

A CHANGE OF STATE

A thermodynamic and cost-effective optimized Trombe wall based on latent heat storage (LHS) for year round application

K.J. Hendriks



A CHANGE OF STATE

A thermodynamic and cost-effective optimized Trombe wall based on latent heat storage (LHS) for year round application

Kees Jan Hendriks | Studentnumber: 4655397

MSc Architecture, Urbanism and Building Sciences | Track: Building Technology
Graduation Master Thesis

MENTORS

Dr. ir. M.J. TENPIERIK

Architectural Engineering +Technology (Building physics)

Prof. dr. ir. T. KLEIN

Architectural Engineering +Technology (Building Product Innovation)

DR. M. TURRIN

Architectural Engineering +Technology (Design Informatics)

DELEGATE OF THE BOARD OF EXAMINERS

Ir. H. Plomp

Architecture and the Built Environment (Education and Student Affairs)



Delft University of Technology

Faculty of Architecture and the Built Environment

Coverpage image: Markinternational (2017). Abstract wallpaper blue. Retrieved from: <http://markinternational.info/abstract-wallpapers-blue/218563602.html>

ABSTRACT

The following graduation thesis "A change of state: A thermodynamic and cost-effective optimized Trombe wall based on latent heat storage (LHS) for year round application" aims to investigate and optimize the thermal energy performance of a Phase change material (PCM) Trombe wall to create an economically feasible product. This passive system reduces the total cost of ownership of the energy system, inside an office building located in The Netherlands, by reducing the energy demand and the maximum peak-loads from the mechanical system. In the European Union (EU) buildings are responsible for almost 40% of the total energy consumption, the energy efficiency of these buildings needs to increase by at least 32,5% by 2030 according to the Sustainable development goals (SDGs) from the EU. Research has shown that the information on the economic feasibility and optimization of PCM within the built environment is somewhat limited, this research will give an in-depth insight in the actual performance on thermodynamics and the cost-effectiveness.

The PCM Trombe wall will be optimized by means of the *Research through design* - method, using different design strategies based on the knowledge of the thermodynamic principles of the PCM. An initial simulation model is used for the energy performance calculations, this model is extended and developed according to the parameters defined for the optimization. A combination of MATLAB and Simulink, a simulation environment based on textual and graphical programming, together with modeFRONTIER is employed. The results from these simulations are first validated with DesignBuilder Software Ltd to verify the legitimacy of the results from the added components and the changed location input data.

The actual performance of the PCM on the reduction of the heating and cooling energy demand, the maximum power-load and the investment cost for the product are determined according to dynamic set-point calculations. A detailed study together with an yearly performance analysis is used, the results from all the different simulations and optimizations are summarized in a design guideline. This guideline gives a clear indication on the differences between the input parameters and the results from the performance of the system. In the end, these results are all brought together in an adaptive and integrated design solution for the application in an office building in the Netherlands.

KEYWORDS: Phase Change Material, Thermodynamics, Cost-effectiveness, Optimization, Total Cost of Ownership, Economic feasibility, Design guideline

ACKNOWLEDGMENT

During my study I created a huge interest in the combination of Building Physics and the use of new innovative materials, subsequently this thesis investigates the use of passive heat and cold storage and concludes my study for a master degree in Architecture, Urbanism & Building Sciences at Delft University of Technology.

I would first like to thank my thesis advisors Dr. ir. Martin Tenpierik, Prof. Dr. ir. Tillmann Klein and Dr. Michela Turrin from the Faculty of Architecture at Delft University of Technology for their insight and encouragement throughout the research process.

Besides this, I would like to give a special thanks to Aytac Balci for his help in speeding up the computational work-flow. The simulations are done using the educational BK Renderfarm platform, which increased the available computing power enormously. I would also like to acknowledge Jan Jacob Trip as the delegate of the Board of Examiners from the Faculty of Architecture at Delft University of Technology for the valuable feedback during the presentation moments.

And finally, I am very thankful to my parents, especially my girlfriend and my friends in Delft and the North of the Netherlands, this achievement would not have been possible without their support and encouragement throughout my whole study and the process of researching for my master thesis.

Kees Jan Hendriks

Delft, The Netherlands

May 2019

GLOSSARY

BEP	Break-even point
BIPV	Building integrated photovoltaic
BMS	Building management system
CEO	Cost-effectiveness optimization
CFD	Computational fluid dynamics
CO ₂	carbon-dioxide
COP	Coefficient of performance
DLS	Dynamic light scattering
DoE	Design of experiments
ECB	European central bank
EER	Energy efficiency ratio
EU	European Union
HTF	Heat transfer fluid
HVAC	Heating, ventilation and Cooling
LCCA	Life cycle cost analysis
LHSU	Latent heat storage unit
LOD	Level of detail
MEP's	Mechanical, Electrical and Public health systems
NSGA	Non-dominated sorting genetic algorithm
PCM	Phase change material
PPD	Percentage people dissatisfied
PWF	Present worth factor
RSM	Response surface methodology
SDGs	Sustainable development goals
SHGC	Solar heat gain coefficient
SNV	Scheduled natural ventilation
TCO	Total cost of ownership
TCS	Thermochemical storage
TEE	Thermal energy efficiency
TES	Thermal energy storage
TIM	Transparent insulation material
TPO	Thermodynamic performance optimization
TRL	Technology readiness level
TWR	Trombe-wall to wall ratio

NOMENCLATURE

q_x	the heat-transfer rate (W/m ²)
dT/dx	temperature gradient in the direction of the heat flow
λ	lambda value (W/(m.K))
d	thickness of the body (m)
m	mass of heat storage medium (kg)
c_p	specific heat (J/(kgK))
T_i	initial temperature (°C)
T_f	final temperature (°C)
T_m	melting temperature (°C)
m	mass of PCM medium (kg)
c_{ps}	average specific heat of the solid phase between t_i and t_m (kJ/(kgK))
c_{pl}	average specific heat of the liquid phase between t_m and t_f (J/(kgK))
f	melt fraction
q	latent heat of fusion (J/kg)
T_w	wall temperature (K)
T_∞	fluid temperature (K)
h	convection heat-transfer coefficient (W/(m ² K))
A	surface area (m ²)
g_{gl}	The fraction of the solar energy transmittance of the window
A_{gl}	The surface area of the window (m ²)
$q_{gl,sol}$	The incident solar radiation on the surface of the window (W/m ²)
$Q_{i,int}$	The internal heat production (W)
A_e	The surface area of the external partitions (m ²)
U_e	The heat transmission coefficient (W/m ² .K)
Q_{tr}	The energy loss (or gain) by transmission and ventilation (W)
$Q_{i,tot}$	The total incoming heat (by people, equipment, lighting and the sun) (W)
M	The accumulation of energy in thermal mass (J/K)
$\rho_1 c_1$	Volumetric heat capacity of air: 1200 J/(m ³ .K)
q_{vr}	The room ventilation flow (m ³ /s)
T_e	Outdoor air temperature (°C)
T_i	Indoor air temperature (°C)
H_{tot}	The total specific heat loss to the exterior (W/K)
α_i	The heat transfer coefficient (W/m ² .K)
i	inflation rate (%)
r	interest rate (%)
C	costs (€)

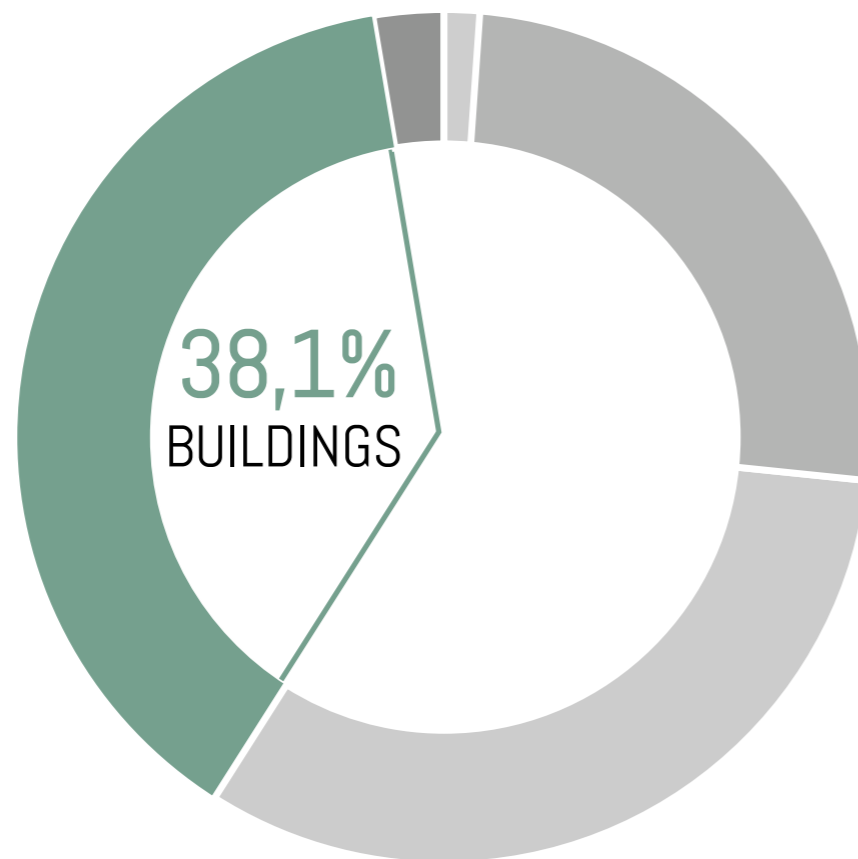
TABLE OF CONTENTS

1. INTRODUCTION	13
1.1 CONTEXT	14
1.1.1 Thermal energy storage (TES)	15
1.2 PROBLEM STATEMENT	15
1.3 SCOPE OF RESEARCH	16
1.4 AIM AND OBJECTIVES	16
1.5 RESEARCH QUESTIONS	17
1.5.1 Sub-questions	17
1.5.2 Constraints and restrictions	18
1.6 RESEARCH APPROACH	19
2. BACKGROUND	23
2.1 THERMAL CONTROL	24
2.2 THERMAL ENERGY STORAGE (TES)	25
2.2.1 Sensible heat storage (SHS)	26
2.2.2 Latent heat storage (LHS)	32
2.3 HEAT TRANSFER	40
2.4 EFFICIENCY OPTIMIZATION	42
2.4.1 Heat transfer enhancement	42
2.4.2 Adaptability of thermal energy storage	53
2.5 CONCLUSION: PART II	56
3. DESIGN CONTEXT	61
3.1 CONTEXTUAL	62
3.1.1 Climate parameters	63
3.1.2 Office typology	64
3.1.3 LHSU typology	65
3.2 ECONOMICAL	66
3.2.1 Parameters cost-effectiveness	67
3.3 CONCLUSION: PART III	70
4. THERMODYNAMICS	73
4.1 ONE-NODE HEAT BALANCE	74
4.1.1 Incoming heat	75
4.1.2 Transmission and ventilation	76
4.1.3 Accumulation	77
4.2 MULTI-NODE HEAT BALANCE	77
4.2.1 Multi-node heat conduction	79
4.2.2 Non-stationary multi-node heat balances	80
4.3 CONCLUSION: PART IV	82
5. COMPUTATIONAL PHASE	85
5.1 SIMULATION METHODOLOGY	86
5.2 PARAMETER SPECIFICATION	88
5.2.1 Benchmark	91
5.2.2 MACRO: PCM Layer thickness	91
5.2.3 MACRO: Coverage (SHGC)	91
5.2.4 MACRO: Melting temperature	92
5.2.5 MACRO: Latent heat of fusion	93
5.2.6 MESO: Trombe wall to Wall Ratio (TWR)	93
5.2.7 MESO: Multi-layered LHSU	94
5.2.8 MESO: Surface area	95
5.2.9 MICRO: Ventilation	95
5.2.10 MICRO: Convective heat transfer enhancement	96
5.2.11 MICRO: Conductivity enhancement	97
5.3 INITIAL MATLAB / SIMULINK	98
5.3.1 Nodes definition	99
5.3.2 Heat transfer mode	99
5.3.3 Fixed simulation parameters	100
5.4 EXTENDED MATLAB/SIMULINK MODEL	101
5.4.1 Multi-layering extension	101
5.5 MODEL VERIFICATION & VALIDATION	108
5.5.1 Internal heat gains	109
5.5.2 External infiltration	110

5.5.3	Solar Gains	111
5.5.4	Air temperature	112
5.6	VALIDATION RESULTS	113
5.6.1	Validation multi-layering	116
5.7	OPTIMIZATION STRATEGY	119
5.7.1	Optimization algorithm	119
5.7.2	Number of evaluations	121
5.8	CONCLUSION: PART V	122
6.	SIMULATION RESULTS	125
6.1	THERMODYNAMIC EVALUATION	126
6.1.1	MACRO: PCM layer thickness	127
6.1.2	MACRO: Coverage (SHGC)	130
6.1.3	MACRO: Latent heat of fusion	131
6.1.4	MACRO: Melting temperature	133
6.1.5	MESO: Trombe wall to wall ratio (TWR)	134
6.1.6	MESO: Multi-layered LHSU	137
6.1.7	MESO: Cavity width	139
6.1.8	MESO: Surface area	140
6.1.9	MICRO: Convective heat transfer	141
6.1.10	MICRO: Conductivity heat transfer	142
6.1.11	Results overview	144
6.2	ECONOMIC EVALUATION	145
6.2.1	Benchmark calculation	146
6.2.2	Results Design of Experiments (DoE)	147
6.3	OPTIMIZATION EVALUATION	150
6.3.1	ONE: Combined optimization	150
6.3.2	TWO: Cooling optimization	152
6.3.3	THREE: Heating optimization	153
6.3.4	FOUR: Total cost of ownership (TCO) optimization	154
6.4	DESIGN GUIDELINE	157
6.5	CONCLUSION: PART VI	

7.	DESIGN PHASE	163
7.6.1	Design requirements	165
7.6.2	Materials and products	167
7.6.3	Module production & assembly	168
7.6.4	Technical detail	172
8.	SYNTHESIS	175
8.1	DISCUSSION	176
8.2	CONCLUSION: FINAL	177
8.2.1	Future research directions	179
9.	REFERENCES	181
	APPENDICES	189
	APPENDIX A	190
	APPENDIX B	192
	APPENDIX C	193
	APPENDIX D	196
	APPENDIX E	199
	APPENDIX F	200
	APPENDIX G	201
	APPENDIX H	202
	APPENDIX I	203
	APPENDIX J	207

Figure 1.1
Energy consumption of different sectors in the EU. Reproduced from "Energy efficiency of buildings", by European Parliament, 2016. Retrieved from [http://www.europarl.europa.eu/RegData/etudes/BRIE/2016/582022/EPRS_BRI\(2016\)582022_EN.pdf](http://www.europarl.europa.eu/RegData/etudes/BRIE/2016/582022/EPRS_BRI(2016)582022_EN.pdf)



1. INTRODUCTION

This section describes the methodology for this research study. First, the context of this study will be elaborated on, after that a brief introduction into thermal energy storage will be given to show the working principle and the reason why it is incorporated in this research study. Secondly, the problem statement will be given followed by the scope of this research study to show the boundaries of this research study. Thirdly, the aim and objectives will be described together with the main research question and sub research questions. Lastly an overview will be given regarding the research approach and method, used to point out the detailed steps within the research framework.

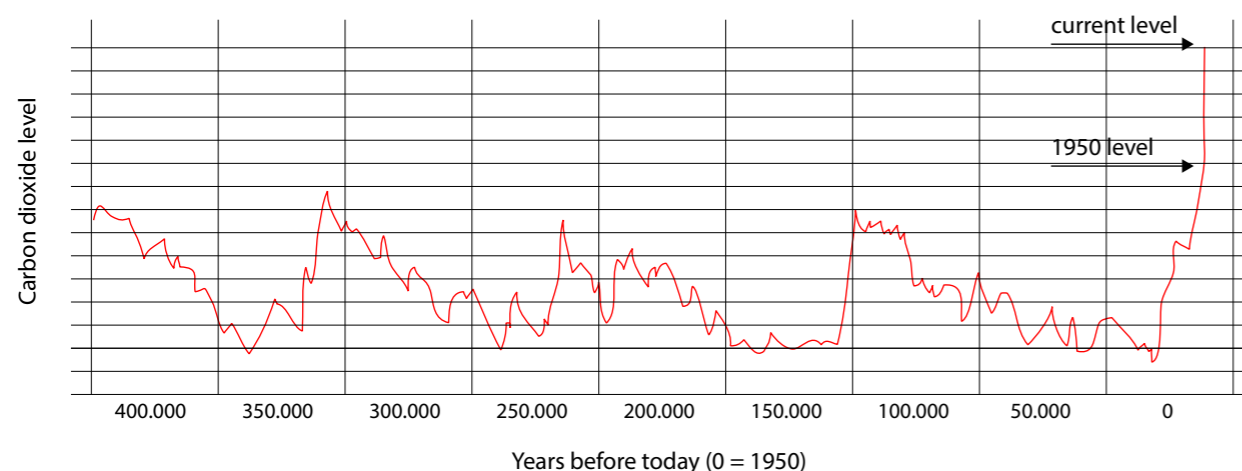
1.1 CONTEXT

In the last decades the growing increase in energy demand and the CO₂-emission (Figure 1.2) is a huge challenge due to the growth in population, industrial innovations and the urbanization, this leads to the exhaustion of fossil energy sources worldwide. It is expected that if this pattern continues the energy demand for heating will rise with 50% in 2050 and for cooling this demand will be tripled (Souayfane, Fardoun, & Biwoleb, 2016). A decrease in energy demand for heating is needed through a socially-fair transition in a cost-efficient manner to reduce the greenhouse gas-emissions in the Netherlands by at least 49% by 2030 compared to 1990 (Rijksoverheid, 2018) and the energy efficiency in the European Union (EU) needs to increase by at least 32,5% (European Commission, 2018). Furthermore, the EU has declared that these greenhouse gas emission need to be net-zero by 2050. This together will contribute to achieve the Paris Agreement temperature from the UN Sustainable Development Goals (SDGs) (European Commission, 2018).

Buildings are responsible for almost 40 percent (Figure 1.1) of the total energy consumption from the EU (European Commission (EC), 2018). In many developed countries the use of active climate control systems from buildings and Heating, ventilation and air-conditioning (HVAC) have an enormous contribution to these total greenhouse gas emissions (European Commission, 2018). Traditional buildings were once built with considerations to environmental conditions to maintain the interior spaces of the building cool in summer and warm in winter (Kumar & Buddhi, 2013). Sophisticated building management systems (BMSs) nowadays are required because these aspects of building construction are forgotten in modern architecture.

Furthermore, buildings are exposed to permanent climatic influences such as diurnal temperature variations, seasonal temperature swings as well as temperature fluctuations due to internal heat gains from human thermoregulation and technological facilities inside the building (Veen & Hakvoort, 2016). These active BMSs are accompanied by high cost of energy and designers, engineers and constructors are under pressure from owners to minimize the total project cost (Ellis, 2007). These HVAC systems can be downsized or even substituted with the use of innovative passive solutions.

Figure 1.2: Climate change over the years considering the CO₂-emissions redrawn. Reproduced from Nasa, n.d., Retrieved November 12, 2018 from <https://climate.nasa.gov/evidence/>



1.1.1 Thermal energy storage (TES)

Research has shown that thermal energy storage (TES) is an efficient way to reduce the energy demand, this technology stores energy from heat or cold in a medium resulting in energy that can be used at another time of the day (Sarbu & Sebarchievici, 2018). Therefore, this technology can be deployed to reduce the need of mechanical systems, which can help to reduce the operation costs for the building, the carbon-dioxide (CO₂) emissions and it helps to create a comfortable and healthy environment for the occupants.

This way of energy management has a lot of potential, but also other purposes can be pursued when using TES in buildings, sustainable heating and cooling with TES in buildings can be achieved through passive systems in building envelopes. In this way it can for instance be used to offset peak loads from sun radiation, which significantly reduces the loads needed for cooling the building.

1.2 PROBLEM STATEMENT

Buildings are responsible for an enormous part of the total energy consumption, new sustainable and innovative passive technological developments are needed in order to achieve the objectives from the SDGs to reduce the final energy consumption from the EU and to achieve the SDGs. Contemporary low energy buildings are based on a combination of controlled ventilation and high insulation values. These lightweight buildings can not respond to high diurnal temperature swings and mechanical cooling is needed to control the environment. A major drawback of conventional TES applications, such as a Trombe wall with thermal mass, is the combination of a low heat capacity and a high density of the material, which results in heavyweight structures with a low thermal capacity (Guarino, et al., 2015). Moreover, another disadvantage of this structure is the reduction in the amount of daylight entering the building. Research showed that Phase change materials (PCM's) have the highest potential considering energy storage capacity, around 5 to 14 times more energy storage is achieved using PCM's (Salunkhe & Shembekar, 2012). This results in a more compact design compared to conventional thermal mass systems and up to 14 times less material is needed. In addition, this simplifies the implementation into contemporary low energy buildings, which makes it much more convenient for application (Hu, He, Jia, & Zhang, 2017; Khudhair & Farid, 2004; Riffat, Mempoou, & Fang, 2013). The correct and practical implementation of these PCM's in buildings is one of the main problems to address (Souayfane, et al., 2016). A transition is needed in the development of TES in buildings to evaluate and optimize these systems considering their energy potentials and cost-effectiveness, subsequently contributing to a wide application of passive TES in low energy buildings. These TES systems need to become economically feasible and attractive to all building owners to make the transition to a more sustainable environment, no reliable research was found on the economic feasibility and optimization of this PCM Trombe wall technique. Therefore, efficient and cost-effective heat transfer enhancement techniques need to be explored. This economic evaluation is essential in assessing the applicability of these systems in buildings, which subsequently leads to a decreased reliance on HVAC-systems.

1.3 SCOPE OF RESEARCH

The research primarily focuses on creating a TES system which is economically beneficial considering the reduction in energy usage, which contributes to downsizing of active climate regulation systems. Subsequently, taking into account the analysis of the life cycle cost for application in a office building. These office buildings have high internal and external loads that need to be managed. This research will lead to an in-depth insight into the evaluation of the cost-effectiveness of this innovative passive energy management system. The Trombe wall is an effective TES system, possibilities for increasing the air flow rate and the use of operable vents increases the efficiency. This system gradually transfers the stored energy within the thermal mass to the interior of the building, in this way it can be used for passive winter heating and summer cooling. The volume of a Trombe wall can be increased for a higher heat storage capacity of the wall. However, this will increase the total weight on the building's structure, which subsequently increases the volume and costs of the structural elements (Hu, He, Jia, & Zhang, 2017). Therefore, the efficiency of the system will be optimized within this research study, this significantly reduces the volume of the system, which results in a more practical system. Hence, a PCM based Trombe wall will be the main focus of this research study, the two benchmarks of this study will be a standard facade with an exterior sunscreen and a conventional Trombe wall system based on concrete thermal mass. A study from Van Unen showed the potential of this type of passive solar wall in the temperate climates due to the high diurnal temperature swings (Unen, 2018), therefore the Trombe wall will be situated in a office building the Amsterdam, the Netherlands.

1.4 AIM AND OBJECTIVES

The aim of this research report is to investigate the thermal energy effectiveness (TEE) of a passive PCM Trombe wall in a non-residential building, this TEE relates to the thermodynamic potentials of the PCM and the economic feasibility of the material considering the balance between input (project costs) and output (energy reduction). In achieving this goal, two main objectives will be strategically addressed:

1. The first objective is to ameliorate the thermal performance of the PCM Trombe wall by improving the energy storage capacity with a focus on thermodynamic optimizations and therefore the effectiveness for application in buildings. Hence, the optimal set of parameters needs to be defined to minimize the year round thermal energy demand of the building compared to a conventional passive Trombe wall.
2. The second objective of this research is to evaluate the costs of the different TES systems, which gives insight in the cost-effectiveness, resulting in minimizing the total life cycle costs (LCC) of these system (including the production of the system and the energy reduction over the lifetime). Subsequently, this contributes to the optimization for an economically feasible application of a passive TES system compared to a Heating, ventilation, and air conditioning (HVAC)-system in a non-residential building.

The cost-effectiveness optimizations (CEO) and the thermodynamic performance optimization (TPO) together will result in an optimized design, which is economically feasible and where the PCM is implemented into a system that makes optimal use of the storage capacity of the material.

1.5 RESEARCH QUESTIONS

The main question addressed in this research study is:

*“What is the most **cost-effective** and **thermodynamic optimized design** for a **passive Trombe wall** based on latent heat storage for **year round application** in an office building in Amsterdam, the Netherlands?”*

Cost effectiveness relates to the different optimization strategies, which will be assessed by a Life-cycle cost analysis (LCCA), this refers to the total project costs made up out of acquisition cost, total facility management (operation and support) costs, and total disposal cost. The optimum relates to the balance between fuel investment costs (including cost for energy supply) and the investment costs for the design variable (including the total life cycle costs). (Ellis, 2007)

Thermodynamic optimized design relates to the design outcome of the Trombe wall based on PCM's, which is optimized in terms of heat-transfer enhancement techniques considering conduction, convection and radiation.

1.5.1 Sub-questions

The following sub-research questions are determined regarding the thermodynamic optimization of the passive Latent heat storage unit (LHSU):

- *A1: Which LHSU's are available considering the production of the materials and the encapsulation?*
- *B1: In which ways can the LHSU be optimized to increase the effectiveness of the PCM Trombe wall application in non-residential buildings?*
- *B2: How can the LHSU be adaptive for year round application considering the different seasons of the year?*

The cost effectiveness of the system will be evaluated and optimized by establishing the following sub-research questions:

- *C1: In which way can the PCM Trombe wall be optimized for the cost-efficiency considering the reduction in energy use of the HVAC-system?*

The design process will be employed using the following research questions:

- *D1: Which parameters need to be taken into account for optimizing the cost-effectiveness and thermodynamics of a PCM Trombe?*
- *E1: What is the most efficient thermodynamic optimization, of a PCM Trombe wall, considering the different heat transfer enhancement techniques?*
- *E2: What is the most cost-effective optimization of a PCM Trombe wall?*
- *E3: What is the best combined design outcome for a cost-effective and thermodynamic optimization of a PCM Trombe wall?*

1.5.2 Constraints and restrictions

Cost-effectiveness:

An assumption will be made for the costs of electricity related to the calculation of energy usage from the climate control system and the reduction in energy by the TES-system. An average electricity price will be determined after analysis of the pricing system from the project location.

Material related costs concerning the indication for a price of PCM's can give certain deviations due to a low Technology Readiness Level (TRL) of most of the products, the market for PCM's is not yet fully developed. Therefore mass production is not included in the calculation of most of these products resulting in relatively high capital costs.

The acquisition costs of the system is mainly defined by the cost for the PCM product and the assembly of the product. This product cost is primarily governed by the cost of the production of the system considering enclosing the material and the cost of the raw PCM material, the remaining parts regarding the more detailed costs such as adhesives and other additives may prove difficulties due to the complexity of the analysis. Therefore these parts will be not be employed.

Thermodynamic optimized design:

A morphological optimization will be left out of consideration by reason of the complexity of this study regarding the input from different climate parameters and sun orientations, this will provide different outcomes for the system. In this research the focus will be on an application, which can be implemented in the Dutch climate and a office typology, the project specific outcome from a morphological optimization will significantly increase the cost of the system. This will decrease the cost-effectiveness of the design outcome and will therefore not be considered. Besides this, the focus is on the yearly energy reduction, including these detailed simulations will lead to long and heavy simulations.

Cardinal direction:

The research study focusses on a cost-effective optimization for the passive Trombe wall, hence this study only takes the south facing façade into account during the digital simulations phase, other cardinal directions are neglected.

1.6 RESEARCH APPROACH

This research will be carried out by means of the *Research through design* - method, whereby the thermodynamic and cost-effective optimizations together with the conceptual design will contribute to the experimental phase, which creates new insights to optimize the design. This process will be iterative where an interaction between the conceptual design and the digital optimization in the end will lead to the final design outcome, the different research steps are illustrated in Figure 1.4 and Figure 1.5 on the next page.

Literature study

First a background analysis will be done using a literature study to define the concept of thermal energy storage and the commonly found applications and implementation in the built environment. This information will be used to do a more in-depth research on the principle of heat transfer and heat transfer enhancement techniques to improve the rate of heat transfer of the passive Trombe wall.

Conceptual design

The research outcomes from the background analysis will be incorporated into the parameters for the conceptual design, the parameters will be used to define the project requirements for the design and optimization phase. This conceptual design phase is used for the simplification of all the different optimization strategies, which results in different optimization typologies to easily evaluate and compare them.

Digital optimization

The digital optimization phase, indicated within the blue yellow research phase, is split into two separate optimization strategies, which in the end will be combined to one final design outcome. The thermodynamic and cost-effective design optimizations are separated due to the expected possible discrepancy in outcome between the two subjects. The results from both the subjects will be evaluated and used as input for a new improved conceptual design. The thermodynamic study will be executed using MATLAB®, the energy efficiency of the system will be evaluated by comparing the results to a benchmark office based on Heating, Ventilation and Air-conditioning (HVAC), this will be combined with a Life Cycle Cost Analysis (LCCA) in Microsoft Excel to evaluate the cost-effectiveness of the optimizations by calculating the total investment cost of the design variable and plotting it against the reduction in energy of the HVAC-system.

Design outcome

As said, the total investment costs (the balance between the investment cost for a LHSU and the reduction in the investment for the HVAC system) will determine the optimal outcome. A study will be done considering the method for defining a deliberate decision for the combination of the multi-objective optimization strategy. This can be evaluated with a Pareto analysis; this analysis is about finding the Pareto optimal solution considering the trade-off between the conflicting objectives. The Pareto front shows the solutions linked to both the objectives. The outcome of this design phase leads to a design framework that presents the main outcomes from this research, which can be used as input for the design phase with PCM's. One general combined design will be created using the results from the optimization study.

Figure 1.3 :
Main flow of research design
showing the general steps

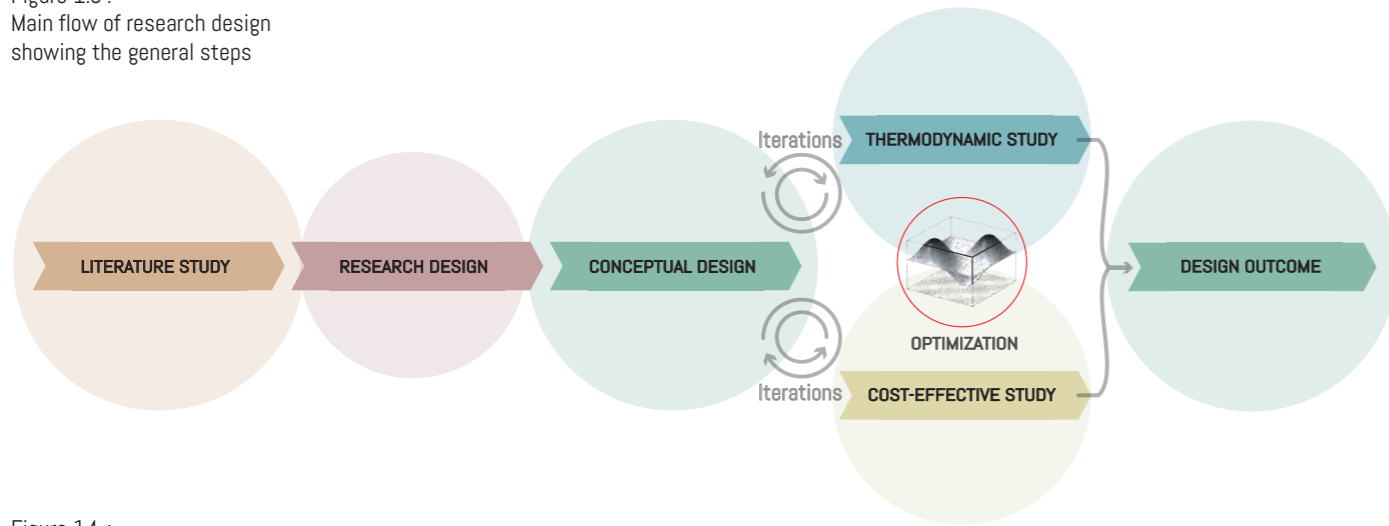


Figure 14 :
Part 1: Reserach framework,
problem identification, literature
study and research design phase.

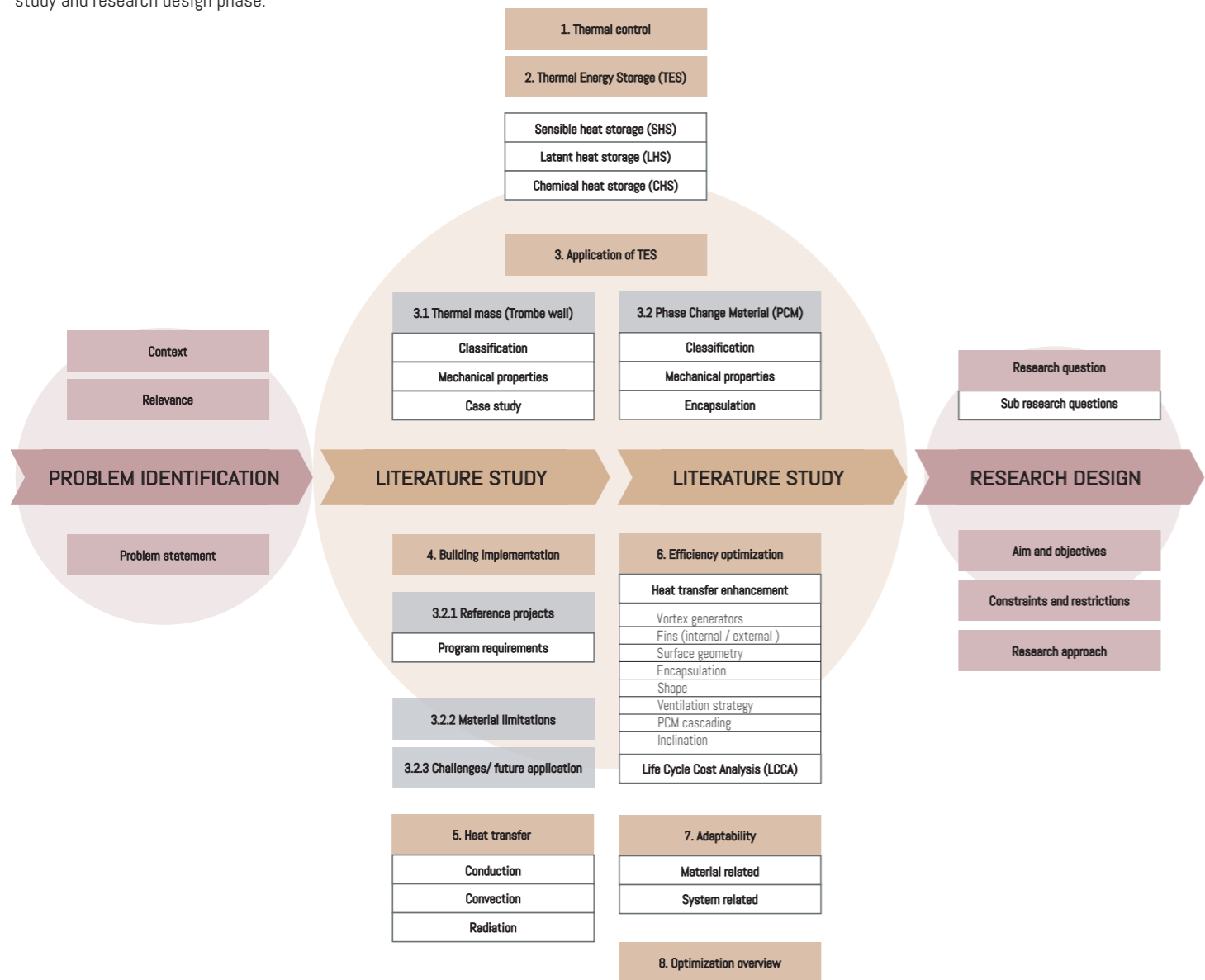


Figure 1.5 :
Part 2: Research framework,
research design and digital
optimization phase

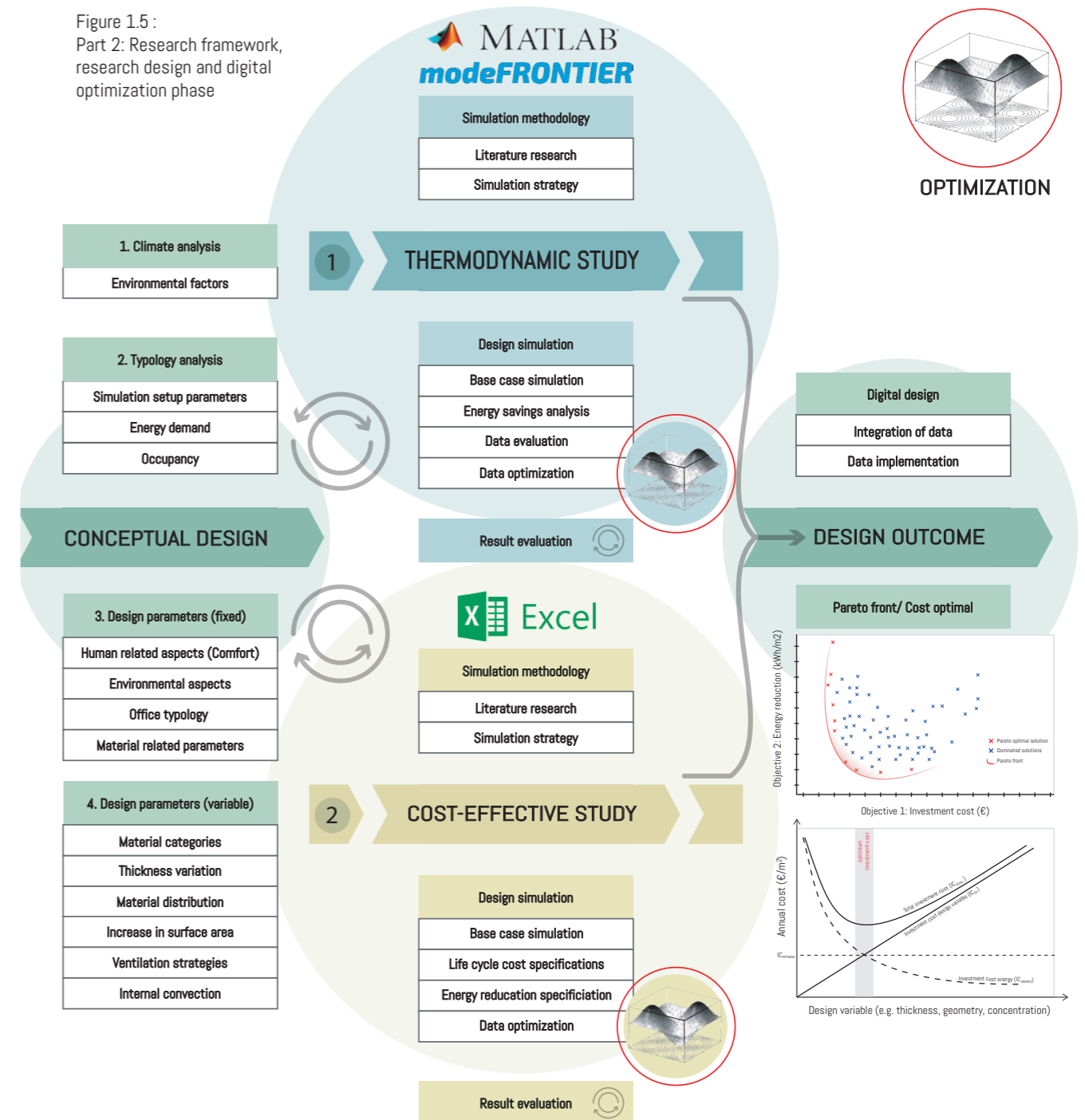


Figure 1.6
PCM modules on a thermal mass wall.
Reprinted from Energyarchitecture,
n.d.. Retrieved from <http://www.energyarchitecture.com.au/projects/norton-summit-ecological-footprint/>



2. BACKGROUND

This section provides the background information regarding the passive thermal management in buildings with Thermal energy storage (TES) and the different advantages and disadvantages. First, thermal comfort will be described according to the standards in the Netherlands. Secondly, the method of thermal energy storage will be described together with the different techniques, this will be used to define the important factors influencing the performance calculations. Thirdly, a study will be shown regarding the working principle of Phase change materials (PCM's) together with the production methods and the products available on the market. Lastly, the different heat transfer enhancement techniques will be described according to numerical and experimental studies from previous researchers, these enhancement techniques will be used to increase the performance of the PCM Trombe wall. A summary will be given with the different techniques for the optimization phase.

2.1 THERMAL CONTROL

Buildings underlay several environmental influences regarding heat management, diurnal and seasonal changes in temperatures in the environment together with internal heat gains. Together they are creating fluctuations in temperature when no thermal management concept is introduced. In addition, these factors are important to take into consideration for an efficient thermal control system (TCS). The solar radiation through windows is one of the factors that creates significant impact on the performance of a building when window to wall ratios are above 20 to 30%, an important property related to this aspects is the Solar heat gain coefficient (SHGC). This coefficient is a property of the window which indicates the amount of energy to pass through the window expressed as a number between 0 and 1 (Straube, 2011). Nowadays buildings are often well-insulated and therefore heat from inside is captured inside this space, it will not escape the building. Subsequently, interior heat gains, regarding heat from the occupants and heat generated by active systems inside the building, are also important for the TCS. Especially in offices this interior heat gain can be high due to the large amount of people and devices per square meter of floor area, in cold weather conditions this heat of-course reduces the heating demand of the building but when it is warmer outside this heat adds to the cooling load of the building. (Straube, 2011)

Table 1.1 : Recommended indoor temperatures for energy calculation, temperature heating and cooling. Reprinted from "Nederlandse norm: NEN-EN 15251 (en)" by CEN, 2007

Type of building or space	Category	Temperature range for heating, °C	Temperature range for cooling, °C
		Clothing ~ 1,0 clo	Clothing ~ 0,5 clo
Offices and spaces with similar activity (single offices, open plan offices, conference rooms, auditorium, cafeteria, restaurants, class rooms, Sedentary activity ~1,2 met	I	21,0 – 23,0	23,5 - 25,5
	II	20,0 – 24,0	23,0 - 26,0
	III	19,0 – 25,0	22,0 - 27,0

The objective for the thermal control of a building is to keep the space of the building on an quasi constant temperature, more specifically to avoid that the temperature raises above a certain comfort threshold, which keeps the occupants satisfied. This comfort level differs from winter and summer due to a difference in perception of temperature and the amount of clothing we are wearing. The NEN-15251 is an European Standard where Indoor environmental input parameters are defined for designing and assessing the performance of the controlled indoor environment (CEN, 2007). The design requirements for thermal comfort, minimum room temperature in winter and maximum room temperature in summer, are given and apply to calculations for windows, building mass and sun shielding. "APPENDIX A" shows the indoor design temperatures for buildings with HVAC. Table 1.1 shows the recommended temperatures for energy calculations by means of a predicted percentage of dissatisfied (PPD) people of 10% (Category II: "APPENDIX A"). (CEN, 2007)

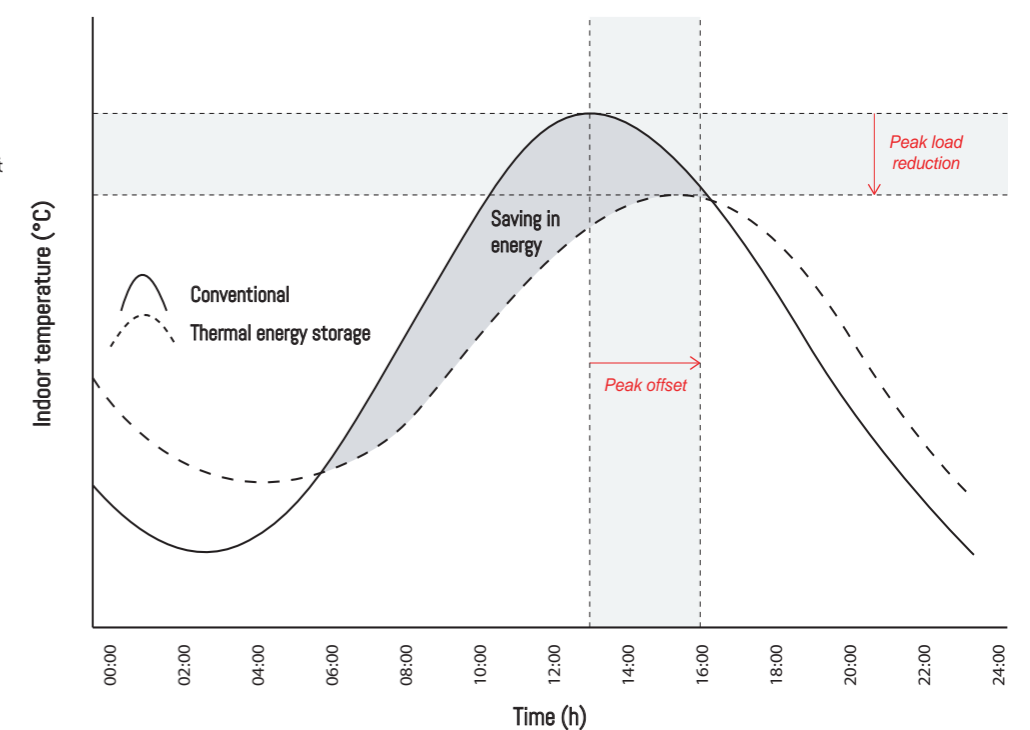
2.2 THERMAL ENERGY STORAGE (TES)

A key function in the thermal control of buildings nowadays is the passive application of Thermal Energy Storage (TES). This way of storing thermal energy is a topic widely discussed and researched due to the positive effects of its storage capacity on developing a sustainable environment, which especially contributes to the energy efficiency of buildings in terms of balancing out the gap between demand and supply and reducing peak loads from solar radiation (Sarbu & Sebarchievici, 2018). This technology stores energy from heat or cold in a medium resulting in energy that can be used at another time of the day, therefore it reduces the need of active building service systems such as Mechanical, Electrical and Public health systems (MEPs) or Heating, Ventilation, and Air-Conditioning systems (HVACs). This can lead to a reduction in operation costs for the building and carbon-dioxide (CO₂) emissions, but also in a comfortable and healthy environment for the occupants. (Sarbu & Sebarchievici, 2018)

The energy storage density is a property of high importance considering the amount of energy that can be stored per unit of volume (Gracia & Cabeza, 2015). Thermal storage systems can be classified in two main categories, thermal energy storage (TES) and thermochemical heat storage (TCS). TCS-system are associated with heat storage and release by a reversible endothermic/exothermic reaction process. For instance, the charging process requires energy to separate material A into two parts (B+C), these separated materials will be stored separately. The energy can later be used at a specific time when the separate parts are mixed at a certain pressure and temperature that fit the requirements (Sarbu & Sebarchievici, 2018). These TES-systems can be sub-divided into sensible heat storage and latent heat storage.

These TES systems can provide significant economical and environmental benefits by providing a passive solution which reduces the need for mechanical systems and therefore the fuel costs of these systems. TES can for instance be used to offset peak loads from sun radiation which significantly reduces the loads needed for cooling the building (Figure 1.7) (Kalnæs & Jelle, 2015).

Figure 1.7 : Peak shifting and reduction by using TES. (Reproduced from "Phase change materials and products for building applications" by Kalnæs & Jelle, 2015)



2.2.1 Sensible heat storage (SHS)

Sensible heat storage materials are using the most simple method for storing heat based on the principle of heating or cooling a liquid or solid medium. A variety of materials are available which can be used for this method such as water, molten salts, rocks or sand and an important medium in building applications, concrete (Sarbu & Sebarchievici, 2018). The price and the fact that it has no toxic additives are the main advantages of this material. The amount of heat that can be stored (Q_s (J)) during the charging and discharging process depends on specific volume of the material, the specific heat and the change in temperature, this is expressed as illustrated in equation (1.1):

$$Q_s = \int_{T_i}^{T_f} mc_p dt = mc_p(T_f - T_i) \quad (1.1)$$

m mass of heat storage medium (kg)

c_p specific heat (J/(kgK))

T_i initial temperature (°C)

T_f final temperature (°C)

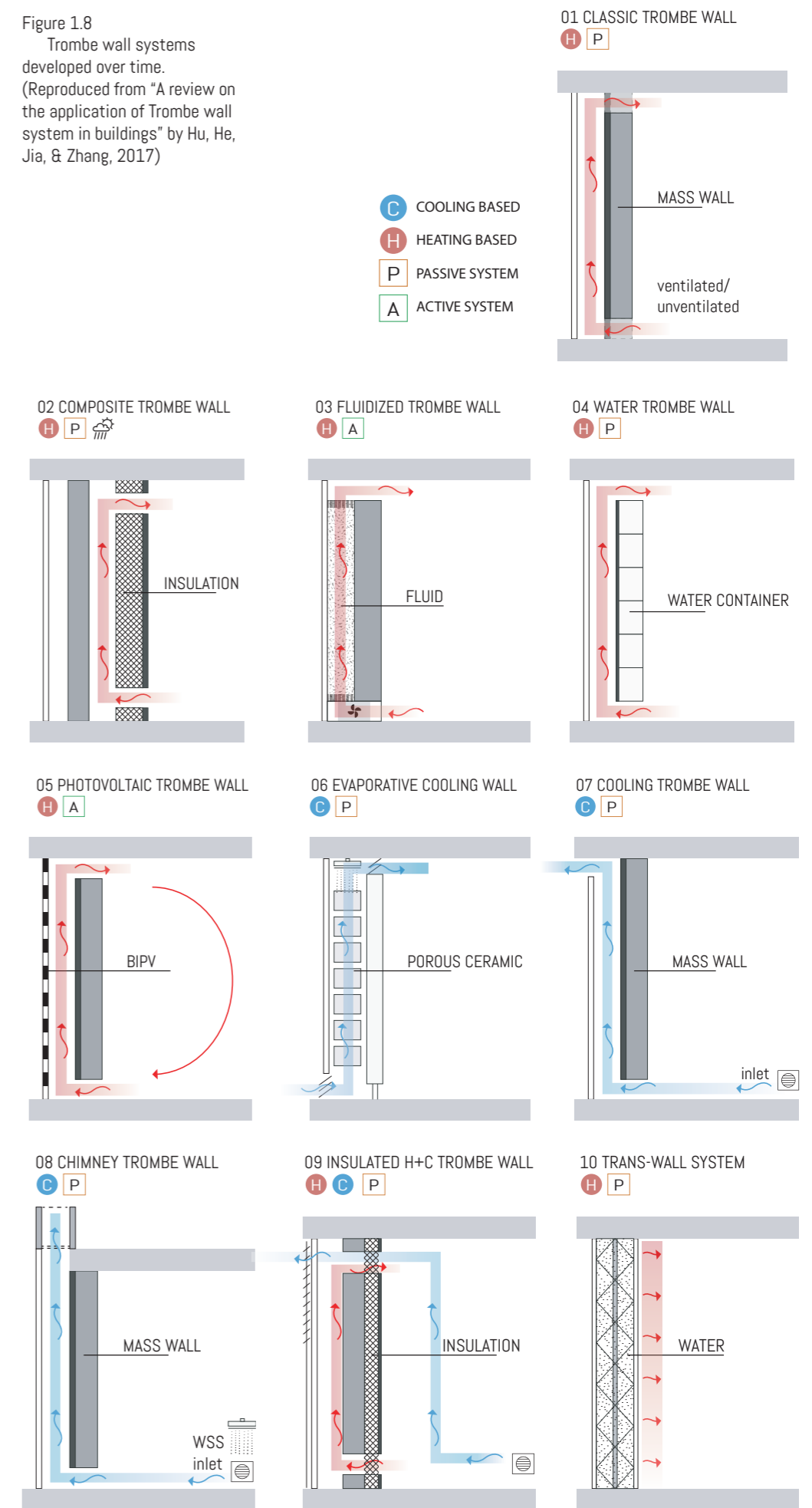
The main disadvantage of this method is the volume required for implementation in the building sector, these materials have a low energy density or specific energy so a large amount of volume is required to store enough heat for effective passive technologies. (Sarbu & Sebarchievici, 2018)

2.2.1.1 Trombe wall

A well-known system based on this SHS principle is the Trombe wall, the concept of this wall is patented by Edward S. Morse in 1881, after that the concept is further developed by Felix Trombe in the 1960s making it a popular system for application in buildings (Hu, He, Jia, & Zhang, 2017). Trombe walls can be classified into two main categories, the heating based type of Trombe wall and the cooling based type of Trombe wall. The classic Trombe wall is a wall constructed out of thermal mass such as stone, brick or adobe which is painted black on the side exposed to the sun, this dark paint increases the amount of heat absorbed by the material (Saadatian, Sopian, Lim, Asim, & Sulaiman, 2012). The wall makes use of indirect solar radiation through a glazing pane which is situated in front of this wall (Figure 1.8), a greenhouse effect is created in the space between the wall and the glazing (Hu, He, Jia, & Zhang, 2017).

This traditional system is always used on the south façade of the building, in northern hemisphere countries, where it absorbs and stores the solar energy. This stored energy will then gradually be transferred to the interior of the building which can be used for passive winter heating, in summer the heat gradient in front of the wall creates a natural air flow for summer cooling. Duffie and Beckman (2013) indicate that the use of vents can improve the performance of the system compared to an unventilated wall (Duffie & Beckman, 2013). With time changes are made in the working principle of this Trombe wall, several researchers developed techniques to increase the heat transfer rate and the storage density of this wall by introducing ventilation strategies and additional elements (Figure 1.8). All these different Trombe wall principles have their own benefits and drawbacks. The information from this study will be used as background information for the optimization strategies of the PCM based Trombe wall. The figures depicted on the next page are connected to the information from Table 1.2.

Figure 1.8
Trombe wall systems developed over time.
(Reproduced from "A review on the application of Trombe wall system in buildings" by Hu, He, Jia, & Zhang, 2017)



The following table shows the description of all the different Trombe wall enhancement strategies to improve the thermal performance of the system, the results are summarized to show the benefits and drawbacks from these specific techniques. A summary of the most important findings is shown in the "Results" overview in Table 1.2.

Table 1.2 Comparison overview of the different Trombe wall optimization strategies

#	Type	Description	Type of study	Results	Reference
01	Classic trombe wall	This classic trombe wall design uses a combination of thermal mass together with a glazed cavity to absorb heat from solar radiation and to store this heat. The air in this cavity is used to heat up the cold fresh air before entering the room.		A small air flow rate tends to give better performance results, an increase in the channel depth increases the mass flow rate. The optimal Trombe wall area to total wall area is $(\alpha)=37\%$. Covering the wall controls the performance of the wall for overheating and heat loss	(Hu, He, Zhang, & Ji, 2017)
02	Composite trombe wall	An important drawback from the classic trombe wall is the heat loss from the inside in cold periods. The composite wall uses an insulated wall as addition on the inside, the heat is transferred by conduction through the wall and is then transferred to the inside by convection.	Numerical study	Better performance for heating the building due to less heat loss, a more stable indoor temperature is observed by using insulation in a cold or cloudy climate	(Shen, Lassue, Zalewski, & Huang, 2007)
03	Fluidized trombe wall	This heating based trombe wall has an addition of highly absorbing and low-density particles within the cavity space. The air, assisted by a fan, flows through this space and is in direct contact with these particles.	Numerical study	The extracted total heat increased from 300W to 500W compared to the conventional trombe wall by using fluidized particles in direct contact with the airflow	(Uysal & Tung, 1991)
04	Water thermal storage wall (WTSW)	This design is comparable to the classic trombe wall, in this case water is used as the thermal mass of the wall. This increases the heat capacity of the wall compared to the conventional trombe wall.	Numerical study	An improved thermal comfort and energy savings is realized by using water as thermal energy storage material (8.6% energy savings)	(Wang, Tian, & Ding, 2013)
05	Photovoltaic trombe wall (PV-TW)	This type of trombe wall generates electricity and provides heating for the interior space by using building integrated photovoltaic (BIPV) on top of the outer glass pane.	Numerical study & experimental study	The BIPV covering can reduce the thermal efficiency of the trombe wall up to 17%, here electrical energy is the addition for a higher overall efficiency	(Sun, Ji, Luo, & He, 2011)
06	Evaporative trombe wall	For both winter and summer season, in summer the space is cooled down using the evaporative cooling wall and in winter the wall works as a conventional trombe wall.	Experimental study	The system is difficult and complex, but a high rate of passivity is obtained with this system.	(Melero, Morgado, Neila, & Acha, 2011)
07	Cooling trombe wall	This is a simple convection based cooling trombe wall, in moderate climates this system can be used efficiently. Here the outdoor temperature can be lower than the indoor temperature. In this situation the trombe wall can be used for natural ventilation by opening a ventilation inlet on the other side of the room, this type is based on the principle of a solar chimney.	Numerical study	In this way the trombe wall can operate in different modes (heating and cooling) by adjusting the air flow. It reduced the heating load by 20% and the cooling load increased by 11%	(Miyazaki, Akisawa, & Kashiwagi, 2006)
08	Chimney trombe wall	This system combines the benefits from the solar chimney principle with the ones from the trombe wall, the wall can be used all year long with this addition and the heat storage of the wall ensures that the solar chimney can operate during late hours of the day.	Experimental study (desert climate)	Water spraying system (WSS) at the channel increases the thermal efficiency of by around 30%. The heat from the trombe wall increases the air flow rate of the chimney. Mainly used for cooling based climates and high ventilation rates	(Rabani, Kalantar, Dehghan, & FaghiehSchool, 2015)
09	Insulated heating and cooling trombe wall	A heating and cooling based trombe wall using 15 cm wool insulation on the inside and two 3 mm thick roll-up curtains in the cavity is created to reduce heat losses and heat gains depending on the season. Ventilation strategies are used to dissipate heat from the interior or from the cavity.	Experimental study (semi-arid climate)	A reduction in energy at peak loads for heating and cooling is respectively 93% and 72%. The indoor temperature is 4 degrees higher in winter and lower in summer compared to a trombe wall.	(Dabaieh & Elbably, 2015)
10	Trans wall	This wall is transparent and modular at the same time, it provides heating and illumination to the interior space. In this way it plays also an aesthetic role due to the visibility of the outside space. Water is placed inbetween two glazing panes within a metal frame.	Numerical study	The convective heat transfer within the trans wall reduces its efficiency, baffels can be implemented to prevent this phenomenon from happening	(Saadatian, Sulaiman, Asim, & Sopian, 2012)

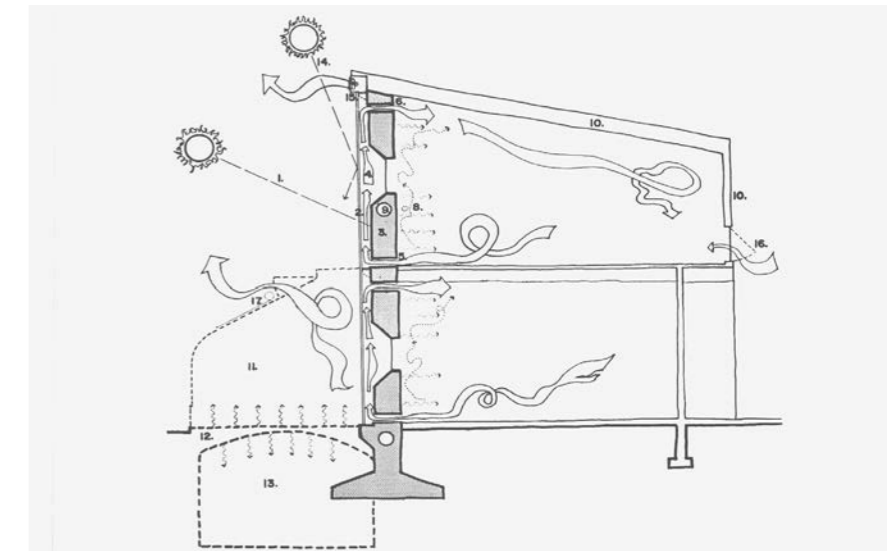
2.2.1.2 SHS case studies

The Kelbaugh House, New Jersey (Douglas Kelbaugh)

The Kelbaugh Solar House is a two floor residential wood-frame building, built in New Jersey between 1974 and 1975. The house uses a passive solar Trombe wall made out of concrete, the wall is placed behind a two storey high greenhouse façade. The sun-side face, orientated to the south, is painted black with a selective coating and the thermal storage capacity of the wall is both used for heating in summer and cooling in winter (Latouche, 2007). The top vent of the wall, situated at the roof ridge, can be opened in summer to prevent the space from overheating and to stimulate air flowing through the house to ventilate. The total thickness of the Trombe wall is 38 centimetres, six windows are placed in the 56 square meter wall to give visibility to the outside and access to the greenhouse (Latouche, 2007).

Measurements used to indicate the indoor temperature show that the indoor temperature was relatively stable, one diurnal cycle showed a temperature swing between 14 and 23 degrees Celsius. The outdoor temperature varied between -13 and 14 degrees, this shows that the wall had significant effect on the preservation of the indoor temperature (Latouche, 2007). Some major problems affecting the overall performance of the Trombe wall are the reverse convection during night-time due to colder air flowing downwards in the cavity and the heat losses through the large opening into the greenhouse (Latouche, 2007). The air can be prevented from flowing back into the house when it is too cold by using a back-draft damper, this manual damper closes when the air is flowing in the wrong direction (Duffie & Beckman, 2013).

Figure 1.9 Section showing air circulation and heat radiation. Reprinted from the Canadian Centre for Architecture, by Latouche, 2007. Retrieved from <https://www.cca.qc.ca/en/issues/19/the-planet-is-the-client/33741/the-kelbaugh-house>



The Solar House, Odeillo (Mitchell Trombe)

This Solar house, built by Mitchell Trombe, is a four room detached house built in Odeillo, the French Pyrenees. The southern façade is constructed out of a large two storey high concrete wall which is used as a passive solar wall. The south face is fully dark painted to improve the absorbency of the wall, this façade is completely blind and no windows are integrated (Figure 1.10), so there is no view to the surrounding landscape and no access to natural daylight from this sunny side (Medici, 2017). The façade is more used as architectural statement on the importance of saving energy, however the architectural quality and

the view from the inhabitants from the interior is not taken into account. The Trombe wall includes two operable vents at the top and the bottom that can be used for the circulation of air within the building. In winter these vents are used to recirculate the air from behind the glass panel inside the building, in this way the air heats up gradually and a stable indoor temperature is achieved. In summer, cross-ventilation is used to allow fresh air to enter the space, the stack effect within the cavity of the solar wall creates a natural air flow. A 35 centimetre concrete wall is used, this thickness is sufficient to provide a heated air flow for most of the night. This thickness and the working principle for ventilation is equivalent to the storage wall and principle from the Kelbaugh house presented before. (Medici, 2017)

These differences between the two cases shows the potentials in architectural expression of the Trombe wall but they are not yet thoroughly explored by the architects, the principles are in the beginning stage of development.



Figure 1.10
South facing façade showing the black painted trombe wall. Reprinted from Manuale Faidate, by Jureidini, 2011. Retrieved from <https://jjureidini.wordpress.com/2011/01/18/trombe-wall-case-studies/>

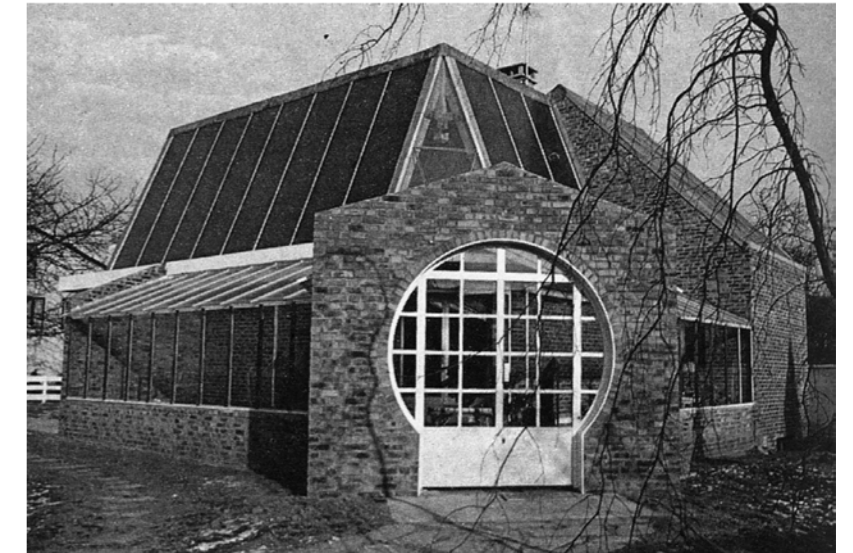
Maison particulière, Argenteuil, Val d'Oise (Marc Vaye and Frédéric Nicolas)

The Maison Argenteuil is a residence built in Val d'Oise Argenteuil (Figure 1.11), the solar technique used in this building is similar to the conventional trombe wall described before. However, in this building the cavity between the massive wall and the glazing is used as usable sun space (greenhouse) and the depth of his space is wider (Figure 1.11), this makes the room behind it darker compared to the conventional Trombe wall. (Medici, 2017)

A manually operable shutter system is situated in front of the thermal mass, this creates a technique where the behaviour of the inhabitants contributes to the performance of the solar wall system. The shutters are used to protect the thermal mass during night-time to prevent for heat losses to the outside, this feature can affect the performance of the wall negatively when the shutters are left closed during daytime due to the manual operation. The cavity is still used for natural air circulation within the building via vents at the top and the bottom of the wall. Another innovation in this building is the use of the southeast façade in combination with the southwest façade, so the wall is divided into two separate cardinal direction and not one in particular. (Medici, 2017)

The house was able to provide 70% of the heating needed, using a combination of this solar wall together with solar collectors integrated in the façade of the first floor. Some mayor issues for this project were access of natural light in the rooms situated behind the solar storage wall, the behaviour of the inhabitants for the operable shutters and the view to the outside. (Medici, 2017)

Figure 1.11
Maison particulière, Argenteuil, Val d'Oise. Main entrance and greenhouse on the south. Reprinted from "The Trombe Wall during the 1970s: technological device or architectural space", by Medici, 2017



Zion Visitor Centre, Springdale, Utah

A more modern example of the application of a Trombe wall is the ventilated masonry wall from the Visitor Centre at Zion National Park in Utah, Colorado. An important design issue is the prevention of overheating of the Trombe wall during the summer season when the sun is high in the sky, several shading techniques can be incorporated into the system to prevent the wall from absorbing the solar radiation. The interior surface of the wall can reach up to 38 °C, this temperature was reduced by 7 °C when the system was covered from the outside for four days (Torcellini & Pless, 2004). A strategically placed overhang is situated at the roof ridge from the Zion Visitor Centre to block the direct sun in summer, in winter the sun elevation will be low so direct radiation will enter the building (Figure 1.12). Windows are placed at the top of the wall allowing for sunlight to enter the building and for more solar radiation in winter. The wall contributes for 20% of the total energy for heating the building. There was no ventilation integrated into the design to drive the air flow of the Trombe wall, the system is mainly based on radiation. (Torcellini & Pless, 2004)

Figure 1.12
South facing Trombe wall Zion Visitor Centre. Reprinted from Green Building Brain, by R. Williamson, n.d.. Retrieved from https://greenbuildingbrain.org/buildings/zion_visitor_center



2.2.2 Latent heat storage (LHS)

Latent heat storage is based on the heat absorption or release when a storage material undergoes a phase change from solid to liquid or liquid to gas or vice versa. At the beginning of the energy absorption the material acts the same as SHS materials, in this period the material is still liquid or solid so energy is stored in a sensible way, the temperature rises linear together with the rise in enthalpy of the system (Figure 1.14). During the nucleation process large changes in enthalpy can be observed at a quasi constant temperature which gives this material the characteristic of storing a large amount of energy at a smaller temperature range compared to sensible heat storage systems (Bourne & Novoselac, 2015). The storage capacity Q_s (J) of a LHS-system is calculated by the following equation, the most important phase for storing energy is the nucleation phase (Sarbu & Sebarchievici, 2018):

$$Q_s = \int_{T_i}^{T_m} mc_p dT + mf\Delta q + \int_{T_m}^{T_f} mc_p dT$$

$$Q_s = m \left[c_{ps}(T_m - T_i) + f\Delta q + c_{pl}(T_f - T_m) \right] \quad (1.2)$$

Figure 1.13 :
Equation latent heat storage
(Sarbu & Sebarchievici,
2018)

- T_m melting temperature ($^{\circ}\text{C}$)
- m mass of PCM medium (kg)
- c_{ps} average specific heat of the solid phase between t_i and t_m (kJ/(kgK))
- c_{pl} average specific heat of the liquid phase between t_m and t_f (J/(kgK))
- f melt fraction
- q latent heat of fusion (J/kg)

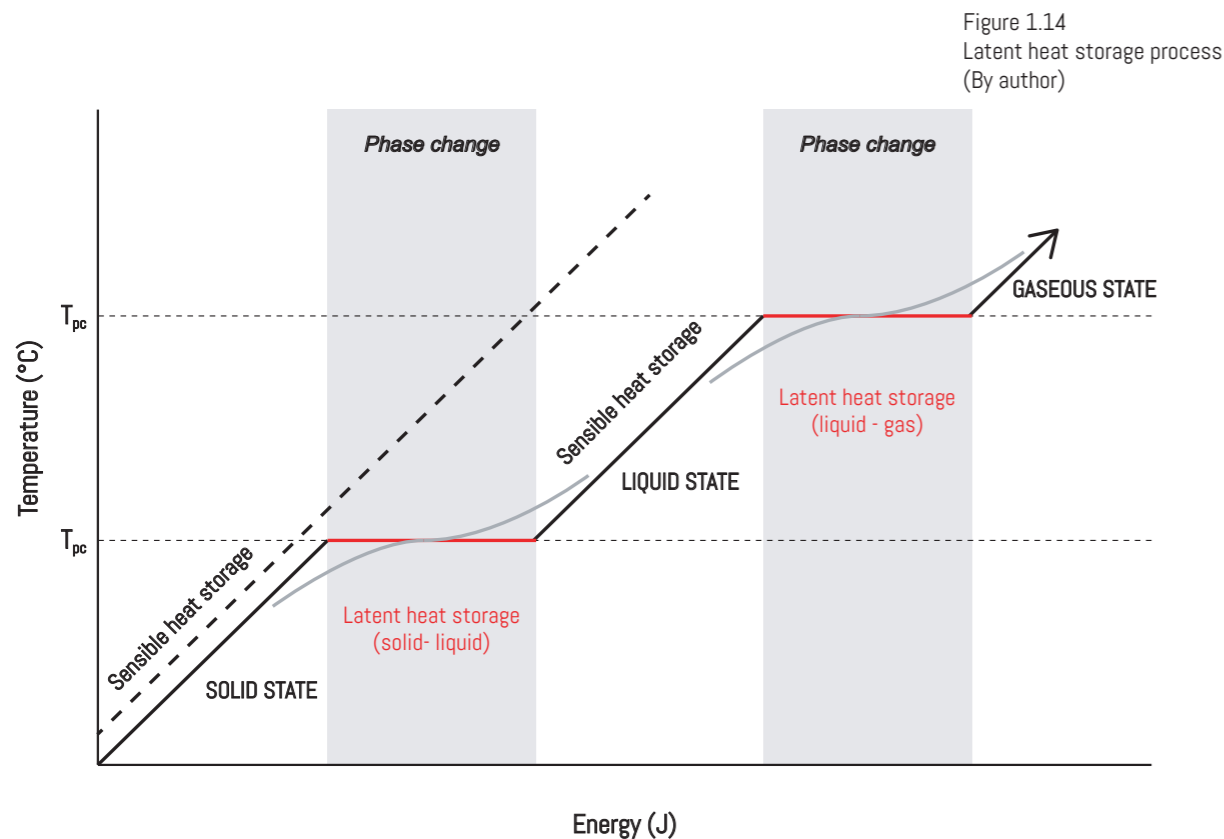


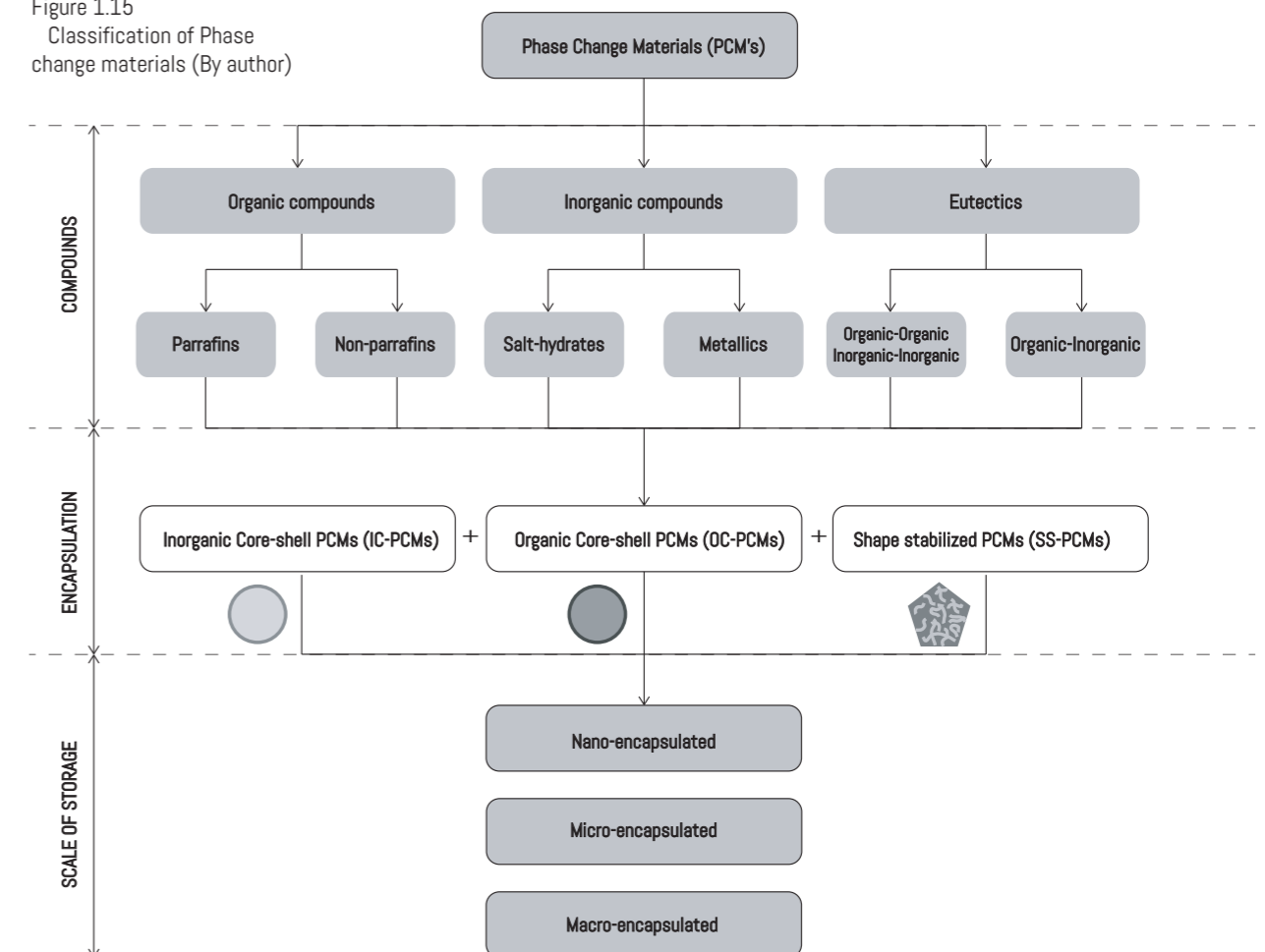
Figure 1.14
Latent heat storage process
(By author)

2.2.2.1 Phase change materials (PCM's)

LHS materials are commonly known as Phase Change Materials (PCM's) because of their ability of storing and releasing heat during the change in physical state. Two type of heat transfer modes can be observed during the absorption of energy, first heat is transferred through the PCM by conduction. Later natural convection takes place within the material due to the transition to a liquid state, the solid material tends to move away from the heat transfer surface (Jegadheeswaran & Pohekar, 2009).

These PCM's can have significant positive effect on the energy performance of a building, including the reduction in the energy demand, peak load shifting and energy conservation which results in a reduction in the consumption for building owners (Qureshi, Nair, & Farid, 2011). The material substances can be classified in three different categories: Organic, Inorganic and Eutectic compounds (Figure 1.15) with each his own mechanical properties and heat storing capacity (Riffat, Mempoou, & Fang, 2013; Khudhair & Farid, 2004). Inorganic phase change materials are mainly Salt-hydrate and Metallic compounds, the latter is not used for building applications due to the weight of this compound and the temperature range is not sufficient for building applications (Kalnæs & Jelle, 2015). Organic substances can be divided into Parrafins and Non-parrafins (Polyethylene Glycol and Fatty acids and derivatives), a drawback from these materials is the relatively high price (Riffat, Mempoou, & Fang, 2013). Eutectic compounds are a mixture of both organic and inorganic or a combination of the two, the adjustment of properties to match the specific requirements is an interesting characteristic of this type of PCM (Kosny, Shukla, & Fallahi, 2013).

Figure 1.15
Classification of Phase
change materials (By author)



The heat storage densities from these LHS-systems can go up to 300 kJ/kg for salt hydrates and 150 kJ/kg for organic phase change materials, which is around 5 to 14 times more energy storage than SHS-systems (Salunkhe & Shembekar, 2012). The change in phase from solid to liquid phase and from liquid to solid phase is defined as the process of charging and discharging (Salunkhe & Shembekar, 2012; Riffat, Mempoou, & Fang, 2013).

Different PCM's have different performance values regarding energy enthalpy for cooling or heating application. But also within one material the partial enthalpy curves for melting and solidification can differ (Figure 1.16), this is important to take into account during the material selection and design specific considerations (Kalnæs & Jelle, 2015). This means a difference in latent heat of melting and solidification and a delay in phase change, the solidification starts at a lower temperature compared to the end temperature of the melting process, this phenomenon is called thermal hysteresis (Bony & Citherlet, 2007). Another important factor to notice in this nucleation process is the difference between the charging cycle and the discharging cycle. The time to charge a PCM heatsink is 1/5th of the total time of operation and the time for discharging is 4/5th (Srikanth, Nemani, & Balaji, 2015), this shows a significant difference which must be kept in mind when designing with PCM's.

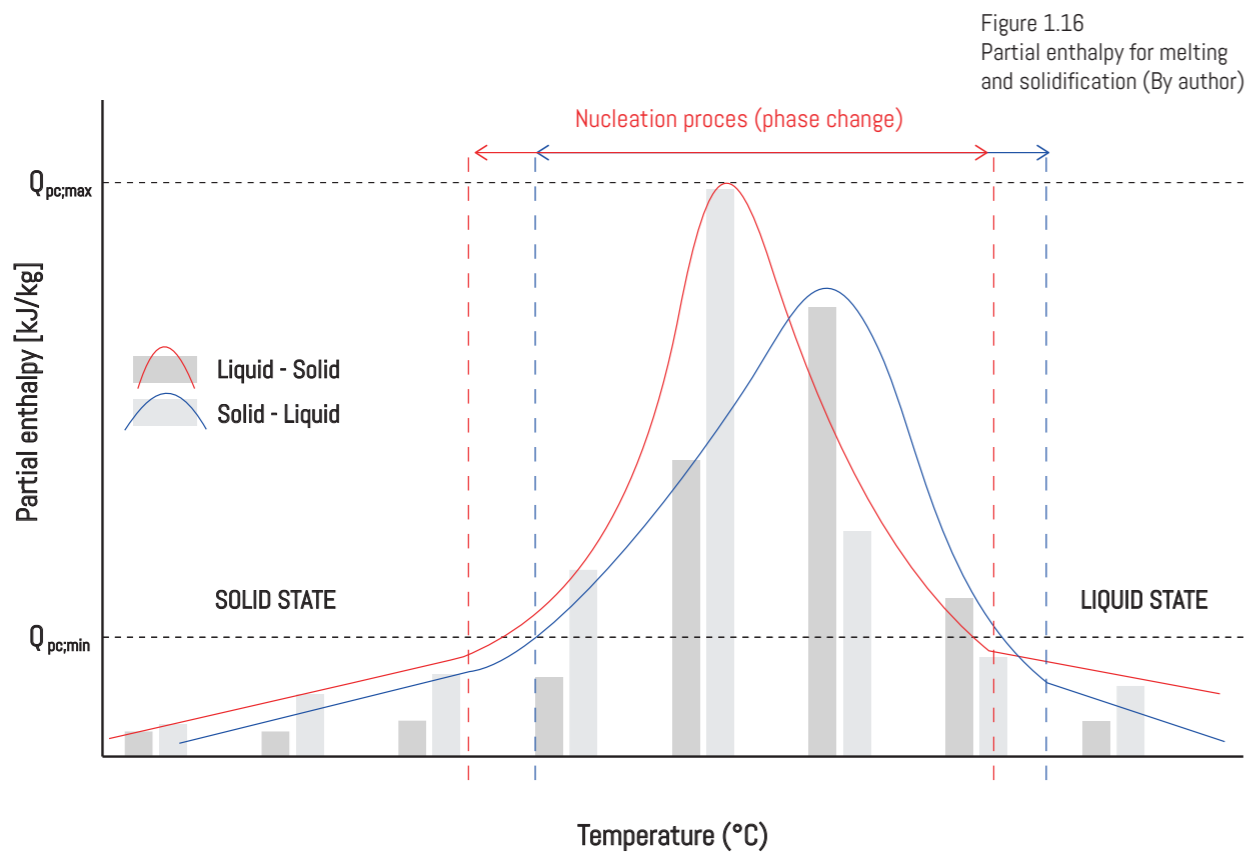


Figure 1.16
Partial enthalpy for melting
and solidification (By author)

Incorporation methods

The techniques for incorporating and encapsulating PCM's in building systems and products have a significant impact on the performance of the final product (Salunkhe & Shembekar, 2012), techniques mainly used in building applications are direct incorporation, immersion and encapsulation (Sun, Wang, Xiao, & Gao, 2013). The three main methods used to encapsulate the PCM's are: Macro-encapsulation (above 1 mm), micro-encapsulation (0-1000 μm) and nano-encapsulation (0-1000nm) (Kosny, Shukla, & Fallahi, 2013; Salunkhe & Shembekar, 2012). These storage containers (micro, macro, nano) can all be used as direct heat exchanger medium or they can be incorporated into conventional building products depending

on the specific project requirements (Khudhair & Farid, 2004).

Macro-encapsulation or packaging of PCM's is commonly used for building applications, the container shapes are mainly tubes, pouches, spherical capsules. or rectangular packages (Kosny, Shukla, & Fallahi, 2013; Salunkhe & Shembekar, 2012). Climator for instance produces rectangular shape pouches incorporated with PCM known as ClimSel™, these pouches are produced out of plastic foil which are integrated with metallics to increase the heat transfer of the system (Climator, 2017). Rubitherm® Technologies GmbH is another well-known manufacturer in Europe, they produce for example rectangular macro-encapsulated rigid containers and transparent polymer pouches (Rubitherm, 2018).

The production of micro-encapsulated PCM's is more complex due to the size of the final particle (less than 1 mm). The benefit from this specific encapsulation is the increase in heat transfer surface area which results in an improved heat transfer between the PCM and the HTF (i.e. air or water). The production costs from this method varies markedly depending on the material used and the production technique (Kosny, Shukla, & Fallahi, 2013). Another factor is that the encapsulation of organic PCM's is more difficult than inorganic PCM's, this can also increase the costs for the final product.

The material and the ratio of the shell is important for the performance of the overall system considering the heat transfer and the mechanical strength of the product. An important factor for the material of the encapsulation is the thermal conductivity, this should be higher than that of PCM, it should not react with the PCM and it needs to withstand the thermal expansion of the material (Salunkhe & Shembekar, 2012).

The encapsulation of these different PCM's can be classified as organic core-shell materials (OC-PCMs), inorganic core-shell materials (IC-PCMs) and shape-stabilized PCMs (SS-PCMs) (Figure 1.15). SS-PCMs are composites of PCM's combined with other materials, the PCM retains within the system by capillary attraction (Milián, Gutiérrez, Grágeda, & Ushak, 2017). Core-shell PCM's are basically particles of PCM's that are covered by another material (Milián, Gutiérrez, Grágeda, & Ushak, 2017). The core-to-shell ratio can vary a lot, this has significant impact on the thermal capacity of the final product, more encapsulation material results in a lower overall performance of the system. Some manufacturers from micro-encapsulated PCM's are Microtek Laboratories (producing Micronal®) and PureTemp LLC, they both produce PCM in dry powder form, wet cake forms and slurry form (Microtek, 2018; PureTemp, 2018).

Application

Several studies are available on the application of PCM's in various passive and active systems to incorporate them into existing building products and building management systems. Micro-encapsulated PCM's are for instance widely incorporated in many different building elements such as Concrete mixes and Cement Mortars, Wallboards, Gypsum plaster, Sandwich panels and Slabs (Konuklu, Ostry, Paksoyd, & Charvat, 2015). And macro-encapsulated PCM's can be found in building systems such as shutter, glazing, blinds, ceiling packages and floor accumulators (Global-e-systems, n.d.; Pomianowski, Heiselberg, & Zhang, 2013).

Vertical and horizontal shutters were tested and simulated in some studies, no practical application of such devices is found (Weinlaeder, Koerner, & Heidenfelder, 2011; Alawadhi, 2012). In one study three centimetre thick shutters were used, this resulted in a reduction of 23% of the heat gain through the windows compared to a conventional shutter. The shutters were made out of aluminium foam filled with

PCM. The regeneration of the PCM inside the shutter was a problem observed by the researchers, the study showed that only tilted windows for ventilating the system is not enough. They suggested that night ventilation should be added to the system in order to discharge the system accurately when talking about climates with low outside air temperatures during night-time. (Weinlaeder, Koerner, & Heidenfelder, 2011)

Global-e-systems is a company specialized in several passive and active PCM products for building application, they sell pure PCM as material together with an underfloor element and a ceiling element. These floor elements, Thermavar™ PCM Climate Floor, are placed under the covering of the floor and they are charged by a floor heating network (Figure 1.17). This is done during the night to use energy during off-peak hours. The PCM is charged with low temperature water ranging between 30°C and 35°C. The PCM used in these element has a melting temperature between 25°C and 28°C. In addition, the floor also stores the energy from the solar radiation that enters the room, in summer this results in a cooling effect and in winter the floor is preheated by the sun. The primary energy reduced by this system is around 50% by combining it with a boiler, central grid or heat pump (Global-e-systems, n.d.).



Figure 1.17
PCM flooring system from Global-e-systems for both heating and cooling the space. Reprinted from Global-e-systems, by GES, n.d.. Retrieved from <https://www.global-e-systems.com/en/products/thermavar-pcm-climate-floor/>

Another practical application from Global-e-systems is the Thermavar™ PCM climate ceiling, this product contains PCM pouches of 570 x 270 mm that are placed on top of an aluminium ceiling tile (Figure 1.18). This product is mainly used for heating and cooling of office spaces, only small changes are needed in the buildings climate management system when retrofitting the system into an office. The ceiling is used for both heating and cooling, heat from the indoor environment is captured by the material to cool the space. In winter the heat is absorbed during daytime and the PCM solidifies when the ambient temperature drops below a certain point, the heat is delivered back to the room. During the night on hot summer days, night ventilation is used to regenerate the PCM to completely solidify before the morning (Global-e-systems, n.d.).



Figure 1.18
PCM ceiling system from Global-e-systems for both heating and cooling the space. Reprinted from Global-e-systems, by GES, n.d.. Retrieved from <https://www.global-e-systems.com/en/products/thermavar-pcm-climate-ceiling/>

The PCM used in this product is a salt-hydrate PCM22 ($\text{CaCl}_2 + 6\text{H}_2\text{O}$) with a process-temperature of 22°C, in some cases PCM18 is used depending on the set-point temperature for the target room. Hence, the heat is captured when the temperature raises above 22°C for the PCM22. In this way, a reduction in energy of 25 to 50% can be achieved for cooling and between 10 and 25% for heating (Global-e-systems, n.d.). So important to notice is the difference in process temperature between the two systems from Global-e-Systems, the set point temperatures for heating and cooling correspond to the comfort temperatures mentioned before in Section "THERMAL CONTROL"

The GlassX product is a glazing system already available on the market, this product is mainly developed to prevent for overheating of buildings with large amounts of glazing. This systems adds thermal mass to modern buildings and absorbs direct radiation without blocking visible sun light from the environment, when the PCM is crystalline around 8 – 28% of the visible light enters the room (GlassX, 2017). The system is made of quadruple glazing system combined with a transparent Dynamic Light Scattering (DLS) prism in the outer segment and a PCM core in the inner segment (Figure 1.19). The DLS prism is used to prevent the summer radiation from entering the building by reflecting the direct sun-rays. In winter the sun elevation is lower ($< 35^\circ$) and radiation passes through the prism to allow for heating (GlassX, 2017). In this way, the SHGC varies between the different seasons. The PCM core is made of a salt-hydrate ($\text{CaCl}_2 + 6\text{H}_2\text{O}$) with a melting temperature between 26 and 28 °C. The indoor temperature is reduced by 5-9°C compared to a building with conventional glazing (GlassX, 2017).

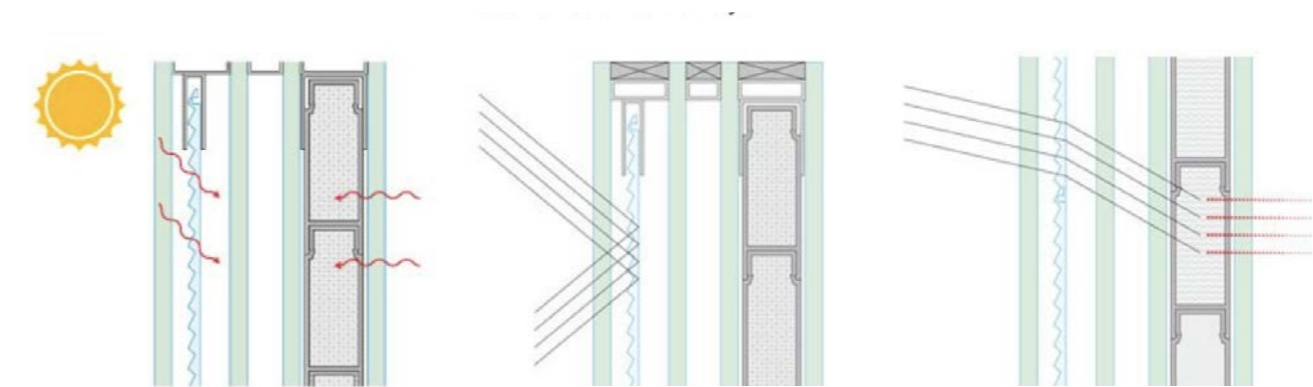


Figure 1.19
GlassX system, working principle for winter and summer situation. Reprinted from: "Introducing GlassX – the world's first Thermodynamic Glazing system", by GlassX, 2017, retrieved from: <https://www.glassxpcm.com/how-glassx-works/>

Summer: Sun high in the sky > 40°
Total reflection of the rays

Winter: Shallow winter sun < 35°
Loss-free passage of the rays

Pomianowski, Heiselberg and Zhang conducted a research study on thermal storage technologies with PCM's. They presented several studies showing the integration of PCM's in glazing systems, tests were done with PCM with the same melting temperatures as mentioned before. The different simulations showed promising results in reducing the heat gain and allowing for daylight to enter. One study, conducted by Owen Lewis, used Transparent Insulation Material (TIM) within the glazing system together with integrated PCM containers to block the direct solar radiation and allow for daylight to enter the room. (Pomianowski, Heiselberg, & Zhang, 2013)

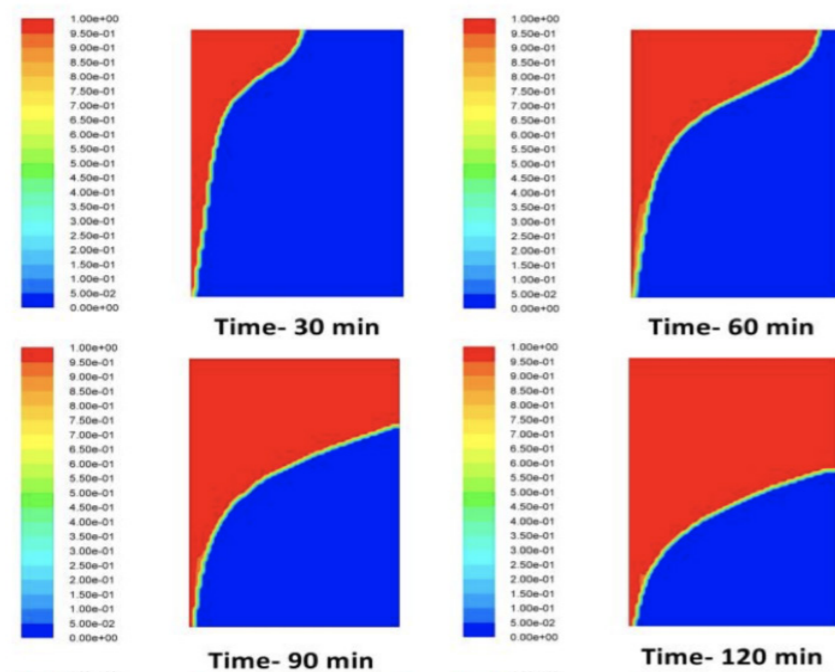
Material limitations

So these PCM show convenient ways of storing thermal energy within compact application methods, but some disadvantages and limitations show up besides all these potentials. All the different compounds have their own drawbacks which must be improved to create products that are feasible for implementation in building structures, a successful implementation of PCM's for TES depends totally on the reliability and the stability of the material. Limitations of the material will be discussed, these limitations will be used as input for the optimization process of the system.

One of the biggest limitations of PCM's in general is the low thermal conductivity, which negatively affects the heat transfer rates of the overall system. It decreases the amount of heat or cold absorbed during the nucleation phase (Bland, Khzouz, Statheros, & Gkanas, 2017).

Zhang, Chen, Wang and Wu (1993) conducted a research study on the melting process of a PCM-unit which is discretely heated at a constant rate, they noticed that during the solid-liquid interface in the very first moment a few small melting region appear. After some time these small regions gradually merged and they became one, during this phase transition natural convection occurs due the difference in temperature from the liquid particles. This leads to ascending of the particles with a higher temperature and descending of particles with a lower temperature (Zhang, Chen, Wang, & Wu, 1993), which results in an irregular melting process between the upper part and the lower part (Figure 1.20). The outcome of this specific phenomenon can be that the melt fraction of the system is low and not all the PCM is efficiently used or the melting time will be longer (Wang & Zhao, 2015).

Figure 1.20 Irregular melting process inside a PCM element, red represents the liquid condition. Reprinted from "Simulation of Melting Process of a Phase Change Material (PCM) using ANSYS (Fluent)", by Vikas, Ankit Yadav, S.K. Soni, 2017



Jegadheeswaran reviewed several other researches, they did various experimental studies on the effect of natural convection in different shapes of encapsulation and all the studies show comparable results, it can be concluded that a higher rate of melting takes place in the top region of the unit due to natural convection inside the system (Jegadheeswaran & Pohekar, 2009). Another leading cause of this phenomenon is the fact that phase segregation takes place within the system, different particles with various densities will separate within the system. This results in a negative effect on the long-term thermal stability of the

system, measures have to be taken to prevent this from happening (Bland, Khzouz, Statheros, & Gkanas, 2017). Stritih (2004) indicates that only the process of melting has natural convection, this does not occur in the case of solidification, the natural convection was found 10 times lower in this case compared to the melting process. The solidified particles took the same shape as the surface of the encapsulation.

Compound specific limitations and properties

For inorganic compounds the following disadvantages occur: corrosive to metals, supercooling, phase segregation, incongruent melting and high change in volume. Supercooling takes place when the solidification of the liquid is below its normal freezing point, this aspect makes the material unreliable because of the delay in solidification (Bland, Khzouz, Statheros, & Gkanas, 2017).

Some disadvantages from organic compounds are: flammability, a low heat storage capacity and a low thermal conductivity. Limited research is available about the limitations of eutectics compound, not many research is done regarding these mixtures, a significant drawback is the costs of eutectics due to the complexity of the production process (Kalnæs & Jelle, 2015). Various other properties of the different PCM categories are summarized in Table 1.3. The before-mentioned limitations of the materials are essential to ensure the long-term stability and economic feasibility of the final LHSU. Improving these aspects will have considerable impact on the thermal performance of the LHS-unit.

Table 1.3 Comparison of the different PCM compound families (Reproduced from "PCMs for Residential Building Applications: A Short Review Focused on Disadvantages and Proposals for Future Development" by Bland, Khzouz, Statheros, & Gkanas, 2017)

	Organic compound		Inorganic compound	Eutectics
	Paraffins	Non paraffins (fatty acid)	Salt hydrates	
Formula	C_nH_{2n+2} ($n = 12-38$)	$CH_3(CH_2)_nCOOH$	$AB \cdot nH_2O$	-
Melting point	-12-17 °C	7,8-187 °C	11-120 °C	4-93 °C
Heat of fusion	190-260 J/g	130-250 J/g	100-200 J/g	100-230 J/g
Costs	- Expensive	- More expensive	- Low cost (availability)	Most expensive
Advantage	- No phase segregation, no supercooling, no corrosion with containers	- Sharp phase transition temperature	- Higher thermal conductivity, high commercial available, sharp melting point, low volume change, high density	No segregation, high conductivity, high heat of fusion
Disadvantage	- Lower thermal conductivity, flammability, high volume change	- Flammability, mildly corrosive	- Higher density, supercooling, corrosion on metal, more segregation of material	Low heat of fusion per unit weight
Compound examples (Melting point (°C), latent heat (J/g))	<i>n</i> -tridecane (4.5, 231), paraffin wax (32, 251), <i>n</i> -tricontane (65, 252)	Acetic acid (16.7, 187), stearic acid (61, 200), lauric acid (42, 178) and other non-paraffins	$CaCl_2 \cdot 6H_2O$ (30, 170-192), $Na_2SO_4 \cdot 10H_2O$ (32, 251), NaCl $Na_2SO_4 \cdot 6H_2O$ (18, 286), $MgSO_4 \cdot 7H_2O$ (48.4, 200)	$Na_2SO_4 + NaCl + KCl + H_2O$ (4, 234), $NH_2CONH_2 + NH_4NO_3$ (46, 95)

A lot of PCM's are available on the market and not all of them are suitable for the application for fast charging and discharging at room temperature in buildings, some important properties for the implementation need to be considered (Souayfane, Fardoun, & Biwole, 2016). These important properties are related to thermo-physical, kinetic, chemical and economic requirements of the PCM to make it thermo-dynamic and cost-effective for application. As mentioned before, each of the specific PCM compound have their own specific characteristics, these can be enhanced by using different enhancement techniques,

these techniques will be discussed later in section "24 EFFICIENCY OPTIMIZATION". So a poor property of a certain PCM compound does not mean that it is not appropriate for application, these properties can be improved. The following list with properties is proposed by Souayfane, Fardoun, & Biwoleb (2016).

Table 14 Thermo-physical, kinetic, chemical and economic requirements of PCMS for application (Souayfane, Fardoun, & Biwoleb, 2016)

Thermo-physical Requirments	Kinetic Requirements	Chemical requirements	Economic
- Melting temperature appropriate to the operating temperature	- High nucleation rate to avoid supercooling of the liquid	- No corrosiveness	- Low price and cost effective
- High latent heat of fusion	- High rate of crystallization or high melting rate to satisfy the amount of heat revored from the system	- No degradation after freeze/ melt cycles	- Good recyclability
- High specific heat		- Non toxic	- Facility of seperation from other materials for disposal or reuse
- High conductivity of the material		- Non-flammable	- Availability
- Congruent melting		- Long term chemical stability of the PCM	- Payback time
- Small change in volume			
- No sub-cooling during solidification			
- Cycling stability			

2.3 HEAT TRANSFER

The knowledge of heat transfer inside and on a body is important in the efficiency optimization for TES-systems. The science of heat transfer is about predicting the transfer of energy within different bodies as result of a difference in temperature, it is used to calculate and predict the rate of heat transfer that takes place (Holman, 1986). The three modes of heat transfer that occur on a body are conduction, convection and radiation.

The heat transfer inside an element can be a steady-state heat flow or a transient state heat flow. For the transient state, the temperature conditions and/or the heat flow differ within a certain time span, so the temperature that goes into a section can differ from the temperature which is released (Straube, 2011). This is because of a continuous fluctuating temperature on the outside of the body or due to different properties of the materials within the body. When talking about a steady-state heat flow an equilibrium is reached between the heat flow and the temperature, so the temperature within the body at all the points does not change with time. (Straube, 2011)

Mode 1: Conduction is the transfer of heat through a medium by direct contact, an energy transfer takes place from the high-temperature field to the low-temperature field. The conductivity of a material is determined by the positive constant property λ which is the lambda value of the material (Holman, 1986). The rate of heat transfer per unit area corresponds to the temperature difference between the bodies, shown in the first equation from Figure 1.21. This mode of heat transfer is most important for solid bodies and sometimes for liquids (Straube, 2011).

The formulas below show the importance of the area and the thermal conductivity of the material for heat transfer enhancement. An increase in surface area with a preservation volume of the bodies increases the rate of conduction between the two bodies.

$$q_x = -\lambda \frac{dT}{dx} \quad q_x = -\lambda \frac{T_1 - T_2}{d} \quad (1.3)$$

Figure 1.21
Equations for thermal conductivity (Holman, 1986)

q_x the heat-transfer rate (W/m²)
 dT/dx Temperature gradient in the direction of the heat flow
 λ lambda value (W/(m.K))
 d thickness of the body (m)

Mode 2: Convection is the transfer of heat due to the movement of molecules within a liquid or gas. This mode of heat transfer is important for the transfer of heat between fluids and solids or within fluids, the process is called convection heat transfer (Straube, 2011).

The overall effect of heat transfer by convection is expressed by the formula shown in Figure 1.22, the most important factors in this heat transfer mode are the surface area of the body and the heat transfer coefficient.

$$q = h(T_w - T_\infty) \quad (14)$$

Figure 1.22
Equation for convective heat transfer (Holman, 1986)

q the heat-transfer rate (W/m²)
 T_w wall temperature (K)
 T_∞ fluid temperature (K)
 h convection heat-transfer coefficient (W/(m²K))

Mode 3: Radiation is the transfer of heat by electromagnetic waves as a result of a temperature difference between two bodies, also called thermal radiation (Straube, 2011). An ideal thermal radiation is called a black-body, this body emits energy at a rate proportional to a fourth of the absolute temperature of the body (Holman, 1986). This mode of heat transfer is most important for the exchange of energy between two solid bodies and this will be left out of consideration in this research study for the LHSU optimization, it has no practical importance on the evaluation for optimizing the performance of the system.

24 EFFICIENCY OPTIMIZATION

Various techniques can be adopted to improve the thermal performance of the LHS-units, the optimization of the efficiency of the system in this study is based on two approaches: (1) Heat transfer enhancement of the system, (2) Cost-effective optimization of the system. The knowledge from the heat transfer enhancement optimization will be used as input for the cost-effective optimization and vice versa. This section describes the different techniques and methods to optimize according to these two objectives.

24.1 Heat transfer enhancement

An important factor for improving the heat transfer is the use of extended surfaces as described in Section "2.3 HEAT TRANSFER". Calculations show that the surface area and the encapsulation is an important parameter which influences the heat transfer rate, which can be adjusted by using different design approaches. Figure 1.23 shows an example of an thermal mass wall in a single residential house, PCM modules are added on top of this mass wall, these modules have an increased surface area by using bulge shapes. The effectiveness and techniques of several methods to increase the heat transfer rate and to improve the performance of heat transfer will be discussed.



Figure 1.23
PCM modules on a thermal mass wall.. Reprinted from Energyarchitecture, n.d.. Retrieved from <http://www.energyarchitecture.com.au/projects/norton-summit-ecological-footprint/>

24.1.1 Fins

Literature study showed that both internal and external fins were used to improve the heat transfer rate of the system, the studies mainly focus on improving the thermal performance of heat exchangers and photovoltaic (PV) systems. Khannaa, Reddy and Mallick (2018) did a research study on the implementation of internal aluminium fins in an aluminium PCM container attached to a PV-system (Figure 1.24), considering variations in fin length, fin thickness and the spacing between the fins (Khannaa, Reddy, & Mallick, 2018)

This PCM unit is used to cool down the PV-system which results in an increased efficiency of the module. The difference in temperature of the PV with and without fins indicates the amount of heat absorbed by the PCM due to the addition of fins. Figure 1.24 shows the results from two of the different objectives, a significant decrease in temperature is observed by the use of fins. The variation in thickness and spacing between the fins shows that an optimum is reached where a small deviation in the results is observed. All the objectives show a significant reduction in the temperature of the PV, which indicates the effectiveness of the fins.

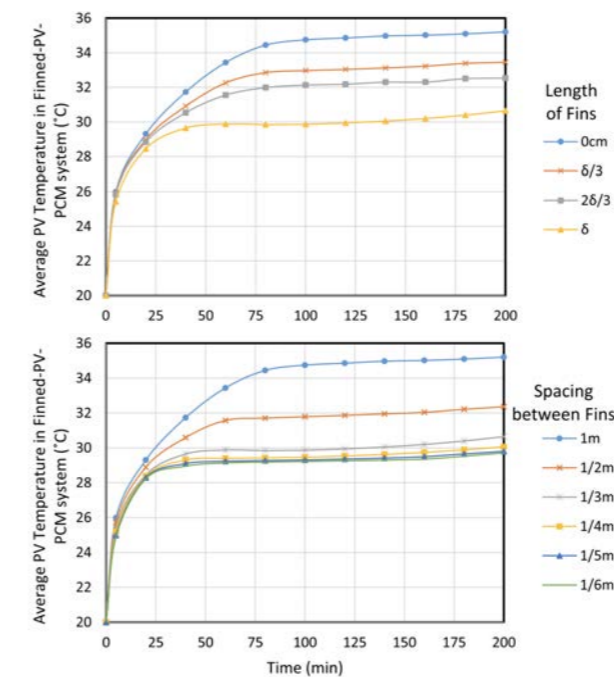
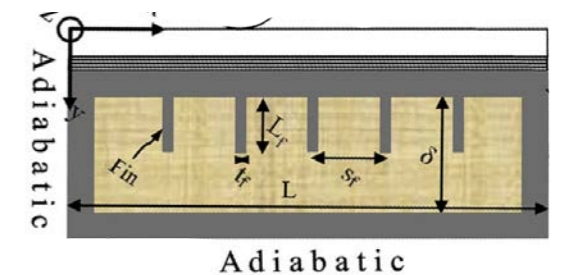


Figure 1.24 Schematic design of PV-module with PCM container and graphical results from different design objectives. Reprinted from "Optimization of finned solar photovoltaic phase change material (finned pv pcm) system", by Khannaa, Reddy, & Mallick, 2018.



24.1.2 External fins

Abbassi and Dehmani (2015) investigated the effect of the addition of vertical thermal fins to the internal Trombe wall surface of an unventilated Trombe wall. The aim of this experiments is to increase the heat transfer rate between the wall and the interior of the building which leads to an improvement in the efficiency of the wall. Two experimental tests were done, a comparison is made between a Trombe wall with and without fins. The results are used to validate the outcome from the numerical study, aluminium fins of 0,7 meter in height, 0,05 meter in depth and 0,002 meter in thickness were used. The spacing between the fins was 0,04 meter, these dimension were the result from the optimization of the numerical study. (Abbassi & Dehmani, 2015)

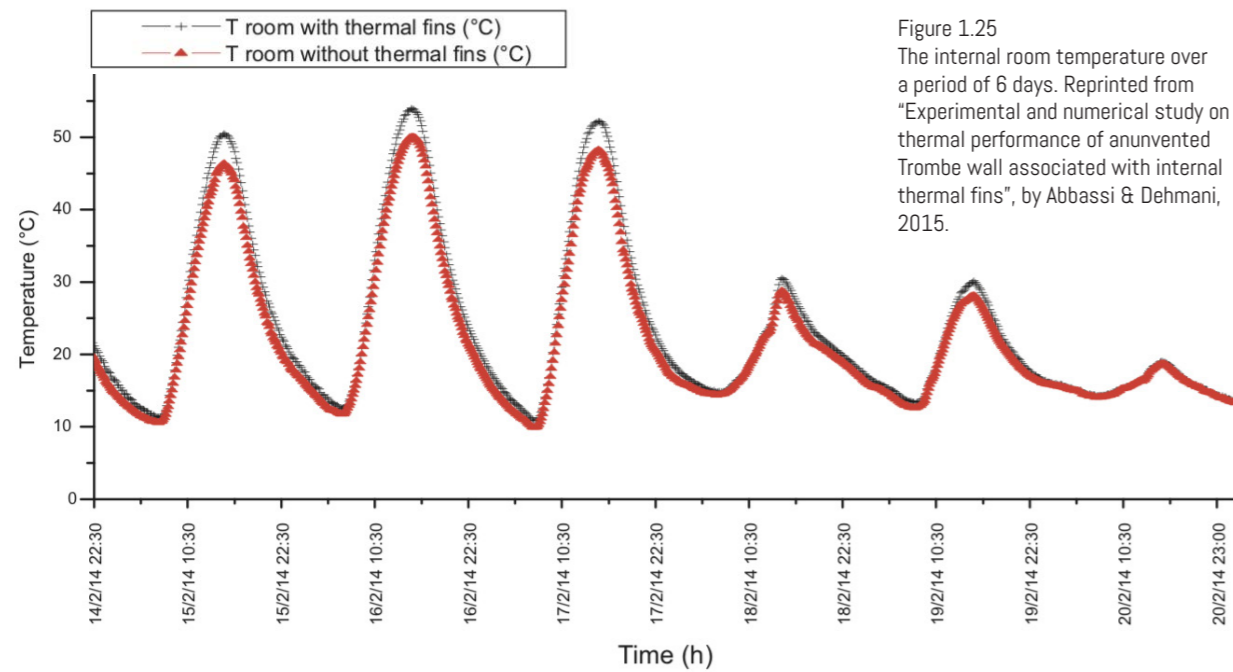


Figure 1.25
The internal room temperature over a period of 6 days. Reprinted from "Experimental and numerical study on thermal performance of an unvented Trombe wall associated with internal thermal fins", by Abbassi & Dehmani, 2015.

Figure 1.25 shows the internal room temperature measured over a period of six days, this experimental setup shows high internal temperatures due to the small test setup of the room. These temperatures do not give an idea about the indoor climate of real scale buildings, this experiment is only used to measure the increase in efficiency of the Trombe wall. In the first few days the solar radiation during daytime exceeded the 500 W/m^2 . The measured temperature difference in the room between the two separate experiments was 3-4 degrees Celsius on these days (Abbassi & Dehmani, 2015). An increase in efficiency of 7% was measured with a solar radiation of 800 W/m^2 . So in general the experiment showed that the addition of thermal fins increased the interior room temperature and decreased the Trombe wall temperature which leads to an improved efficiency of the system with just a small intervention. (Abbassi & Dehmani, 2015)

24.1.3 Encapsulation

Increasing the surface area of the PCM unit can significantly increase the heat transfer rate as mentioned before. Another way to increase this surface area is by adopting existing production techniques such as micro-encapsulation. Veerappan, Kalaiselvam, Iniyar and Goic (2009) investigated the effect of the encapsulation of PCM particles, considering spherical PCM encapsulated particles. Five different particle sizes were analysed, all with the same encapsulated material (Veerappan, Kalaiselvam, Iniyar, & Goic, 2009). The large sized spherical took noticeably more time to completely solidify compared to the smaller sized spherical, heat has to travel smaller distances from the heat transfer surface to the core of the spherical. A significant difference in solidification can be observed, the spherical PCM with a diameter of four centimetre is already solidified at the time of 20 minutes compared to a solidification time of almost 200 minutes for the 12 centimetre spherical. In this way, a specific process time period can be established using various sizes of spherical PCM's inside a structure. (Veerappan, Kalaiselvam, Iniyar, & Goic, 2009)

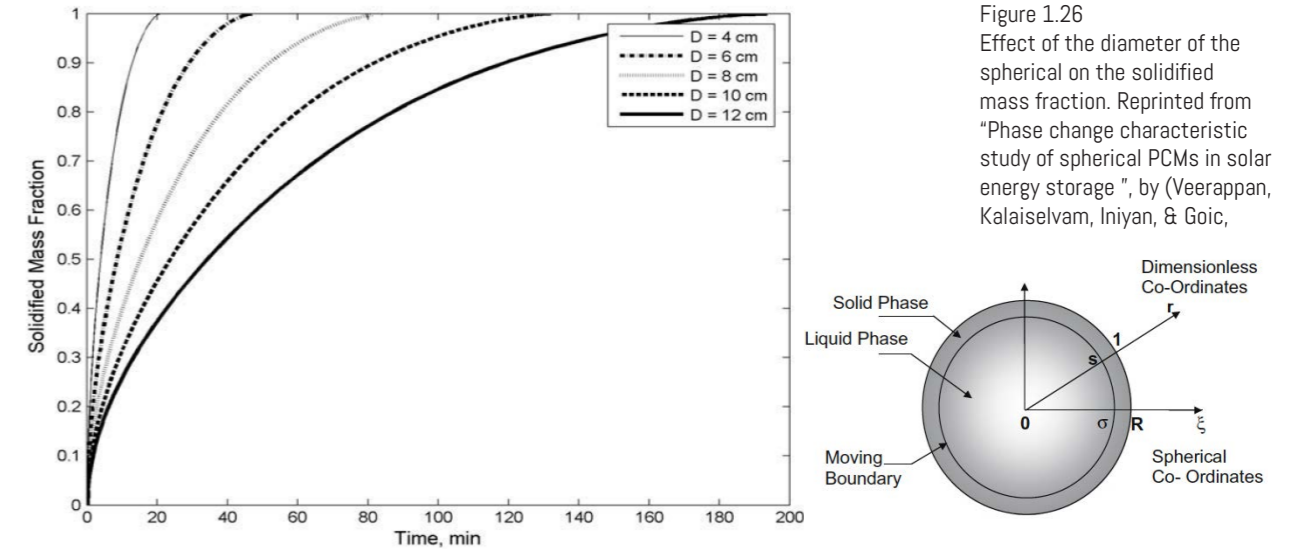


Figure 1.26
Effect of the diameter of the spherical on the solidified mass fraction. Reprinted from "Phase change characteristic study of spherical PCMs in solar energy storage", by (Veerappan, Kalaiselvam, Iniyar, & Goic,

Ismail, Henriquez and Silva (2003) conducted a similar research study comparing different encapsulated spherical with various internal radii as shown in Figure 1.27 (Ismail, Henríquez, & Silva, 2003). The results from this study correspond to the results from the study shown before, the same range in solidification time is observed. So a better thermal performance of micro-encapsulated PCM's can be expected compared to conventional PCM's, these micro-encapsulated PCM's can for example be incorporated into slurries. These slurries are substances with a heat transfer fluid (HTF) and PCM particles, the encapsulation of these particles can be made out of a wide range of materials including natural and synthetic polymers. (Jegadheeswaran & Pohekar, 2009)

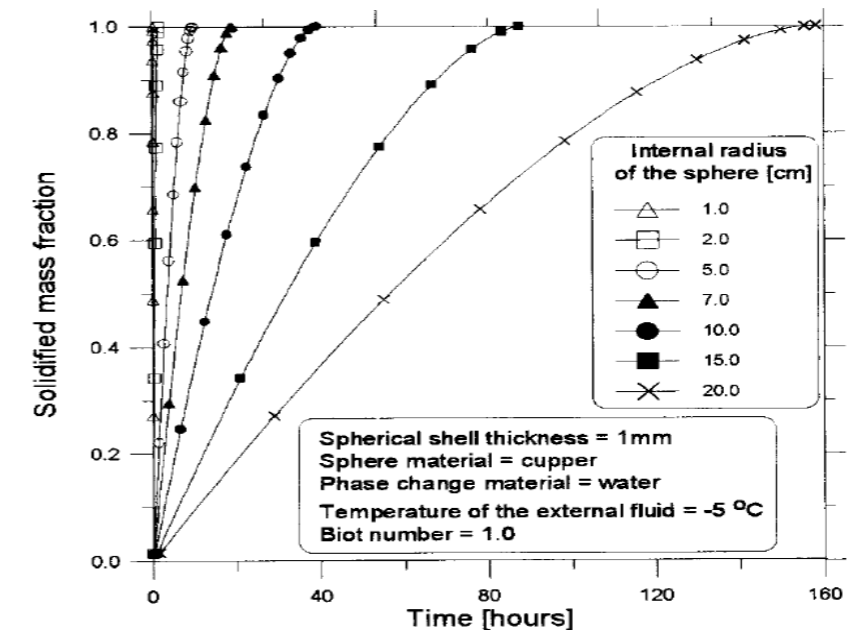
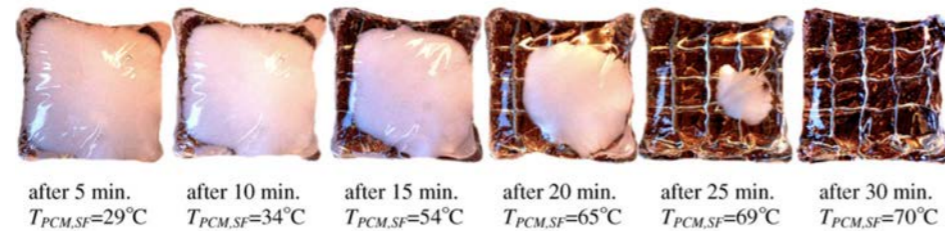


Figure 1.27
Solidification process of various spherical PCM's considering the solidified mass fraction. Reprinted from "A parametric study on ice formation inside a spherical capsule Ismail, Henriquez, & Silva, 2003

Zukowski (2007) conducted an experimental study on the effect of the encapsulation using Polyethylene bags on the charging and discharging time of the PCM, the benefit of these bags is the relatively thin encapsulation of the PCM which may result in an improved heat transfer compared to solid containers. Several small bags filled with Paraffin (Figure 1.27) are placed next to each other in an experimental setup where the climatic conditions of a room are simulated (Zukowski, 2007). The results from the experiment

showed that the discharging time during cooling occurred faster than the charging time. The time for the solidification process ranged from 50 to 90 minutes and for the melting process ranged from 80 to 240 minutes. Normally this discharging process takes around 4/5 of the time and the charging process 1/5 as mentioned in Section "2.2.2.1 Phase change materials (PCM's)". This indicates that the thickness of the 'container' and the material used for the encapsulation plays an important role in the charging and discharging process and especially in the deviation in nucleation time between melting and solidification. (Zukowski, 2007)

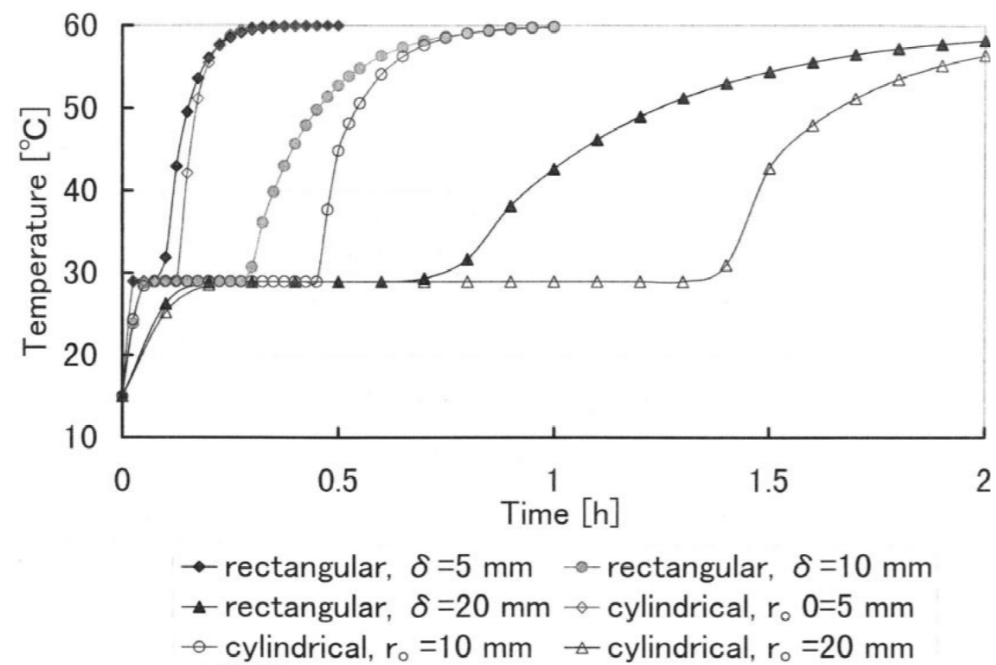
Figure 1.28 Paraffin PCM encapsulated with Polyethylene bags, particular stages of melting. Reprinted from "Experimental study of short term thermal energy storage unit based on enclosed phase change material in polyethylene film bag" by Zukowski, 2007.



24.14 Shape

Zivkovic and Fujii (2001) investigated the effect of shape on the melting time and the temperature inside the PCM unit. A comparison is done between rectangular and cylindrical containers (ranging from 200 to 400 mm) with the same volume (i.e. comparable mass of the PCM inside the container) and heat transfer surface area between the HTF and wall of the container (Zivkovic & Fujii, 2001). The comparison between the largest volumes show that the melting time of the rectangular container required nearly half of the melting time compared to that of the cylindrical container with the same volume, Figure 1.29 shows the results of the temperature measured in the core of different specimens with various radiuses over a period of time. (Zivkovic & Fujii, 2001)

Figure 1.29 Effect of the shape on the melting time, temperature in the core measured. Reprinted from "An analysis of isothermal phase change of phase change material within rectangular and cylindrical containers" Zivkovic & Fujii, 2001



24.1.5 Surface geometry

Cupkova and Azel (2015) conducted a research study on the effect of surface geometry on the rate of heat transfer in TES systems. They compared different geometrical configurations with an increase in surface area while maintaining the volume of the specimen. This increase in surface area is used as strategy for a higher rate of heat transfer by convection along the wall.

A less effective performance optimization was observed for the specimens with a smooth geometry compared to the ones with rougher geometries. The rate of heat gain and loss for different surface geometries are shown in Figure 1.30, the lighter tiles are the configurations of geometric families with the more smooth surfaces and the darker tiles are the families with more rough surfaces (Cupkova & Azel, 2015). The tiles more to the right show a higher rate in heat gain and loss compared to the base line. It can be noticed that the results in rate decrease (degree/minute) for the repetitive rough geometries results in the same outcomes as the more complex geometries. The sections in Figure 1.31 show a more detailed performance indication comparing a sinusoidal surface to a rectangular geometry, this simulation shows a shorter thermal lag for sinusoidal surfaces and an increase in the heat transfer rate due to more direct contact with the air flow. The opposite is observed for the rectangular specimen due to small air pockets created by the surface. (Cupkova & Promopattum, 2017)

Also for the performance trends for changing rates of increasing and decreasing in temperature were tested, and different configurations show different rates of heat gain and heat loss (Figure 1.33). It can be concluded that surface morphology can have noticeable effect on the rate of heat transfer of TES systems, considering the release of heat and thermal absorption (Cupkova & Azel, 2015). In this way the thermal mass can be significantly improved in a passive way resulting in better performance characteristics for managing the indoor climate of a building. Besides this, the actuation of surface geometry can improve the aesthetic quality of the wall by just simple configurations.

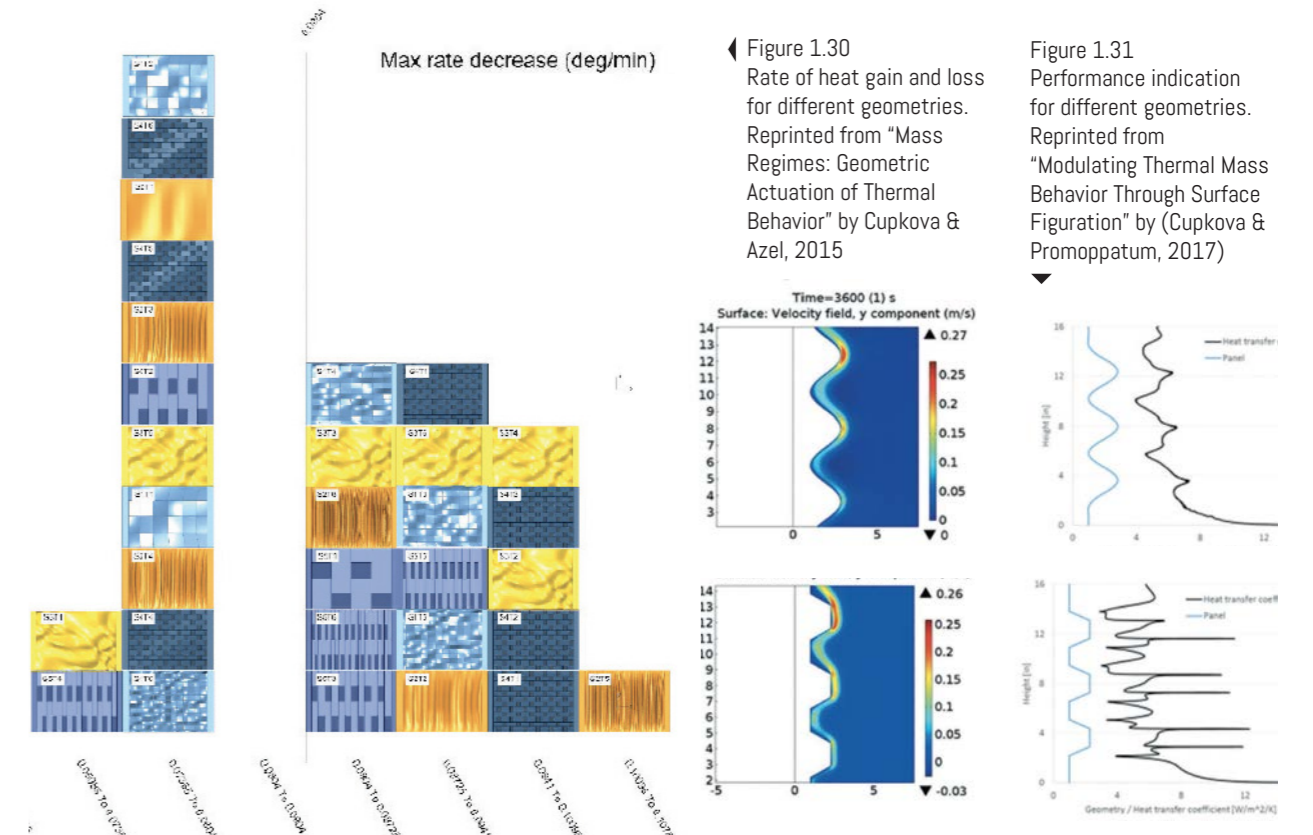
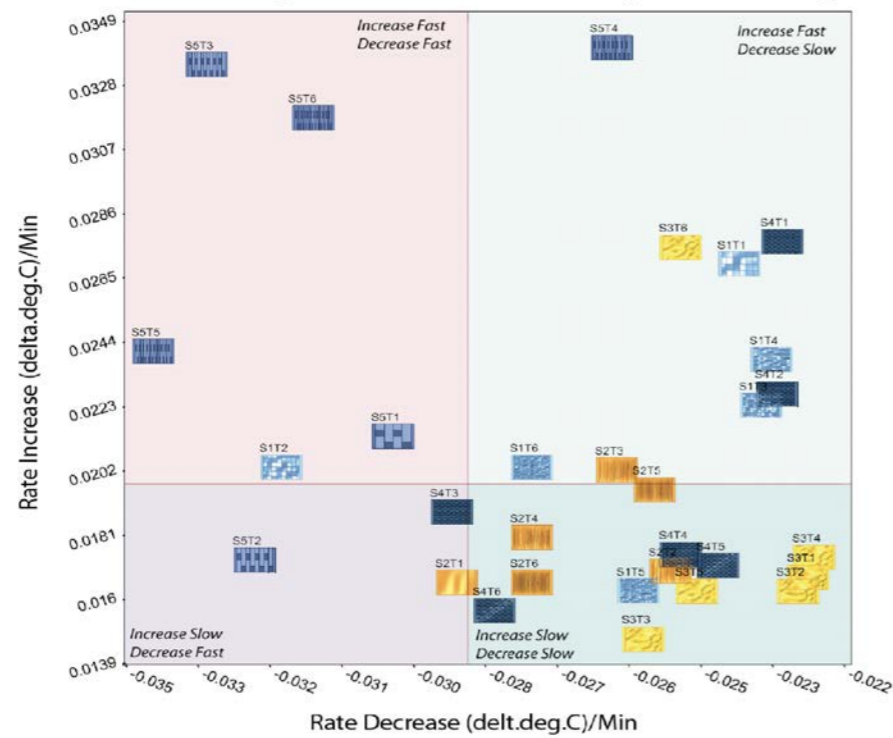


Figure 1.33 : rate of heat gain and loss for different geometries. Reprinted from "Mass Regimes: Geometric Actuation of Thermal Behavior" by Cupkova &

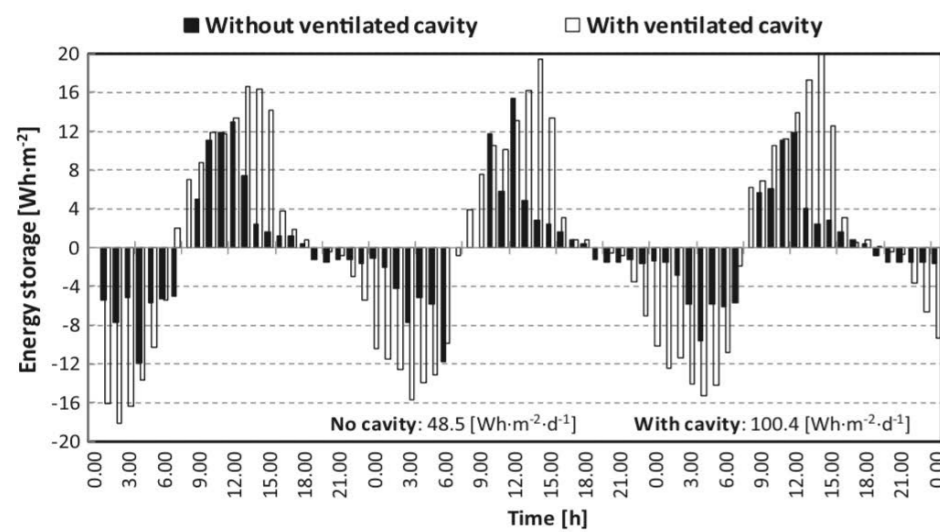


24.1.6 Ventilation strategy

As shown in Section "2.2.1.1 Trombe wall" convection plays an important role in the performance of a Trombe wall system, the transfer of heat between the wall and the air is by convection. David, Kuznik and Roux (2011) studied the effect of the natural convection on the performance of a PCM wall. The results from this study show a remarkably influence on the store and release process of the wall by convection.

The simulations show that the amount of energy stored by the PCM wall is more affected by convective heat than the wall without PCM. The variation in energy absorbed by the PCM wall with an air flow of 0 m/s compared to an airflow of 1 m/s is more than 30%, so an increase in heat absorbed due to the air flow (David, Kuznik, & Roux, 2011). This increase in heat transfer rate leads to a decrease in melting and solidification time of the system. For melting this means an increase in the outlet temperature and for solidification a decrease in outlet temperature (Halawa & Saman, 2011).

Figure 1.34 Effect of the cavity on the energy storage. Reprinted from "Simulation of a ventilated cavity to enhance the effectiveness of PCM wallboards for summer thermal comfort in building" by Evolaa, Marlettaa, & Sicurella, 2014



Evola, Marlettaa and Sicurella (2014) studied the effect of a cavity between the PCM wall and the outer skin to increase the efficiency of the PCM wallboard. Fresh air enters from the outside and improves the solidification process of the PCM and the heat transfer for night ventilation. Figure 1.34 shows the results of this system compared to a PCM wallboard without cavity ventilation, an increase in energy storage from 42.4% to 78.2% is observed (Evolaa, Marlettaa, & Sicurella, 2014).

So the effectiveness of the system is influenced by the distance between the PCM wall and the outer skin but also by the dimensions of the inlet and outlet of air to the room and from the outside. This increase in heat transfer can also be obtained by employing other techniques on different scales of the design. The venturi effect can for example be used to increase the air flow by air pressure due to the size difference in the inlet of the and the outlet of the air channel within the Trombe wall

Zamora and Kaiser (2009) investigated the natural convective flow in an converging channel for a Trombe wall and solar chimney, different inclinations were observed to analyse the effect on the heat transfer rate. An increase in turbulent kinetic energy is observed, this leads to a higher heat transfer rate at the lower wall of the channel but not in an increase in the overall heat transfer rate of the system. (Zamora & Kaiser, 2009)

Behbahani, Kazerouni and Davar (2014) optimized the geometry of the Trombe wall regarding free heat by convection. They optimized the system according to several parameters such as the distance between the glass and the wall, the upper and lower channels and the edges and geometry of the channel. Sharp corners were removed at the channel, this resulted in an increased Nusselt number which leads to an increased heat transmittance and a higher indoor room temperature (Behbahani, Kazerouni, & Davar, 2014). The same is observed in the numerical simulations from Corasaniti, Manni, Russo and Gori, they state that the channel with the "guided air flow" the best performances showed but only for narrow channels. Four blades are placed inside the cavity next to the bottom vent (Figure 1.35). This guided flow improves the air flow within the channel compared to the conventional rounded edges. (Corasaniti, Manni, Russo, & Gori, 2017)

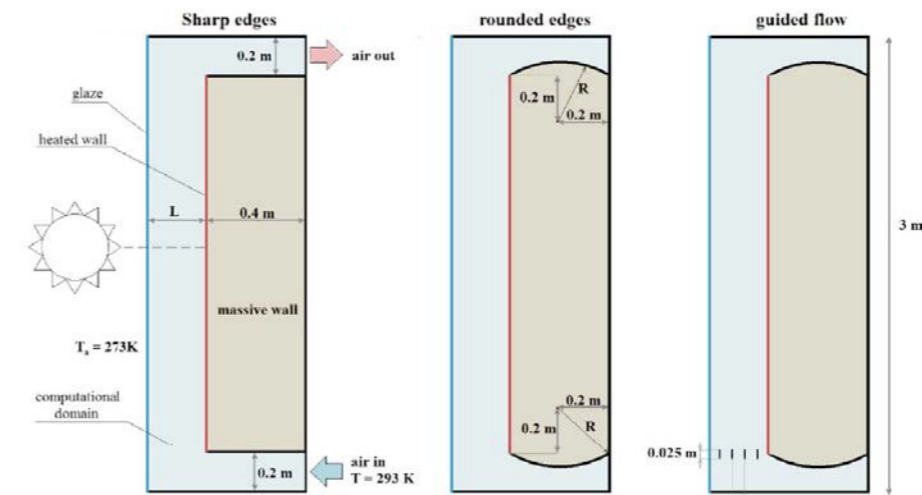
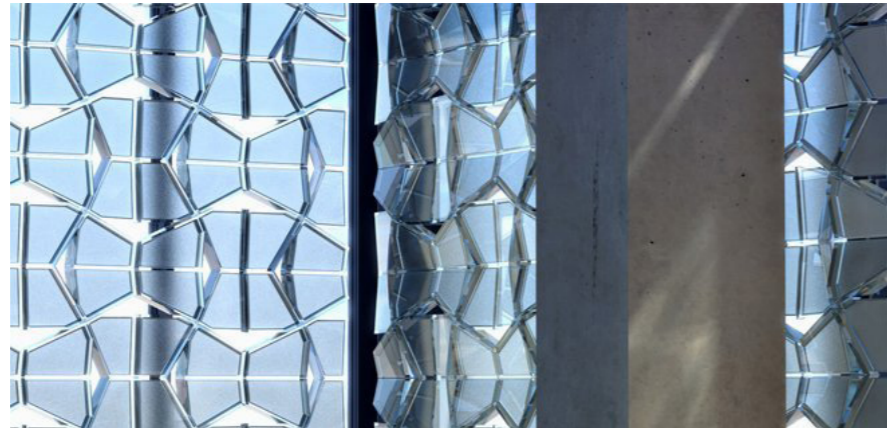


Figure 1.35 The configurations of optimization setup for the convective flow of a trombe wall. Reprinted from "Numerical simulation of modified Trombe-Michel Walls with exergy and energy analysis" by Corasaniti, Manni, Russo, & Gori, (2017)

Wattez, Cosmatu, Tenpierik, Turrin and Heinzelmann (2017) also studied the effect of ventilation on the energy performance of a PCM based Trombe wall system. They conducted a multi-objective optimization study to improve the efficiency of this system compared to a conventional Trombe wall. For the enhancement regarding the ventilation strategy they observed the effect on energy reduction by varying the amount of openings, the size of these openings and the place of the opening in the wall. This is done to improve the

ventilation rate together with an increase in the view to the outside environment. The results showed that a Trombe wall with 10% of physical openings provides the highest energy savings, in winter 38% savings were observed and in summer 24% of savings. This 10% was the minimum of opening for visibility of the outdoor environment according to their program of requirement, less openings showed better results. Openings up to 20% of the Trombe wall area can be adopted when a temperature loss of 0,7°C is accepted. (Wattez, Cosmatu, Tenpierik, Turrin, & Heinzelmann, 2017)

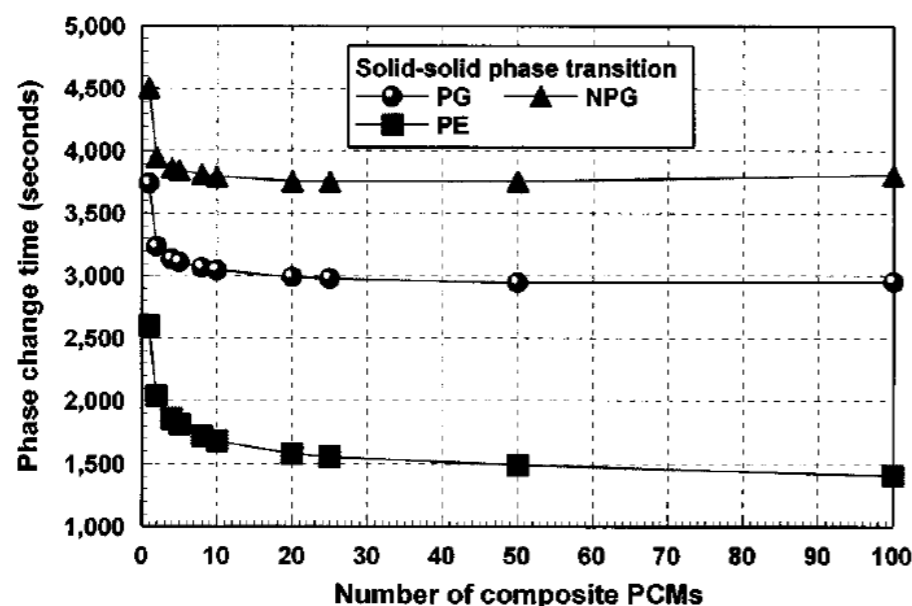
Figure 1.36
PCM based trombe wall with openings for ventilation and view to the outside. Reprinted from "Renewed Trombe wall passively reduces energy consumption" by Wattez, Cosmatu, Tenpierik, Turrin, & Heinzelmann, 2017



24.1.7 Multiple families of PCM

Section "2.2.2.1 Phase change materials (PCM's)" showed the limitations of the PCM's nucleation process during melting and solidification. Natural convection within the system results in a difference in temperature between the lower part and the upper part, this is an important factor which influences the melt ratio of the PCM and therefore the efficiency of the system. Wang, Chen and Jiang (1999) studied already in 1999 the effect of the implementation of a novel homogeneous phase change process in materials (HPCP). In this process several PCM's with different melting temperatures were combined to control the irregular melting process within the system. They noticed that the nucleation process of the PCM decreases when the number of the PCM's increased, between 5-10 different PCM's showed the best result for a steady phase change (Figure 1.37). (Wang, Chen, & Jiang, 1999)

Figure 1.37
Effects of composite PCM number on complete phase change time. Reprinted from "Theoretical study on a novel phase change process" by Wang, Chen, & Jiang, 1999



This HPCP method shows a feasible amount of single PCM's for application in buildings. Several volumetric shapes were tested and calculated considering the following: (1) Spherical PCM, (2) Cylindrical PCM and (3) Flat plate PCM, a significant deviation was observed between the separate shapes. The complete operation time of the nucleation process, compared to the conventional method, was reduced with 60% for (1), with 50% for (2) and with 33% for (3) (Wang, Chen, & Jiang, 1999). So the HPCP showed a considerable improvement of the operation time, however the researchers were not specific in the elaboration on the arrangement of the PCM's and the distribution within the three systems. With the HPCP the PCM is used in a more efficient way, less unused material will be implemented in the system and therefore the weight of the PCM unit can be reduced remarkably which is very important for the construction of buildings. As alternative, a higher efficiency can be obtained which can lead to a reduction of the HVAC systems needed to control the temperature

Several other researchers showed also the benefits of implementing multiple PCM's in numerous applications in combination with use of HTF's and the air conditioning principle (Ezra, Kozak, Dubovsky, & Ziskind, 2016; Mosaffa, Farshi, Ferreira, & Rosen, 2014; Seeniraj & Narasimhan, 2008). However, non of the researchers showed the use of passive application of multiple PCM's.

Figure 1.38
Finned tube multi PCM LHS unit. Reprinted from "Performance enhancement of a solar dynamic LHTS module having both fins and multiple PCMs", by Seeniraj & Narasimhan, 2008

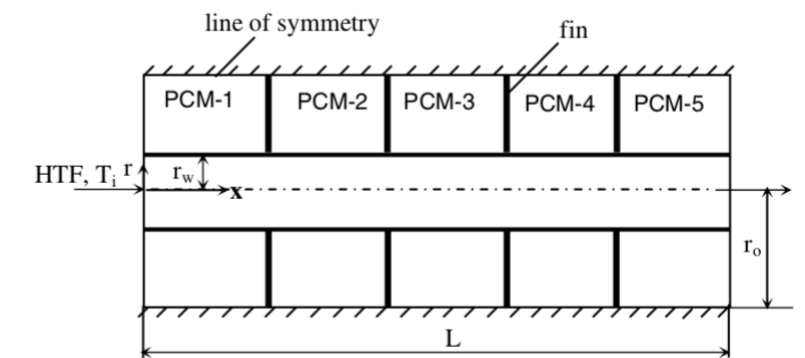


Figure 1.39
Effects of composite PCM number on complete phase change time. Reprinted from "Analysis and optimization of melting temperature span for a multiple-PCM latent heat thermal energy storage unit" by Ezra, Kozak, Dubovsky, & Ziskind, 2016

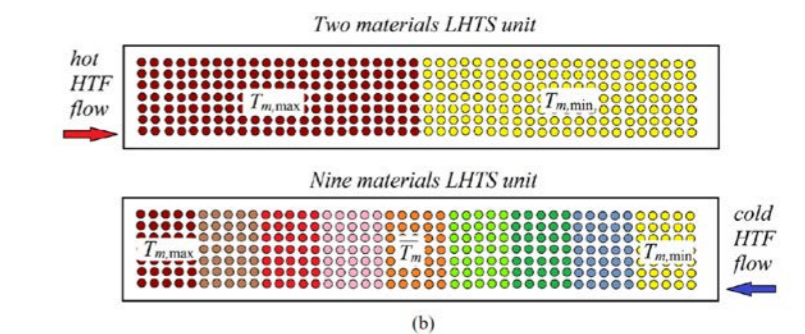
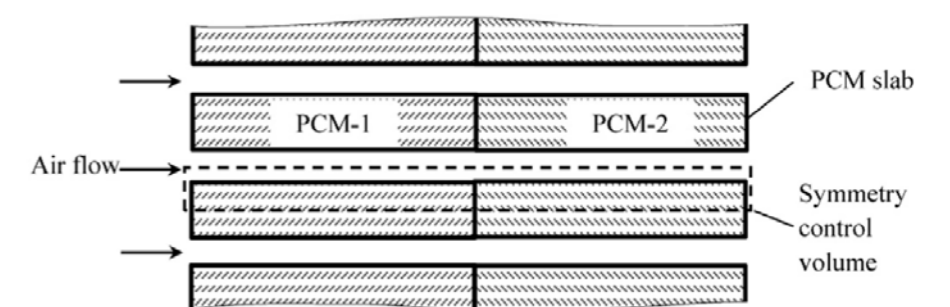


Figure 140
Schematic LHS unit with multi PCM's. Reprinted from "Energy and exergy evaluation of a multiple-PCM thermal storage unit for free cooling applications" by Mosaffa, Farshi, Ferreira, & Rosen, 2014



24.1.8 Inclination of the PCM

Section "Material limitations" already showed that natural convection plays a major role in the heat transfer process during the nucleation of the PCM. Using this phenomenon to increase the heat transfer rate of the unit can have significant impact on the performance.

Kamkari, Shokouhmand and Bruno (2014) investigated the melting of PCM in a rectangular enclosure at three different inclination angles considering the internal thermal behaviour of the material. Several experiments were employed for different inclination angles (0° , 45° and 90°), the experiments were conducted using wall temperatures of 55°C , 60°C and 70°C . Figure 141 shows the difference of total melting time versus inclination angle for the different operation temperatures (Kamkari, Shokouhmand, & Bruno, 2014). For all inclination angles, melt fractions increase almost linearly with time, remarkable in this observation is the increase in melting time between the 45° inclined unit and the 90° inclined unit, the lower the temperature the greater the difference between the two. In this experiment the heat source is projected on one specific surface, this differs from the application in buildings. However, a positive effect can be obtained by inclining the unit towards the sun to create a more evenly distributed heat transfer surface. The inclination showed significant benefits regarding the internal formation of convection currents and therefore an increase in the heat transfer rate and a reduction in melting time. On average a reduction in melting time between 35% and 53% was achieved compared to the vertical enclosure, respectively. (Kamkari, Shokouhmand, & Bruno, 2014)

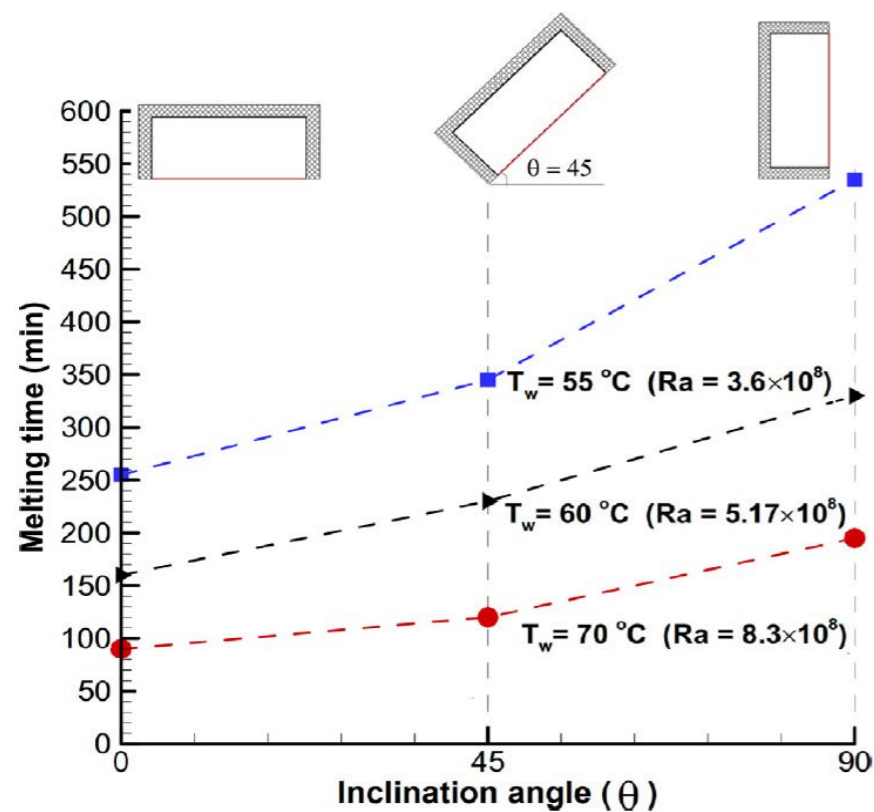
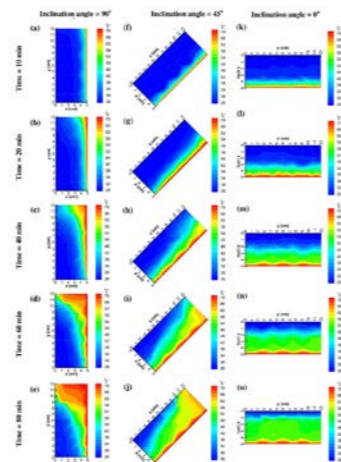


Figure 141
Variation of total melting time versus inclination angle for different wall temperatures. Reprinted from "Experimental investigation of the effect of inclination angle on convection-driven melting" by Kamkari, Shokouhmand, & Bruno, 2014



different angles (0° , 30° , 60° and 90°). They also concluded that the inclination strongly defines the internal convective vortex and improves the melting process (Figure 142), the inclination shows a pattern that tends to a Rayleigh–Bénard convection pattern. This indicates that a more regular and evenly distributed pattern develops within the specimen, this results in higher melting rates and a faster energy transport. (Webb & Viskanta, 1986)

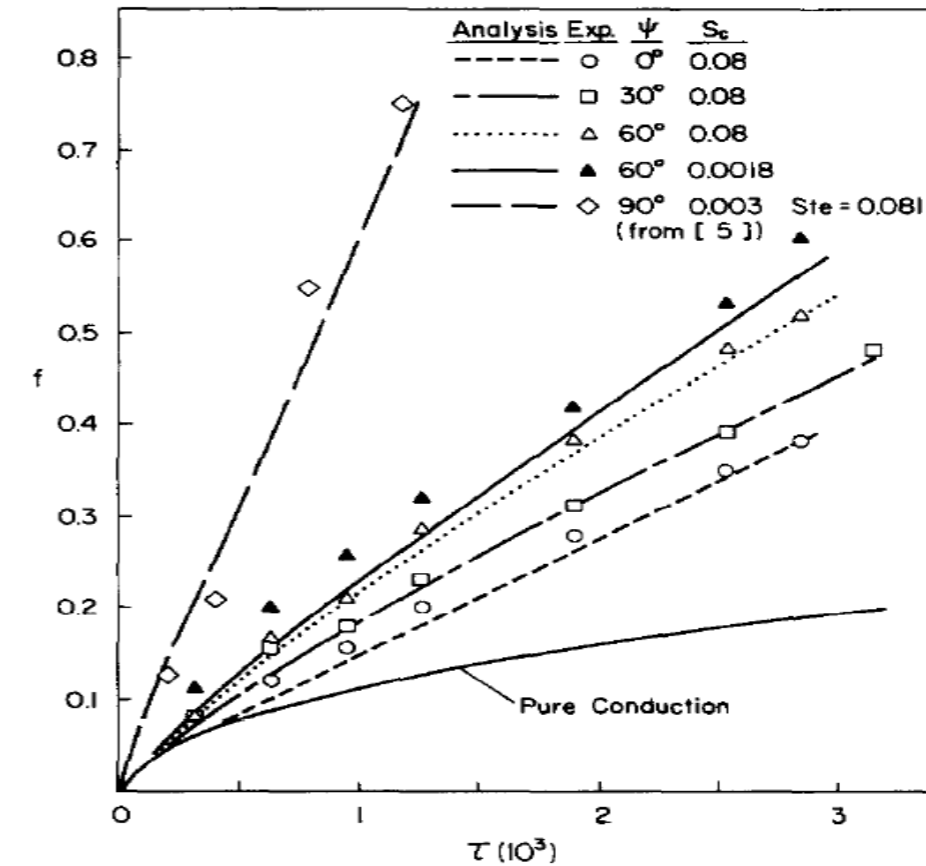


Figure 142
The molten fraction (f) of the various inclinations with dimensionless time (T). "Natural-convection-dominated melting heat transfer in an inclined rectangular enclosure", by Webb & Viskanta, 1986

24.2 Adaptability of thermal energy storage

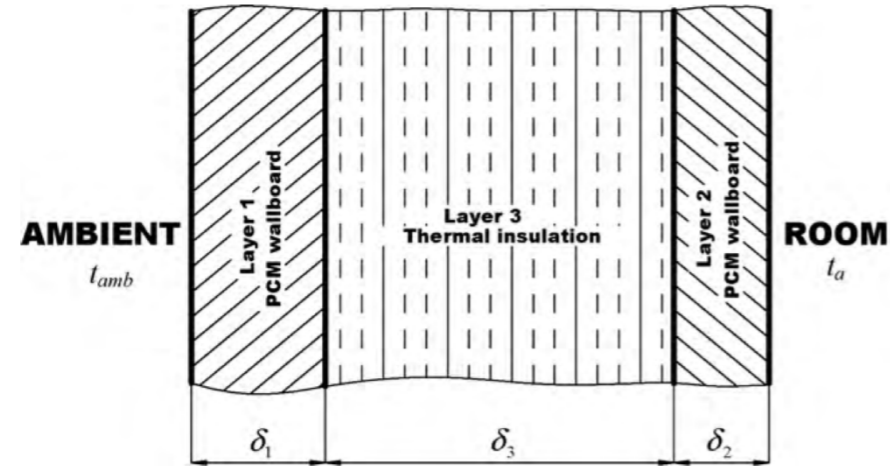
The adaptability of the LHSU to the ambient temperature is important for the overall efficiency of the system concerning the application of PCM's in climates with both winter and summer season. Making it adaptable to this climate increases the yearly operation time of the LHSU, several optimization method will be described.

24.2.1 Multi pcm layers

Izquierdo-Barrientos, Belmonte, Rodríguez-Sánchez, Molina and Almendros-Ibáñez conducted a research study on the effect of the location of a layer of PCM in the wall, the different climatic conditions and the melting temperature of the PCM. This study is carried out to find the optimal transition temperature for both winter and summer season, this means a temperature that reduces the heat gain in summer and heat loss in winter. The results obtained indicate that no such optimum phase change temperature is possible for both seasons, the melting temperature needs to be considered for one target application or multiple layers need to be considered (Izquierdo-Barrientos, Belmonte, Rodríguez-Sánchez, Molina, & Almendros-Ibáñez, 2012).

This implementation of multiple layers in building applications have been reported in several research studies. Diaconu and Cruceru (2010) studied the implementation of two separate PCM layers with both different melting temperatures. The system contains three functional layers, the external PCM wallboard layer (active during summer season), an inner thermal insulation layer and the internal PCM wallboard layer (active during winter season) as shown in Figure 143. The external layer has a higher PCM melting point compared to the internal layer. (Diaconu & Cruceru, 2010)

Figure 143
Structure of the multi layered composite LHSU. Reprinted from "Novel concept of composite phase change material wall system for year-round thermal energy savings" by Diaconu & Cruceru, 2010.



They stated the most important thermo-physical properties for the efficiency of the system are the melting temperature and the latent heat of the system. Using two different PCM melting temperature resulted in the highest efficiency considering energy savings, the melting temperatures for this specific application are illustrated in Figure 144.

Figure 144
Values for melting temperature of the two PCM layers for cooling and heating. Reprinted from "Novel concept of composite phase change material wall system for year-round thermal energy savings" by Diaconu & Cruceru, 2010.

	Heating	
Condition	$Q_{H,annual} = \min$	$\max(Q_H) = \min$
Melting point	$t_{m2} = 24.4^\circ\text{C}$	$t_{m2} = 33.4^\circ\text{C}$
	Cooling	
Condition	$Q_{C,annual} = \min$	$\max(Q_C) = \min$
Melting point	$t_{m1} = 20.0^\circ\text{C}$	$t_{m1} = 19.3^\circ\text{C}$

The outer layer prevents the heat from entering the building and reducing the heat load significantly, peak loads were reduced by 354% and the energy savings for heating were 12,8%. For cooling the peak load reduction was 24,3% and 1% for annual energy savings from the AC (Diaconu & Cruceru, 2010). However, no optimization of the parameters was considered so they expect that once these parameters are adjusted more savings can be achieved for the annual energy savings from the AC (Diaconu & Cruceru, 2010).

24.2.2 Adaptable system

Wattez, Cosmatu, Tenpierik, Turrin and Heinzelmann investigated the energy savings of an adaptable Trombe wall system in the "Double face"-project. This project is a innovative Trombe wall system based on PCM which can be used for both winter and summer season. Several small containers with pcm are

integrated into a storey high system, the back of the containers has a layer of aerogel to guide the direction of the heat transfer (Figure 145). In summer, the system faces towards the interior and absorbs the excessive heat from the interior space produced by the occupants and by other heat sources such as technological devices. This heat is released during the night by facing the elements towards the façade. In winter, the system is rotated towards the exterior and absorbs the heat from the sun during the day, this heat is released at night to prevent the space from cooling down to much.

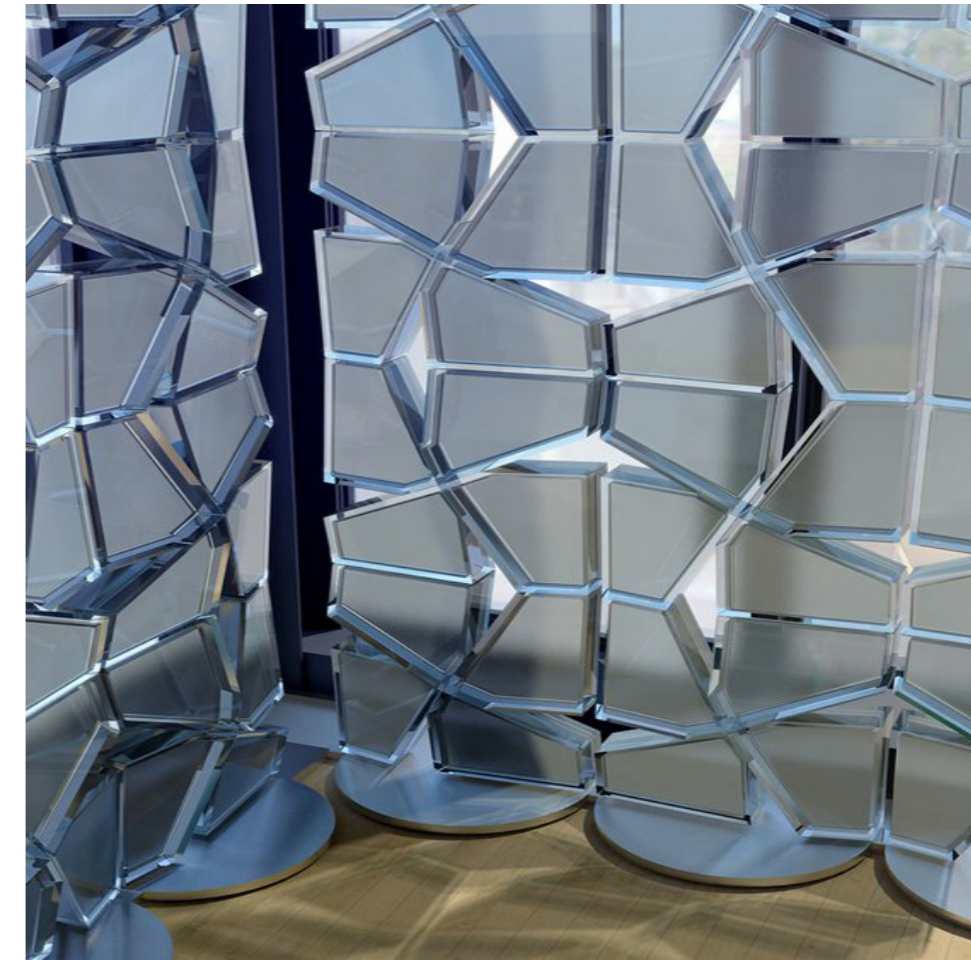


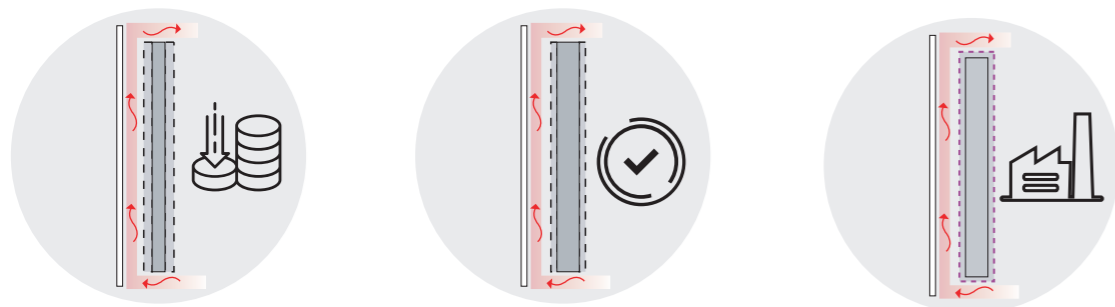
Figure 145
Double face project, PCM base translucent trombe wall Reprinted from 4TU Federation, by Delft University of Technology, n.d.. Retrieved from <https://www.4tu.nl/bouw/en/LHP2014/doubleface/>

The results showed that the energy demand for heating could be reduced by 30% by using 2 centimetre of PCM together with 1 centimetre of aerogel. However, this thickness heats up to fast due to the high values for solar radiation. A thicker PCM layer is needed in winter to prevent this from happening (around 5 centimetres of PCM is needed), but this extra layer is not needed in summer due to negative effect on the melting and solidification. In summer the heat is absorbed from the interior, here the temperature differences is smaller compared to the situation with the PCM facing the exterior. Another drawback from this system is the fact that it cools the room unwanted on cloudy days. (Wattez, Cosmatu, Tenpierik, Turrin, & Heinzelmann, 2017)

2.5 CONCLUSION: PART II

CHAPTER: "2. BACKGROUND"

The thermodynamic and cost-effectiveness of the optimization depends on several variable parameters. The before mentioned heat transfer enhancement techniques for optimizing the effectiveness of the PCM can be adopted to increase the heat transfer rate, which results in a higher reduction of the energy produced by the auxiliary system, a summary showing the techniques that can be adopted for the simulation can be seen on the next page. However, also some other basic strategies can be used to reduce the energy, three other design variables have been considered. These strategies include the quality of the PCM (i.e. high/low latent heat of fusion), the quantity of the PCM (i.e. the total volume of the system), the production method considered (i.e. the encapsulation) and the price of the system depending on the availability.

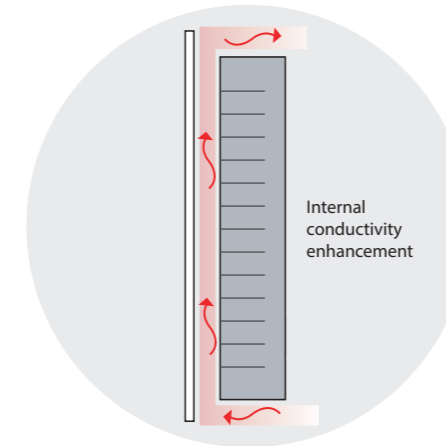


2.5.2.1 Important enhancement techniques obtained from Trombe wall study

- The heat loss coefficient of the wall is highly related to the air velocity in the cavity, a small wind speed tends to give better performance results. The channel depth and the dimensions of the inlet and outlet influences the mass flow rate in this area.
- The south facing facade is the most effective orientation for the design of a building with a Trombe wall in the northern hemisphere.
- Important to consider when designing with PCM are the possibility for overheating, incongruent melting and the fact that inorganic compound are corrosive to metals.
- A composite, or insulated, Trombe wall results in an increase in efficiency for cold or cloudy climates. Less heat loss is observed during the heating season and less heat gain during the cooling season.
- A higher surface area shows an increase in the efficiency of the wall. However, the optimal ratio of the Trombe wall area to the total south wall area seems to be $(a)=37\%$.
- The visibility from the inside seems an important feature when designing a Trombe wall, openings in the wall allows for light and solar radiation to enter the space directly and improves the architectural quality of the wall and the space.

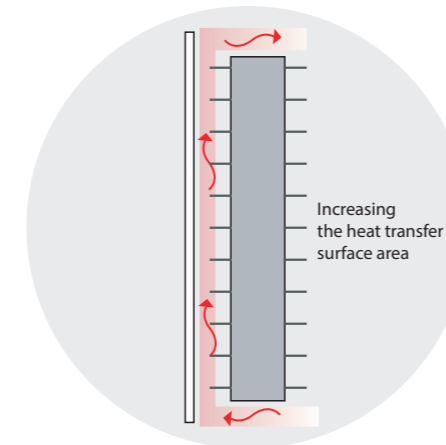
2.5.2.2 Important enhancement techniques PCM

A literature study showed different possible enhancement techniques for the heat transfer of the PCM Trombe wall, this includes extended heat transfer surface, increased conductivity (encapsulation material and thickness), ventilation strategies, multiple PCM's and the adaptability of the system. The following pages summarizes these different heat transfer enhancement techniques observed in the literature.



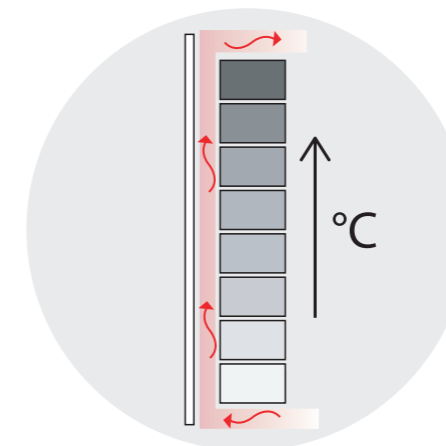
CONDUCTIVITY - Internal fins:

The research study showed a significant increase in the heat transfer of the element by varying the fin length, fin thickness and the spacing between the fins. In this way the property for the low conductivity of the material will be compensated by a high conductive addition within the system.



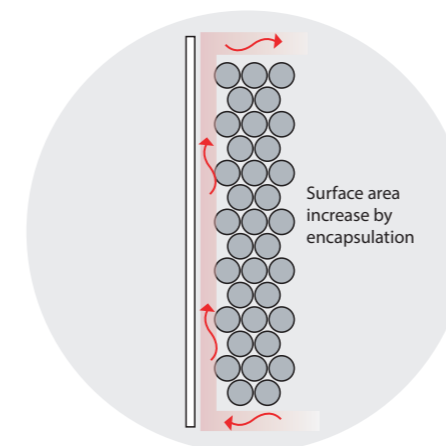
CONDUCTIVITY - External fins:

The effect of the addition of vertical aluminium thermal fins to the trombe wall surface of an unvented trombe wall was measured, this addition of thermal fins increased the interior room temperature which resulted in an increase in efficiency of 7% with a solar radiation of 800 W/m^2 . These fins can have significant impact by combining a ventilation strategy.



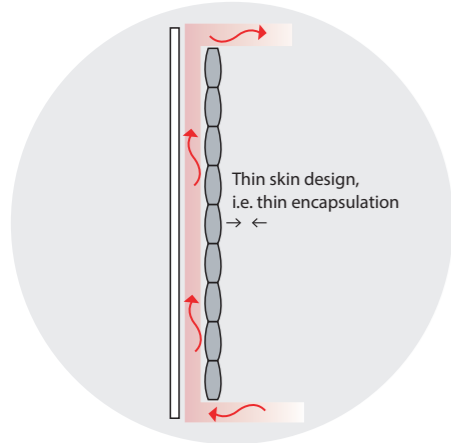
INTERNAL CONVECTION - Cascading of PCM:

A major problem from PCM wall systems is the irregular melting pattern within the LHSU due to thermal convection within. A lower melting temperature is needed in the lower parts of the system. The results from the study show that the time for nucleation process of the PCM decreases when the number of the PCM's increased, between 5-10 different PCM's showed the best result for application in a heat exchanger.



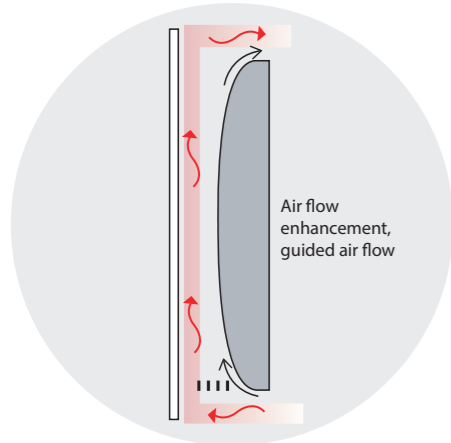
HEAT TRANSFER: Spherical encapsulation:

The heat transfer rate of the LHSU can be improved by increasing the surface area of the encapsulation. A difference in the time of solidification is observed, the spherical with a diameter of four centimeter is already solidified at the time of 20 minutes compared to a solidification time of almost 200 minutes for a the 12 centimeter spherical. An optimal melting time can be created in this way this way.



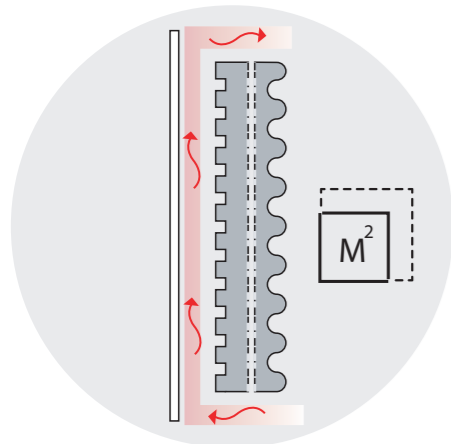
CONDUCTIVITY - Encapsulation with pouches:

Polyethylene bags can be used for the encapsulation of PCM, this method improves the charging and discharging time of the PCM. The benefit of these bags is the relatively thin encapsulation of the PCM, this results in a melting and solidification time close to each other. So a smaller deviation between melting and solidification is observed.



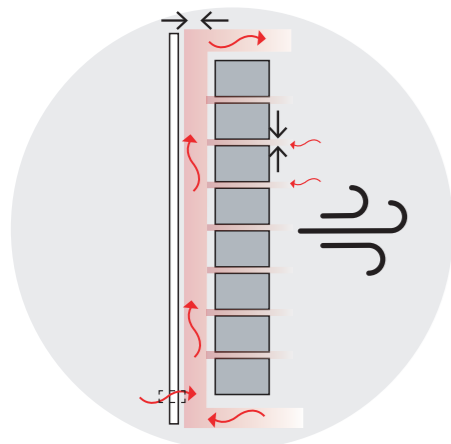
CONVECTIVE HEAT TRANSFER - Improved air flow :

The shape of the wall together with several small fins in the bottom layer increases the air flow along the wall by guiding it. Removing the sharp corners increases the Nusselt number which results in an higher heat transmittance at the surface of the wall to the air in the cavity. A higher room temperature is observed.



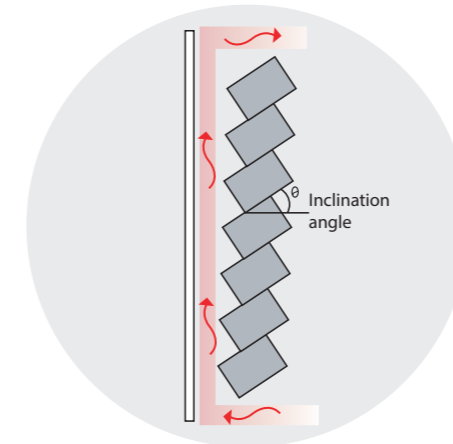
CONVECTIVE HEAT TRANSFER - Smooth surface:

A rectangular geometry creates small air pockets when air is flowing along the wall, this reduces direct contact between the air flow and the surface of the wall which create a longer heat lag. The sinusoidal surface showed the opposite results, a higher heat transfer rate and a shorter heat lag. A rough surface showed better results for the heat transfer rate compared to smooth surfaces.



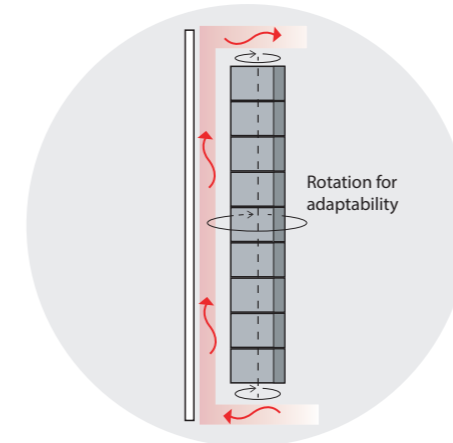
OPENINGS - Ventilation openings:

The effectiveness of the PCM Trombe wall system is influenced by the distance between the PCM wall and the outer skin but also by the dimensions of the inlet and outlet of air to the room and from the outside. So variations can be made using different design strategies to attain a higher air flow rate when needed.



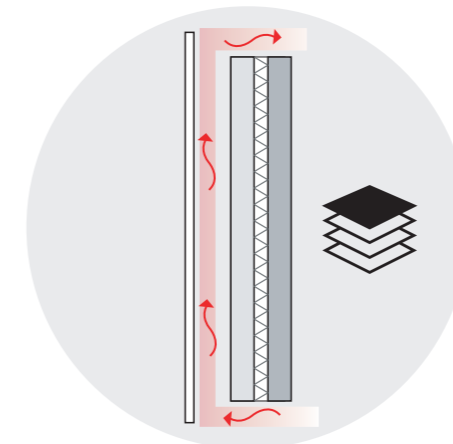
ORIENTATION - Inclination:

Inclining the PCM module showed significant benefits regarding the internal formation of convection currents and therefore an increase in the heat transfer rate and a reduction in melting time. On average a reduction in melting time between 35% and 53% was achieved compared to the vertical enclosure, respectively. The heat transfer surface also faces perpendicular to the sun with this intervention increasing the amount of radiation on the surface



ADAPTABILITY - Adaptive by rotation:

The efficiency of the system can be improved by integrated a rotative system, in this way the PCM can be rotated towards the most important side at that specific time of the day. In this way, the system can capture for instance internal heat during the day and release this heat during the night towards the façade. The most effective configuration can be defined according to the specification from the typology and climate.



MULTILAYERING - Adaptive by multi-layering:

Results from the literature study indicate that not one optimum phase change temperature is possible for both seasons, multiple layers of PCM can be considered to increase the effectiveness of the system. This can be achieved by choosing two PCM's, one with a melting temperature close to the comfort temperature for cooling and one for heating.

Figure 146
Laignel, E (Photographer). (2016).
Saatchi & Saatchi Offices – New
York City [digital image]. Retrieved
from <https://officesnapshots.com/2017/02/27/saatchi-saatchi-offices-new-york-city/>



3. DESIGN CONTEXT

This section, related to the "*Conceptual design-phase*", describes the input parameters for the simulations. A study will be employed considering the parameters from the context such as the target climate and the building typology. These parameters from the building typology contain the fixed parameters for the optimization regarding the temperature set-point, the occupancy, the internal heat gain, the volume of the optimization model, the auxiliary system and the facade requirements. For the climate, the sun radiation, the temperature and the sun angles are most important for the optimization calculations. All these optimization parameters and corresponding values are summarized in the "*Parameter overview*" supplementing this chapter.

To attain an optimal design for the PCM Trombe wall based on a Thermodynamic and Cost-Effective Optimization (TCEO), several parameters must be taken into account. These parameters are defined using the background study on PCM, the Trombe wall and environmental aspects such as the parameters for climate and the office typology. These parameters will be listed down in two categories, fixed parameters and variable parameters. These fixed parameters are determined using the requirements for the offices typology, the environmental influences at the location and the properties from the auxiliary system. The variable parameters are mainly the parameters from the heat transfer enhancement techniques regarding the shape, the material, the encapsulation and the overall working of the system. A summary of all the parameters included within this study is illustrated in Table 1.5 and Table 1.6 at the end of this section.

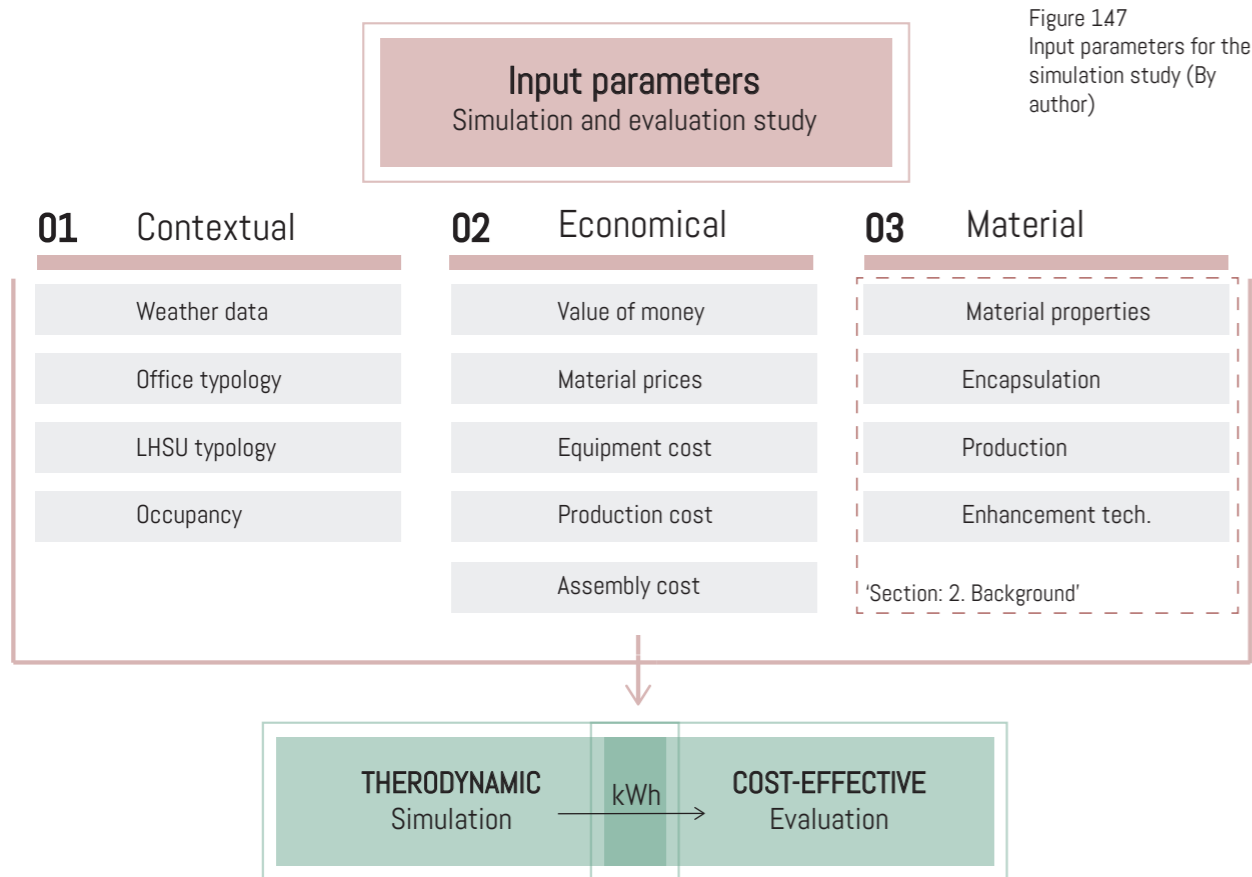
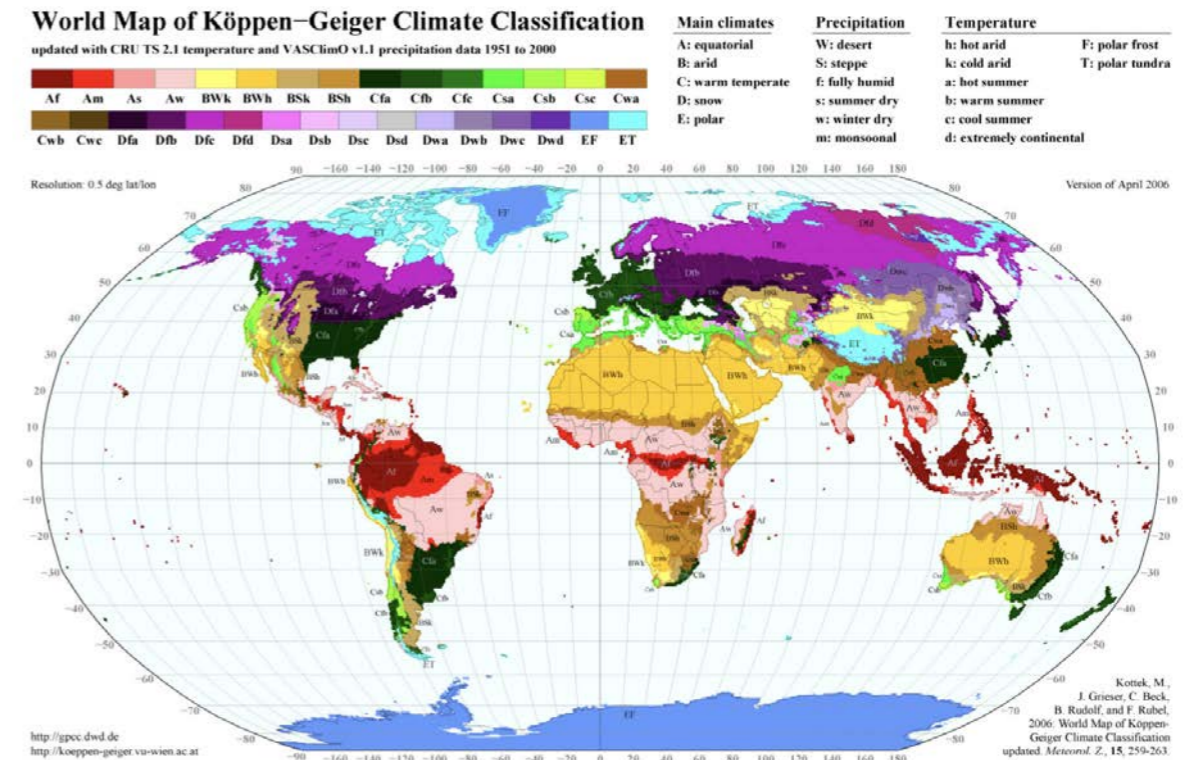


Figure 147
Input parameters for the simulation study (By author)

3.1 CONTEXTUAL

The TCEO will be applied to an office building located in Amsterdam, the Netherlands. Van Unen conducted a research study on the effect of PCM integrated in a Trombe wall based on different climates and building typologies (Unen, 2018). It can be concluded from this study that the PCM Trombe has the most effect in climates with a large diurnal temperature swing observed in the Temperate Climate Marine West-coast climate (Cfb) according the Köppen-Geiger Climate Classification (Figure 149). This temperate climate has dry seasons and a warm summer. Besides that, offices show a potential due to the large internal loads from the inhabitants and the technological devices. For this reason, the context of this research study will be set to an office building located in Amsterdam, The Netherlands. The performance of this office building will be based on the Dutch regulations from the Bouwbesluit. In Europe, offices with rooms for groups or private offices are commonly used, an assumption will be made for the dimensions of this office.



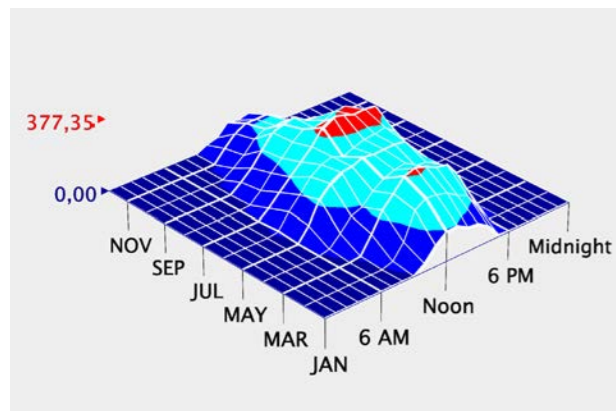
Dwa: Cold/dry winter/hot summer.
Csa: Temperate/dry summer/hot summer.
Cfb: Temperate/without dry season/warm summer.
Dfb: Cold/without dry season/warm summer.
Dfa: Cold/without dry season/hot summer.
Csb: Temperate/dry summer/warm summer.
Dfc: Cold/without dry season/cold summer.
Cwa: Temperate/dry winter/hot summer.
Cfa: Temperate/without dry season/hot summer.
Af: Tropical/rainforest.
BSk: Arid/steppe/cold.
Am: Tropical/monsoon.

Figure 148
World map of Köppen-Geiger Climate classification showing the different countries with a Cfb climate. Reprinted from "A Database for Climatic Conditions around Europe for Promoting GSHP Solutions", by Carli, et al., 2018

3.1.1 Climate parameters

The location for this research study is Amsterdam, the Netherlands, the climate from this location is analysed using Climate Consultant 6.0 (Built 11 version 6.0.11) together with the NLD_Amsterdam weather-file (Climate Consultant 6.0, 2018), information from this study will be used as guideline knowledge for the simulations. The analysis contains the monthly annual dry bulb temperatures, wind speed, the illumination and the direct normal radiation for surfaces perpendicular to the sun (Figure 149). The angles from the sun related to the surface of the facade is also important for the simulation, the different angles on the days of the year will be simulated using climate data from the NEN5060-B2: Hygrothermal performance of buildings (NEN, 2008).

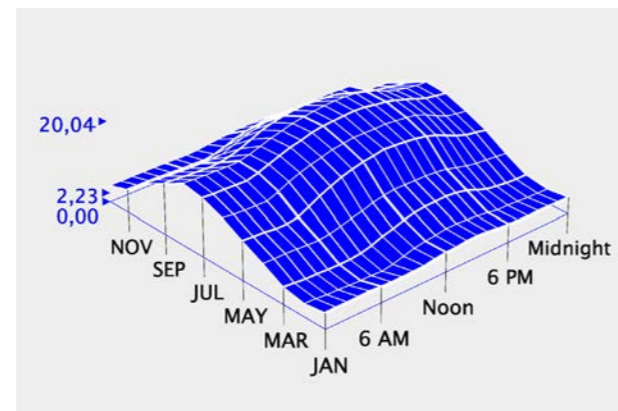
The peak monthly direct normal radiation is around 540 Wh/m², this peak is observed in the summer month July, the minimum mean radiation is around 70 Wh/m² and this happens in December. As said before, the diurnal temperature swing is important for the solidification of the PCM, this swing is relatively large in the Netherlands, this makes the application of the PCM in this type of climate interesting. The average diurnal swing observed from the analysis is around 7 degrees in summer and 2 °C in winter, with a peak difference of around 20 °C between day and night in summer periods. And lastly, the annual peak for the wind velocity is 8,5 m/s and the annual minimum wind velocity is 2,5 m/s, the highest average monthly peak is from January and is 11,5 m/s. The lowest monthly average wind velocity is 1,5 m/s, this velocity counts for all the summer months (May, June, July and August) (Climate Consultant 6.0, 2018).



DIRECT NORMAL RADIATION
(Wh/sq.m)

54%	Night Time
22%	4 - 158
22%	158 - 316
2%	316 - 474
0%	> 474

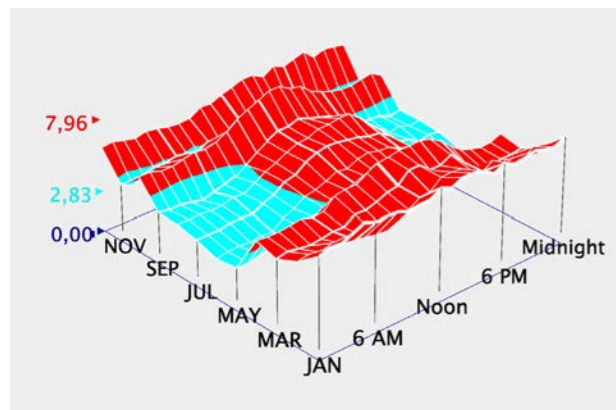
Figure 1.49
Direct normal radiation
NLD_Amsterdam (By author
reprinted from Climate
Consultant 6.0, 2018)



DRY BULB TEMP
(degrees C)

0%	< 0
100%	0 - 21
0%	21 - 27
0%	27 - 38
0%	> 38

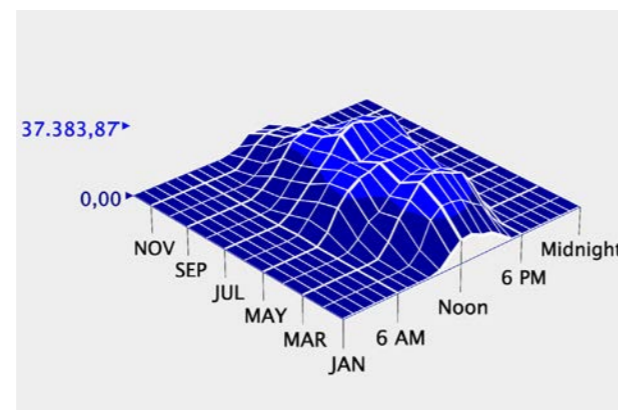
Figure 1.50
Dry bulb temperature
NLD_Amsterdam (By author
reprinted from Climate
Consultant 6.0, 2018)



WIND SPEED
(m/s)

0%	< 2
0%	2 - 3
30%	3 - 5
70%	5 - 9
0%	> 9

Figure 1.51
Wind speed NLD_Amsterdam
(By author reprinted from
Climate Consultant 6.0,
2018)



DIRECT NORMAL ILLUMINATION
(lux)

81%	< 20000
19%	20000 - 40000
0%	40000 - 60000
0%	60000 - 80000
0%	> 80000

Figure 1.52
Direct normal illumination
NLD_Amsterdam (By author
reprinted from Climate
Consultant 6.0, 2018)

3.1.2 Office typology

As mentioned before, the office dimensions of the space will be assumed, this is done according to a calculation based on the NEN (guideline NEN 1824: 2010). For a normal office a minimum of 10 m² per employee needs to be taken into account (Wit, 2018). This is based on the private space for the employee, the cabinets needed and a meeting room. A room with six employees will be assumed, which accounts for a total office area of 60 m² (Wit, 2018). Some basic requirements for the office model will be listed below, which are based on the Dutch regulations and standard office typologies:

- The office is only occupied during working hours, these hours are from 8 00 am till 18 00 pm
- The auxiliary system used in the office is a Heating, Ventilation and Air-conditioning (HVAC) system, this system is active during the occupied hours from the office.
- The set-point temperatures are based on the literature study from Section "2.1 THERMAL CONTROL" according to the NEN-EN 15251. The temperature set-point for heating (winter period) will be set on 20 °C and for cooling (summer period) will be set on 26 °C, based

on offices with an open plan space in Category II (predicted percentage of dissatisfied (PPD) people of 10%)

- A vertical external partition from a office space needs to fulfil certain heat resistance according to the Dutch Buildings Decree 2012. Section 5.3 from this code specifies a heat resistance of 4,5 m²K/W for the façade and 6,5 m²K/W for the roof structure (Bouwbesluit, 2018).
- Construction (materials)
- The u-value for windows in the building envelope needs to be at least 1,65 W/m²K (Bouwbesluit, 2018). Clear double glazing will be used for this envelope, this showed best results for the reduction in energy in offices according to the study from Van Unen (2018), in this case more solar radiation can be used by the LHSU. For the south facade a WWR of 90% will be assumed to allow daylight to enter the building, the simulation study will be used to determine the optimum percentage of Trombe wall.
- The internal heat gain from the occupancy of people doing office work is 120 W/P, the heat gain from the devices at the work station and people together represent around 25 W/m² of office (Menezes, Cripps, Buswell, Wright, & Bouchlaghem, 2014).

3.1.3 LHSU typology

Important for the optimization of the LHSU is the Level of Detail (LOD) of the specification of the costs. Research has shown some important factors which have to be taken into account for the design of a LHSU, the most important requirements for designing system and choosing the materials for encapsulation:

- Environmental conditions: The operation temperature is important to specify if the encapsulation material is suitable. The operating temperature will be 45 °C at maximum.
- Corrosion protection: Especially metals but also plastics can need protective treatments.
- Flammability: When the PCM inside the container is flammable retardants need to be considered for the shell.
- Sealing; Different sealing methods are possible for the macro-encapsulation (Figure 1.53), Fleischer (2015) indicates that this storage needs to be permanently sealed with methods such as brazing, welding or soldering to prevent from them from leakage.
- Physical properties (Macro-encapsulation): Yield strength, density
- Thermophysical properties (PCM): Melting enthalpies and temperatures, heat capacities, densities and thermal conductivities

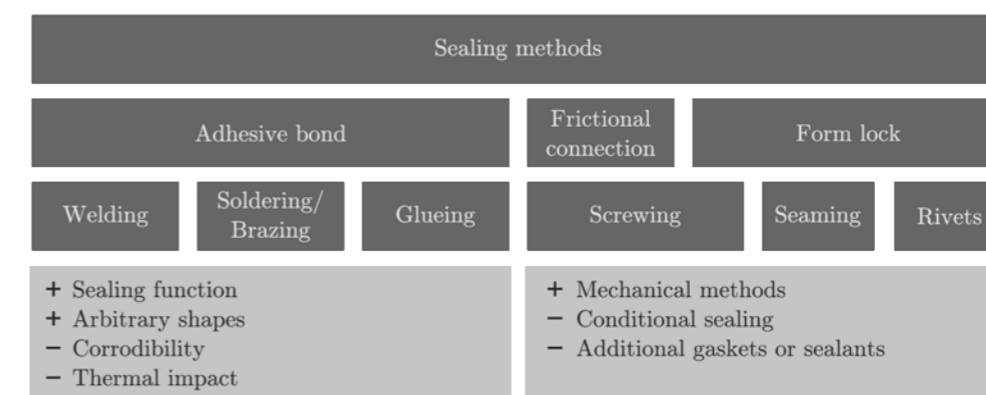


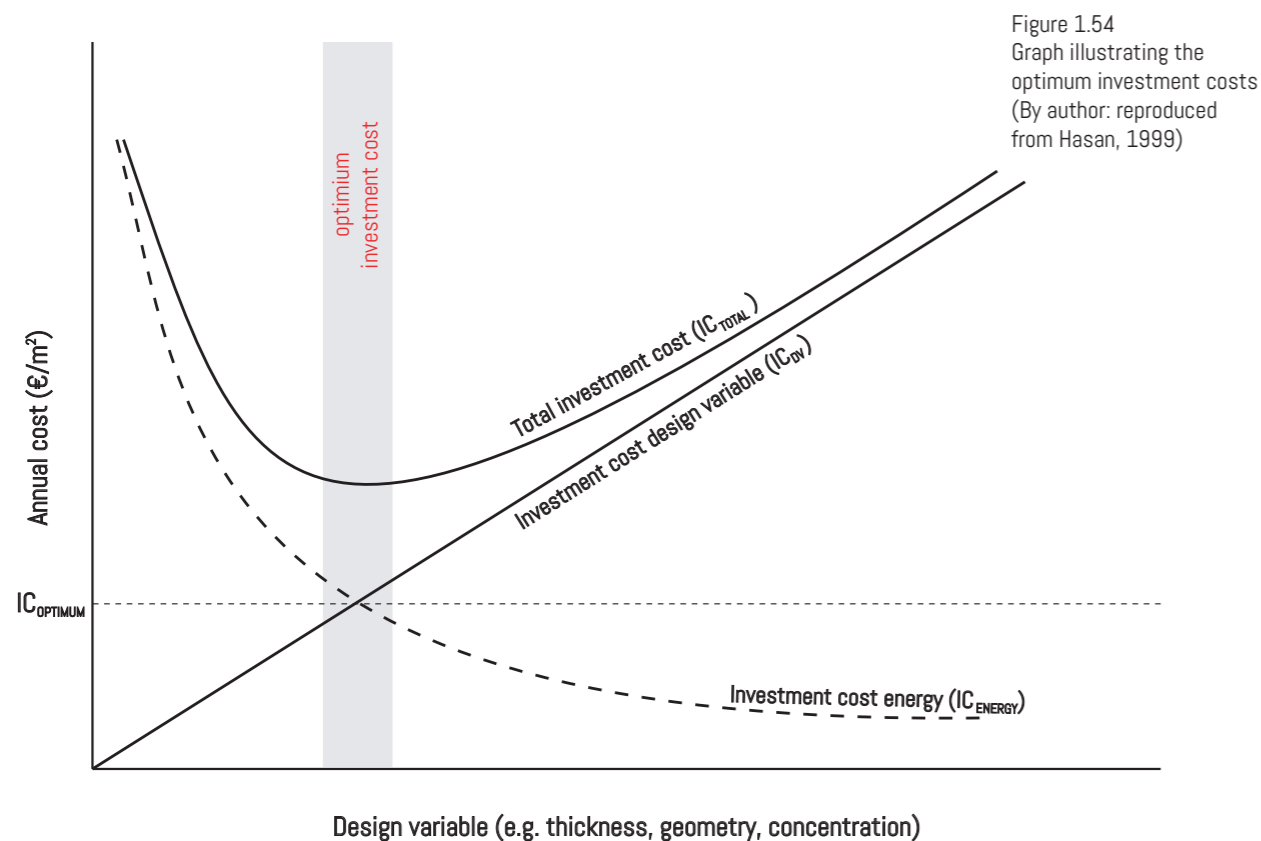
Figure 1.53
Different sealing methods
for macro-encapsulated
PCMs. Reprinted from
"Macro-Encapsulation
of Inorganic Phase-
ChangeMaterials (PCM)
in Metal Capsules", by
Höhlein, König-Haagen, &
Brüggemann, 2018)

3.2 ECONOMICAL

The aim of this research study is to investigate the Thermodynamic and Cost-Effective Optimization (TCEO) potentials to create an economic feasible product which can be implemented in an efficient way in an office building located in the Netherlands. So the system needs to be optimized from both the thermodynamic and the cost-effective objectives, this section describes the method and strategies that will be used for the cost-effective optimization.

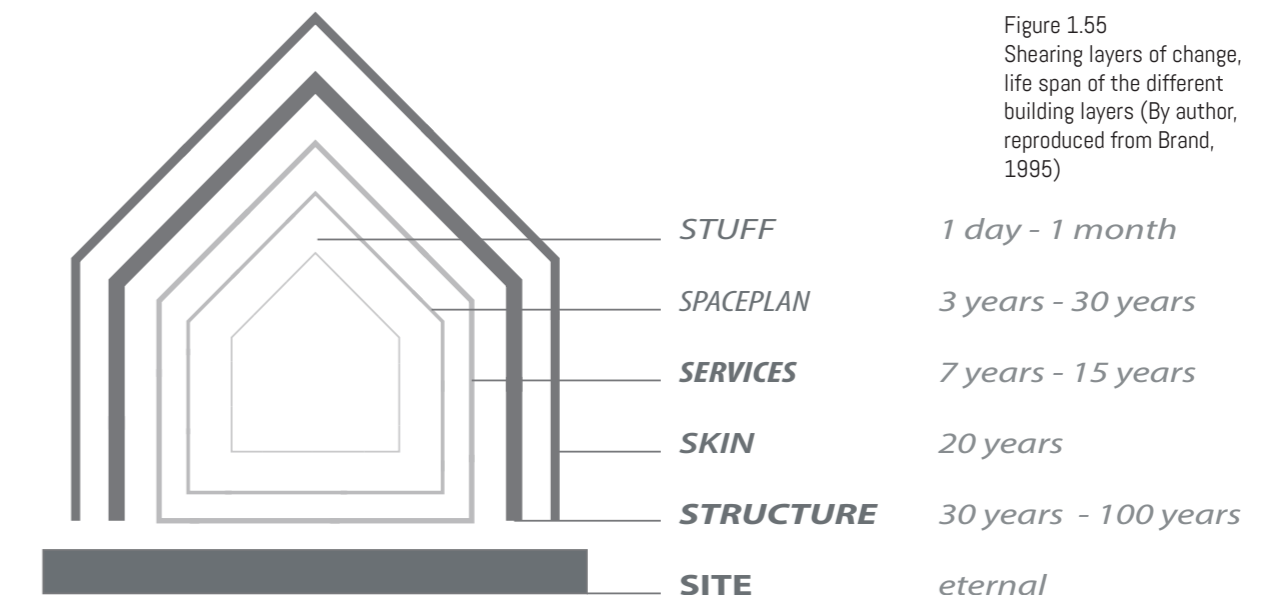
Several researchers studied the cost-effective design process within various applications, an economic analysis will be used as method to evaluate different design alternatives which includes a Life Cycle Cost Analysis (LCCA) (Jaber & Ajib, 2011; Kharbouch, Mimet, Ganaoui, & Ouhsaine, 2018; Hasan, 1999). A cost-effective building application with PCM is obtained by finding a balance between the energy savings and the investment costs for the PCM, therefore a calculation for the optimum investment costs ($IC_{OPTIMUM}$) should be considered (Figure 1.54).

At this optimum point the total investment costs of the design variable (IC_{DV}) is equal to the investments costs for energy (IC_{ENERGY}) from the building during its lifetime (N) in years. The investment costs for energy relates to the annual sum of the electrical equipment's consumption costs ($C_{EQUIPEMENT}$), so the total cost of ownership for these specific installations. Subsequently, this results in the a minimum total investment costs (IC_{TOTAL}) for operating the building (Kharbouch, Mimet, Ganaoui, & Ouhsaine, 2018; Hasan, 1999). These equipment consumption costs include the operation costs, maintenance costs and capital costs (the one-time expenses for the purchase of the system) multiplied by the Present Worth Factor (PWF). The design variables refer to the different heat transfer enhancement techniques discussed in Section "24.1 Heat transfer enhancement".



A more detailed calculation method will be described in the Section "6. SIMULATION RESULTS", a detailed simulation method together with the formulas will be discussed. The different parameters needed for this section will be described here, some basic assumption will be made for the lifespan, the economics and material costs to calculate the estimated cost of the whole system. An overview of the PCM material costs is given in Table 1.5 on page 68.

Steward Brand (1995) studied the existing layers inside and around a building, he states that the building consists out of 6 layers, all with their own life-span. These layers are illustrated in Figure 1.55 and can be used to determine the expected life-span of these separated layers. This research study focusses on the implementation of a PCM Trombe wall into a building, this wall is part of the skin layer of the building. A life span of 20 years is expected from this layers (Brand, 1995), this number will be used to determine the life span of the Trombe wall for the Thermodynamic and Cost-Effective Optimization (TCEO) and for the auxiliary heat system. An estimation can be made for the replacement strategy for the PCM regarding the thermal cycles and degradation of the material.



3.2.1 Parameters cost-effectiveness

The costs-effective optimization of the PCM Trombe wall system is based on several variables, these variables are depended on the economics of the country, the availability of the product and the energy demand of the target building. The total investment cost (IC_{TOTAL}) is based on the Present Worth Factor (PWF) taking into account the interest rate (r) and the inflation rate (i), which indicates the value of money over a certain time. The target inflation rate in Europe is around 2 percent, the past few years this rate decreased within the Netherlands but the long-term inflation rate is going to trend around 2% (CBS, 2017; ECB, 2018), this number will be assumed for the calculations. The interest rate is determined by the Governing Council of the European Central Bank (ECB) in Europe and is 0.25% (ECB, 2018).

The electricity prices together with the value for heating the HVAC and the efficiency of the system is needed to determine the costs for the total HVAC system. The electricity prices for non-household consumers in the Netherlands, including levies and taxes, is around 17.7 eurocent per kWh according to the European Statistical Office (Eurostat, 2018).

The measurement of energy efficiency of installations that are used for heating and cooling the building is determined according to the COP (Coefficient of Performance) or the EER (Energy Efficiency Ratio). A assumption will be made for the efficiency of the installations used in the benchmark situation. Oeffelen, Spiekman and Bulavskaya (2013) conducted a research study on the most commonly used installations within office buildings. It can be concluded that a compression cooling installation is used in most office buildings, around 70% of the buildings with a office function uses this type of cooling. And for heating a HR-boiler is mostly used in office buildings, around 88% of the buildings has this type of heating (Oeffelen, Spiekman, & Bulavskaya, 2013). The HR107-boiler is a common type, this boiler has a efficiency of 107%. A standard COP of 3,0 will be employed for the compression cooling, this indicates the efficiency at full-load operation within one year (KWA Bedrijfsadviseurs B.V., 2011). A heat-pump, with a higher efficiency compared to the older equipment, will be used within the calculation to include the transition to the more modern offices, this heat-pump will have a COP of 3. These values are summarized in Table 1.6.

Personal contact via e-mail with Rubitherm for prices and systems, Stefanie Klaiber in an email to the author gave details on the prices of the products sold by RubiTherm (S. Klaiber, personal communication, December 20, 2018). An overview of the product information and the prices is illustrated in "APPENDIX C".

Table 1.5 Summarized overview of the parameters used for the price of PCM (S. Klaiber, personal communication, December 20, 2018)

Variable parameters					
#	Type	Parameter	Value Unit	Reference	
02.1	Pure material (10.000 kg)	RUBITHERM RT 15 ($\Delta H = 180$ kJ/kg)	4,13 €/kg	(Rubitherm, 2018)	
		RUBITHERM RT 18	4,25 €/kg	(Rubitherm, 2018)	
		RUBITHERM RT 21 ($\Delta H = 155$ kJ/kg)	4,48 €/kg	(Rubitherm, 2018)	
		RUBITHERM RT 25	4,67 €/kg	(Rubitherm, 2018)	
		RUBITHERM RT 31 ($\Delta H = 165$ kJ/kg)	4,66 €/kg	(Rubitherm, 2018)	
		RUBITHERM RT 18 HC ($\Delta H = 260$ kJ/kg)	9,11 €/kg	(Rubitherm, 2018)	
	02.2	Accumulators	RUBITHERM RT 21 HC ($\Delta H = 190$ kJ/kg)	9,32 €/kg	(Rubitherm, 2018)
			RUBITHERM RT 28 HC ($\Delta H = 250$ kJ/kg)	9,11 €/kg	(Rubitherm, 2018)
			RUBITHERM SP15 ($\Delta H = 180$ kJ/kg)	2,18 €/kg	(Rubitherm, 2018)
			RUBITHERM SP21E ($\Delta H = 170$ kJ/kg)	2,14 €/kg	(Rubitherm, 2018)
			RUBITHERM SP24E ($\Delta H = 180$ kJ/kg)	2,01 €/kg	(Rubitherm, 2018)
			RUBITHERM SP25E ($\Delta H = 180$ kJ/kg)	1,89 €/kg	(Rubitherm, 2018)
			RUBITHERM SP26E ($\Delta H = 180$ kJ/kg)	1,88 €/kg	(Rubitherm, 2018)
			RUBITHERM SP29Eu ($\Delta H = 200$ kJ/kg)	1,80 €/kg	(Rubitherm, 2018)
			RUBITHERM SP31 ($\Delta H = 210$ kJ/kg)	2,92 €/kg	(Rubitherm, 2018)
			R1 (170x85x25) (filled with RT or SP)	5,95 €/st	(Rubitherm, 2018)
			R1 (170x85x25) (filled with RT HC)	10,95 €/st	(Rubitherm, 2018)
			R2 (210x130x25) (filled with RT or SP)	10,95 €/st	(Rubitherm, 2018)
R2 (210x130x25) (filled with RT HC)	15,95 €/st	(Rubitherm, 2018)			
R3 (320x290x25) (filled with RT or SP)	15,95 €/st	(Rubitherm, 2018)			
R3 (320x290x25) (filled with RT HC)	25,95 €/st	(Rubitherm, 2018)			
02.3	Pouches	Aluminium pouch (340x340)	15 €/st	(Rubitherm, 2018)	
		Polymer bag (130x290)	15 €/st	(Rubitherm, 2018)	
		Aluminium pouch: ClimSel C21 (150x370)	4 €/st	(ClimSel, 2018)	

*RT = Organic phase change material
 *SP = Salt hydrate phase change material
 *HC = High latent heat capacity
 * ΔH = Latent heat of fusion (kJ/kg)

Table 1.6 Summarized overview of the parameters used for the simulation setup within MATLAB/Simulink

Fixed parameters				
#	Type	Parameter	Value Unit	Reference
Context				
01.1	Climate	Temperate Climate Marine West-coast climate (Cfb)		(Carli, et al., 2018)
		Temperature file	$Te_NEN5060B2_1p_double$	(NEN, 2008)
01.3	Office	Direct normal radiation	variable	(NEN, 2008)
		Minimum radiation	variable	(NEN, 2008)
01.4	People occupancy	Sun radiation file	$qsol_NEN5060B2_1p_double$	(NEN, 2008)
		Room size (10 m ² /person)	60 m ²	(Wit, 2018)
01.4	People occupancy	Number of occupants	6 Persons	
		Schedule	8 00h - 18 00h (Mon-Fri)	
01.5	Electric equipment	Schedule (High power)	8 00h - 11 00h (Mon-Fri)	
		Schedule (Low power)	11 00h - 17 00h (Mon-Fri)	
01.5	Electric equipment	Equipment type	HVAC -	
		Heating and cooling	Heatpump	
01.5	Electric equipment	Coefficient of performance (COP)	3	
		Gas consumption (heating)	12,5 m3/m2	(Sipma, 2016)
01.6	Heating and cooling setpoint	Heating setpoint (HS)	20 °C	(CEN, 2007)
		Cooling setpoint (CS)	26 °C	(CEN, 2007)
01.7	Heat production	Heat rate internal heat	25 W/m ²	(Menezes, et al., 2014)
		Metabolic heat rate (<i>included</i>)	120 W/P	(EngineeringToolBox, 2003)
01.8	Ventilation	Mechanical ventilation rate	2.0/3600 (s ⁻¹)	(Unen, 2018)
		Natural ventilation ($A_{inlet} = A_{outlet}$)	0,025 * A_{facade} m ²	(Unen, 2018)
01.8	Ventilation		$C_d = 0.8$	
		Night ventilation (mechanical + natural)	$T_{room,oper} > 24$ °C $T_{room,oper} > Te$	
Building construction				
02.1	Building envelope	Wall: Heat resistance (R_c)	4,5 m ² K/W	(Bouwbesluit, 2018)
		Window: U-value (U_{gl})	1,6 W/m ² K	
		Solar heat gain coefficient (SHGC)	0,7	
02.2	Heat transfer coefficient	Infiltration rate	0,2/3600 (s ⁻¹)	
		south façade: α_i	2,7 W/m ² K	
		south façade: α_e	25,0 W/m ² K	
02.3	Latent heat storage unit (LHSU)	adiabatic walls: α_e	0 W/m ² K	
		Insulation thickness	10 mm	
		Latent heat of fusion	180 kJ/kg	
02.3	Latent heat storage unit (LHSU)	Thermal conductivity	0,6 W/m.k	
		Specific heat capacity	2000 J/kg.K	
		Control volume layers	$nl_pcm = 10$ $nl_ins = 3$	
Economics				
03.1	Present Worth Factor	Interest rate	0.25 %	(ECB, 2018)
		Inflation rate	2 %	(CBS, 2017; ECB, 2018)
03.2	Electricity	Dutch non-household consumerprice	0,085 €/kWh	(Eurostat, 2018)
03.3	Miscellaneous	Maintenance factor	3 %	
		Salvage factor	10 %	
03.3	Miscellaneous	Life span (façade)	20 years	(Brand, 1995)

3.3 CONCLUSION: PART III

CHAPTER: "3. DESIGN CONTEXT"

The main objective of this research study is to create an optimal design for the PCM Trombe wall based on a Thermodynamic and Cost-Effective Optimization (TCEO), to pursue this several parameters must be taken into account. Therefore, this chapter defines the main criteria for the simulation environment including the contextual parameters such as the climate parameters, the office typology and the LHSU typology. Besides this, also the economical context is defined to determine the parameters needed to evaluate the cost-effectiveness of the design optimization and simulation.

The PCM Trombe wall performs best in climates with large diurnal swings, this is seen within the Temperate Marine West-coast climate (Cfb), therefore the location for this research will be Amsterdam, the Netherlands. The PCMs also show a lot of potential for the application within offices, these buildings have a large internal heat production which can effectively be accumulated by the PCM. A standard eight to six office schedule will be considered, the office has an internal heat production of 25 W/m² and the envelope partition properties according to the Bouwbesluit. The auxiliary system will be based on an Heating, ventilation and air conditioning (HVAC) system with a predefined air change rate and a fixed heating and cooling set-point (Table 1.6). The application of PCM within the Built Environment is accompanied by several requirements for the design regarding safety, material properties and the cost-effectiveness. Important factors are the maximum operation temperature of 45°C, the sealing methods and corrosion protection for the encapsulation of the material and the flammability when considering organic compounds.

For the economic evaluation of the feasibility of the product several factors need to be taken into account, first of all the value of money over time is determined by the Present Worth Factor (PWF). The PWF is based on a combination of the interest rate and the inflation rate at the specific location. This factor will be multiplied by the operation costs, the energy and maintenance costs (Table 1.6). Secondly, the facade of the office has a life span of 20 years, this life span will be used as guideline to determine the payback time of the PCM product. And in the end the performance of the auxiliary system will be used to define the actual operation cost according to the fuel price. All these factors will be used to assess the performance of the LHSU on the reduction in the energy demand and the costs

4. THERMODYNAMICS

This section describes briefly the background knowledge needed to determine the indoor temperature and related energy flows within the building. This knowledge is needed to understand the initial working principle of the MATLAB/Simulink simulation model which is used in the DoubleFace 2.0 project. First the basic principle of a heat balance calculation will be elaborated on, this will be followed up by a more detailed multi-node heat balance calculation which can be used to determine the temperature and energy flows within a room. These energy flows are directly related to the energy demand within the room, which is important to determine the performance of the PCM trombe wall. In the end a matrix definition will be shown, this calculation method will be used to simplify and combine all the calculations in one matrix notation.

4.1 ONE-NODE HEAT BALANCE

To determine the required power for heating or cooling a building two types of heat balance calculations can be adopted, the steady-state heat balance and the non-stationary heat balance. The first is only used to calculate the required energy for heating and cooling for time-independent situations (Spoel, 2017). The latter is used when temperatures and heat fluxes vary with time, they can be used to calculate the temperature inside a building or the energy needed to heat or cool a building over time. In this way, variations in temperature and solar radiation within different seasons or days can be incorporated (Spoel, 2017). Another important aspect which can be taken into account with this type of calculation is the effect of thermal mass.

These non-stationary heat balance calculations are based on the sum of the heat flows within the system. A simple model to determine the temperatures and heat fluxes at time (t) inside a building is the one-node model (Figure 1.56), the model of the room is also called the 'Control volume' (Spoel, 2017). The arrow indicates the direction of the corresponding energy flow, an incoming arrow implies a positive sign in the heat balance equation and a negative sign is used for the outgoing arrow. So if heat is flowing out of the control volume, this heat is lost from the *Control volume* to the surrounding environment and the numerical value of Q will be negative.

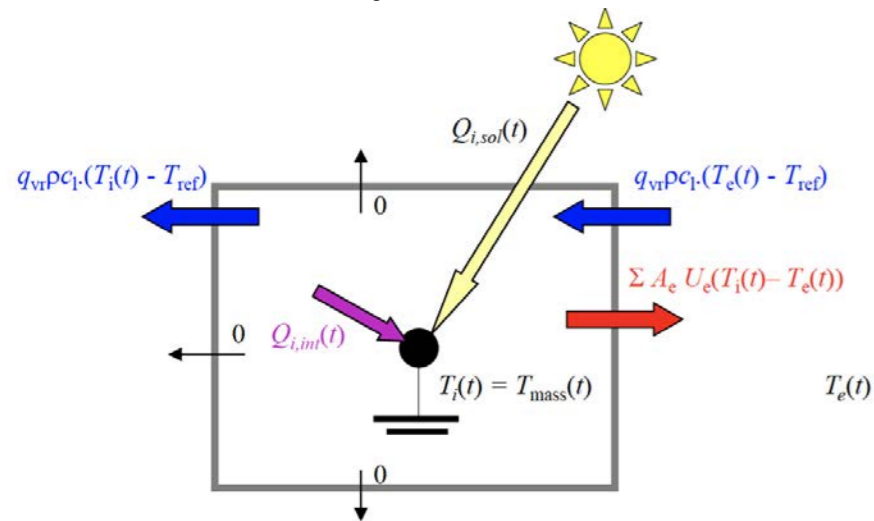


Figure 1.56
Graph illustrating the optimum investment costs
(By author: reproduced from Hasan, 1999)

The energy flows used to determine the temperature in the building (T_i) and therefore the energy needed for cooling or heating the building are related to the characteristics of the building and to its location. This heat balance is expressed in the following time dependent equation as sum of all the different energy flows:

$$g_{gl} A_{gl} q_{gl,sol}(t) + Q_{i,int}(t) + \sum A_e U_e \cdot (T_e(t) - T_i(t)) + q_{vr} \rho_l c_l (T_e(t) - T_i(t)) - M \frac{dT_i(t)}{dt} = 0 \quad (1.5)$$

g_{gl}	The fraction of the solar energy transmittance of the window
A_{gl}	The surface area of the window [m ²]
$q_{gl,sol}$	The incident solar radiation on the surface of the window [W/m ²]
$Q_{i,int}$	The internal heat production [W]

A_e	The surface area of the external partitions [m ²]
U_e	The heat transmission coefficient from the opaque external partitions [W/m ² .K]
Q_{tr}	The energy loss (or gain) by transmission and ventilation [W]
$Q_{i,tot}$	The total incoming heat (by people, equipment, lighting and the sun) [W]
M	The accumulation of energy in thermal mass [J/K]
$\rho_l c_l$	Volumetric heat capacity of air: 1200 J/(m ³ .K)
q_{vr}	The room ventilation flow [m ³ /s]
T_e	Outdoor air temperature [°C]
T_i	Indoor air temperature [°C]
H_{tot}	The total specific heat loss to the exterior [W/K]

This equation is expressed more concisely in the following equation, which is the sum of the three main energetic aspects:

$$Q_{i,tot}(t) + Q_{tr}(t) - M \frac{dT_i(t)}{dt} = 0 \quad (1.6)$$

With the internal loads and the loads from transmission expressed as follows:

$$Q_{i,tot}(t) = Q_{i,sol}(t) + Q_{i,int}(t) \quad (1.7)$$

$$Q_{tr}(t) = H_{tot}(T_e(t) - T_i(t)) \quad (1.8)$$

And where the indoor temperature is calculated using the following explicit expression, the loads assumed in this calculation are the average loads that occurred between time t and $t+\Delta t$.

$$T_i(t + \Delta t) = T_i(t) + \frac{\Delta t}{M} (Q_{i,tot}(t + \Delta t) + Q_{tr}(t)) \quad (1.9)$$

4.1.1 Incoming heat

The total incoming heat is the sum of the internal heat sources [W] and the incoming solar heat [W] as expressed in Equation (1.7). The internal heat gains of the building are a result of the heat produced by the people, appliances and devices. In offices these loads are important due to the high density of electrical equipment inside the building, such as computers, printers, coffee machines and other electrical appliances. An average load from all the devices together can be assumed for the total internal load ($Q_{i,app}$) on the relevant floor area of the space (A_{sp}), this is expressed in the following equation.

$$Q_{i;devices} = \sum A_{sp} q_{i;app} \quad (1.10)$$

The heat produced by people inside the space depends on the activity of the work (Menezes, Cripps, Buswell, Wright, & Bouchlaghem, 2014), the total heat produced by the people ($Q_{i;people}$) is the sum of the loads from the persons ($Q_{i;ps}$) with different activities for the amount persons in the room (n_{ps}). In this specific situation people doing normal office work will be assumed.

$$Q_{i;people} = \sum n_{ps} Q_{i;ps} \quad (1.11)$$

The incoming solar radiation penetrates the building through the transparent faces and is absorbed by the opaque surfaces of the envelope. This solar radiation is not absorbed by the air inside the room but by the construction parts such as the floor and the walls and by reflections towards other surfaces, this radiation is absorbed and increases the temperature at the surface. When this surface temperature exceeds the temperature from the room this heat is transferred to the room by conduction and convection (Figure 1.57). This heat can be absorbed by the thermal mass of the building to reduce these internal loads, this accumulation of heat will be explained in Section "4.1.3 Accumulation".

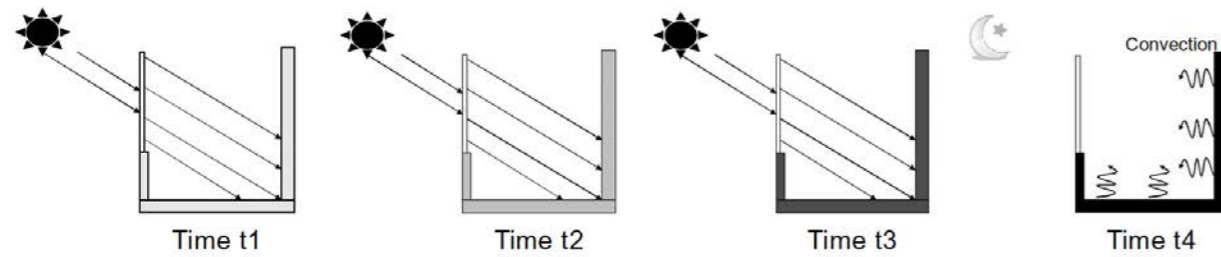


Figure 1.57
The process of absorption of solar radiation into the construction. Reprinted from " Sustainable Urban Environments by Itard, 2012

The heat gains from solar radiation depend mainly on the orientation, size (A_{window}) and properties of the windows (Itard, 2012). The percentage of solar radiation transmitted through the glass is referred to as the g-value (g_{glass}) or the solar heat gain coefficient (SHGC). This factor applies also to the exterior and interior sun shading (g_{shade}). In this calculation the effect of the thermal mass is neglected, this is included separately in the total heat balance. The total incoming solar radiation is expressed in the following equation:

$$Q_{i;sol} = \sum g_{glass} A_{window} g_{shade} q_{i;rad} \quad [W] \quad (1.12)$$

4.1.2 Transmission and ventilation

The difference in temperature between the exterior and the interior stimulates a heat flow through the envelope (i.e. walls, glazing, roof and floors). The amount of heat loss or gain depends on the temperature difference between the room (T_i) and the exterior (T_e). The transmission and ventilation are grouped together using the term H_{tot} . The transmission through the structure depends on the U-value, this is the overall heat transfer coefficient in W/m^2K , the surface area (A) of the structure in m^2 . The energy flows into or out of the building through openings (e.g., windows or grilles) or systems (e.g., mechanical ventilation) is determined

using the ventilation rate (q_{vr}), the density of the air (ρ) and the specific heat of the air (c_l) (Itard, 2012).

$$Q_{tr}(t) = H_{tot}(T_e(t) - T_i(t)) \quad (1.13)$$

$$H_{tot} = \sum U_e A_e + q_{vr} \rho_l c_l \quad (1.14)$$

The u-value can be calculated according to Equation (1.15), the R_c -value is the thermal resistance of the wall, this value can be calculated using the width of the wall and the thermal conductivity λ , a low thermal conductivity results in a high thermal resistance (Equation (1.16)). The α_o and α_i are the combined heat transfer coefficients for convection and radiation. For the interior surface (α_i) a value of $7.5 W/m^2K$ can be assumed because of a low air velocity inside the building.

$$U = \frac{1}{\frac{1}{\alpha_i} + R_c + \frac{1}{\alpha_o}} \quad [Wm^{-2}K^{-1}] \quad (1.15)$$

$$R_c = R_{c1} + R_{c2} + R_{c3} = \frac{d_1}{\lambda_1} + \frac{d_2}{\lambda_2} + \frac{d_3}{\lambda_3} \quad [m^2KW^{-1}] \quad (1.16)$$

4.1.3 Accumulation

The accumulation of heat within the building depends on a combination of the thermal mass M (J/K) within the building and the dependence on the temperature with time (Spoel, 2017). The thermal mass is determined according to the sum of all the components n with mass m_n and the specific heat c_n of the body (Equation (1.17)). This includes for instance the construction of the building (i.e. the walls, floors or ceiling), the air volume, and furniture (Spoel, 2017). In this way, high cooling loads within the building are avoided, which subsequently reduces the energy needed.

$$M = \sum_n (m_n c_n) \quad (1.17)$$

4.2 MULTI-NODE HEAT BALANCE

The aforementioned one-node heat balance model is only used when the single *Control volume* used to determine the indoor temperature is in direct contact with the surrounding environment. The *Control volume* in this research study is a single room which is part of a larger building, so two or more rooms are connected to this volume. More nodes will be added in the heat balance, each connected room will have a one-node room model to simulate the different temperatures from the adjacent rooms. First, an introduction will be given in the Two-node heat balance equations, this will be used as base for the more complicated multi-node heat balance. Heat flows between the rooms exist due to the exchange in air, this is indicated with the blue arrows between the rooms (Figure 1.58). The following equation applies to this two-node

room model and contains the sum of all the different heat flows with t' as the continuous time variable:

$$Q_{1,sol} + Q_{1,int} - \sum A_{1,e} U_{1,e} \cdot (T_1(t') - T_e(t')) - \sum A_{1,2} U_{1,2} \cdot (T_1(t') - T_2(t')) + (q_{v,1 \rightarrow e} + q_{v,1 \rightarrow 2}) \rho c_f T_1(t') + q_{v,e \rightarrow 1} \rho c_f T_e(t') + q_{v,2 \rightarrow 1} \rho c_f T_2(t') - M_1 \frac{dT_1(t')}{dt'} = 0 \quad (1.18)$$

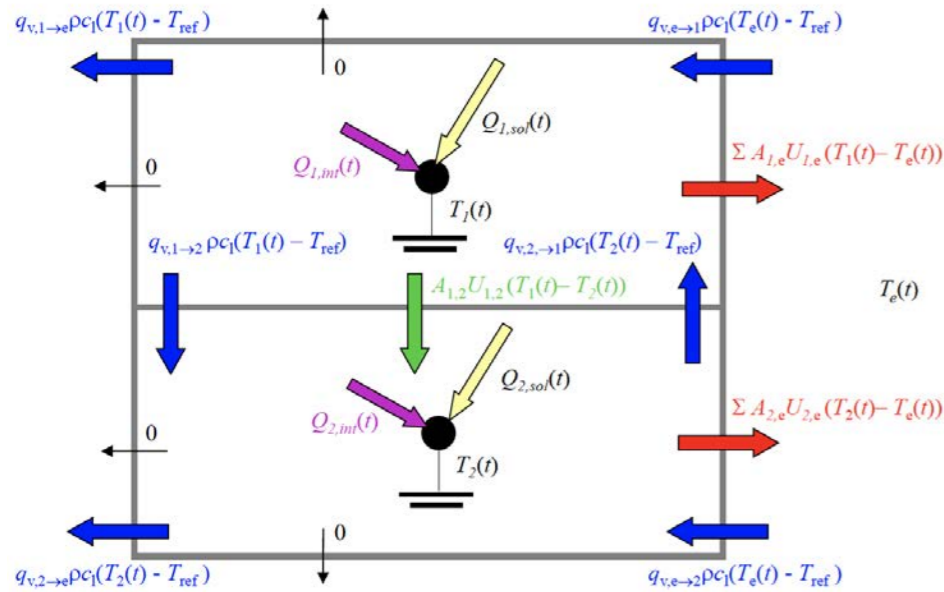


Figure 1.58
A two-node room model of two adjacent rooms. Reprinted from "Playing with heat balances" by Spoel, 2017

Equation (1.18) can be written more concisely by grouping the terms for ventilation and transmission in as $S_{1,e}$ and $S_{2,e}$ and the $Q_{1,tot}$ and $Q_{2,tot}$ groups the different heat loads affecting the temperature. The following two equations apply to room one and room two (Spoel, 2017):

$$Q_{1,tot} - S_{1,e} T_e(t') - S_{1,1} T_1(t') - S_{1,2} T_2(t') - M_1 \frac{dT_1(t')}{dt'} = 0 \quad (1.19)$$

$$Q_{2,tot} - S_{2,e} T_e(t') - S_{2,1} T_1(t') - S_{2,2} T_2(t') - M_2 \frac{dT_2(t')}{dt'} = 0 \quad (1.20)$$

And here the explicit expression of the temperature for room one reads as follows, again the loads assumed in this calculation are the average loads that occurred between time t and $t+\Delta t$:

$$T_1(t + \Delta t) = T_1(t) + \frac{\Delta t}{M_1} (Q_{1,tot}(t + \Delta t) - S_{1,e} T_e(t) - S_{1,1} T_1(t) - S_{1,2} T_2(t)) \quad (1.21)$$

4.2.1 Multi-node heat conduction

An important method which needs to be included in the final simulation for the heat balance of the room is the multi-node heat conduction. This equation simulates the heat that flows through the structure to the interior, this equation does not necessary result in a zero. When a heat flux is calculated to the room, the temperature inside this space will increase. This rate in temperature change is based on the thermal capacity M (J/K) of the control volume as shown in the following equation. This thermal capacity depends on the materials included in the room, when these materials are homogeneous the equation is expressed as shown in Equation (1.23).

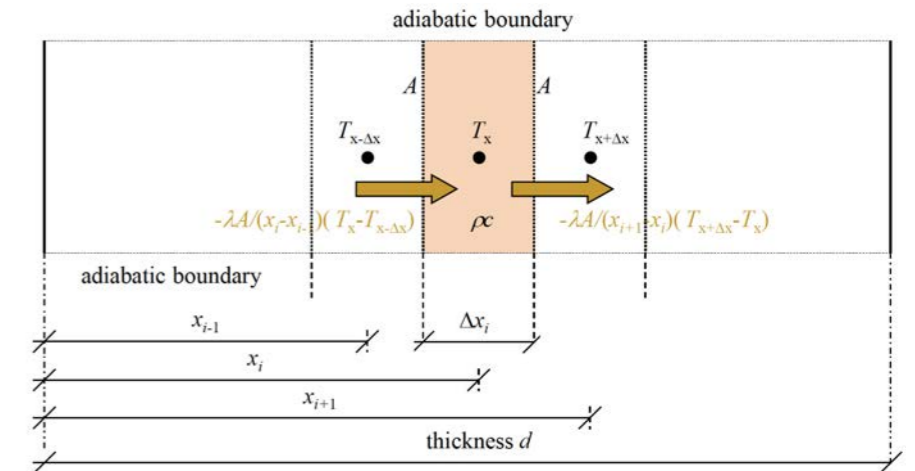
$$\sum Q = M \frac{\partial T}{\partial t} \quad (1.22)$$

$$M = \rho c V \quad (1.23)$$

Here the thermal capacity M is defined by the volume (V) of the control volume, the material's mass density (ρ) and the specific heat capacity (c) of the material.

The heat balance equation for conduction is based in the model shown in Figure 1.59, here the problem domain is subdivided in different layer slabs or control volumes. These volumes are numbered using the index i starting with number 1 at the left-side and counting towards to right and they all add up to the total number of control volumes (N) (Spoel, 2017). All the layers have a equal thickness expressed as (Δx_i), the temperature inside the control volume at position x_i is expressed as T_{x_i} [°C] which is positioned in the centre of the control layer. So the control volume depicted in Figure 1.59 is at located position $x = x_i$.

Figure 1.59
The one-dimensional heat conduction in a solid. Reprinted from "Playing with heat balances" by Spoel, 2017



Important for the heat balance equation are the relevant properties for conduction, these are the density of the material (ρ), the heat conduction coefficient in W/m.K (λ), the surface of the material in m^2 (A) and the specific heat capacity of the material (c). The equation is based on Equation (1.22) and is written as following:

$$\frac{-\lambda A}{x_i - x_{i-1}}(T_{x_i} - T_{x_{i-1}}) - \frac{-\lambda A}{x_{i+1} - x_i}(T_{x_{i+1}} - T_{x_i}) = \rho c A \Delta x_i \frac{\partial T_{x_i}}{\partial t} \quad (1.24)$$

The change in temperature from time $t(n)$ to $t(n+1)$ can be determined according to the following explicit scheme:

$$T_{x_i}^{(n+1)} = T_{x_i}^{(n)} + \frac{\Delta t^{(n)}}{\rho c A \Delta x_i} \left(\frac{-\lambda A}{x_i - x_{i-1}}(T_{x_i}^{(n)} - T_{x_{i-1}}^{(n)}) - \frac{-\lambda A}{x_{i+1} - x_i}(T_{x_{i+1}}^{(n)} - T_{x_i}^{(n)}) \right) \quad (1.25)$$

When not considering a homogeneous solid but multiple layers of material with different properties, the heat flux calculation must be expressed as shown in Equation (1.26). Here the different control volumes with varying properties such as the thermal capacity, the density and the heat conduction coefficient are indexed by the volume number shown as (i) or (i+x). In this situation the nodes are also placed in the centre of the control volume (Figure 1.60).

$$\frac{-A(T_{x_{i+1}} - T_{x_i})}{\frac{\Delta x_i}{2\lambda_i} + \frac{\Delta x_{i+1}}{2\lambda_{i+1}}} \quad (1.26)$$

The the scheme of the heat balance of a control volume $x = x_i$ which is situation adjacent to a different material is expressed as follows:

$$\frac{-A(T_{x_i} - T_{x_{i-1}})}{\frac{\Delta x_i}{2\lambda_i} + \frac{\Delta x_{i-1}}{2\lambda_{i-1}}} - \frac{-A(T_{x_{i+1}} - T_{x_i})}{\frac{\Delta x_i}{2\lambda_i} + \frac{\Delta x_{i+1}}{2\lambda_{i+1}}} = \rho_i c_i A \Delta x_i \frac{\partial T_{x_i}}{\partial t} \quad (1.27)$$

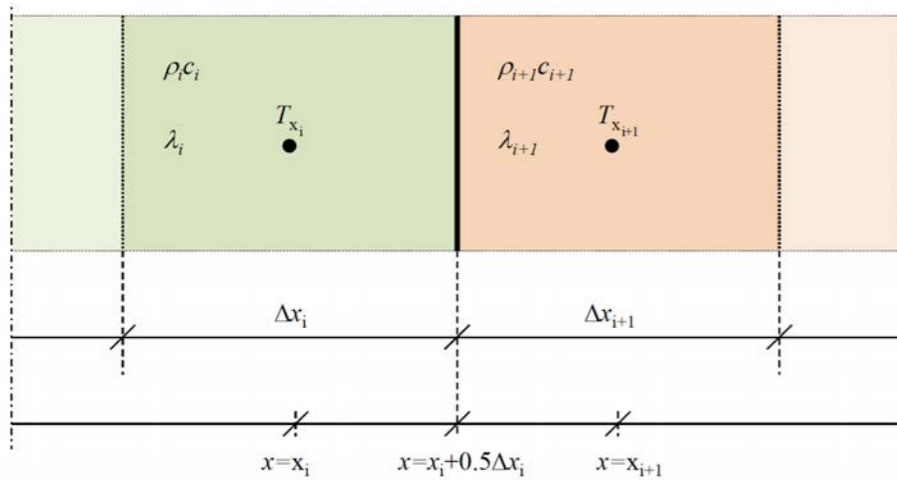


Figure 1.60
The one-dimensional heat
conduction in a solid.
Reprinted from "Playing with
heat balances" by Spoel,
2017

4.2.2 Non-stationary multi-node heat balances

The schemes become more complex when considering a practical situation for the heat balance

calculation, here more than just the one-dimensional heat conduction will be incorporated. Software tools are necessary for doing such calculations. MATLAB/Simulink will be used as simulation program for these calculations. A combination of all the heat balances together will be written down concisely in matrices, which include multiple calculations to define temperatures within different nodes spread across the control room. The working principle of these matrices will be illustrated using the Equations (1.19) and (1.20) from the two-node heat balance equation, here t is used instead of t' :

$$Q_{1,tot} - S_{1,e}T_e(t) - S_{1,1}T_1(t) - S_{1,2}T_2(t) - M_1 \frac{dT_1(t)}{dt} = 0 \quad (1.28)$$

$$Q_{2,tot} - S_{2,e}T_e(t) - S_{2,1}T_1(t) - S_{2,2}T_2(t) - M_2 \frac{dT_2(t)}{dt} = 0 \quad (1.29)$$

These equations can be expressed shorter using the following matrix notation:

$$\begin{pmatrix} Q_{1,tot} \\ Q_{2,tot} \end{pmatrix} - \begin{pmatrix} S_{1,e} \\ S_{2,e} \end{pmatrix} T_e(t) - \begin{pmatrix} S_{1,1} & S_{1,2} \\ S_{2,1} & S_{2,2} \end{pmatrix} \begin{pmatrix} T_1(t) \\ T_2(t) \end{pmatrix} - \begin{pmatrix} M_1 & 0 \\ 0 & M_2 \end{pmatrix} \begin{pmatrix} \dot{T}_1(t) \\ \dot{T}_2(t) \end{pmatrix} = 0 \quad (1.30)$$

Which is even expressed shorter by the following notation:

$$\mathbf{M}\dot{\mathbf{T}} + \mathbf{S}\mathbf{T} = \mathbf{Q} \quad (1.31)$$

In this notation the M is the mass matrix, S the stiffness matrix, Q the load vector, and T the vector with the (time-) dependent variables (Spoel, 2017). These different matrices contain a certain number (N) of equations denoted with $i = 1, 2, \dots, N$. All these equations together can be written down in the following matrix notation:

$$\begin{pmatrix} M_1 & & & & & & \\ & M_2 & & & & & \\ & & M_3 & & & & \\ & & & \ddots & & & \\ & & & & M_{N-2} & & \\ & & & & & M_{N-1} & \\ 0 & & & & & & M_N \end{pmatrix} \begin{pmatrix} \dot{T}_1 \\ \dot{T}_2 \\ \dot{T}_3 \\ \vdots \\ \dot{T}_{N-2} \\ \dot{T}_{N-1} \\ \dot{T}_N \end{pmatrix} + \begin{pmatrix} S_{1,1} & S_{1,2} & & & & & \\ S_{2,1} & S_{2,2} & S_{2,3} & & & & \\ & S_{3,2} & S_{3,3} & S_{3,4} & & & \\ & & \ddots & \ddots & \ddots & & \\ & & & S_{N-2,N-3} & S_{N-2,N-2} & S_{N-2,N-1} & \\ 0 & & & & S_{N-1,N-2} & S_{N-1,N-1} & S_{N-1,N} \\ & & & & & S_{N,N-1} & S_{N,N} \end{pmatrix} \begin{pmatrix} T_1 \\ T_2 \\ T_3 \\ \vdots \\ T_{N-2} \\ T_{N-1} \\ T_N \end{pmatrix} = \begin{pmatrix} Q_1 \\ Q_2 \\ Q_3 \\ \vdots \\ Q_{N-2} \\ Q_{N-1} \\ Q_N \end{pmatrix} \quad (1.32)$$

This matrix notation will be incorporated in the MATLAB/Simulink model, the differential equations for the temperature as a function of time are then solved by the program (Spoel, 2017). Important remarks for the inclusion of this matrix notation within this research study are the following:

- The mass and stiffness matrix contain positive values at the diagonal. For the stiffness matrix the off-diagonal values are always negative and for the mass matrix this can vary;
- The amount of control volumes and the numbering of these volumes is not important, the final solution for the temperature (T) will remain the same. (Spoel, 2017)

The incorporation of this information from the equations and the matrices in MATLAB will be explained in the following Section "5. COMPUTATIONAL PHASE".

4.3 CONCLUSION: PART IV

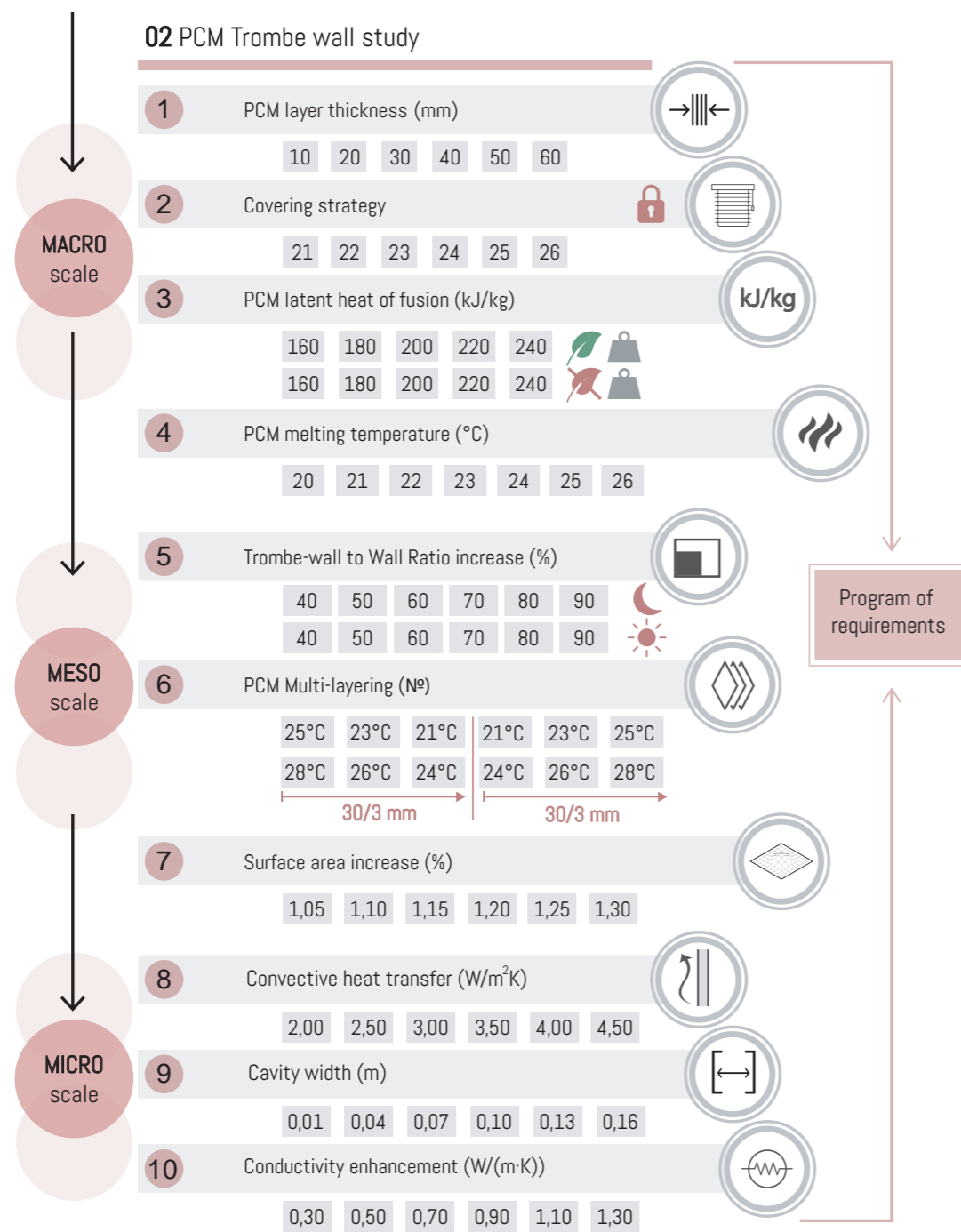
CHAPTER: "4. THERMODYNAMICS"

The knowledge from this chapter will be used as base knowledge for the development and the understanding of the thermodynamic principles within the simulation software that will be used. This thermodynamic principle is based on the non-stationary multi-node heat balance, three main flows of energy are determined within this heat balance, the incoming heat, transmission and ventilation and accumulation.

The incoming heat is the sum of the internal heat sources and the solar heat gains, these internal heat gains are for instance heat produced by the people, appliances and the devices. This design case focuses on heat balances in offices, here the internal heat gains are relatively high due to a high equipment density. Transmission and ventilation is the amount of heat lost to or gained through the structure or openings within the envelope due to the difference in temperature between the interior and the exterior. This is mainly based on the insulating properties of the wall, the size of the openings and the air flow rate from the mechanical ventilation. The accumulation of heat within the Control room is a combination of the thermal mass included within the building and the temperature. This thermal mass includes all the components within the building such as the construction partitions, the air within the room and the furniture for example, this thermal mass can be used to avoid cooling loads within the building.

The more detailed Multi-node heat conduction method is explained, this principle will be used to define the heat flows within the materials of the structure to know the exact temperature flow within the material. All these heat flows together result in complex and long equations, a matrix notation (Equation (1.32) on page 81) will be used to simplify these equations. They include multiple calculations to define temperatures within different nodes spread across the control room, simulation software is needed to undertake these complex calculations, a combination of MATLAB/Simulink will therefore be used.

Figure 1.61
Parameter indication for the Design of
Experiments within the computational study
(By author)



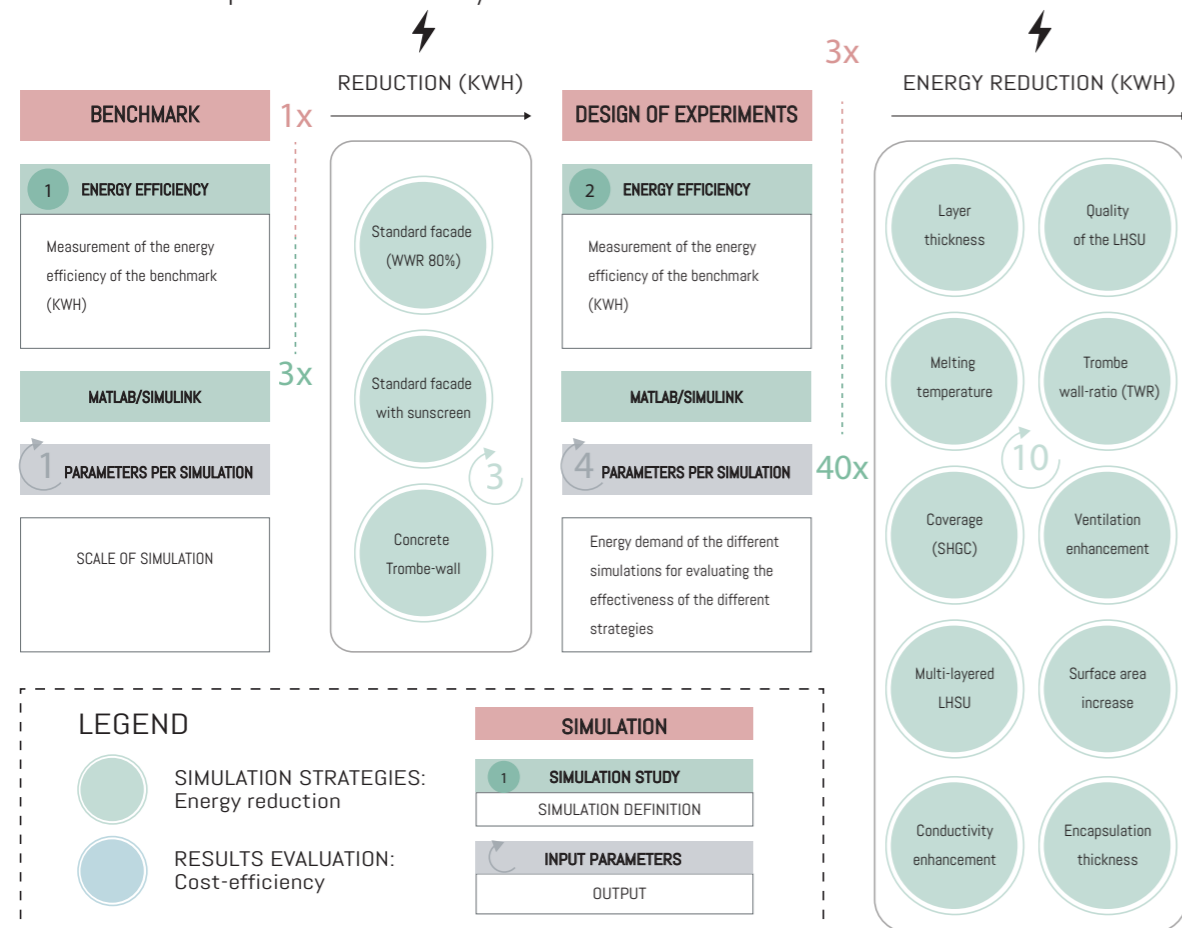
5. COMPUTATIONAL PHASE

This section elaborates on the simulation and optimization methodology, the use of the different parameters that will be adopted within the study and the verification and validation of the results from the simulation platforms. The first section will focus on the general work-flow of the simulation and the optimization. Secondly, an explanation is given on the parameters that will be used within the study together with the simulation setup within MATLAB/Simulink. Thirdly, a brief explanation on the extended simulation model is shown together with the verification and validation of the results from this model. Lastly, the optimization strategy is explained, all the information within this sections is the base for the actual simulation and optimization.

5.1 SIMULATION METHODOLOGY

Results from the literature study showed that different geometries and design additives can be used to improve the performance of a PCM Trombe-wall. The purpose of these simulations is comparing the different strategies on the actual energy reduction and cost-effectiveness. This will be evaluated using a combination of MATLAB® and Simulink®. This is a combination of textual and graphical programming, which can be used to design the thermal model of the office control room. The working principle of the systems is based on the code from MATLAB to define the temperatures at different nodes within model (Mathworks, 2019). These codes are used as input for the thermal room model in Simulink. The modeFRONTIER platform will be connected with this MATLAB/Simulink setup to optimize the results from the simulations using genetic algorithms, a more detailed explanation will be employed in Section "5.7 OPTIMIZATION STRATEGY"

A simplification of the strategies will be adopted due to the complexity of the total simulation, within this research study the focus will be on MATLAB and Simulink, no Computational Fluid Dynamics (CFD) will be used, in this way long simulation times are avoided. The more in-depth working principle of these simulation platforms and the model setup will be given in Section "5.3 INITIAL MATLAB / SIMULINK", an initial model of a PCM Trombe-wall will be used in this research study. The general work-flow of the simulation is shown below, the results from two benchmark studies together with ten optimization strategies from the Design of Experiments (DoE) will be used as input for the first evaluation on the cost-effectiveness. These thermodynamic studies will be employed using the MATLAB/Simulink setup, the results from this phase are mainly the temperatures within the room and the PCM Trombe-wall and the absolute energy reduction of the wall. The temperatures will be used to evaluate the performance more in detail and the energy reduction shows the overall performance of the system.



The detailed output per simulation strategy is given in Section "5.2 PARAMETER SPECIFICATION". This first phase is used to indicate the actual influence of each simulation parameter on the thermal performance, during the second phase the trombe wall will be optimized according to four optimization strategies. First the heating and cooling optimization are separated and after that a combined optimization will be done together with the economic optimization, in this way the impact of the different parameters on heating, cooling and costs can be evaluated. The results from all these simulation studies will be used as input for the program of requirements for the design phase, all these results will be summarized in a design guideline. Some basic limitations from this simulation study are:

1. All simulation studies will be done according to a 2D setup and the heat transfer is one-dimensional;
2. The sensible heat transfer within the PCM during the nucleation process is negligible;
3. The thermal properties of the PCM are kept constant within the simulation;
4. A pressure difference due to the effect of wind on the facade is neglected, a basic utilization factor will be assumed within this section according to a sensitivity analysis, elaboration on this in Section "5.6 VALIDATION RESULTS".
5. The surface depended optimization strategy will be simplified by using different characteristics of the wall such as the surface area and the convective heat transfer of the wall;

These limitations make use of some assumption regarding the convective heat transfer, self-shading of the system and no internal convection is accounted for within the study. Results from the literature study will be used to define the most effective methods for improving the internal convection and the heat transfer of the element. The next sections will elaborate more in detail on the definition of the parameters and the use of the simulation and optimization platforms.

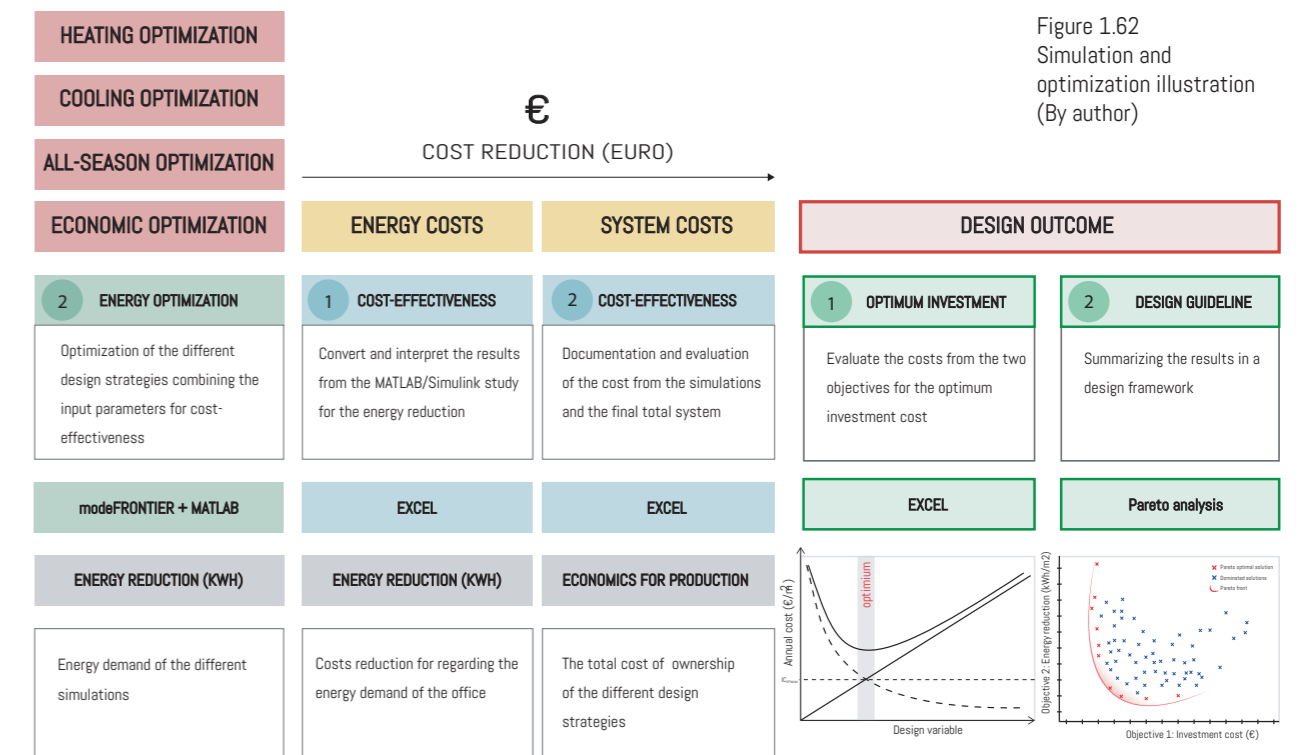


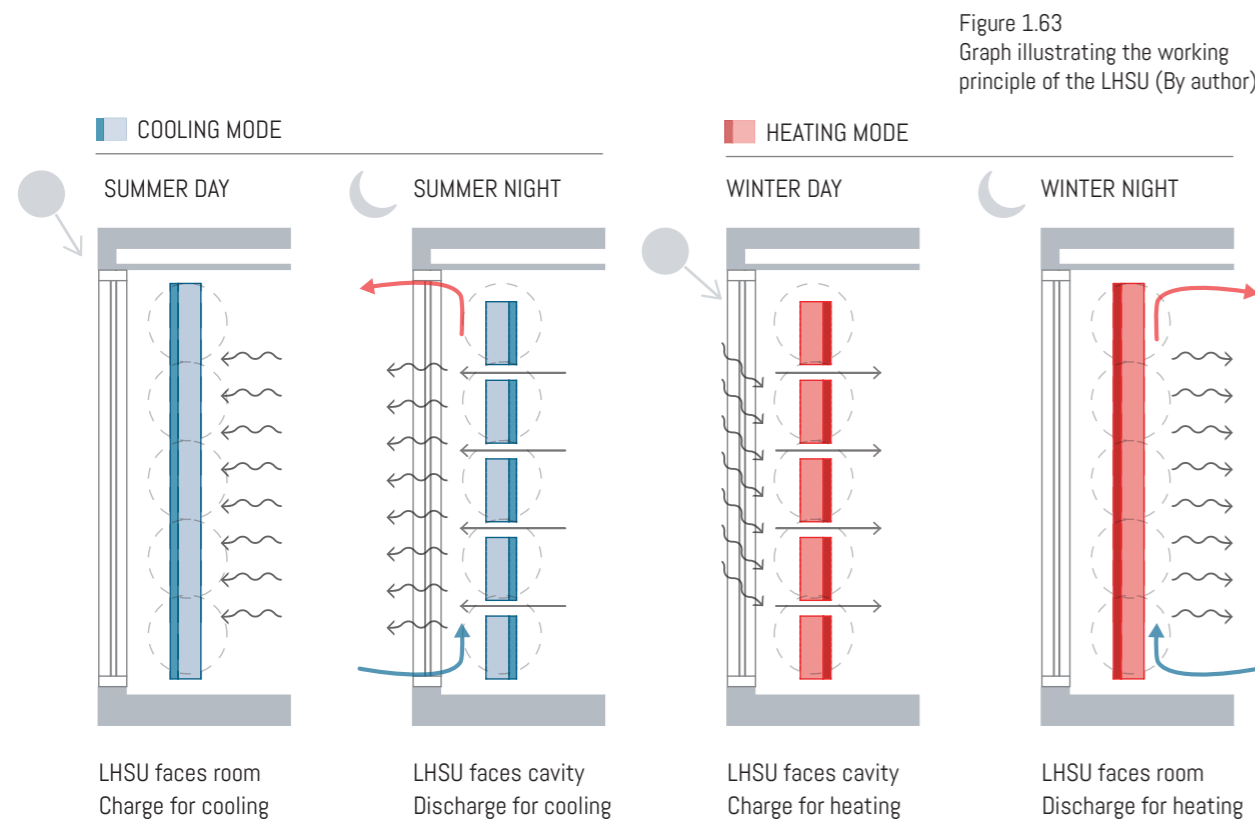
Figure 1.62 Simulation and optimization illustration (By author)

5.2 PARAMETER SPECIFICATION

As explained before, the LHSU will be used for year round application to reduce the energy of the office building. The most interesting part is the expected discrepancy in the results between the different seasons, the rate of heat change and the amount of heat stored for a simple passive design within a certain time span without sun radiation is determined by the following equation (Bokel, 2017):

$$E_{pcm} \cdot V_{pcm} \cdot \rho_{pcm} = \int \alpha_{pcm} \cdot Area_{pcm} \cdot (T_i - T_{pcm}) dt \quad (1.33)$$

Here it can be noticed that the time of heat storage (dt) depends on the temperature difference (ΔT), the properties of the PCM (E_{pcm} , ρ_{pcm} , α_{pcm}) and the dimension of the specimen (V_{pcm} and $Area_{pcm}$). These values for temperature will differ according to the different seasons of the year, higher temperatures differences between the interior and the exterior will lead to higher transmission values. In addition, a higher radiation will also increase the surface temperature of the specimen which subsequently increases the air temperature in the cavity. At a certain point, the longer it takes for the PCM to melt the lower the melt fraction of the system and therefore less PCM is activated. This must be prevented to create a system which makes optimal use of the material. The starting point of this simulation study uses the following charging and discharging setup for the heating and cooling season during the day and at night:



Some basic assumption will be done according to the working principle of the LHSU, the following assumptions are based on results from previous researchers to simplify the simulation study. In this way a more detailed simulation can be carried out and less time is needed to simulate these set-ups.

- A cavity thickness of 47 mm is advised (Tenpierik, et al., 2018) and will be used to prevent self-shading of the system from the overhang of the facade;
- An insulated Trombe wall is more effective in colder climates since less heat is lost to the

exterior (Hu, He, Jia, & Zhang, 2017). A u-value of around 0,020 W/m².K is advised to improve the efficiency (Tenpierik, et al., 2018);

- An adjustable Trombe wall increases the efficiency using a rotation principle as illustrated in Figure 1.63 (Tenpierik, et al., 2018);
- The LHSU will have a standard height of 2.700 mm, according tot he room height;
- Double clear glazing will be used on the outside of the LHSU, research from Van Unen (2018) showed the best performance with this type of glazing.
- The starting properties of the PCM will be based on the SP25E inorganic compound from Rubitherm, these properties are listed in Figure 1.64 (LHSU Properties, information from Section "3.1 CONTEXTUAL").
- The predefined parameters regarding the properties of the Control room and the users are also specified in Figure 1.64 (information from Section "3.1 CONTEXTUAL").

The other more detailed parameters with reference to for instance the ventilation rate, the hysteresis dead band and the absorption coefficients of the different materials are defined in Table 1.6 in "3. DESIGN CONTEXT".

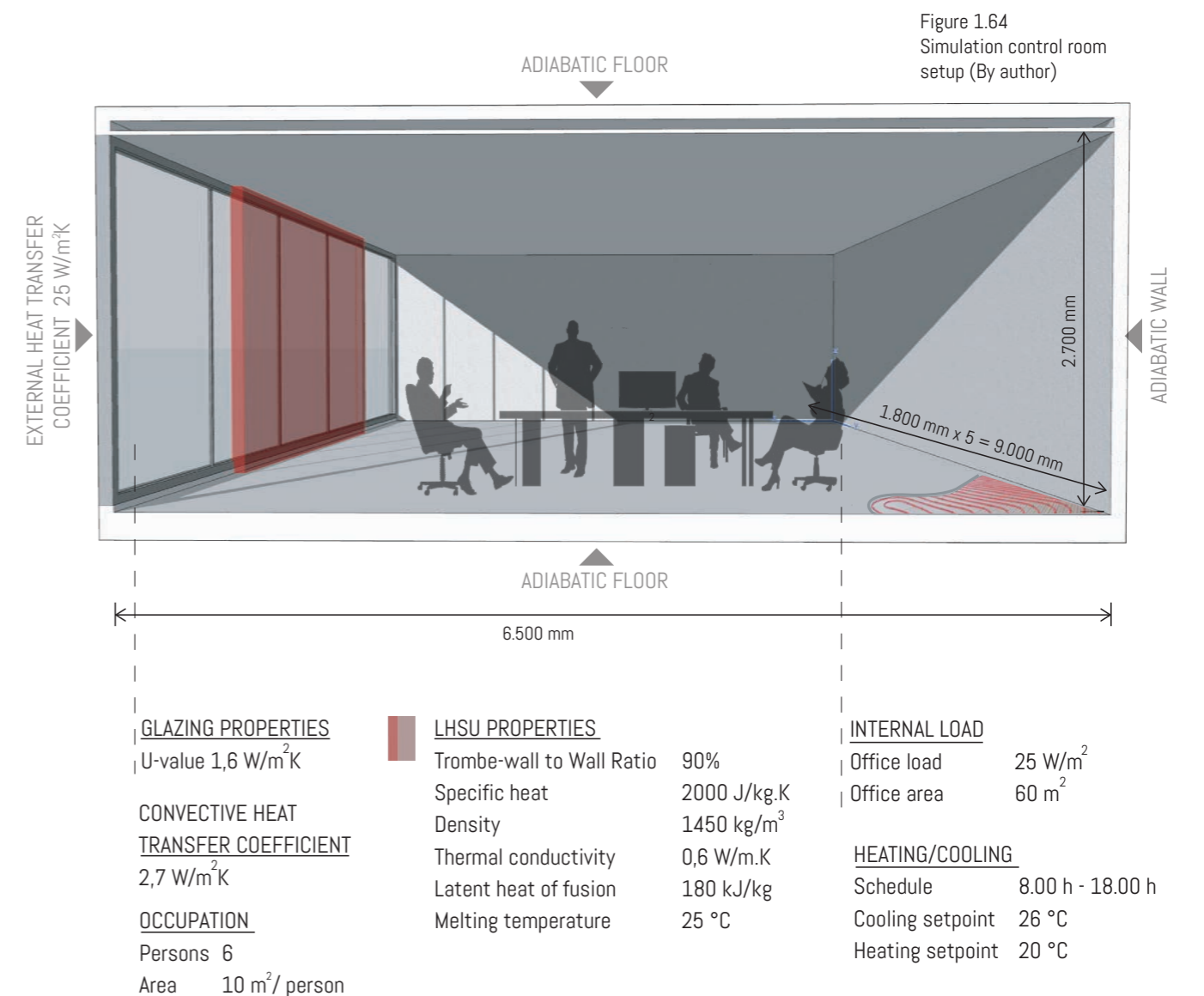
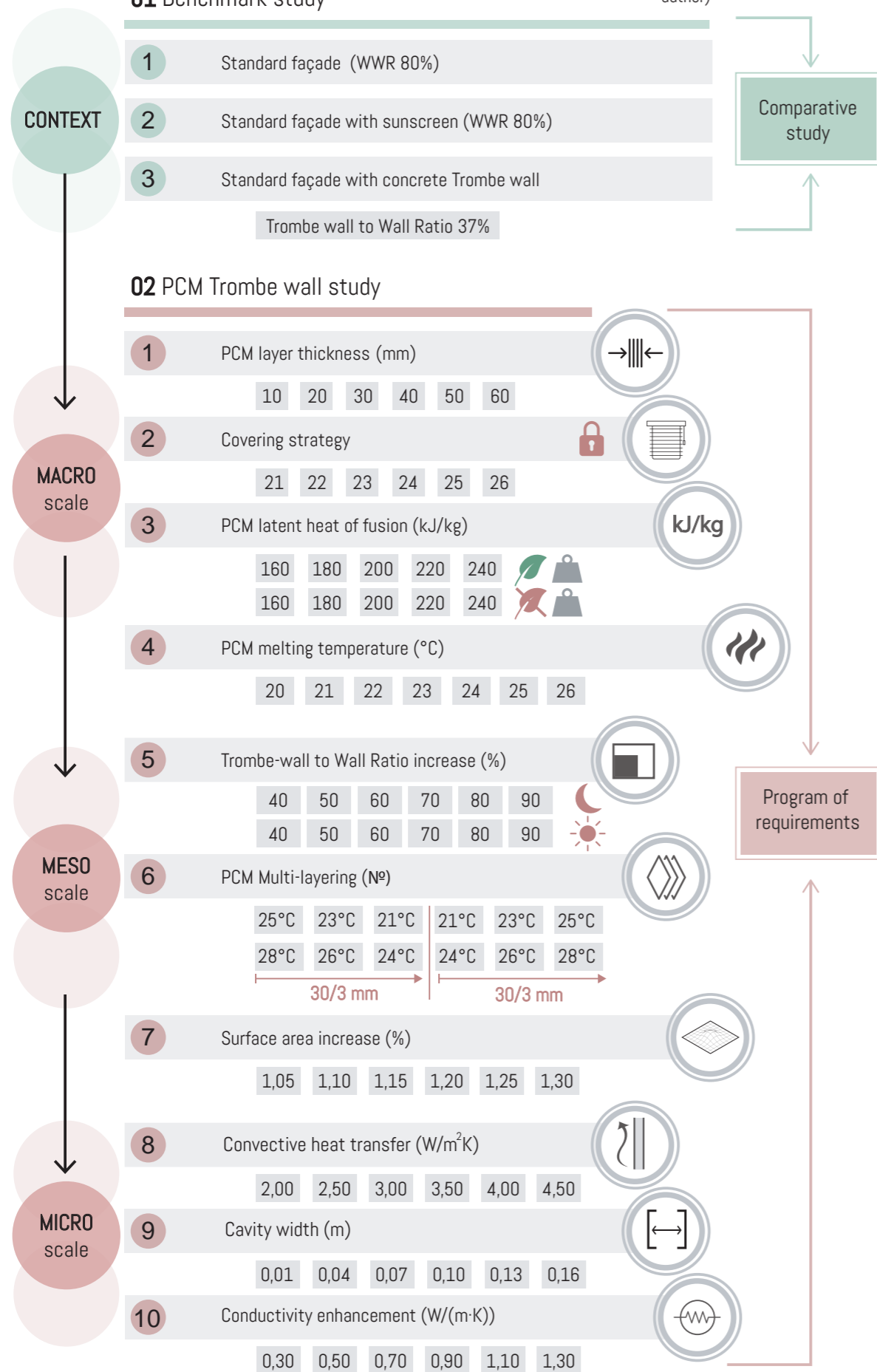


Figure 1.65
Simulation methodology and
enhancement techniques (By
author)



5.2.1 Benchmark

During this simulation first three benchmark studies will be done to define the basic energy consumption of the office room (Figure 1.65). The first simulation is based on a facade with a window-to-wall ratio of 80%, a modern building with a fully glazed south facade. The second and third simulations are based on a facade with a sunscreen or a concrete trombe wall, these situations are used to compare the effectiveness of the PCM with the more conventional systems. The variable parameters that will be considered during this research study will now be discussed. Here, the layer thickness, the material properties, the Trombe-wall to Wall Ratio (TWR), the ventilation enhancement, the SHGC enhancement and the insulation values will be simulated to increase the effectiveness of the LHSU. An overview of these simulation steps and the corresponding parameter values is illustrated in Figure 1.65 (PCM Trombe wall study). The symbols below each simulation strategy indicate the output from that specific simulation to evaluate the performance.



5.2.2 MACRO: PCM Layer thickness

The layer thickness of the PCM within the LHSU is important to evaluate the amount of PCM activated within the different seasons. So which thickness is most effective considering the energy reduction and cost-effectiveness. Important for the performance of the system is preventing the material from overheating, the organic PCM mixture with a melting temperature of 21 °C from Rubitherm Technologies GmbH (RT21) has for instance a maximum operation temperature of 45 °C (Rubitherm, 2019).

A first simulation will show the general differences between the thicknesses within the seasons, an assumption will be made for the material properties, the SP25E mixture from Rubitherm will be used to define the thickness. A second simulation will be done to evaluate the difference in thickness more in detail. The results in energy reduction and cost-effectiveness from different thicknesses will be used as input for the following simulations.



5.2.3 MACRO: Coverage (SHGC)

Different strategies can be adopted to improve the solar heat gain coefficient of the system, in standard situation a sunscreen is used to block direct solar radiation and to prevent room from overheating. A study from Koo, Lee, An and Lee (2018) showed that the SHGC also improves by using different ventilation strategies, they improved the SHGC by around 52% using ventilation in a cavity compared to a situation without ventilation (Koo, Lee, An, & Lee, 2018), a simplification of these strategies will be used in this simulation. Only the value of the SHGC will be changed together with the moment of activation. On a warm

summer day the direct solar radiation on the LHSU must be blocked and on the in-between season this same amount of radiation is desired due to lower outdoor temperatures. The results will show the effect of improving this SHGC in the different seasons. It is expected that this covering strategy significantly increases the performance of the system, therefore the most optimum result from this simulation will be used as new starting point for the following simulations.



5.2.4 MACRO: Melting temperature

Literature showed that the melting temperature is best to be chosen close to the comfortable set-point temperature for heating and cooling, this results in a different set-point temperature for both seasons. The difference in energy reduction from choosing two different types of PCM will be compared to the outcome by using a single type of PCM for both heating and cooling to indicate the actual difference in energy reduction. Information from several manufacturers shows that different melting temperatures are accompanied with various values for the latent heat of fusion and the conductivity, the material types from two reliable manufacturers (Rubitherm and PlusIce) show that higher melting temperatures contain a higher latent heat of fusion. The optimization of these properties will be separated to indicate the differences. The latent heat of fusion and other properties will in this case be defined according to the properties of the SP25E (Figure 1.64).

Table 1.7 Summarized overview showing the properties of different PCM types used in the Built environment, information obtained from "APPENDIX D"

#	Type	PCM Type	Value Unit	Conductivity	Reference
01.1	Pure material (10.000 kg)	Rubitherm SP21E ($\Delta H = 170 \text{ kJ/kg}$)	2,14 €/kg	0,6 W/m.K	(Rubitherm, 2018)
		Rubitherm SP24E ($\Delta H = 180 \text{ kJ/kg}$)	2,01 €/kg	0,6 W/m.K	(Rubitherm, 2018)
		Rubitherm SP25E ($\Delta H = 180 \text{ kJ/kg}$)	1,89 €/kg	0,6 W/m.K	(Rubitherm, 2018)
		PlusICE S21 ($\Delta H = 170 \text{ kJ/kg}$)	2,00 €/kg	0,54 W/m.K	www.pcmproducts.net
		PlusICE S22 ($\Delta H = 175 \text{ kJ/kg}$)	2,00 €/kg	0,54 W/m.K	www.pcmproducts.net
		PlusICE S23 ($\Delta H = 175 \text{ kJ/kg}$)	1,75 €/kg	0,54 W/m.K	www.pcmproducts.net
		PlusICE S24 ($\Delta H = 180 \text{ kJ/kg}$)	1,50 €/kg	0,54 W/m.K	www.pcmproducts.net



5.2.5 MACRO: Latent heat of fusion

As said, PCMs with different melting temperatures also have a difference in the latent heat capacity. Besides this also different qualities and types of PCMs are available on the market, Rubitherm Technologies GmbH in particular manufactures a high quality organic mixture (PCM RT-line) with a higher latent heat capacity. The RT21 HC for instance has an increase capacity of 35 kJ/kg, however the price of these mixtures is also double compared to the standard organic mixtures from Rubitherm ("APPENDIX E"). And they also manufacture inorganic PCMs (PCM SP-line), the difference between these organic and inorganic mixtures is mainly the density and the conductivity of the material, which results in a higher heat capacity per unit volume (kJ/m³.K). Therefore two simulations will be done comparing the outcome from organic and inorganic mixtures, the inorganic compound will have the values from the starting point (Figure 1.64) and the organic compound is based on the values shown in Table 1.8. The results will be used to indicate the difference in energy reduction from the different mixtures. The materials that will be considered are listed below:

Table 1.8 Overview of the values that will be employed within the latent heat simulation, information obtained from ""

#		Latent heat of fusion Unit	Density Unit	Conductivity	Value Unit
01.1	Organic	160 kJ/kg	850 kg/m ³	0,2 W/m.K	€/dm ³
		180 kJ/kg	850 kg/m ³	0,2 W/m.K	€/dm ³
		200 kJ/kg	850 kg/m ³	0,2 W/m.K	€/dm ³
		220 kJ/kg	850 kg/m ³	0,2 W/m.K	€/dm ³
		240 kJ/kg	850 kg/m ³	0,2 W/m.K	€/dm ³
01.2	Inorganic	160 kJ/kg	1450 kg/m ³	0,6 W/m.K	€/dm ³
		180 kJ/kg	1450 kg/m ³	0,6 W/m.K	€/dm ³
		200 kJ/kg	1450 kg/m ³	0,6 W/m.K	€/dm ³
		220 kJ/kg	1450 kg/m ³	0,6 W/m.K	€/dm ³
		240 kJ/kg	1450 kg/m ³	0,6 W/m.K	€/dm ³



5.2.6 MESO: Trombe wall to Wall Ratio (TWR)

This simulation will include the ratio of the total surface area of the LHSU related to the total south facade, a fully glazed south facade will be considered. The objective is to find the optimal ratio of the wall in the different seasons of the year, a reduction of the total area of the Trombe wall on the south facade is beneficial for the visual accessibility and the amount of daylight entering the building. A difference in result is expected due to the unwanted direct solar radiation in summer and the useful direct solar radiation in winter. Results from the literature study showed a optimal TWR of 37% for a normal concrete Trombe wall,

however this is based on year round application. This simulation will contain two steps, the first step is to give a general overview of the impact of the difference in TWR. The results from this study will be adopted in a more detailed simulation. Important is the actual improvement in energy reduction, a 100% covered south-facade will not be beneficial if the difference in energy and cost reduction is small.



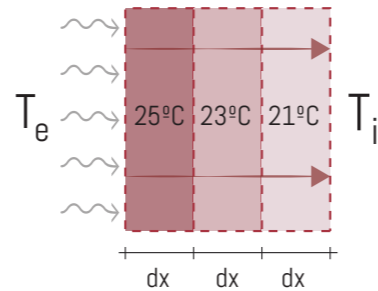
5.2.7 MESO: Multi-layered LHSU

In the multi-layered simulation the objective is to find the optimal amount of PCM layers. A vertical cascading strategy will be adopted in which the system is constructed out of various layers, all with different melting temperatures as shown below. The different ascending and descending melting temperatures in are listed Table 1.9 together with the corresponding thicknesses. The multi-layered system will have a fixed dimension according to the optimal thickness from the first optimization study. A second study will be used to show the difference in energy reduction by preserving a layer thickness of 30 mm as shown in Table 1.9 (data-sheet 01.1 and 01.3).

A fixed TWR will be determined for both seasons to simplify the simulation. So the optimization strategy will vary between the different seasons regarding the thickness, melting temperature strategy and the amount of layers.

Table 1.9 Summarized overview of the values that will be employed within multi-layered optimization

#	Melt temperature	Thickness Unit
01.1 Layers 1-2-3	21-23-25 °C	10-10-10 mm
Layers 1-2	21-25 °C	15-15 mm
Layer 1	21 °C	30 mm
01.2 Layers 1-2-3	25-23-21 °C	15-15-15 mm
Layers 1-2	25-21 °C	15-15 mm
Layer 1	25 °C	15 mm
01.3 Layers 1-2-3	23-25-27 °C	10-10-10 mm
Layers 1-2	23-27 °C	15-15 mm
Layer 1	23 °C	30 mm
01.4 Layers 1-2-3	27-25-23 °C	10-10-10 mm
Layers 1-2	27-23 °C	15-15 mm
Layer 1	27 °C	30 mm



5.2.8 MESO: Surface area

Results from literature study showed already the effect of increasing the heat transfer rate by an increased surface area. Different shapes can be used to increase the heat transfer coefficient of the specimen. Figure 1.54 shows the effect of the depth and width of the articulation of the surface, important to notice is that the heat transfer coefficient is higher for the surface area with the more wide and smooth surface, the morphing of the surface in horizontal direction shows less effect on the heat transfer rate (Cupkova & Promopattum, 2017). A minimum of 25 mm in depth and 100 mm in width showed the best results. The coefficient becomes greater when the temperature increases, the second specimen (S1_B) showed the most promising results regarding the improved heat transfer coefficient. The ratio of surface increase in this research study is around 1.25 and 1.30, this number will be used as the maximum ratio of the increase in surface area. A higher number means a more protruded surface, which can affect the performance due to a higher change for self-shading. A simplified strategy will be adopted for the simulation, the surface area will be changed but no 3D shape will be simulated, in the actual performance the shape will effect the amount of heat transferred. A more smooth surface creates more direct contact with the air and increases the rate of heat transfer.

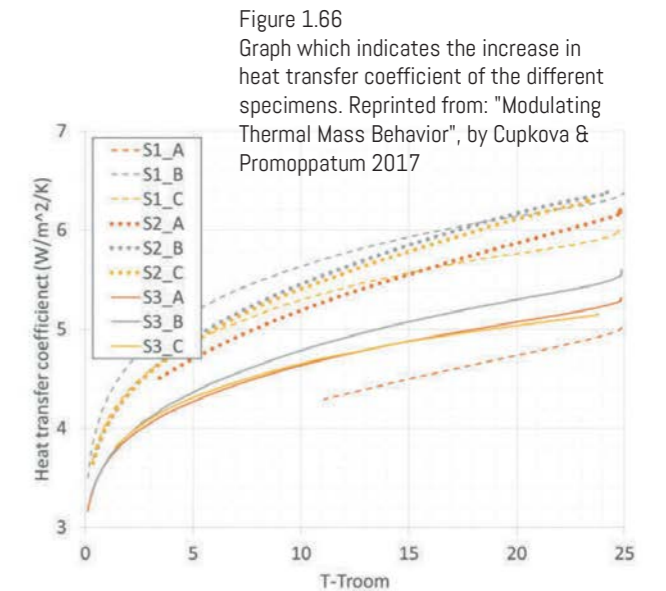
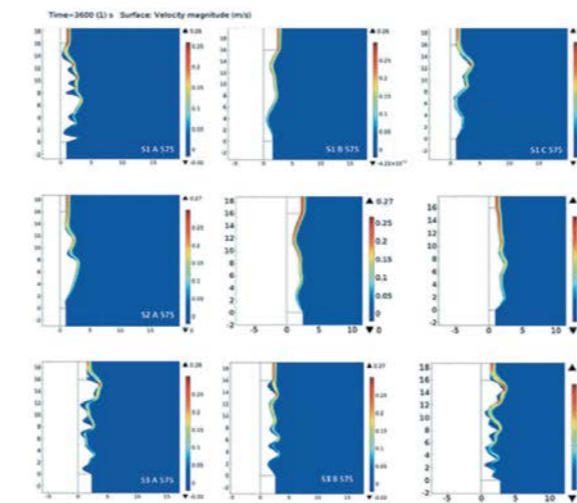


Figure 1.66 Graph which indicates the increase in heat transfer coefficient of the different specimens. Reprinted from: "Modulating Thermal Mass Behavior", by Cupkova & Promopattum 2017



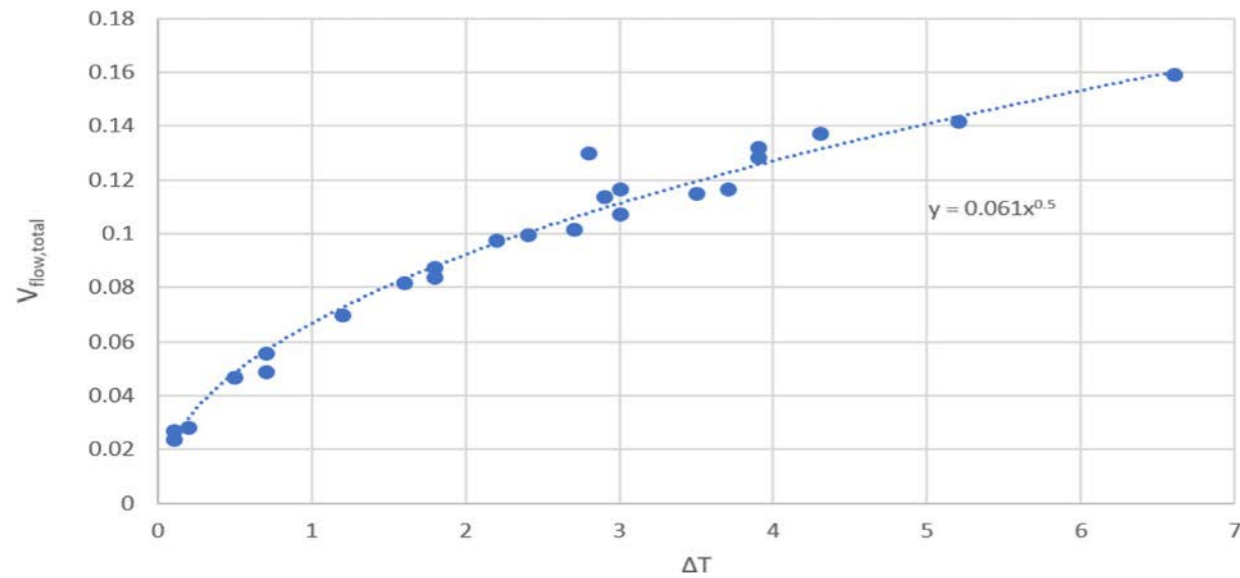
5.2.9 MICRO: Ventilation

The heat loss coefficient of the wall is highly related to the air velocity in the cavity. The ventilation flow (m³/s) between the cavity and the room is determined according to the temperature difference between the two, the effective area of the opening between and the height difference from these openings. The coefficient C_1 is used to define the rate of the ventilation between the two spaces, which emulates the effect of the air exchange based on the temperature difference between the cavity and the room (dT). This coefficient (C_1) will be changed within the MATLAB/Simulink, a direct correlation between the openings and the coefficient will be added. A study from Van Unen (2018) showed the coefficient for an opening size

of 10%, this coefficient is calculated according to the curve fitting method (Figure 1.67). In this way the coefficient changes with the change in opening size, these are directly related to each-other (Designbuilder, n.d.). This direct correlation will be adopted within the MATLAB script, the $C_1 = 0.061$ relates to an opening size of $3.6 \times 2.7 \times 10\% = 0.972 \text{ m}^2$ (Unen, 2018).

$$Q_f = C_1 (dT)^{Cn} \quad [\text{m}^3/\text{s}] \quad (1.34)$$

Figure 1.67
Graph used to determine the flow coefficient.
Reprinted from: "The energy and Comfort Performance of a Lightweight Translucent Adaptable Trombe Wall", by Unen 2018



5.2.10 MICRO: Convective heat transfer enhancement

The properties related the surface of the LHSU can be improved to increase the amount of heat transferred between the surface of the wall and the adjacent air. The literature study showed that different surface geometries and different materials affect the convective heat transfer coefficient ($\text{W}/\text{m}^2/\text{K}$). Figure 1.66 shows that this coefficient can go up to $6.5 \text{ W}/\text{m}^2/\text{K}$ for the heat transfer at room temperature level. This research from Cupkova and Promoppatum (2017) showed that a rough smooth finished surface increases this heat transfer coefficient, but small air pockets arise when the surface is too rough. These air pockets negatively affect the heat transfer between the two bodies. For this study an upper bound of $6.5 \text{ W}/\text{m}^2/\text{K}$ will be used and a lower bound of $2.5 \text{ W}/\text{m}^2/\text{K}$.



5.2.11 MICRO: Conductivity enhancement

As mentioned before, the conductivity of the material is important for the heat transfer rate through the unit, high conductive additives such as graphite and nickel particles or by using a high conductive addition within the system such as metal fins. The aqueous dispersion of r-GO (Graphene oxide) is for instance an interesting candidate to improve this thermal conductivity of salt-hydrates, this material can directly be used as additive within this compound. A research study from Zhang et al. (2018) showed that the thermal conductivity could be increased by 80% while reducing the latent heat of fusion by just 2,7%. For a normal salt-hydrate from Rubitherm this means an increase in thermal conductivity from $0,6 \text{ W}/\text{m}\cdot\text{K}$ to around $1,08 \text{ W}/\text{m}\cdot\text{K}$. For this simulation study this value will be used as maximum increase in conductivity to evaluate the possible effect of using this strategy.

In the design phase this increase in conductivity is related to different aspects indicated in the literature study, this study showed that the internal conductivity can be improved by increasing the density of the product (i.e. different material), by incorporating high conductive additives or by adding external conduction members such as fins.

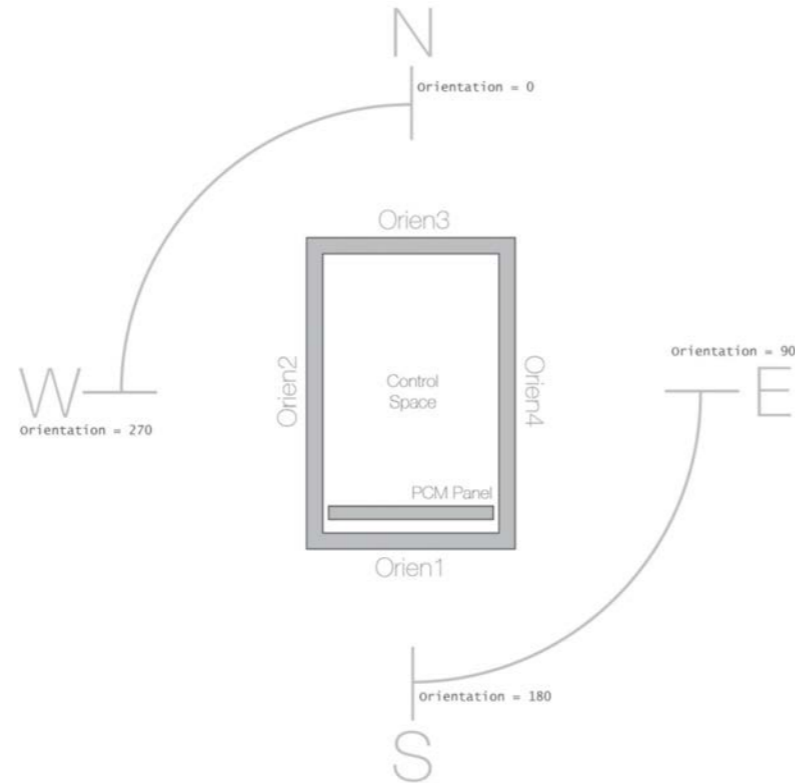


5.3 INITIAL MATLAB / SIMULINK

The simulation model that will be used for this thermodynamic analysis is obtained from the DoubleFace 2.0 research project (Tenpierik, Wattez, Turrin, Cosmatu, & Tsafou, 2018), this model is further developed by Van Unen (2018) to analyse the behaviour of the PCM within different climates and building typologies. This base model will be adapted to evaluate the energy performance of the wall considering the different detailed design optimization strategies. The model is developed using a combination of MATLAB® and Simulink®, this combines textual and graphical programming to design a system in a simulation environment (Mathworks, 2019).

The initial simulation model is based on a simple cubicle room known as the 'Control room' (Figure 1.68). The PCM facade panel is set behind the south facing facade (Orien1), this will stay fixed within the simulation. The other walls are named Orien2, Orien3 and Orien4, which will be referred to according to the corresponding cardinal orientation. So the Orien1 facade refers to an orientation of 180 degrees, which is in south direction. The command used for this orientation is: `Orientation = 180`

Figure 1.68
Definition of the control space and the orientations.
Reprinted from: "Thermal simulations, DoubleFace Project", by Lara, Tenpierik, Spoel, & Turrin, 2015



The dimension of this 'Control room' are determined using the following commands, these command are separated from each-other in the script. The depth of the room is variable and determines the width, volume and area within the script.

```
% ----- VARIABLES -----
orientation = 0;      % 0 = north, 90 = east, 180 = south, 270 = west
room.depth = 4.45;   % 4.45 = small room, 10.00 = big room
% ----- SCRIPT -----

room.width = room.depth;           % in this case in orien2-orien4 direction
room.height = 2.7;                 % 2.7 in every simulation
room.volume = room.depth*room.width*room.height; % air volume room, depth x width x height [m3]
room.area = room.depth*room.width;
```

5.3.1 Nodes definition

The nodes within the definition of the model are used to determine the different layers of the construction envelope. In total 25 nodes are used to define the structure, each facade and roof structure is constructed out of three separates layers with a node at every demarcation, so four nodes per element. And one final node is placed in the middle of the 'Control volume', all these nodes are used to determine the temperature at all these specific points in the model.

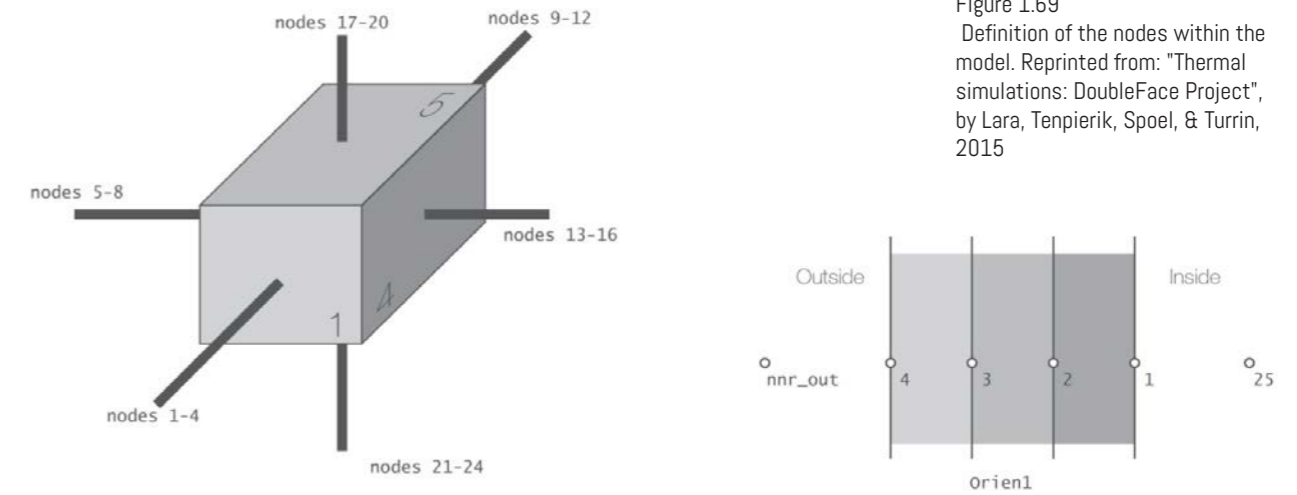


Figure 1.69
Definition of the nodes within the model. Reprinted from: "Thermal simulations: DoubleFace Project", by Lara, Tenpierik, Spoel, & Turrin, 2015

The nodes within the LHSU is defined by the number of control volume layers of the PCM ($n1_{pcm}$) and of the insulation ($n1_{ins}$) together. The total amount of layers is for the simulation is one for the $n1_{ins}$ and three for the $n1_{pcm}$, which results in a total of 6 nodes within the LHSU (Figure 1.70). And the final node, number 32, is represented by the outside air. All these number of nodes from the construction envelope stayed the same within the different calculations.

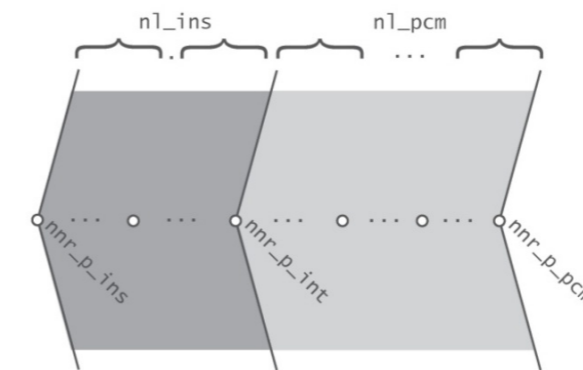


Figure 1.70
Modes of heat transfer within the model. Reprinted from "Thermal simulations: DoubleFace Project", by Lara, Tenpierik, Spoel, & Turrin, 2015

5.3.2 Heat transfer mode

The modes of heat transfer within the constructions are defined by Lara et al. (2015) according to the three main modes of heat transfer that occur on a body. Two schematic figures show the heat transfer mode for the different layer volumes of the standard walls (Figure 1.71) and for the PCM Trombe wall (Figure 1.72).

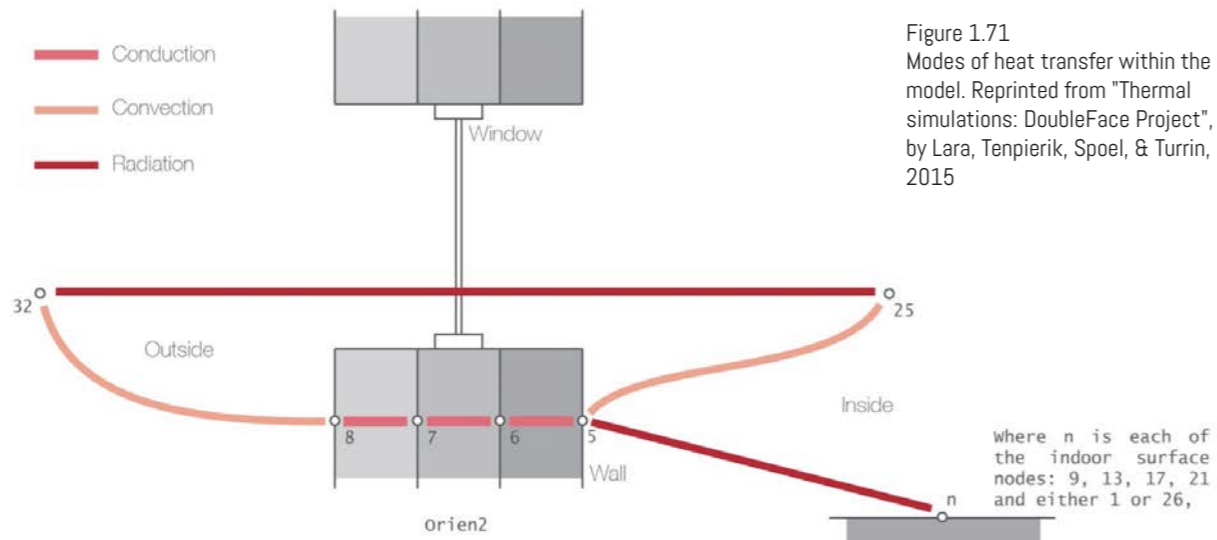


Figure 1.71
Modes of heat transfer within the model. Reprinted from "Thermal simulations: DoubleFace Project", by Lara, Tenpierik, Spoel, & Turrin, 2015

Each layer within the structure contains one node, the amount of control layers within the PCM and insulation differ from the standard wall. The standard structure contains 4 nodes and the PCM Trombe wall accommodates 5 nodes in total as shown below.

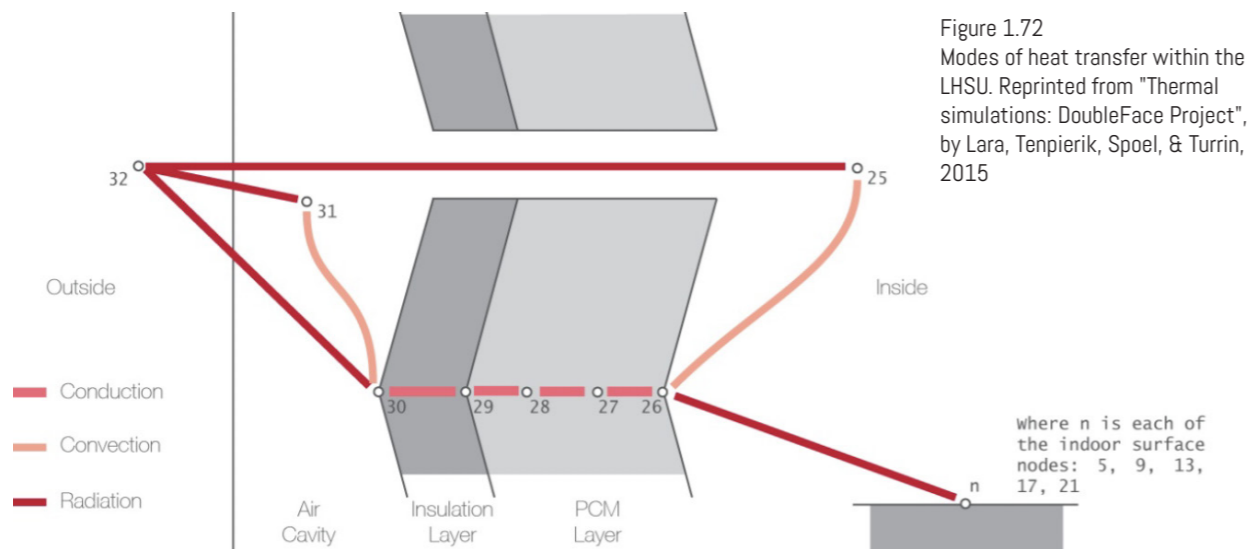


Figure 1.72
Modes of heat transfer within the LHSU. Reprinted from "Thermal simulations: DoubleFace Project", by Lara, Tenpierik, Spoel, & Turrin, 2015

5.3.3 Fixed simulation parameters

As mentioned before, the target climate of this study will be the temperate climate from Amsterdam, the Netherlands, a new office building will be simulated in this climate. In medium-weight office buildings in a temperate climate the trombe wall performance best in absolute sense (Van Unen, 2018), so the highest annual energy savings were recorded in these buildings for both heating and cooling (`building_method_type = 2`).

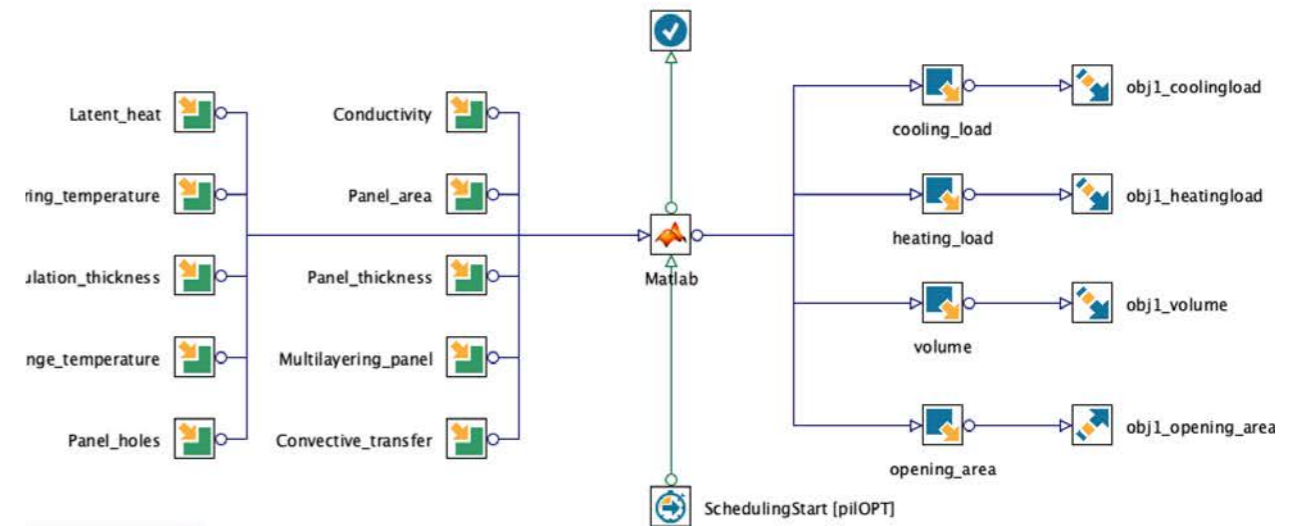
A Trombe-wall with clear double-glazing is better for cooling and a Trombe-wall with coated double-glazing has a better performance for heating the building. Clear double-glazing will be assumed for this research study (`glazing_type = 1`), the SHGC will be adjusted as a variable design parameter, so the effectiveness of covering the wall will be evaluated within this research study. This all results in the following commands for the simulation in MATLAB / Simulink.

```
glazing_type = 1; % 1=double clear glazing, 2=double coated glazing, 3=triple clear glazing, 4=triple coated glazing
building_function_type = 1; % 1 = office, 2 = residence
building_age_type = 1; % 1 = new, 2 = old
building_method_type = 2; % 1 = lightweight, 2 = mediumweight, 3 = heavyweight
panel_present = 1; % 0 = no, 1 = yes
climate_type = 2; % 1 = Cold, 2 = Temperate, 3 = Dry, 4 = Tropical
```

54 EXTENDED MATLAB/SIMULINK MODEL

The MATLAB/Simulink simulation model will be used in combination with modeFRONTIER, this platform will be used to optimize results within MATLAB by employing smart genetic algorithms, the principle of this optimization strategy will be explained in Section "5.7 OPTIMIZATION STRATEGY". A direct connection is created between these two platforms, MATLAB/Simulink will be started automatically and the input and output from the models will be exchanged. In this way objectives can be defined to optimize the system, the node definition illustrated below shows the work-flow that combines the two. On the left the input parameters are defined by incorporating an upper and lower bound, or minimum and maximum value, the right part defines the optimization objectives and output variables. Here the objectives are to minimize the heating and cooling load, the volume and the heat capacity (i.e. the quality of the material). These objectives are defined as output parameters within MATLAB/Simulink, these one-value parameters will be send to modeFRONTIER. In this way these objectives can be analysed and the effect of each design can be evaluated.

These four objectives are important for creating a optimal system for energy reduction with the least amount of material needed to make it thermodynamically optimal and the same time cost-effective. The '*SchedulingStart*' environment is used to define the algorithm and the initial set of input parameters.



54.1 Multi-layering extension

First the `nl_system` parameter together with the new melting and solidification temperatures are added to define the temperature for the second layer, also a new node definition is created for this layer as seen in Figure 1.73. The melting and solidification temperatures for the second layer will be lower compared to the first layer, in this way they will start melting at the same time.

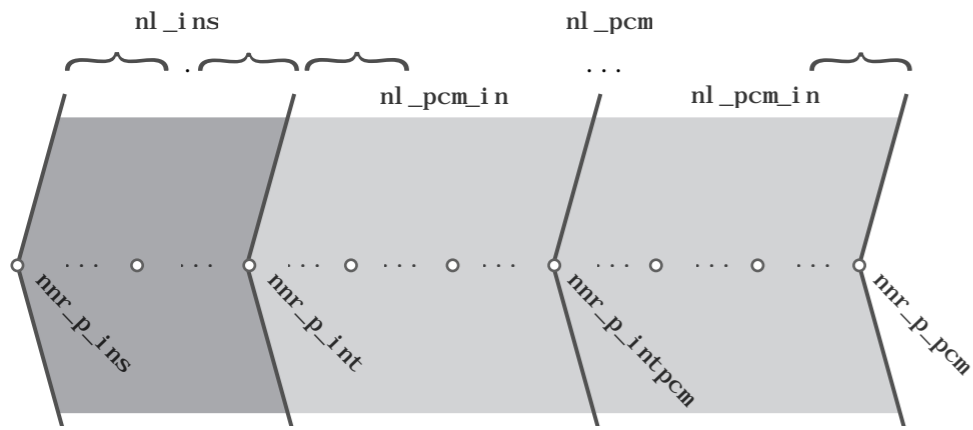


Figure 1.73
New extended node number
definition within the model
(By author)

```

if nl_system == 3
    nl_pcm = 9; % number of PCM control volume layers, minimum = 1
    nl_pcm_in = nl_pcm/3; % number of PCM control volume layers of first layer, minimum = 1
    nl_pcm_inin = nl_pcm*2/3; % number of PCM control volume layers of first layer, minimum = 1
else
    nl_pcm = 10; % number of PCM control volume layers, minimum = 1
    nl_pcm_in = nl_pcm/2; % number of PCM control volume layers of second layer, minimum = 1
end

```

%MELTING TEMPERATURE

```

Ts_pcm = 23; % temperature below which PCM is solid [C]
Tl_pcm = 26; % temperature above which PCM is liquid [C]

```

```

Ts_pcm1 = Ts_pcm; % temperature below which PCM is solid [C] 23
Tl_pcm1 = Tl_pcm; % temperature above which PCM is liquid [C] 26

```

```

if nl_system == 2
    Ts_pcm2 = Ts_pcm+3; % temperature below which PCM is solid [C] 23
    Tl_pcm2 = Tl_pcm+3; % temperature above which PCM is liquid [C] 26
else
    Ts_pcm2 = Ts_pcm+1.5; % temperature below which PCM is solid [C] 23
    Tl_pcm2 = Tl_pcm+1.5; % temperature above which PCM is liquid [C] 26
end

```

```

Ts_pcm3 = Ts_pcm+3; % temperature below which PCM is solid [C] 23
Tl_pcm3 = Tl_pcm+3; % temperature above which PCM is liquid [C] 26

```

The thermal mass for each separate control volume layer (nl_pcm) is calculated according to the mass matrix principle as explained in the "4.2 MULTI-NODE HEAT BALANCE". In the multilayer principle this mass matrix is divided into two parts depending on the amount of layers to be accessed. The code on the next page shows the addition for the two layered variant (nl_system == 2). M_r_l is used to define the thermal mass of the first layer and M_r_l2 defines the thermal mass of the second layer and also the third layer is included in MATLAB. The Simulink model shown below states which part of the mass matrix is accessed, together with the input temperature for each layer, this simulink block definition is linked to the mass matrix script shown below.

%mass matrix latent part

```

M_r_l = zeros(nnr_r+nl_pcm+nl_ins+2,nnr_r+nl_pcm+nl_ins+2);
M_r_l2 = zeros(nnr_r+nl_pcm+nl_ins+2,nnr_r+nl_pcm+nl_ins+2);
M_r_l3 = zeros(nnr_r+nl_pcm+nl_ins+2,nnr_r+nl_pcm+nl_ins+2);

```

```

if nl_pcm == 1
    M_r_l(nnr_r+1,nnr_r+1) = 0.5*panel_pcm.dx*panel_pcm.rho*panel_A*panel_pcm.h/(Tl_pcm-Ts_pcm);
    M_r_l(nnr_r+2,nnr_r+2) = 0.5*panel_pcm.dx*panel_pcm.rho*panel_A*panel_pcm.h/(Tl_pcm-Ts_pcm);

elseif nl_system == 1
    M_r_l(nnr_r+1,nnr_r+1) = 0.5*panel_pcm.dx*panel_pcm.rho*panel_A*panel_pcm.h/(Tl_pcm-Ts_pcm);
    for i = 2:nl_pcm
        M_r_l(nnr_r+i,nnr_r+i) = panel_pcm.dx*panel_pcm.rho*panel_A*panel_pcm.h/(Tl_pcm-Ts_pcm);
    end
    M_r_l(nnr_r+nl_pcm+1,nnr_r+nl_pcm+1) = 0.5*panel_pcm.dx*panel_pcm.rho*panel_A*panel_pcm.h/(Tl_pcm-Ts_pcm);

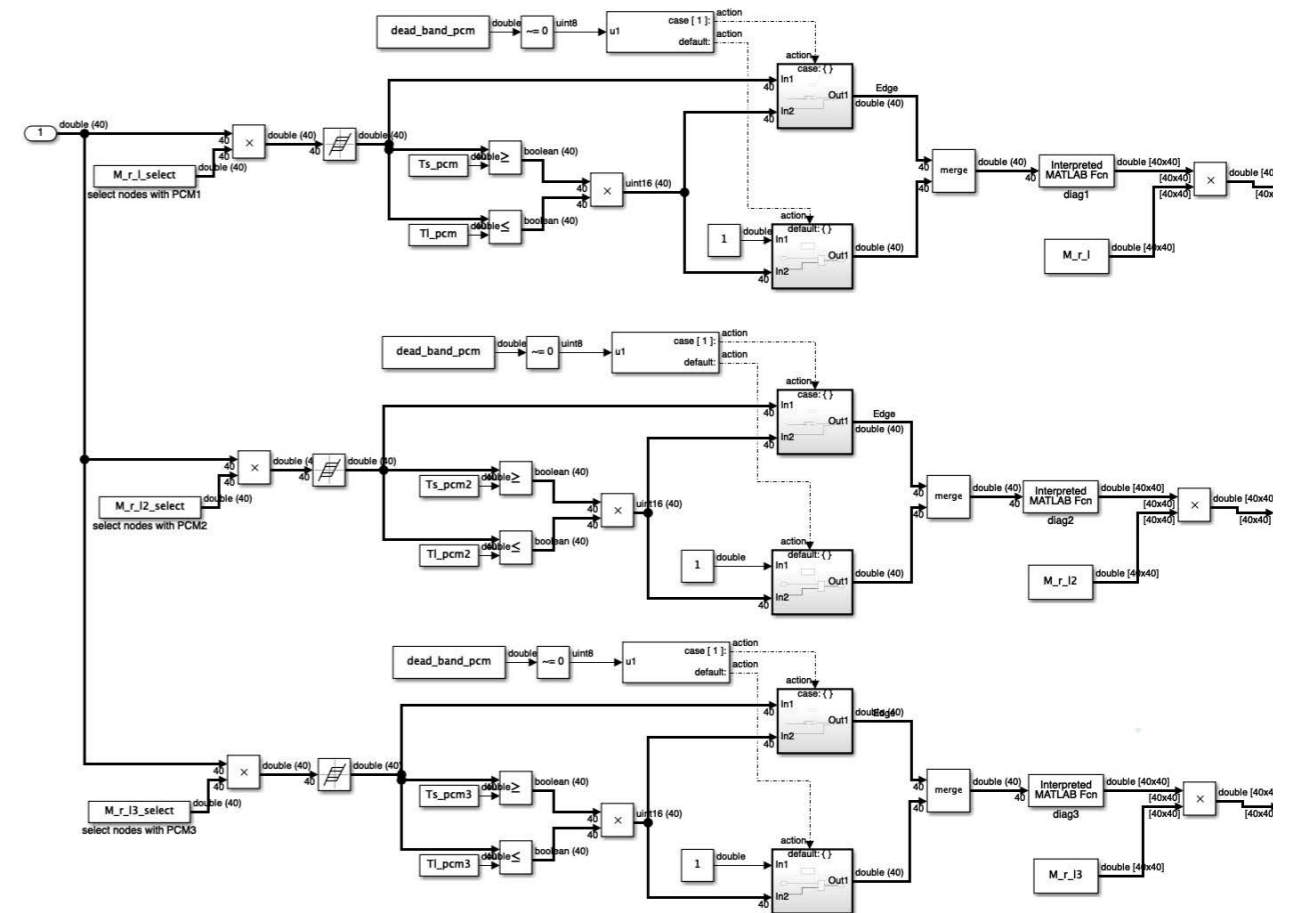
```

```

elseif nl_system == 2
    M_r_l(nnr_r+1,nnr_r+1) = 0.5*panel_pcm.dx*panel_pcm.rho*panel_A*panel_pcm.h/(Tl_pcm-Ts_pcm);
    for i = 2:nl_pcm_in
        M_r_l(nnr_r+i,nnr_r+i) = panel_pcm.dx*panel_pcm.rho*panel_A*panel_pcm.h/(Tl_pcm-Ts_pcm);
    end
    M_r_l(nnr_r+nl_pcm_in+1,nnr_r+nl_pcm_in+1) = 0.5*panel_pcm.dx*panel_pcm.rho*panel_A*panel_pcm.h/(Tl_pcm-Ts_pcm);
    M_r_l2(nnr_r+nl_pcm_in+2,nnr_r+nl_pcm_in+2) = 0.5*panel_pcm.dx*panel_pcm.rho*panel_A*panel_pcm.h/(Tl_pcm2-Ts_pcm2);
    for i = nl_pcm_in+2:nl_pcm
        M_r_l2(nnr_r+i,nnr_r+i) = panel_pcm.dx*panel_pcm.rho*panel_A*panel_pcm.h/(Tl_pcm2-Ts_pcm2);
    end
    M_r_l2(nnr_r+nl_pcm+1,nnr_r+nl_pcm+1) = 0.5*panel_pcm.dx*panel_pcm.rho*panel_A*panel_pcm.h/(Tl_pcm2-Ts_pcm2);

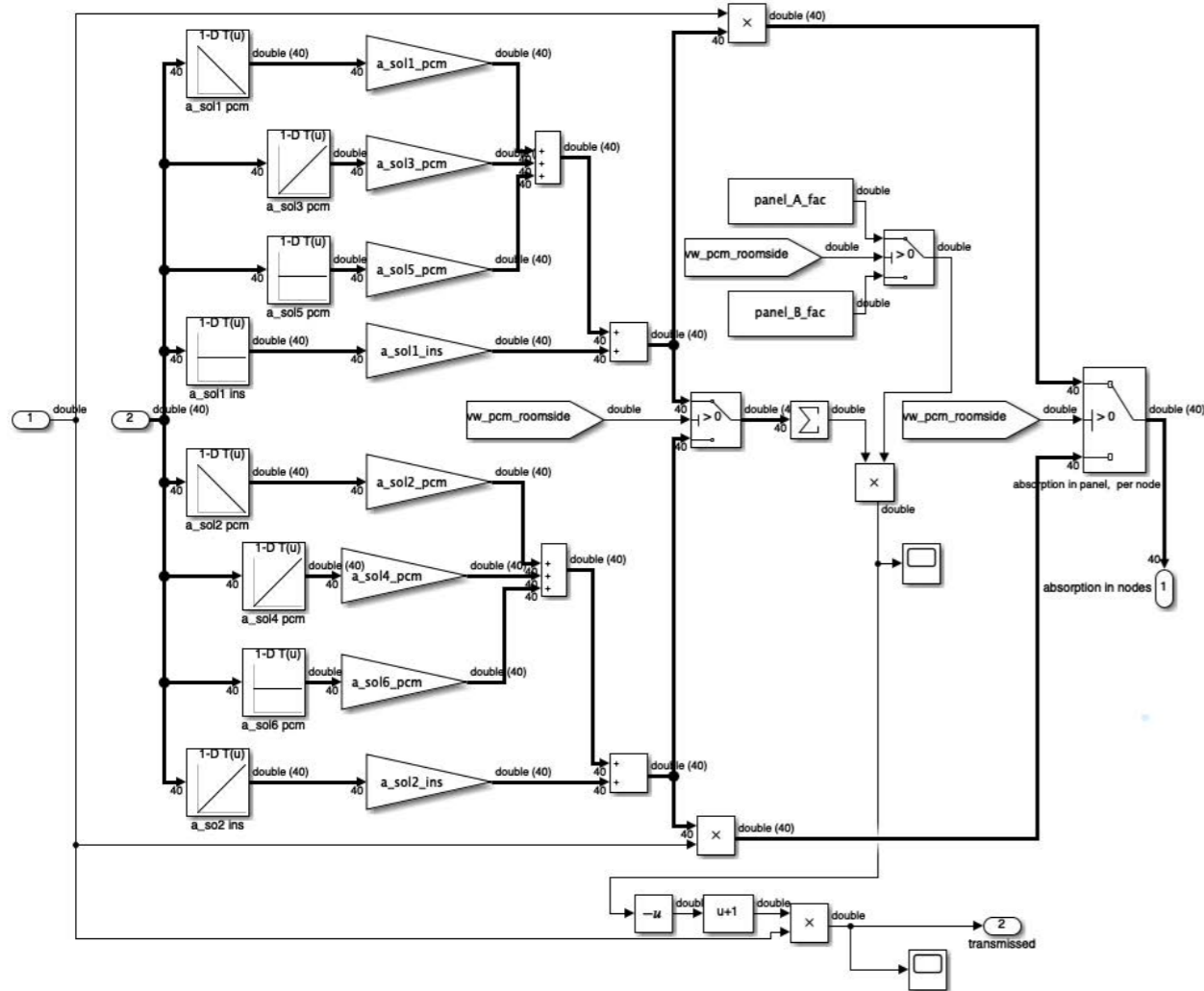
```

The effective mass of the PCM is subsequently executed using the following Simulink setup, the top part contains the first layer of the PCM system, the second part for the second layer and the bottom part is the third layer of the wall. This first layer will always be accessed, the others depend on the state of nl_system.



For instance, when nl_system is equal to one the $M_r_I_select$ picks all the nodes, when nl_system is equal to two this first part part picks just half of the nodes. The other half of the nodes is accessed by the $M_r_I_select2$ function within Simulink, this subsystem is similar to the effective PCM mass shown by Van Unen (2018) but picks the nodes from the second layer. All the values for the thermal mass of each layer are in the end summed up to define the total thermal mass of the multi-layered system.

Another important factor within the multi-layered system is the solar absorption of the system, different values are considered for the liquid and the solid state of the PCM. This also needs to be defined within the MATLAB/Simulink model to account for the right amount of energy absorbed. The Simulink block illustrated below defines the solar absorption for each of the layers for both the situations when the PCM panel faces the room and when the PCM panel faces the cavity (defined in the left part). A distinction is made for the multiplication with the surface area of the panel, the strategy for the optimization defines two different opening areas to allow for more direct sun radiation in the winter situation, therefore the solar absorption is multiplied with either $Panel_A_fac$ or $Panel_B_fac$ (defined in the right part). The result from this block is one part transmitted to the interior and one part absorbed within the PCM panel.



The simulink block calls for the script shown on the next page, here the solar absorption is divided into two parts. The first parts specifies the different solar absorption coefficients for each layer, these are used within the Simulink model to determine the amount of solar energy absorbed for both the liquid

and the solid phase. The measured solar absorption coefficient for a layer of four centimetre PCM in solid phase is 0.97 and the amount absorbed in liquid phase is 0.63 (Tenpierik et al., 2018), this directly means 0.03 is transmitted in solid phase and 0.37 in liquid. This coefficient changes by varying the thickness of the panel, in Equation (1.35) the fourth root is taken for the solar energy absorption to convert the solar absorption coefficient to one centimetre thickness.

$$\alpha_{ab,sol; pcm s} = \sqrt[4]{0.97} = 0.992$$

$$\alpha_{ab,sol; pcm l} = \sqrt[4]{0.63} = 0.891$$
(1.35)

These two coefficient are in the script directly connected to the thickness of the panel in centimetres, in this way the coefficient changes with the change in thickness, the calculated coefficient is defined in the following script. The bottom part shows the coefficient for the 2 layered system ($nl_system == 2$), a definition is made for each of the layers within MATLAB.

```

% SOLAR ABSORPTION
panel_d = panel_pcm.d*100; %thickness in centimetre fro the solar absorption

a_absol_pcm_s = 0.992^(panel_d); % part of incident solar energy absorbed in solid phase for 1 centimetre of PCM
a_trsol_pcm_s = 1-a_absol_pcm_s; % part of incident solar energy transmitted in solid phase for 1 centimetre of PCM

a_absol_pcm_l = 0.891^(panel_d); % part of incident solar energy absorbed in liquid phase for 1 centimetre of PCM
a_trsol_pcm_l = 1-a_absol_pcm_l; % part of incident solar energy transmitted in liquid phase for 1 centimetre of PCM

elseif nl_system == 2
% PCM PANEL FACES THE ROOM
a_sol1_ins_s = 0.09; % part of incident solar energy on panel absorbed by the insulation layer, solid state, when PCM
a_sol1_ins_l = 0.09; % part of incident solar energy on panel absorbed by the insulation layer, liquid state, when PCM
% linear interpolation between solid and liquid state based on volume-averaged PCM temperature
a_sol1_pcm_s = 0.91*a_absol_pcm_s^(1/2); % part of incident solar energy on panel absorbed by the PCM layer, solid sta
a_sol1_pcm_l = 0.91*a_absol_pcm_l^(1/2); % part of incident solar energy on panel absorbed by the PCM layer, liquid stati
a_sol3_pcm_s = 0.91*a_trsol_pcm_s^(1/2)*a_absol_pcm_s^(1/2); % part of incident solar energy on panel absorbed by the
a_sol3_pcm_l = 0.91*a_trsol_pcm_l^(1/2)*a_absol_pcm_l^(1/2); % part of incident solar energy on panel absorbed by the P
a_sol5_pcm_s = 0; % part of incident solar energy on panel absorbed by the PCM layer, solid state, when PCM faces roo
a_sol5_pcm_l = 0; % part of incident solar energy on panel absorbed by the PCM layer, liquid state, when PCM faces roo

% PCM PANEL FACES THE CAVITY
a_sol2_pcm_s = a_absol_pcm_s^(1/2); % part of incident solar energy on panel absorbed by the PCM layer, solid state
a_sol2_pcm_l = a_absol_pcm_l^(1/2); % part of incident solar energy on panel absorbed by the PCM layer, liquid state
a_sol4_pcm_s = a_trsol_pcm_s^(1/2)*a_absol_pcm_s^(1/2); % part of incident solar energy on panel absorbed by the P
a_sol4_pcm_l = a_trsol_pcm_l^(1/2)*a_absol_pcm_l^(1/2); % part of incident solar energy on panel absorbed by the PCM
a_sol6_pcm_s = 0; % part of incident solar energy on panel absorbed by the PCM layer, solid state, when PCM faces roo
a_sol6_pcm_l = 0; % part of incident solar energy on panel absorbed by the PCM layer, liquid state, when PCM faces roo

a_sol2_ins_s = a_trsol_pcm_s^(1/2)*a_trsol_pcm_s^(1/2)*0.09; % part of incident solar energy on panel absorbed by the ir
a_sol2_ins_l = a_trsol_pcm_l^(1/2)*a_trsol_pcm_l^(1/2)*0.09; % part of incident solar energy on panel absorbed by the insi
% linear interpolation between solid and liquid state based on volume-averaged PCM temperature

```

The second part shown on the next page calls for all the nodes within the PCM layer, different solar absorption coefficients are used for each of the layers. Each of these nodes is multiplied with this solar absorption coefficient within the previous mentioned Simulink block. The total thickness of the PCM panel is subdivided in either one, two or three layers.

```

% definition of solar absorption values in the panel, when PCM is facing the room,
%still excluding actual absorption which is calculated in Simulink
a_sol1_pcm = zeros(nkl_tot,1);
a_sol3_pcm = zeros(nkl_tot,1);
a_sol5_pcm = zeros(nkl_tot,1);

```

```

if nI_system == 1
a_sol1_pcm(nnr_p_pcm) = 0.5*panel_pcm.dx/panel_pcm.d;
for i=nnr_p_pcm+1:nnr_p_int-1
a_sol1_pcm(i) = panel_pcm.dx/panel_pcm.d;
end
a_sol1_pcm(nnr_p_int) = 0.5*panel_pcm.dx/panel_pcm.d;

```

```

elseif nI_system == 2
a_sol1_pcm(nnr_p_pcm) = 0.5*panel_pcm.dx/panel_pcm.d;
for i=nnr_p_pcm+1:nnr_p_intpcm-1
a_sol1_pcm(i) = panel_pcm.dx/panel_pcm.d;
end
a_sol1_pcm(nnr_p_intpcm) = 0.5*panel_pcm.dx/panel_pcm.d;
a_sol3_pcm(nnr_p_intpcm) = 0.5*panel_pcm.dx/panel_pcm.d;
for i=nnr_p_intpcm+1:nnr_p_int-1
a_sol3_pcm(i) = panel_pcm.dx/panel_pcm.d;
end
a_sol3_pcm(nnr_p_int) = 0.5*panel_pcm.dx/panel_pcm.d;

```

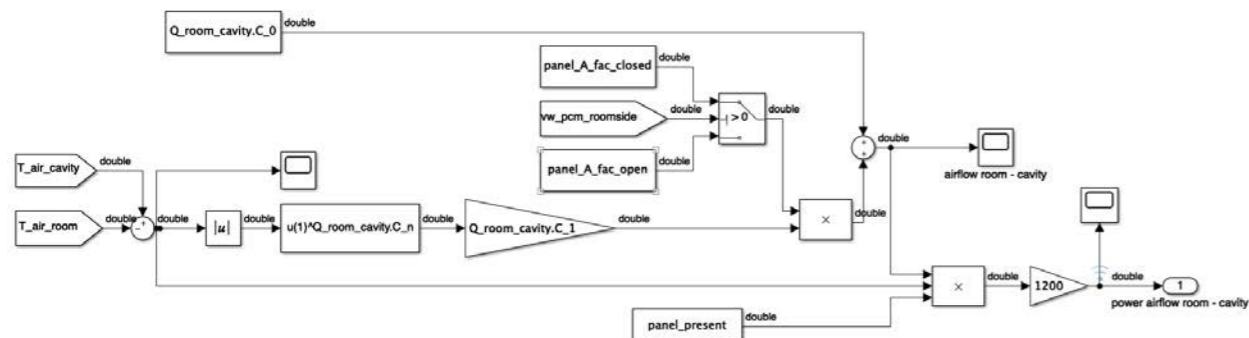
This section explained the principle of the implementation of the multi-layering strategy within MATLAB/Simulink, the validation of the multi-layering system will be employed within Section "5.6.1 Validation multi-layering". As mentioned, in the description for the previous Simulink block, two different opening percentages will be taken into account according to the rotating strategy defined in Section "5.2 PARAMETER SPECIFICATION". This opening strategy is already defined in the solar absorption block, however also the amount of air flowing from the cavity towards the room changes by varying the size of the openings. This affects the flow coefficient of the PCM panel, which is defined in MATLAB/Simulink. This coefficient will now be based the opening size, therefore the following script is extended and connected to the flow coefficient which defines the amount of air flowing between the two spaces.

```

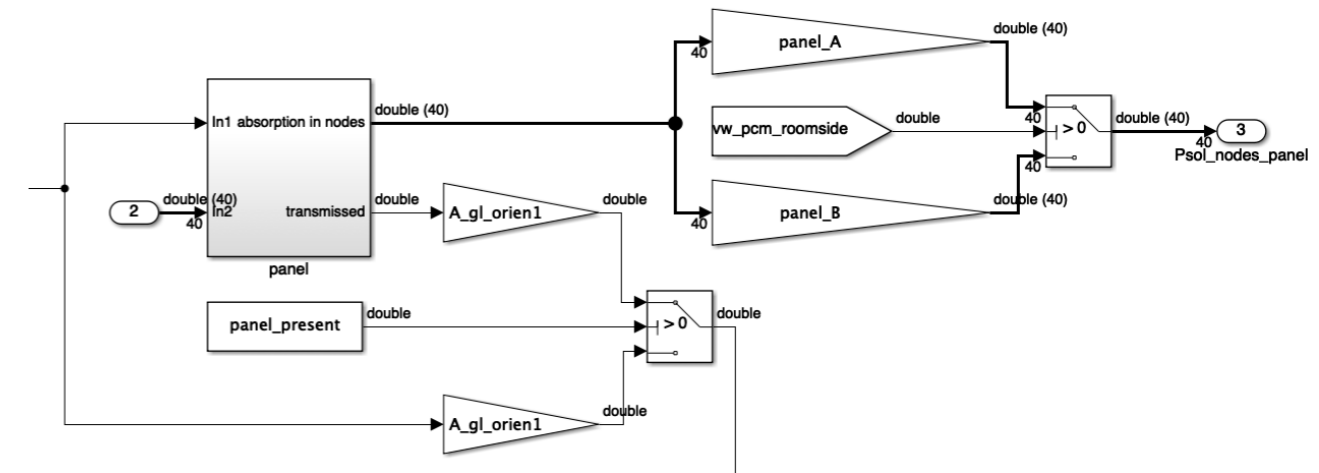
panel_A_fac = 0.9; % fraction of the panel surface area not consisting of holes. So when panel_A_fac = 1,
                  %the panel is closed and completely covers the orien1 facade
panel_B_fac = 0.6; % fraction of the panel surface area not consisting of holes facing Cavity. So when panel_B_fac = 1,
                  %the panel is closed and completely covers the orien1 facade

panel_A_fac_closed = (1-panel_A_fac)*A_gl_orien1; % fraction of the panel surface area not consisting of holes.
%So when panel_A_fac = 1, the panel is closed and completely covers the orien1 facade
panel_A_fac_open = (1-panel_B_fac)*A_gl_orien1; % fraction of the panel surface area not consisting of holes.
%So when panel_A_fac = 1, the panel is closed and completely covers the orien1 facade

```



The same applies to the absorption and the transmittance of solar energy, the opening area is varied within the model. Depending on this variation also the amount of solar energy absorbed by the panel changes, this is seen in the simulink block below. This method is an assumption on the actual solar absorption, this principle is based on the situation where the volume of the panel is preserved and the opening size changes. This is exactly how it needs to work, however the self-shading effect is not considered when varying the opening. Within this simulation only the surface area changes, in a real application the amount of self-shading depends on the design of the product. This self-shading effect negatively affects the amount of energy absorbed by the panel, this needs to be taken into consideration when designing the wall.



Another optimization strategy is the use of an extended surface area to increase the amount of heat transfer at the surface of the panel, this extension affects the convective heat transfer and the heat transfer by radiation between the room nodes and the PCM. The volume of the panel is preserved, in this way the actual effect of the surface extension can be evaluated and no extra PCM has to be added. In the MATLAB script a new factor is added that determines the percentage of the extension, the coefficient added for this principle is the *panel_R_fac* which is multiplied by area as seen below.

```

panel_R_fac = 1.3; % Multiplication ratio of surface area (1.3 indicates an area increase of 30%)

switch panel_present
case 1
Y_r1(25,nnr_p_pcm) = p_alpha_i*panel_A*panel_R_fac; % convection between room air and inner surface
%PCM side of panel
Y_r1(5,nnr_p_pcm) = 5*e2_constr_A/(A_total-panel_A)*panel_A*panel_R_fac; % radiation exchange
Y_r1(9,nnr_p_pcm) = 5*e3_constr_A/(A_total-panel_A)*panel_A*panel_R_fac; % radiation exchange
Y_r1(13,nnr_p_pcm) = 5*e4_constr_A/(A_total-panel_A)*panel_A*panel_R_fac; % radiation exchange
Y_r1(17,nnr_p_pcm) = 5*e5_constr_A/(A_total-panel_A)*panel_A*panel_R_fac; % radiation exchange
Y_r1(21,nnr_p_pcm) = 5*e6_constr_A/(A_total-panel_A)*panel_A*panel_R_fac; % radiation exchange

for i = nnr_p_pcm:nnr_p_pcm+nl_pcm-1
Y_r2(i,i+1) = panel_pcm.la*panel_A/panel_pcm.dx; % conduction
end
for i = nnr_p_pcm+nl_pcm:nnr_p_pcm+nl_pcm+nl_ins-1
Y_r2(i,i+1) = panel_ins.la*panel_A/panel_ins.dx; % conduction
end
Y_r2(nnr_p_pcm,nnr_cav) = p_alpha_cav*panel_A*panel_R_fac; % convection between cavity air and surface PCM side of panel

```

5.5 MODEL VERIFICATION & VALIDATION

The validation of the adopted and transformed MATLAB and Simulink model is important for the legitimacy of the result. The model is already validated considering the components for calculating the energy reduction in a situation with PCM and without PCM (Unen, 2018). Some changes are made regarding the design input such as the weather-data and the configuration of the control room, besides this the calculations within the script are adjusted to fulfil the needs for this specific research study. A sensitivity analysis is needed to verify and validate the changed model to determine whether this model is accurate. This means: *“Substantiation that a computerized model within its domain of applicability possesses a satisfactory range of accuracy consistent with the intended application of the model”* (Schlesinger, et al., 1979). The model can be considered valid when the outcome from the simulation conditions are consistent when varying the internal parameters, those sensitive parameters cause significant changes in the overall outcome from the simulation (Sargent, 2011). The purpose of the model within this research study is to determine the effect of using different configurations of PCM's within a office building compared to a situation without PCM's. A comprehensive validation and verification of the model considering the use of ventilation, air exchange, room configuration and glazing properties is already done by Van Unen (2018). Different techniques can be adopted to validate the model, the most accurate technique is to compare the results to experimental studies. Due to the lack of time for these studies another technique will be used, a comparison to another, already valid, simulation platform using the following extreme situations (Figure 1.74):

1. A bare window facade, no exterior shading is used;
2. A facade with only exterior shading;
3. A facade with both exterior shading and a PCM trombe wall.

The overall heat balance of the room is based on some predefined factors which together determine the final room temperature and the heating and cooling energy needed to preserve the comfortable temperatures of the room. These factors are calculated according to several formulas, the calculated results from the two simulation platform will be compared to determine whether the output is valid. The most important factors for this heat balance are:

- Internal heat gains
- Solar heat gains
- External infiltration
- Air temperature

These different factors will be compared to determine the overall difference in heat balance between the two platforms. The results within MATLAB will be adjusted according to a comparative study with Designbuilder. DesignBuilder Software Ltd is a fully-integrated performance analysis tool which can be used to determine the performance of a building considering: energy and comfort, HVAC, daylighting, costs, design optimisation, CFD and BREEAM/LEED credits (Designbuilder, n.d.). This platform is tested and validated and gives accurate results when compiling corresponding input values within the model.

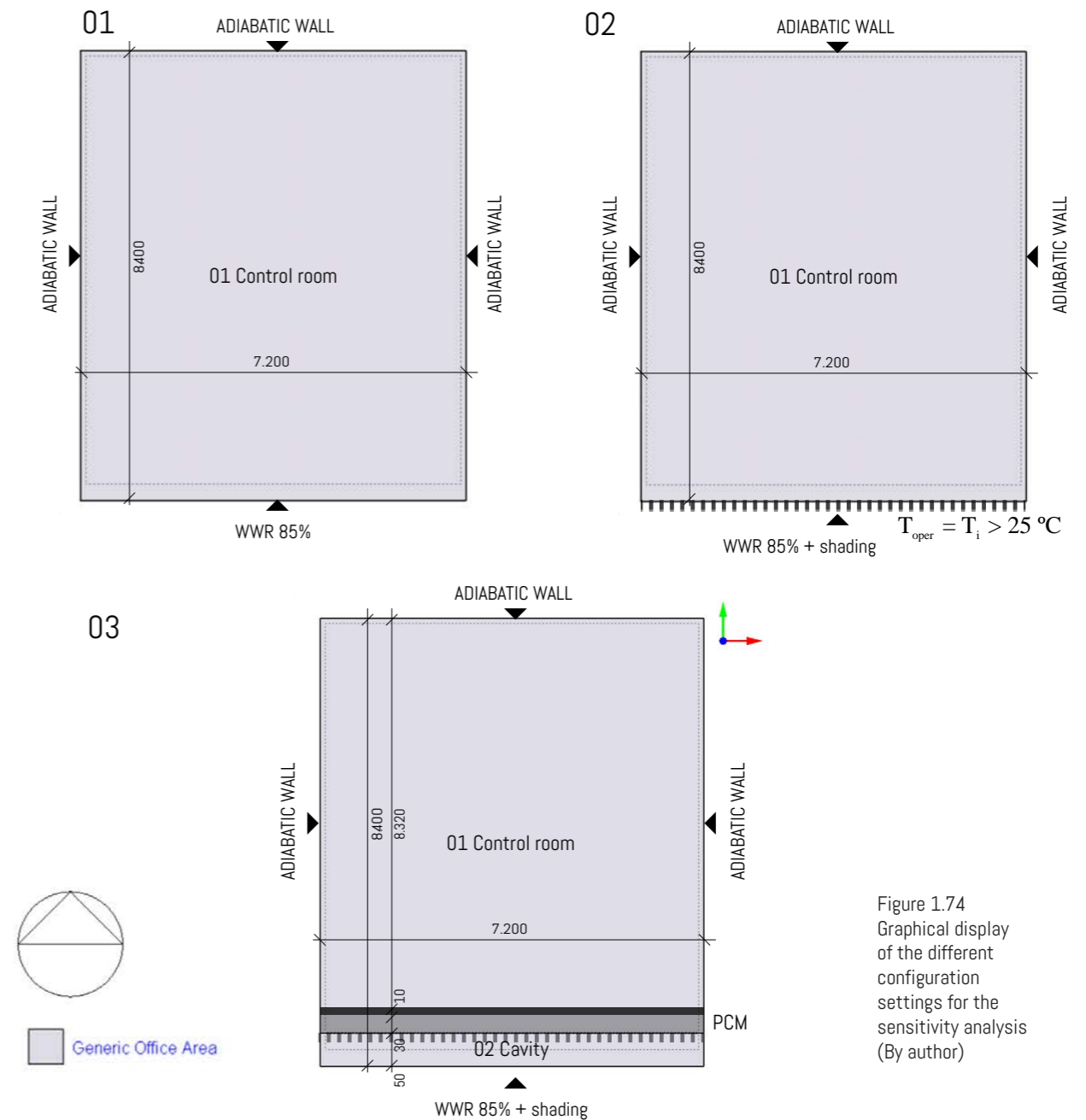


Figure 1.74
Graphical display
of the different
configuration
settings for the
sensitivity analysis
(By author)

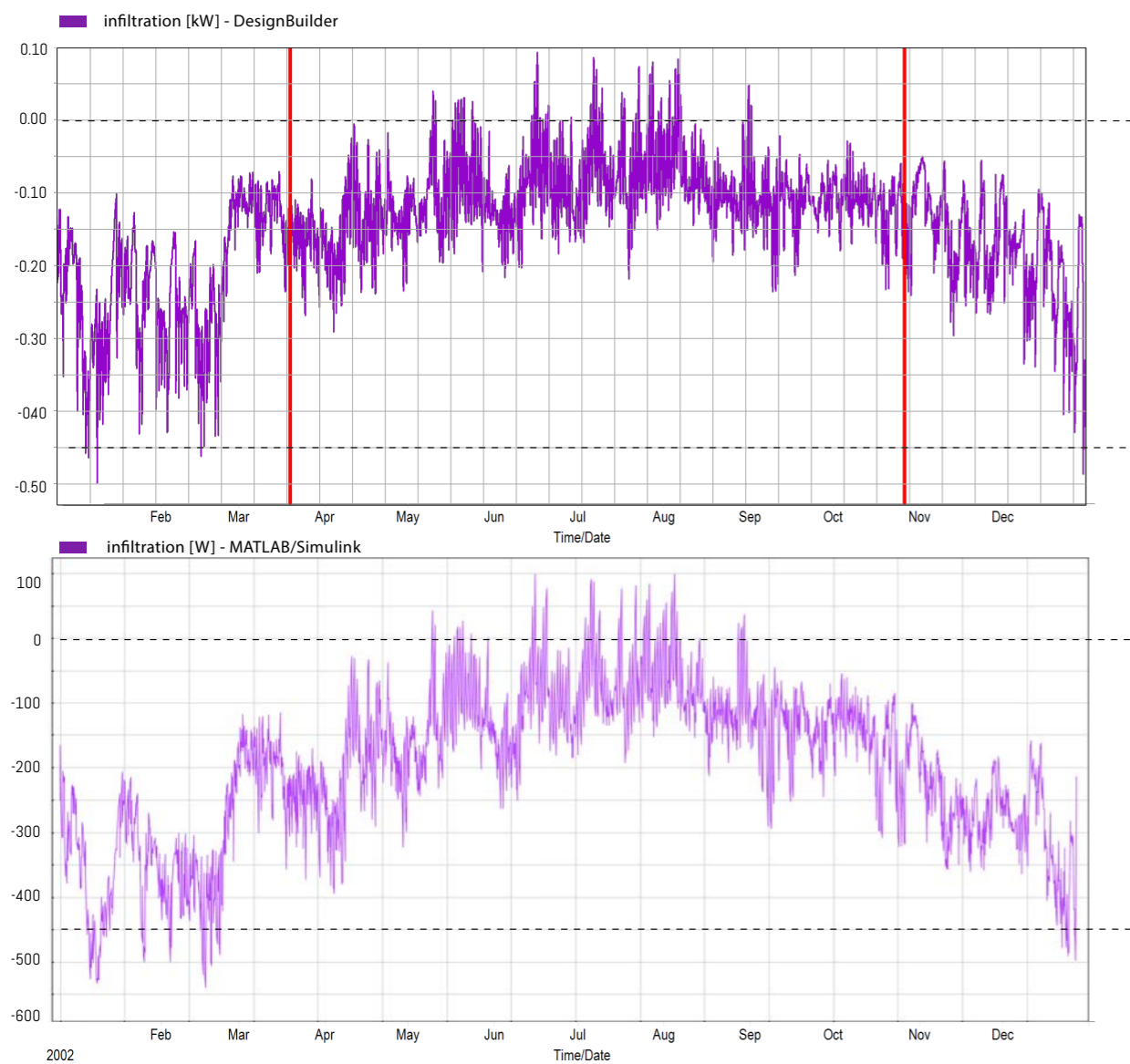
5.5.1 Internal heat gains

The internal heat gains are predefined using a constant value of 25 W/m² for the occupancy and the gains from the office equipment such as computers. This constant value is multiplied by the floor area of the control room, therefore no difference is observed between the two simulation platforms. The output graphs showed that in both simulation a constant value of 1.500 W was accounted for, this was expected due to the basic principle that defines this load. A constant value is given and multiplied by the area of the control room.

5.5.2 External infiltration

The external Infiltration is the heat gain through air infiltration (non-unintentional air entry through cracks and holes in building fabric), the calculated natural ventilation method is used within DesignBuilder to account for the amount of air flowing between the cavity and the interior space for the situation with the PCM Trombe wall. The resulting values from the external infiltration in MATLAB/Simulink seemed to be to opportunistic when comparing them to the results from the Designbuilder Software Ltd, the infiltration power accounted for in the heat balance were significantly lower resulting in a lower heat load and a higher cooling load. This deviation is presumably caused by the difference in calculation method, Designbuilder also takes the pressure difference by wind into account where The MATLAB script did not. A utilization factor is added to the MATLAB model which accounts for this difference in load, the factor is defined by trial and error comparing the resulting graphs. For the external infiltration a utilization factor of 1.25 is used, still some small deviations can be observed but the overall mean of the graph now is the same, these peaks are based on the wind pressure difference between the two platforms.

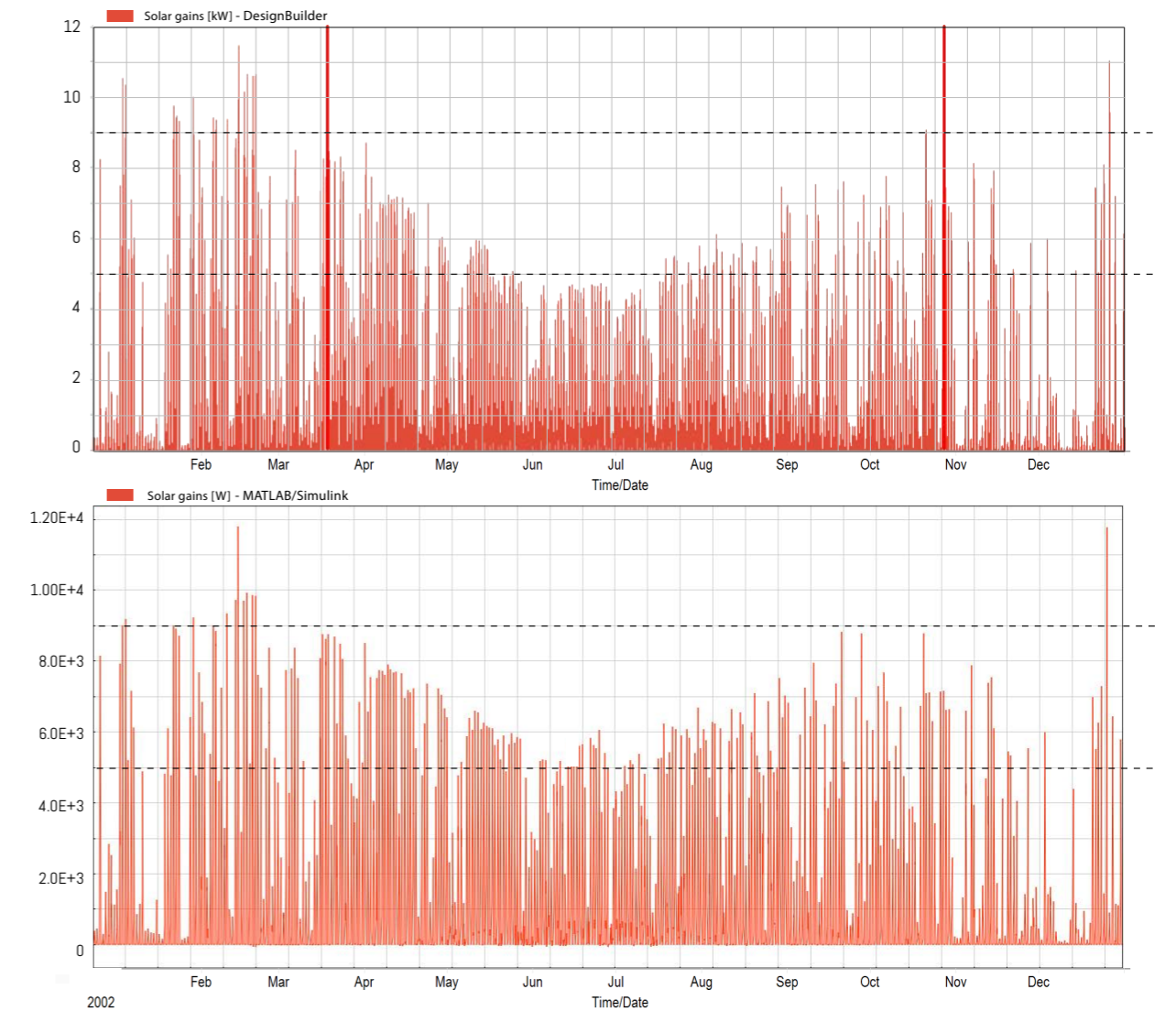
Figure 1.75
Graphs showing the external infiltration throughout the year from Designbuilder (top) and MATLAB (bottom) (By author)



5.5.3 Solar Gains

This section compares the short-wave solar radiation transmission through all external windows. For a bare window, this transmitted radiation is the solar energy that passes through the glass and additionally a small part of diffuse radiation is reflected from the outside window frame, when this is present. When considering a window with shading, this transmitted solar radiation is diffuse. Long-wave solar radiation reflected back from the ground outside is not subtracted. The activation set-point for shading is predefined using the solar gains on the window. The script in MATLAB is based on a minimal solar gain of 100 W/m^2 and a minimal operation temperature of 22°C , this combination of set-points is not possible within Designbuilder, therefore the activation set-point is limited to the use of the solar gains on the envelope, a solar radiation set-point of 100 W/m^2 is used. The first results from MATLAB showed a significant deviation compared to the results from Designbuilder, much higher solar gains were taken into account. This resulted in higher cooling loads and lower heating loads. For these solar gain a utilization factor of 0.80 is used to diminish this deviation, the final results are shown in Figure 1.76.

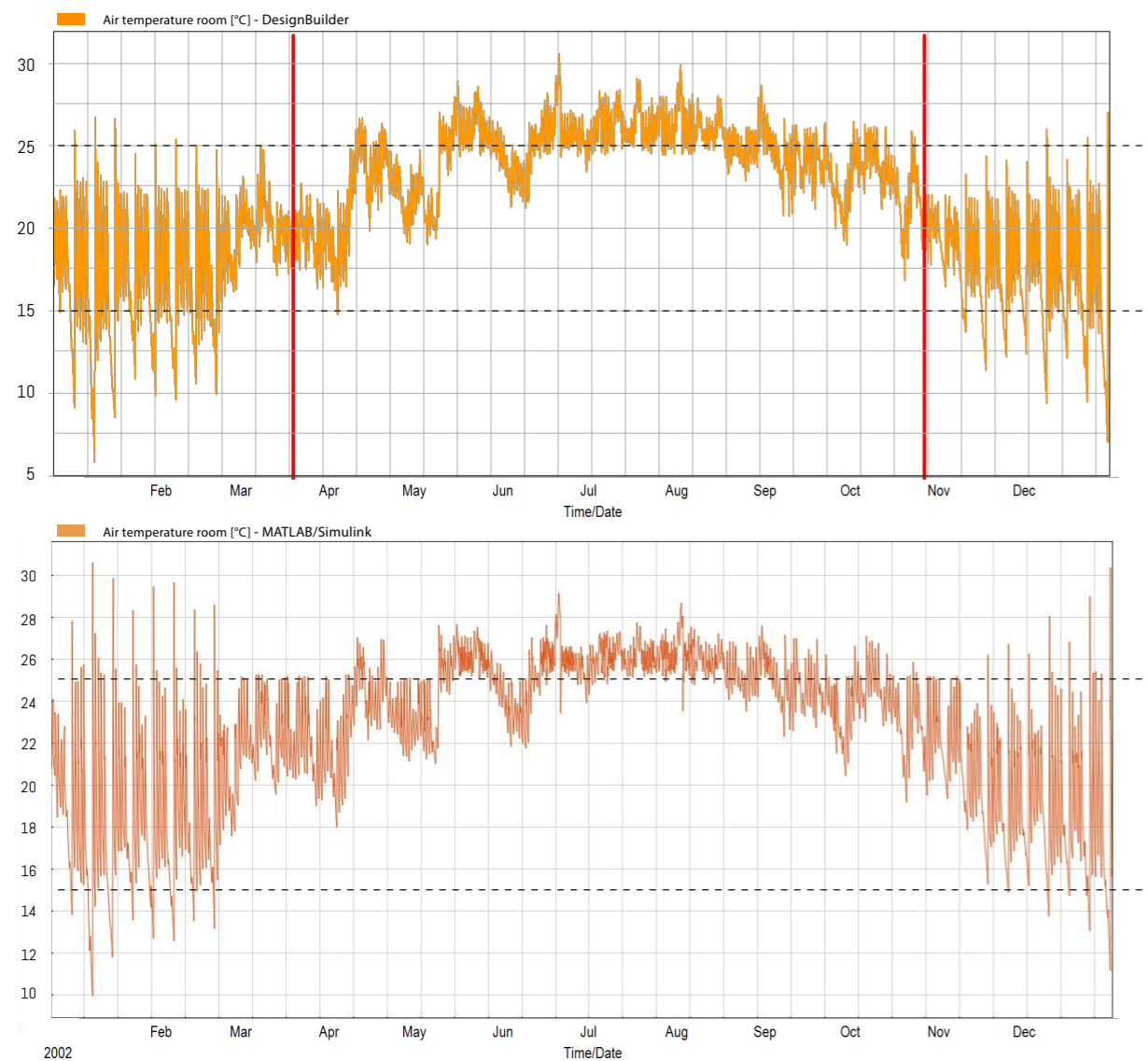
Figure 1.76
Graphs showing the solar gains behind a window without shading throughout the year from Designbuilder (top) and MATLAB (bottom) (By author)



5.54 Air temperature

The dry-bulb outside temperature is for both the simulation platform exactly the same, the temperature is based on the NEN5060-B2: Hygrothermal performance of buildings - Climatic reference data (NEN, 2008). This data is converted to formats suitable for the platforms. Analysis showed that the temperature curves are exactly the same. The last factor that is important to validate before comparing the final energy demand is the resulting indoor temperature. This temperature shows the results from the heat balance calculation, deviations within these temperatures would show a difference in the final energy demand. Figure 1.77 shows the results from both the platforms, a small difference is observed in the peaks of the graph but the overall temperature distribution is comparable to each-other. These results indicate that the overall heat balance from the simulation gives the same outcome. The next section "5.6 VALIDATION RESULTS" will show the real outcome from the energy demand.

Figure 1.77
Graphs showing the indoor air temperature of a room with shading throughout the year from Designbuilder (top) and MATLAB (bottom) (By author)

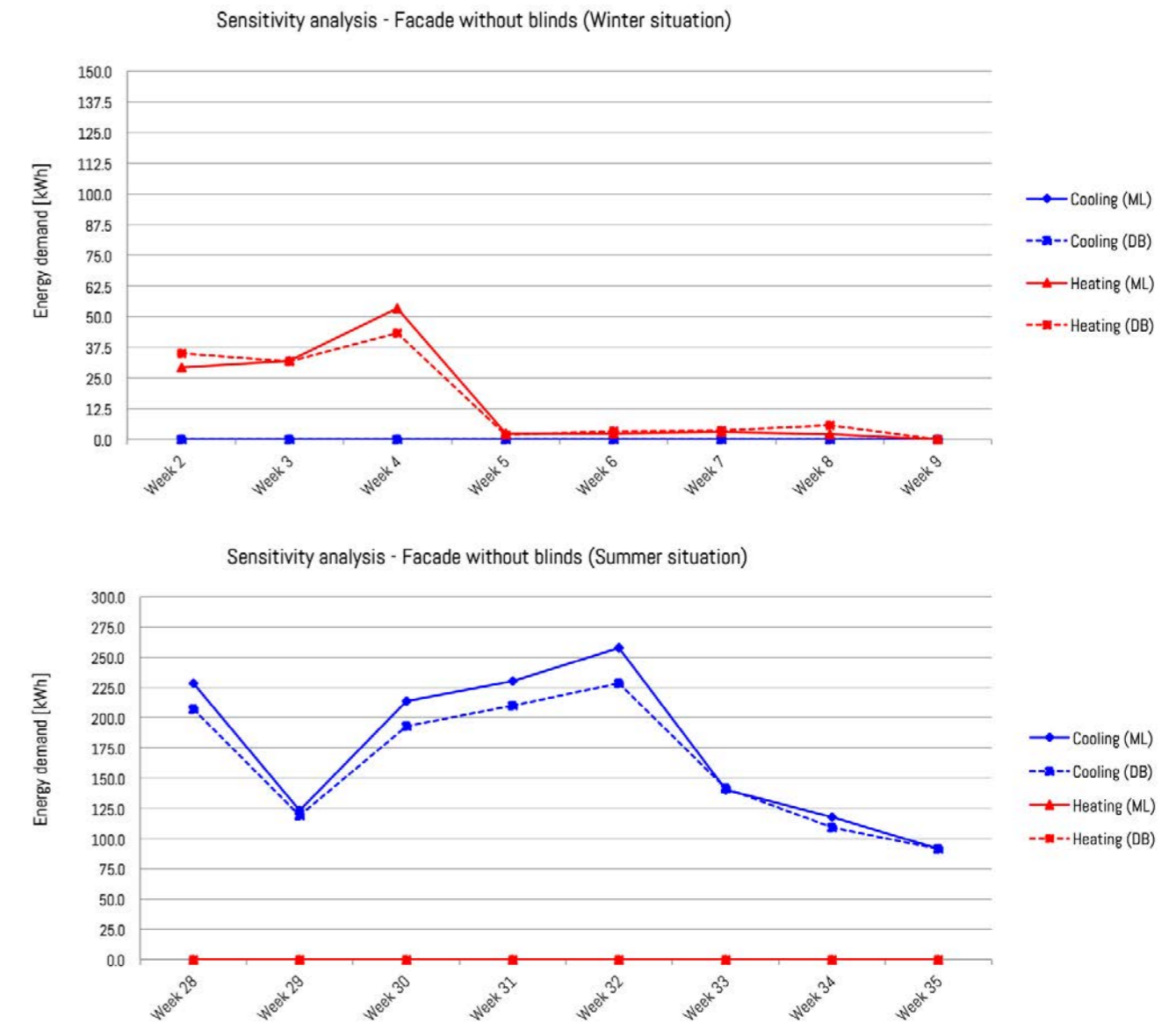


5.6 VALIDATION RESULTS

The first sensitivity analysis shows the results from a bare window with scheduled infiltration and mechanical ventilation. Linear interpolation is used between the results from the different weeks in Designbuilder and MATLAB to indicate the deviation between the two simulation programs.

The total energy demand on yearly base for the summer situation is 4175.0 kWh in Designbuilder and 4294.0 kWh in MATLAB, which means a deviation of 2.77% for cooling. In winter situation the total energy demand is 241.6 kWh for heating within Designbuilder and 274.86 kWh within MATLAB, showing a difference of 12.2% for heating. The results on weekly base during the peak periods are shown in Figure 1.78, important to notice in these graphs are the peaks that occur on the same time. This shows that all the loads accounted for in the heat balance calculations are comparable. The differences observed in this sensitivity analysis are probably based on the small deviations in infiltration power and solar gains.

Figure 1.78
Graphs showing the sensitivity analysis of a bare window in both winter and summer situation (By author)



The second sensitivity analysis shows the difference in results from the situation using a sun-shading device, a simple solar heat gain coefficient (SHGC) of 0.70 is used for the shading to determine the amount of heat entering the rooms through the facade. As mentioned before, the sunshade is scheduled using a minimal solar gain of 100 W/m², the shade will be closed below this value. The total energy demand on yearly base for the summer situation is 1015,0 kWh in Designbuilder and 1030,0 kWh in MATLAB, a deviation of 1,4% for cooling for the total year. In winter the total energy demand is 641.69 kWh in Designbuilder and 666.5 kWh in MATLAB, a difference of 3,7% between the two platforms. Figure 1.79 shows the differences in energy demand on weekly base.

The Scheduled Natural Ventilation (SNV) option is not used for the third sensitivity analysis, this analysis is based on a PCM Trombe wall consisting of small equally distributed holes to provide an airflow to the interior. This SNV-method does not account for the air flow through holes but is determined according to a constant air change rate. The Calculated Natural Ventilation-option determines the airflow through openings according to the pressure difference between the two sides, this difference in pressure is based on the wind pressure, the temperature difference and the discharge coefficient, which is related to the dimensions of the openings. (Designbuilder, n.d.). The total yearly energy demand for cooling in Designbuilder is 574,64 kWh and in MATLAB this is 543,00 kWh, which indicates a deviation of 5,5% in the energy demand. For heating the energy demand in Designbuilder is 406,50 kWh and in MATLAB 431.60 kWh, a total deviation of 5,8%. The graphs in Figure 1.80 show the difference on weekly base in the most crucial months.

Figure 1.79
Graphs showing the sensitivity analysis of a window with sun-shading in both winter and summer situation (By author)

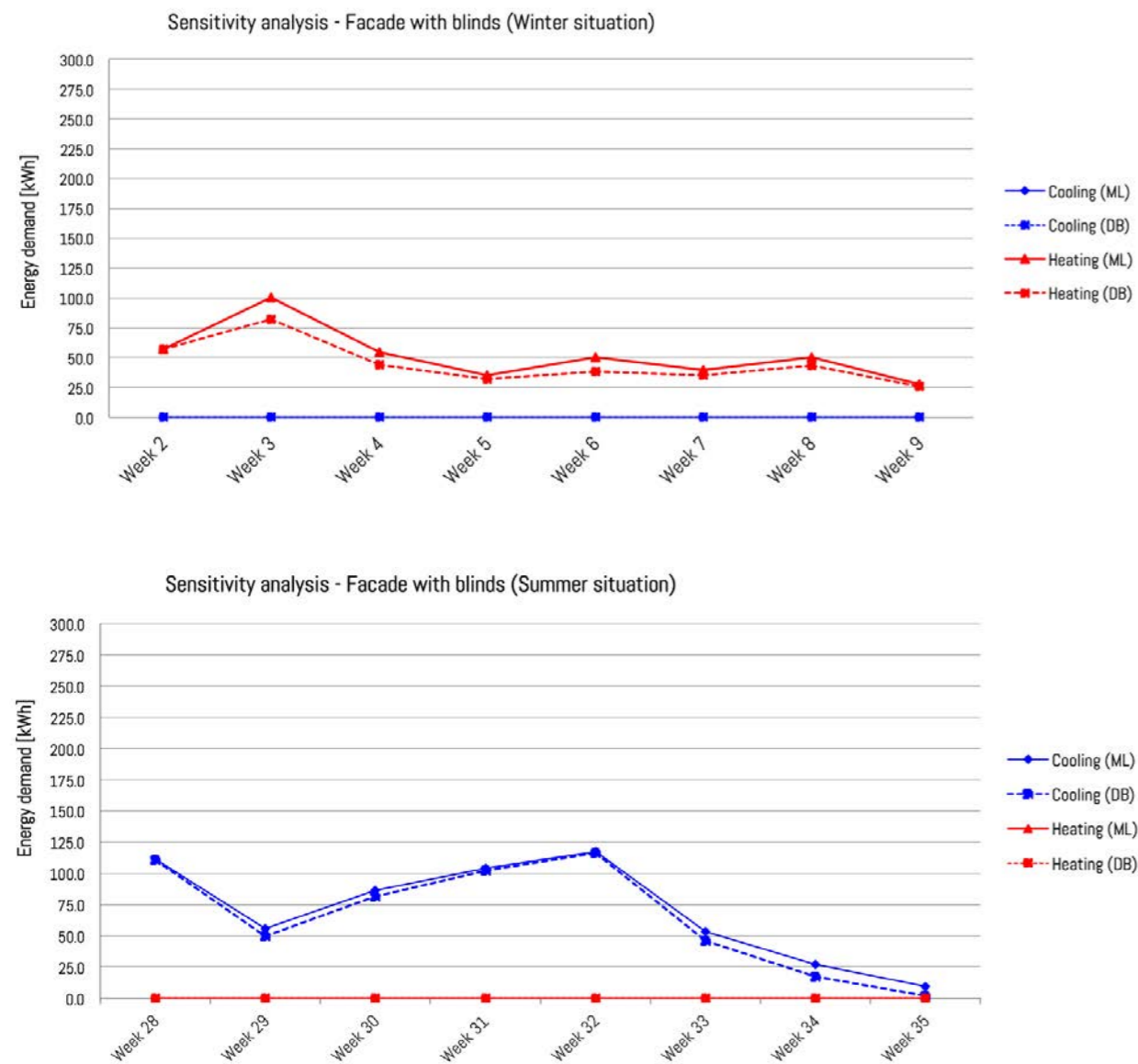
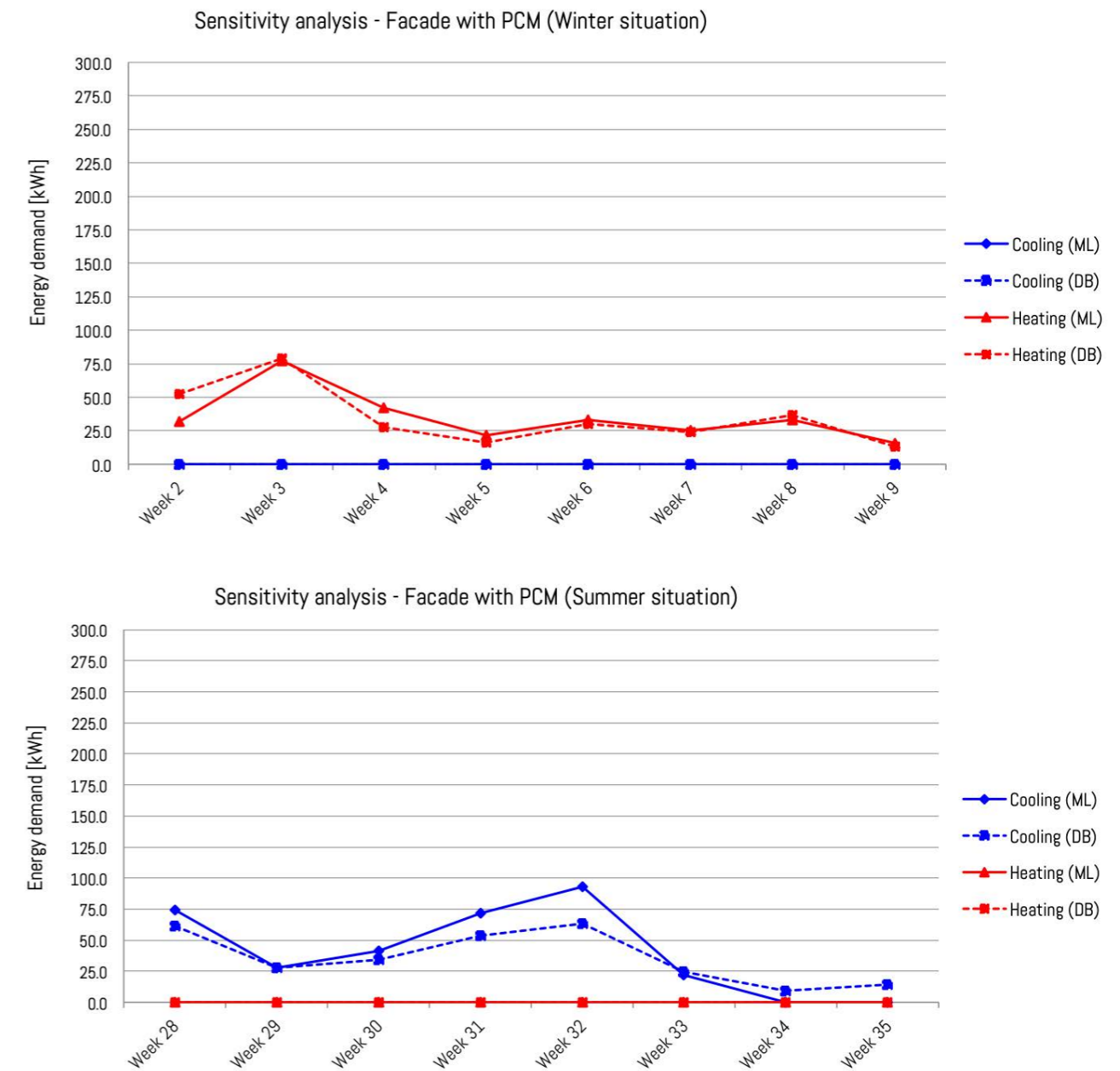


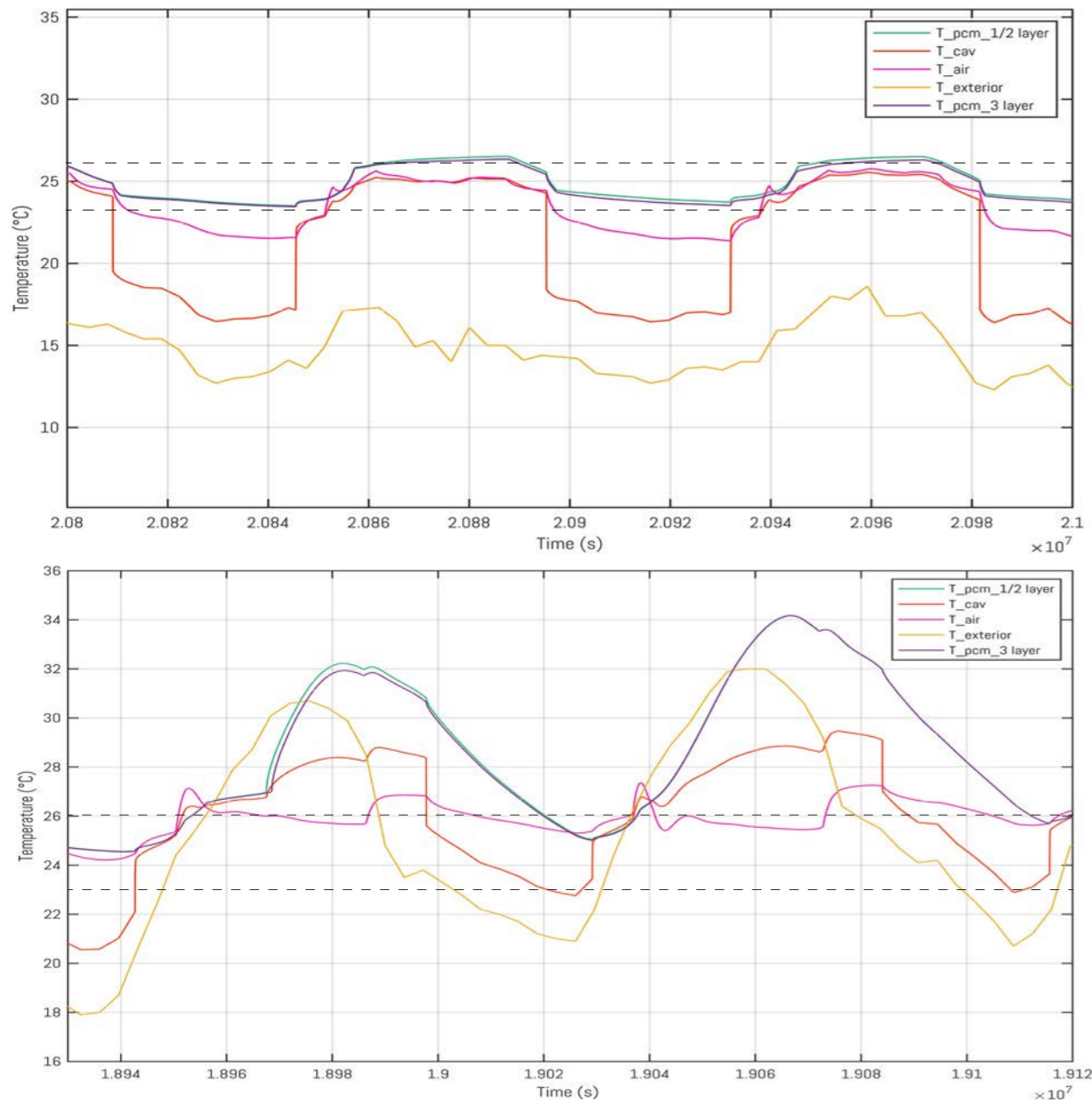
Figure 1.80
Graphs showing the sensitivity analysis of a window with sun-shading in both winter and summer situation (By author)



5.6.1 Validation multi-layering

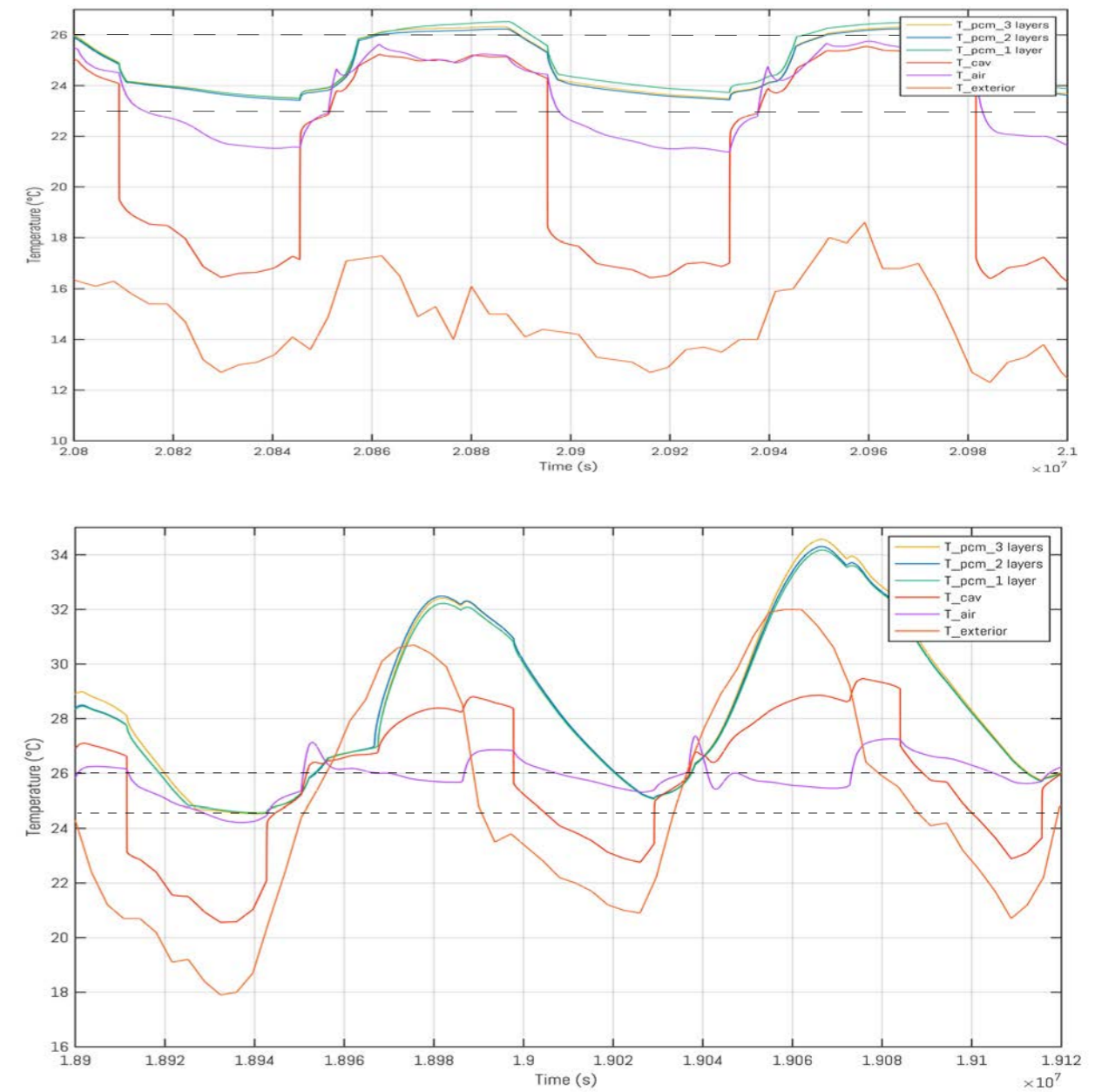
Another validation is needed for the addition of the multi-layering principle within MATLAB/Simulink. The new definition for the solar absorption and the thermal mass for each layer is added together with the corresponding melting temperatures for each layer. First a simulation is carried out to check the validity and the accuracy of the system using the same melting temperature for each layer for the addition of the thermal mass. The results in temperature from the 3 different situations are shown in Figure 1.81, the graph illustrates two typical days and two extreme days within the summer situation, some small differences in the surface temperature of the PCM are observed for the three layered system. A possible cause is the difference in node definition between the one/two layered system (10 nodes) and the three layered system (9 nodes), as mentioned before this difference is needed to get a round number for the nodes.

Figure 1.81
Graphs showing the temperature validation for the thermal mass addition for the multi-layering system, typical summer situation (top) and extreme summer situation (bottom) (By author)



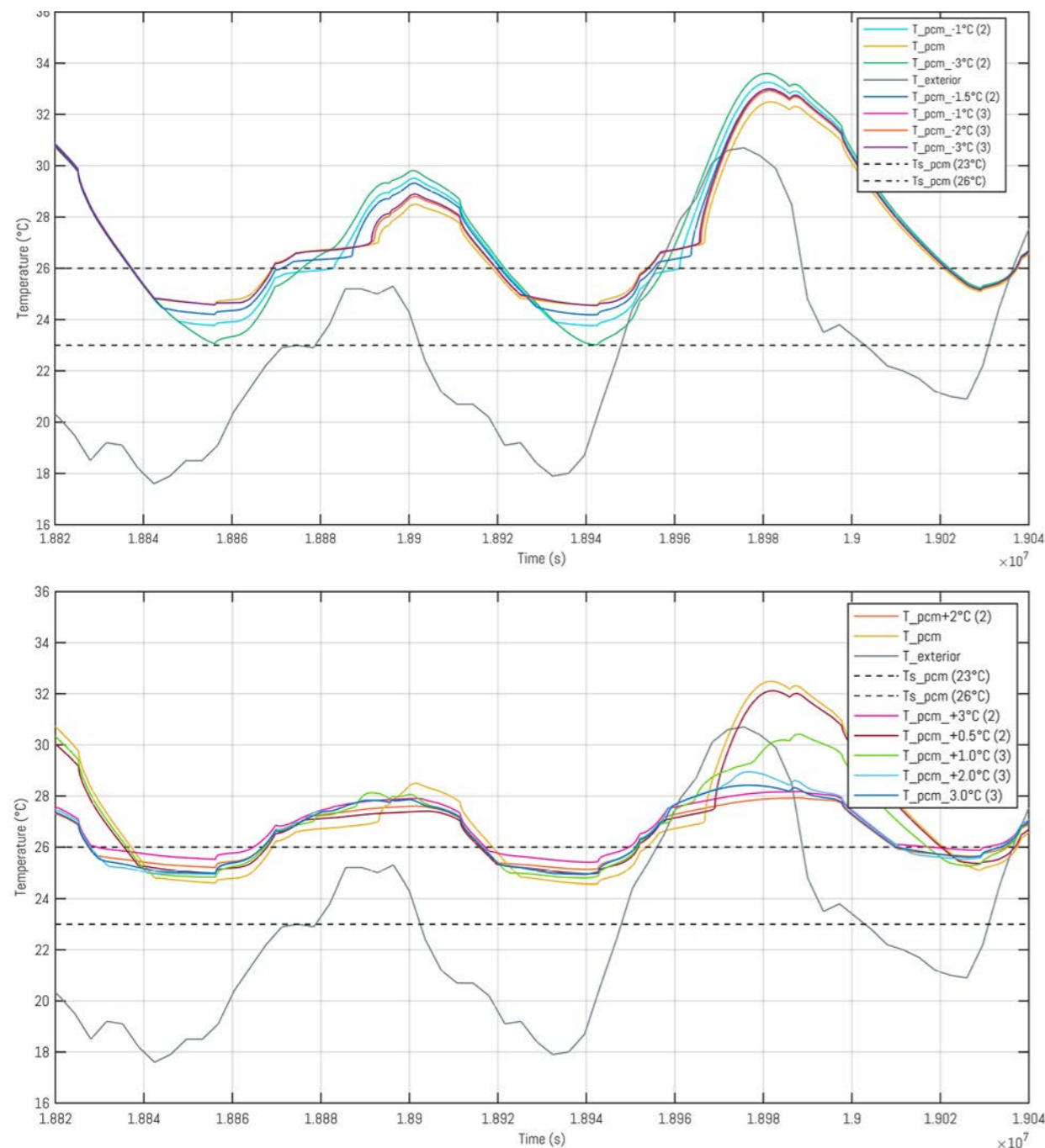
The difference in surface temperature is also evaluated for the two situation when considering the change in the solar absorption for the multi-layering system to indicate eventual discrepancies between the results. For the three different layers only small deviations in the surface temperature of the PCM are observed, a difference of around 0.3 degrees Celsius is observed for both the typical and the extreme situations. This indicates that only small deviations are seen, these differences seem valid for the simulations, so the addition of multiple layers did not significantly affect the results from the air temperature. Now the PCM temperature of each layer will be varied to consider whether the results show inadequate trends.

Figure 1.82
Graphs showing the temperature validation for the solar absorption within the multi-layering system, typical summer situation (top) and extreme summer situation (bottom) (By author)



Now changing the parameters from the different layers will give differences in results, these differences will be evaluated to check whether the simulation within MATLAB is valid. The graphs in Figure 1.83 show the temperature distribution on the surface of the PCM with various deviations between the melting temperatures of the different layers. The yellow line indicates the surface temperature of the normal situation with the same melting temperatures for each layer. The value between the brackets indicates the number of layers and the definition of the line defines the temperature difference between the first and the last layer. The results show no extraordinary deviations only small steps in the temperature curve are seen, this indicates that by varying the temperatures within the layers the model responds well.

Figure 1.83
Graphs showing the temperature distribution for the different melting temperatures within the multi-layering system, descending temperature situation (top) and ascending temperature situation (bottom) (By author)



5.7 OPTIMIZATION STRATEGY

Four main optimization strategies will be used, one that focuses on reducing the heating load, one for the reduction in cooling load, one for the all-season energy reduction and one for the actual cost-effective optimization. In the end, these four will be combined either to one design or to an adaptive design, this method is used to give a more deep insight on the effect of the configuration of the PCM Trombe wall in both heating and cooling mode. The final optimization targets three main objectives and two sub-objectives to create a cost-effective and thermodynamically optimized design, these objectives are illustrated in Figure 1.84. More objectives will reduce the accuracy of the optimization due to the complexity in finding the optimal solution, each of the input variables needs to be optimized according to these objectives and this reduces the capability of getting as close to an optimal solution. The objectives will not contain any constraints, when the results are lower also the overall production costs of the system will be reduced, which is wanted.

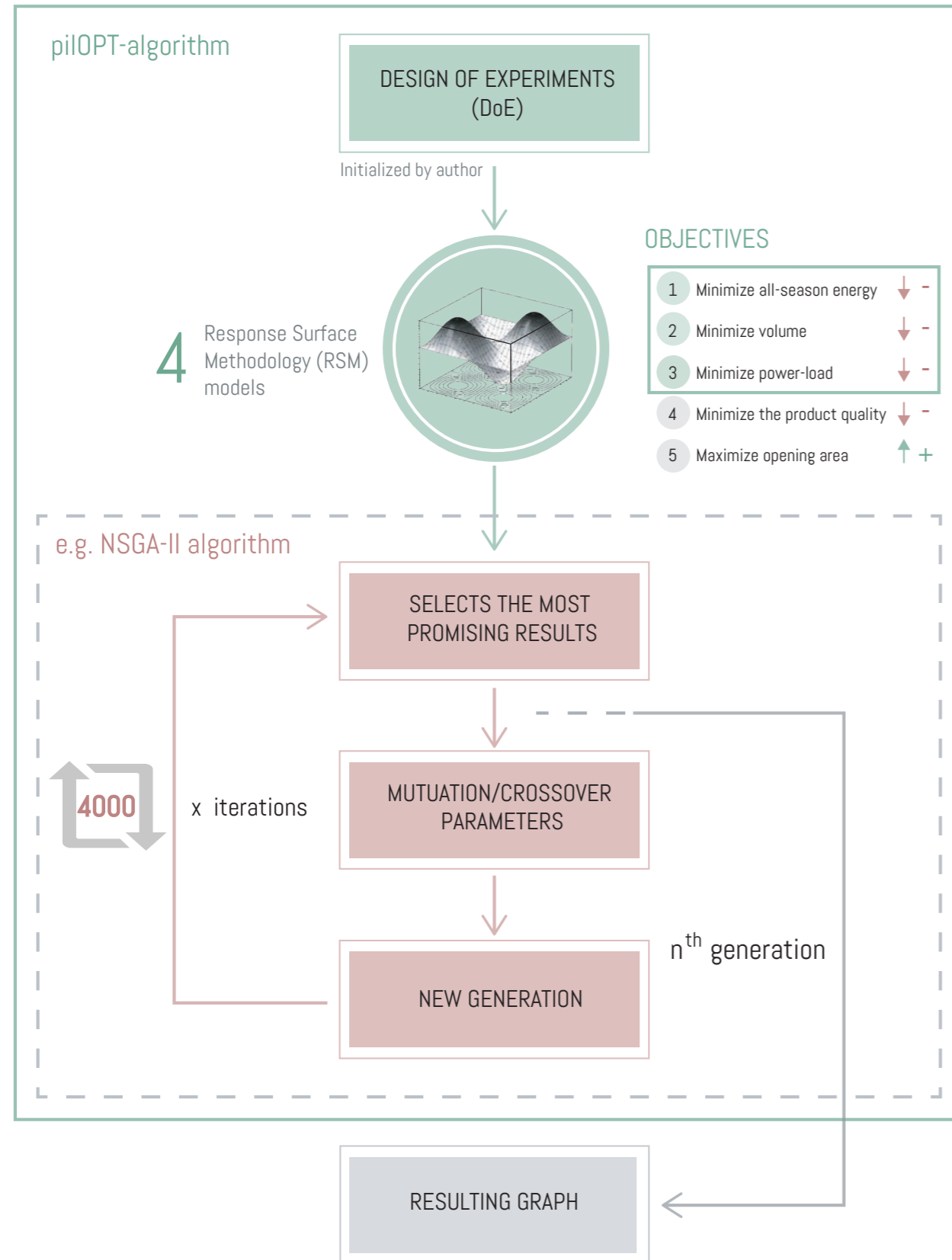
5.7.1 Optimization algorithm

MATLAB/Simulink computes and calculates the heating and cooling loads and modeFRONTIER, a design optimization tool by ESTECO SpA (2018), integrates these simulation codes and uses them to optimize, analyse and visualize the corresponding results in an automatic optimization loop. Different optimization algorithms can be used for this optimization process, Genetic Algorithms (GAs) seem to be the most applied optimization algorithm in Building Performance Simulations (BPS) when considering a first, less detailed, global optimization (Nguyen, Reiter, & Rigo, 2014). This research study focuses on this global search to point out the differences between various input variables by comparing them, here a quasi-optimal solution gives a first indication on the actual performance of the PCM regarding its cost-effectiveness.

GAs are meta-heuristic algorithms inspired by the process of natural selection as seen in nature (Nguyen, Reiter, & Rigo, 2014). The Non-dominated Sorting Genetic Algorithm II (NSGA-II) is commonly used for multi-objective optimizations with continuous variables (ESTECO SpA, 2018), the selection process is guided towards a uniformly distributed Pareto front of the optimization. In this way, the dominated design solutions are neglected and only the optimal solutions are combined with each-other to create new generations using Cross-over and Mutation (ESTECO SpA, 2018). They are popular due to the capability of handling multi-objective optimization problems and discontinuity in the results without being trapped in local minimums, in summary a robust and reliable simulation algorithm (Nguyen, Reiter, & Rigo, 2014; ESTECO SpA, 2018). Here robustness refers to getting as close as possible to the optimum solution from the objective function, the absolute extreme (ESTECO SpA, 2018). Another important concept within optimization algorithms is the convergence rate of the algorithm, this specifically refers to the efficiency in finding an optimal solution, or to reach convergence, within as little generations as possible (ESTECO SpA, 2018). A disadvantage of these genetic algorithms is the low convergence rate when a relatively high accuracy is required for more detailed processing (ESTECO SpA, 2018).

The performance of this optimization method can be enhanced using a Genetic Algorithm combined with the Response Surface Methodology (RSM), this reduces the simulation time needed for optimization. A similar optimization approach has been used by Manzan & Clarich (2017), a RSM model has been used to reduce the runtime of an integrated thermal and daylight optimization for an external shading device. RSM creates meta-models that approximate the input and output behaviour of the optimizations using the

Figure 1.84
Illustration of the optimization process using a combination of a genetic algorithm and RSM modelling (By author)



information from previously evaluated designs (Manzan & Clarich, 2017), this method falls within the domain of machine learning. Different types of meta-models can be trained, modeFRONTIER has some built in RSM options based on Interpolating RSMs or Approximating RSMs. The different meta-models can be compared to rank them based on their accuracy and performance, the more accurate the model the more accurate the final results (ESTECO SpA, 2018).

- Interpolating RSMs: K-nearest, Kriging and Radial, Basis Function;
- Approximating RSMs: Polynomial SVD, Parametric Surfaces, Gaussian Processes, Neural Networks and Evolutionary Design. (ESTECO SpA, 2018)

Each objective from the optimization is used as input for the RSM training, in this way the effectiveness is evaluated for each meta-model in all the optimization cases (Manzan & Clarich, 2017). The multi-strategy pilOPT-algorithm within modeFRONTIER combines this previously mentioned optimization method into one strategy, the algorithm learns from the genetic algorithm and uses this information as input for new RSM models to increase the accuracy of these models (ESTECO SpA, 2018). There is a constant interaction between the real optimization from for example the NSGA-II algorithm and the virtual optimization from the RSM models, this improves the robustness of the process and the quality of the optimization.

5.7.2 Number of evaluations

The number of evaluations within the optimization study is determined by a convergence of the model. The time for the convergence of the simulation is determined by estimating the number of evaluations needed, a greater population size will lead to more evaluations needed to converge to the optimal solution within the available time. Some test simulation runs showed that the pilOPT-algorithm converges relatively quick and already within a few hundred simulations the algorithm converges towards the pareto-front and neglects the dominated solutions. Post-processing of the results will be done by evaluating the results from several generations in between the start and the final result, at every new generation the results will be plotted to define the effect of each variable. The Design of Experiments (DoE) is initialized by the author to first generate plots based on varying just one variable at a time and keeping the other variables constant, in this way more knowledge is created on the resulting principle of each variable on its own and its effect on the performance of the system.

For each optimization around 4000 iterations will be used, the process of the optimization will be assessed during the run. The optimization can be considered complete when the simulation converges to a quasi optimal solution and when a large number of designs is grouped together at the pareto-front. An online server network will be used to execute all these optimization iterations, up to 16.000 iterations are needed and this is only possible using heavy computing systems. Therefore the BK Renderfarm from the Delft University of Technology will be used, combining this with the Concurrent Design Evaluations-function within modeFRONTIER significantly speeds up the process. In this way all the optimization can run parallel on multiple cores. The results from the optimization will be evaluated more in detail in Section "6.3 OPTIMIZATION EVALUATION" to give insight into the effect of each optimization on the input parameters and the most effective parameters for each solution.

5.8 CONCLUSION: PART V

CHAPTER: "5. COMPUTATIONAL PHASE"

The aim of this research study is comparing the different design strategies on the performance in thermodynamics and the cost-effectiveness, this will be evaluated using a combination of MATLAB® and Simulink®. With these simulation platforms the yearly energy demand of the room can be calculated, no complex computational fluid dynamics (CFD) analysis will be included. An initial simulation model is adopted within this research, this model is developed and extended according to the needs from the different design strategies. The initial simulation model is based on a simple cubicle room known as the '*Control room*'. The PCM facade panel is directly placed behind the south facing facade with a small cavity in-between the south facing window and the panel.

First the model is validated using the DesignBuilder simulation software, exactly the same setup is created to evaluate and compare the results from both the platform. Three extreme situations are simulated to indicate the change in the results, these sensitive parameters cause significant changes within the model. The results show that a maximum 12.2% difference (equal to 30 kWh) on yearly base is observed for the heating situation, the other results vary between 2.7% and 5.5% difference. These results indicate relatively small deviations, this implies that the model is valid for the application with the use of the referenced weather files. Also the peaks in the graphs are compared to evaluate the trend of the temperature within the model, here it is noticed that the only difference is found in the height of the peaks. After that the changes made to this model are concisely validated according to the expectation on the behaviour of the model, no unexpected behaviour may occur within the model.

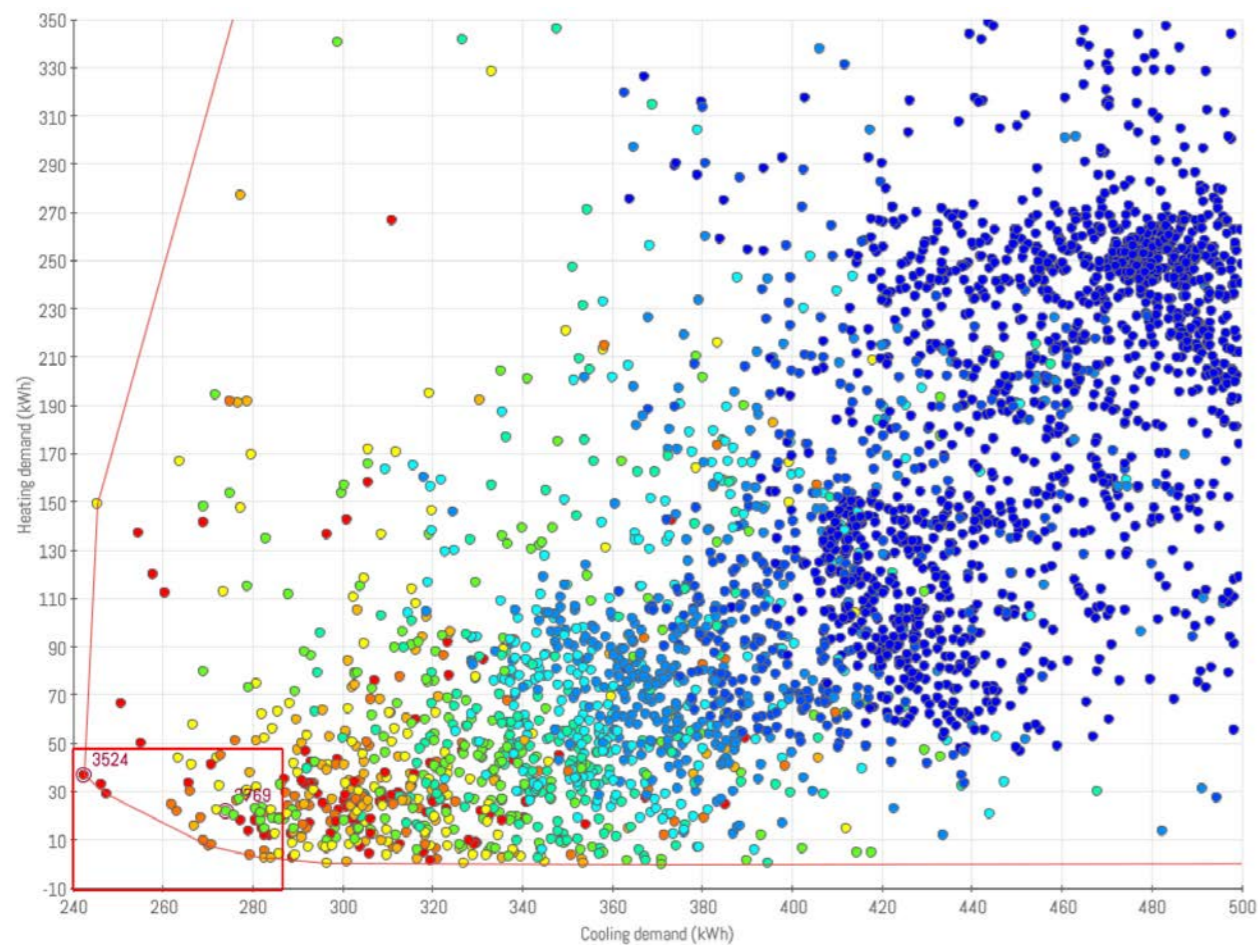
The simulation and optimization phase is based on three main principles, the Design of Experiments (DoE) regarding the thermodynamics, the DoE regarding the cost-effectiveness and lastly the different optimization strategies. For the thermodynamic DoE ten main strategies are adopted to evaluate the performance of each parameter by changing one parameter at the time. The results from this study will be compared with each-other to indicate the differences in energy reduction between the different designs for each target solution (summer, winter, all-season). The cost-effective DoE is introduced to reveal the differences between the energy reduction and the actual cost reduction. Results from this first study will be used as input for the optimization phase, within this optimization four main categories will be targeted (cooling, heating, all-season and economic optimization). The final optimization focused on finding an economically interesting design, which is based on three main objectives, the reduction in the heating and cooling energy demand, minimizing the volume needed and reducing the maximum power-loads within the room. The last one reduces the size of the equipment to cut down the total cost of ownership. All the information gathered from the simulation and optimization studies will be summarized in a design guideline and in one specific office design case as illustrated in the simulation flow in Figure 1.62 on page 87.

6. SIMULATION RESULTS

This section answers the sub-research questions: *What is the most efficient thermodynamic optimization, of a PCM Trombe wall, considering the different heat transfer enhancement techniques?* and *What is the most cost-effective optimization of a PCM Trombe wall?* The thermodynamic optimization deals with the use of energy and the relation with the indoor air temperatures within the building to evaluate the performance of the system more in detail. First a Design of Experiments (DoE) is used, with this method one parameter at a time is varied. The results from each strategy will be evaluated considering the extreme temperatures for winter and summer situations, these situations will give a clear insight in the effectiveness on the energy performance.

The cost-effective optimization is defined by the total cost of ownership of the overall auxiliary system, including the PCM Trombe wall. Three main principles will be used to assess and optimize the wall, these are the reduction in the yearly energy usage, the reduction in the maximum power-load and the reduction of the cost of the PCM product. These two evaluation and optimization strategies will be brought together in the end to summarize and identify the actual differences, a design guideline will be given to illustrate these differences. This guideline is used to give a clear overview of the deviations, the detailed results from this chapter together with the design guideline can be used as input for designing a PCM Trombe wall.

Figure 1.85
Scattered chart with the different design variants from all-season energy optimization (By author)



6.1 THERMODYNAMIC EVALUATION

This section describes the thermodynamic analysis of the Design of Experiments, the stepped analysis diagram shown below illustrates the input parameters for this simulation. The analysis focuses on a more detailed study in understanding the main trend within each variable and to assess whether overheating occurs or other discrepancies within the results are observed, the energy reduction performance gives insight on the yearly performance for an 60 m² office. A detailed overview with the input parameters is given in "APPENDIX D". The extreme winter situation is from day 54 (23 Februari) till day 58 (27 Februari) and the extreme summer situation starts on day 190 (9 July) until day 194 (13 July). The benchmark energy demand results for heating (329 kWh) and for cooling (1132 kWh) are used for comparison on the actual performance improvement ("APPENDIX D").

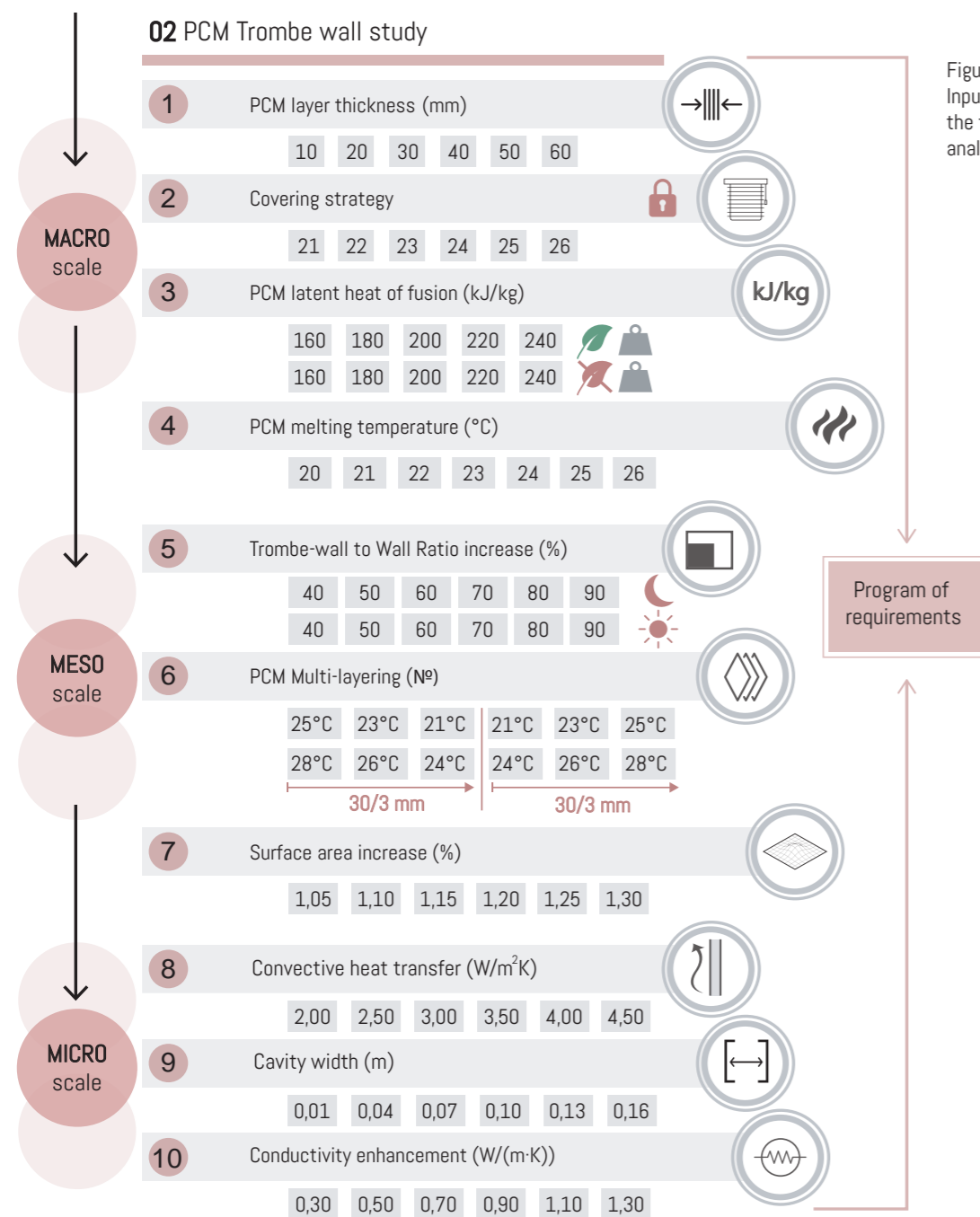


Figure 1.86
Input parameters for the thermodynamic analysis (by author)

6.1.1 MACRO: PCM layer thickness

First an overview is given from a combination of extreme and typical days within summer and winter period (Figure 1.87), this overview is used to indicate the actual effect of the variation in thickness on the PCM temperature and the indoor air temperature. In summer situation the rather typical day on the left shows almost no differentiation in air temperature between the thicknesses. On the extreme days the temperature is more stabilised for the 3 to 4 centimetre situations (Figure 1.87: red indication), less peaks are seen during these days. On the extreme winter days the results show that the thickness between 2 and 3 centimetres in winter situation is crucial for the performance of the system, the temperature of the PCM exceeds the limits for overheating which is around 45 °C, on extreme days the PCM temperature rises up to 60 °C for the 1 and 2 centimetre panels, so for salt hydrates in this climate at least 3 centimetre is needed to prevent from overheating.

Figure 1.87
Graphs with results from the variation in panel thickness for several running days in summer (top) and winter (bottom) situation (By author)

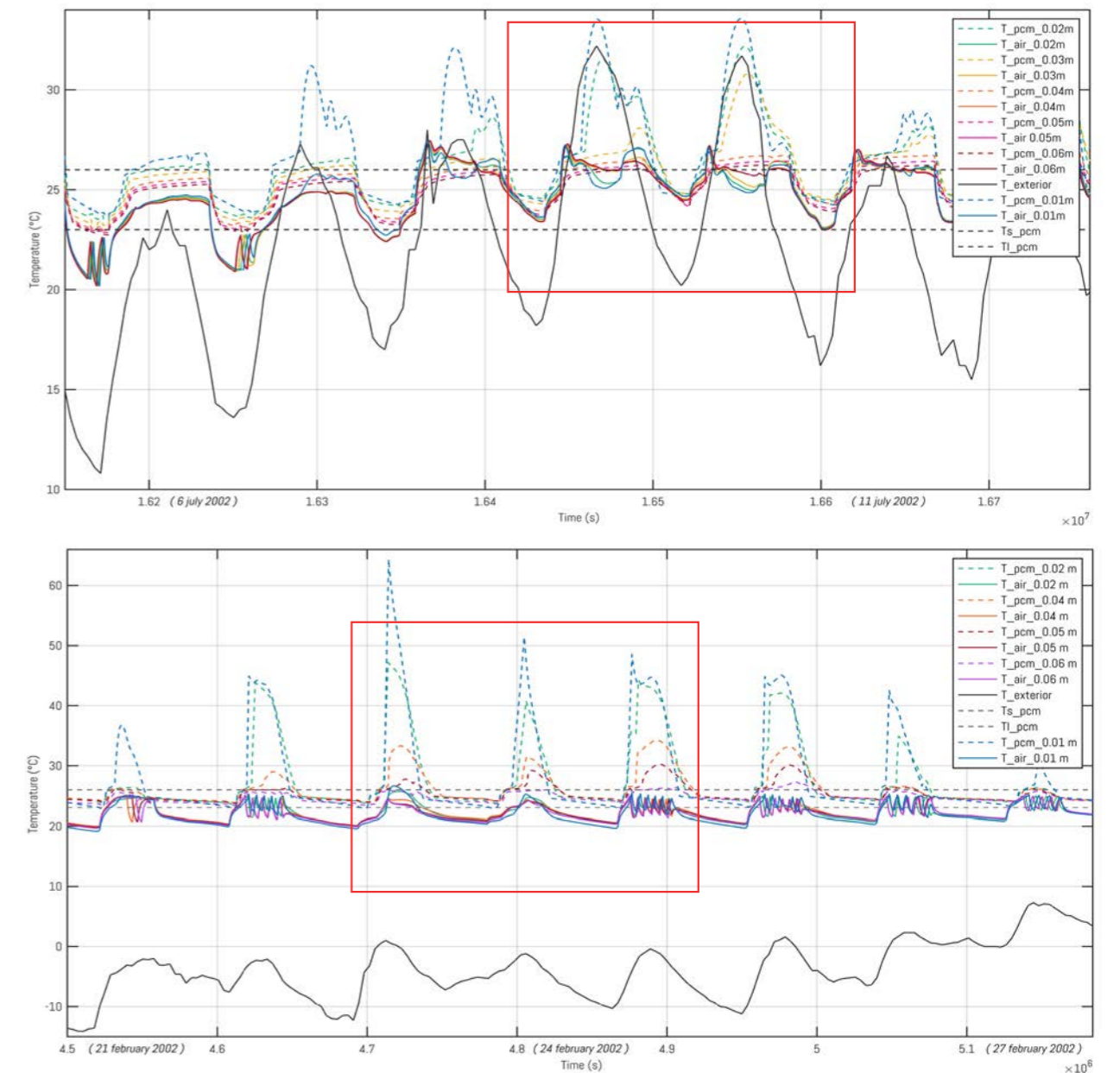


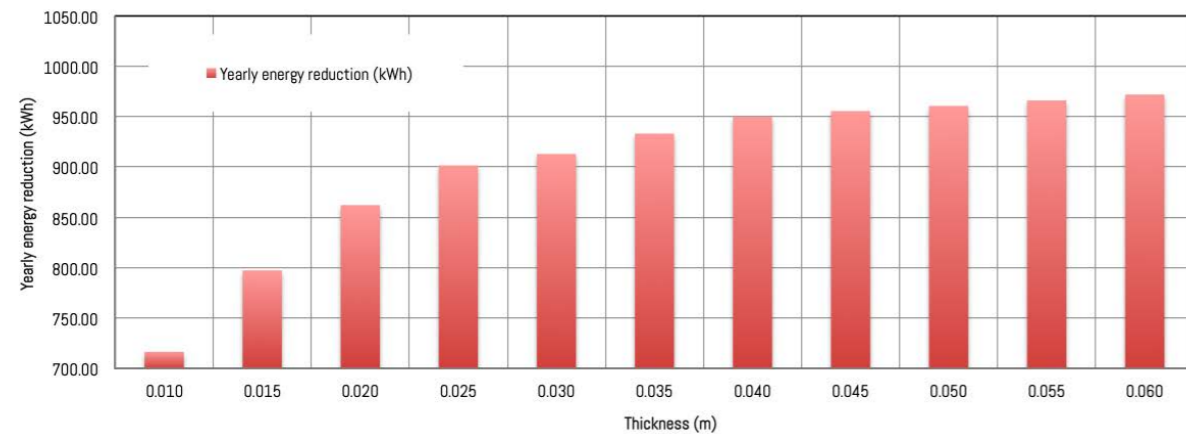
Table 1.10 Overview energy usage and energy reduction considering various PCM layer thicknesses

ID (#)	Panel thickness (m)	Cooling energy usage (kWh)	Heating energy usage (kWh)	Cooling reduction (%)	Heating reduction (%)	Cooling reduction (kWh)	Heating reduction (kWh)	Yearly energy reduction (kWh)
1.1	0.010	582.65	161.84	48.53	50.82	549.35	167.26	716.61
1.2	0.015	531.88	131.79	53.01	59.95	600.12	197.31	797.43
2.1	0.020	480.94	117.92	57.51	64.17	651.06	211.18	862.24
2.2	0.025	465.95	93.52	58.84	71.58	666.05	235.58	901.64
3.1	0.030	455.55	92.61	59.76	71.86	676.45	236.49	912.94
3.2	0.035	444.74	83.17	60.71	74.73	687.26	245.93	933.19
4.1	0.040	435.65	75.38	61.51	77.09	696.35	253.72	950.07
4.2	0.045	432.90	72.64	61.76	77.93	699.10	256.46	955.55
5.1	0.050	434.26	66.18	61.64	79.89	697.74	262.92	960.66
5.2	0.055	422.64	72.34	62.66	78.02	709.36	256.76	966.12
6	0.060	424.49	64.61	62.50	80.37	707.51	264.49	972.00

The objective for this variable is to reduce the amount of PCM needed, a smaller pcm layer results in less capital costs and has a lower impact on the usable area within office. The difference between the rentable square meters and the usable square meters needs to be as low as possible, the combination of the thickness and the width of the cavity are important for this consideration. Besides this, a reduction in material will also reduce the price of the latent heat storage unit, the material price of the PCM is rather expensive compared to the other materials that need to be included.

The results from the heating and cooling energy reduction (Table 1.10) show that a higher performance is achieved for the thicker PCM sections, however from a thickness of 3,5 centimetres the reduction becomes less as seen in Table 1.11, from this point the investment will not be worth the actual reduction in energy..

Table 1.11 Overview energy usage and energy reduction considering various PCM layer thicknesses



The first graph from the summer situation (Figure 1.88) shows a peak in the indoor air temperature which is reduced while the PCM temperature stays the same, at this moment the PCM absorbs the energy (indicated with red). A more horizontal the PCM temperature curve results in a more stable indoor climate and a lower air temperature at night, subsequently this gives a lower starting temperature for the next day which is beneficial considering the cooling load of the room. In winter the PCM needs to lift the air temperature to a higher temperature in the evening/night, Figure 1.89 shows that the 4 centimetre PCM creates the most stable temperature on an extreme diurnal cycle for the winter situation, this thickness gives a normal indoor temperature at day and a higher temperature at night.

The same benefit is observed in the summer situation, a thicker section in summer does not add to the performance of the system and in winter it reduces the air temperature within the building. Especially for the cooling season there is not much differentiation observed from panels with a thickness of 4 centimetre and higher, the same is observed in the energy demand results (Table 1.11).

Figure 1.88
Graphs with results from the variation in panel thickness for the extreme summer (By author)

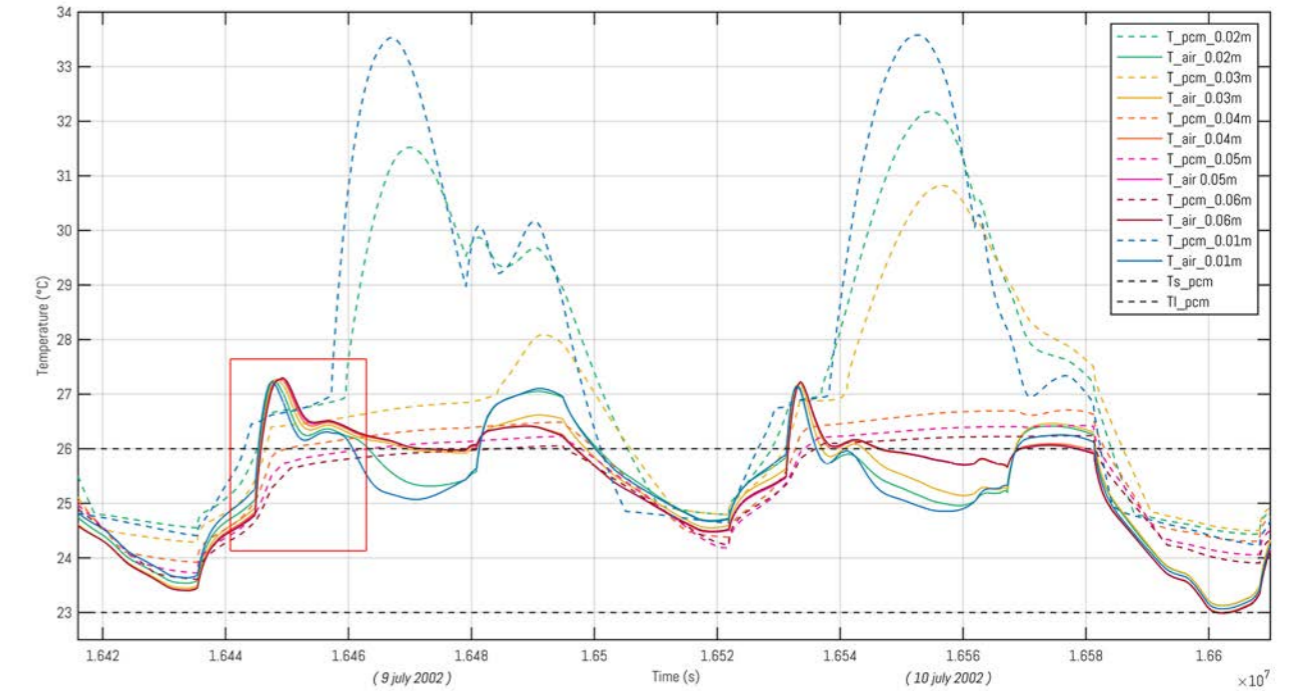
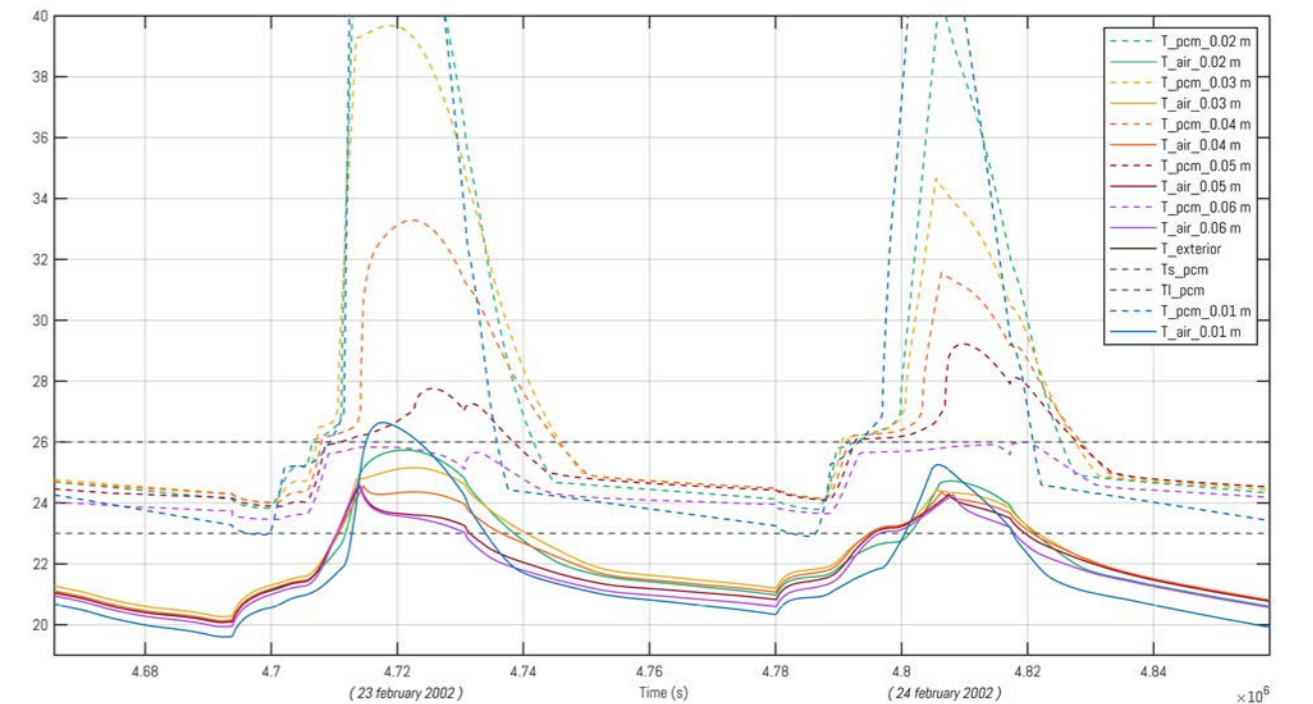


Figure 1.89
Graphs with results from the variation in panel thickness for the extreme winter situation (By author)



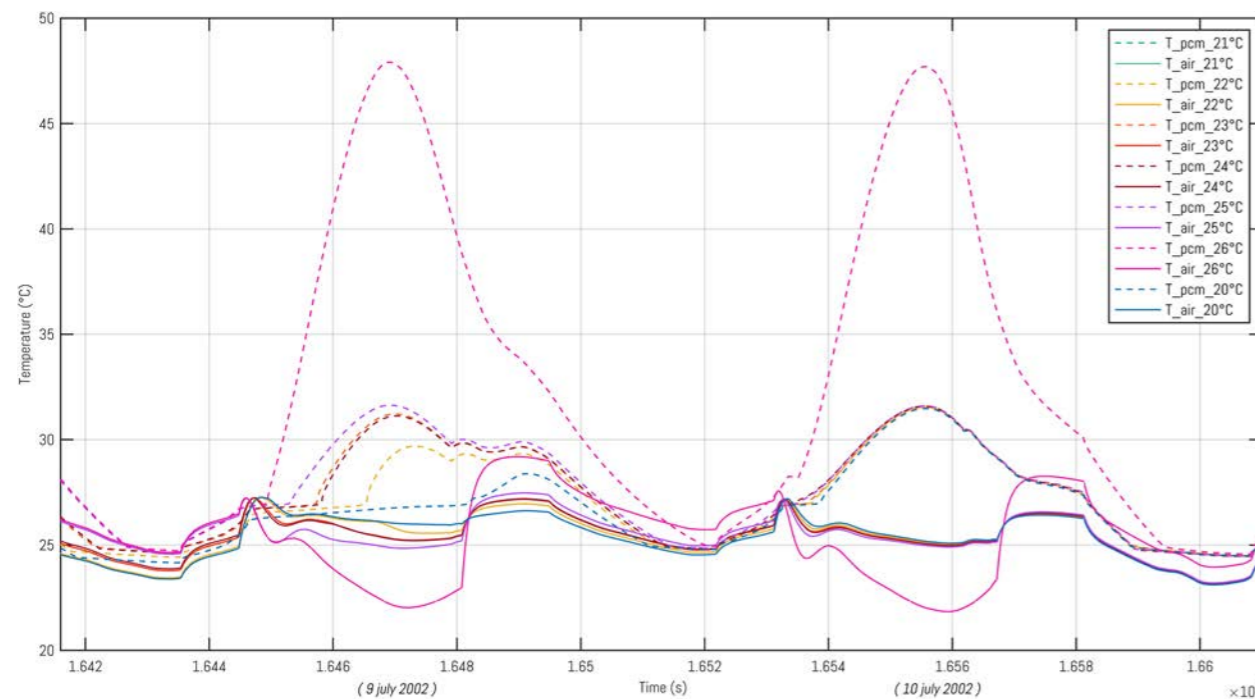
6.1.2 MACRO: Coverage (SHGC)

Table 1.12 Overview energy usage and energy reduction considering the different set-point temperatures for the sun-shading

ID (#)	Blind covering (°C)	Cooling energy usage (kWh)	Heating energy usage (kWh)	Cooling reduction (%)	Heating reduction (%)	Cooling reduction (kWh)	Heating reduction (kWh)	Yearly energy reduction (kWh)
7	20.00	447.12	163.91	60.50	50.19	684.88	165.19	850.07
8	21.00	445.06	129.46	60.68	60.66	686.94	199.64	886.57
9	22.00	465.95	93.52	58.84	71.58	666.05	235.58	901.64
10	23.00	580.24	82.24	48.74	75.01	551.76	246.86	798.62
11	24.00	829.40	79.02	-	75.99	-	250.08	250.08
12	25.00	3029.17	75.15	-	77.16	-	253.95	253.95
13	26.00	3328.89	72.90	-	77.85	-	256.20	256.20

The most important season for the shading strategy is the cooling season, the covering is used to reduce the external loads from the direct sun radiation. A standard solar heat gain coefficient (SHGC) of 0.7 is used for the glazing and 0.25 for the blinds in front of the glazing. In summer the PCM temperature in extreme situations goes up to 48°C (Figure 1.90), this will cause overheating of the PCM during warm summer days. A higher set-point temperature performs of-course better for the heating energy reduction, however the difference are negligible, the best performing set-point temperature for both seasons is 22°C. On extreme summer days this temperature also results in an relatively stable indoor air temperature, higher temperatures will create too high PCM and air temperatures. This set-point value will be fixed for the following simulations.

Figure 1.90
Graphs with results from the variation in set-point temperatures the for summer situation (By author)



6.1.3 MACRO: Latent heat of fusion

Table 1.13 Overview energy usage and energy reduction considering the latent heat of fusion for the organic PCM

ID (#)	Latent heat storage: organic (J/kg)	Cooling energy usage (kWh)	Heating energy usage (kWh)	Cooling reduction (%)	Heating reduction (%)	Cooling reduction (kWh)	Heating reduction (kWh)	Yearly energy reduction (kWh)
14	1.60E+05	538.08	139.14	52.47	57.72	593.92	189.96	783.88
15	1.80E+05	539.14	135.27	52.37	58.90	592.86	193.83	786.69
16	2.00E+05	532.68	119.86	52.94	63.58	599.32	209.24	808.56
17	2.20E+05	535.58	101.70	52.69	69.10	596.42	227.40	823.82
18	2.40E+05	531.85	103.41	53.02	68.58	600.15	225.69	825.84

Table 1.14 Overview energy usage and energy reduction considering the latent heat of fusion for the inorganic PCM

ID (#)	Latent heat storage: inorganic (J/kg)	Cooling energy usage (kWh)	Heating energy usage (kWh)	Cooling reduction (%)	Heating reduction (%)	Cooling reduction (kWh)	Heating reduction (kWh)	Yearly energy reduction (kWh)
19	1.60E+05	472.62	107.62	58.25	67.30	659.38	221.48	880.86
20	1.80E+05	465.95	93.52	58.84	71.58	666.05	235.58	901.64
21	2.00E+05	465.08	85.48	58.92	74.02	666.92	243.62	910.54
22	2.20E+05	458.99	70.20	59.45	78.67	673.01	258.90	931.90
23	2.40E+05	445.60	76.31	60.64	76.81	686.40	252.79	939.19

For the different organic mixtures [#14-18] the PCM temperature rises too much for the winter situation (Figure 1.91), in this particular situation the solar altitude angle is lower compared to the summer situation. Therefore, more direct solar radiation is received at the PCM surface, this significantly increases the temperature of the PCM and the risk for overheating of the PCM. With the simulated 2,5 centimetre PCM overheating will occur, the temperature of the PCM rises up to 47°C (Figure 1.91). As mentioned before the maximum temperature aloud within the PCM is around 45°C for inorganic sal-hydrates from Rubitherm, for the organic PCM this is around 55°C depending on the melting temperature of the compound (Rubitherm, 2019). Increasing the thickness of the PCM also increases the amount of solar energy absorbed by the material, this reduces the overheating effect. Some extra thicknesses are simulated to evaluate the PCM temperature for these values, these are shown in Figure 1.91 (0.035m and 0.045m). The purple and pink line illustrate this effect of the increase in thickness with the same latent heat of fusion (240 kJ/kg), only these thicknesses seem valid for the application of inorganic PCMs in this specific design case. This is specifically needed for the organic PCM due to a combination of a lower material density, this results in a lower latent heat capacity of the material. It can be noticed that the PCM also stays longer within the transition phase, however these differences are relatively small and will not create significant differentiation for the energy performance. The oscilattion seen on the last three days (Figure 1.91) indicates the opening of the cavity vents from the Trombe wall, when the air temperature rises over 23°C these vents are opened to allow for a natural airflow, below th 22°C they are closed.

For the inorganic mixture (Figure 1.92) it can be noticed that on extreme days only the 4,5 centimetre PCM is activated by the drop in the temperature at the beginning of the day. For the total energy reduction,

the highest latent heat of fusion (#23) increases the yearly performance of the unit with just 6.7% compared to the lowest (#19). So in general, the organic PCM has not enough capacity for the application when considering heat storage units with a small thickness to surface area ratio. The PCM tends to overheat due to a lower latent heat capacity compared to inorganic PCMs, all the simulated latent heat of fusion values for the standard 2,5 centimetre panel show too high PCM temperatures. Comparing the two situations no large deviations are observed in the air temperatures, the biggest difference is the possibility for overheating between the two different compounds. The results show a performance increase of 12.1% for the energy performance index (825,84 / 939,19 kWh) comparing the inorganic and the organic compound.

Figure 1.91
Graphs with results from the variation in the latent heat of fusion for organic PCM in winter situation (By author)

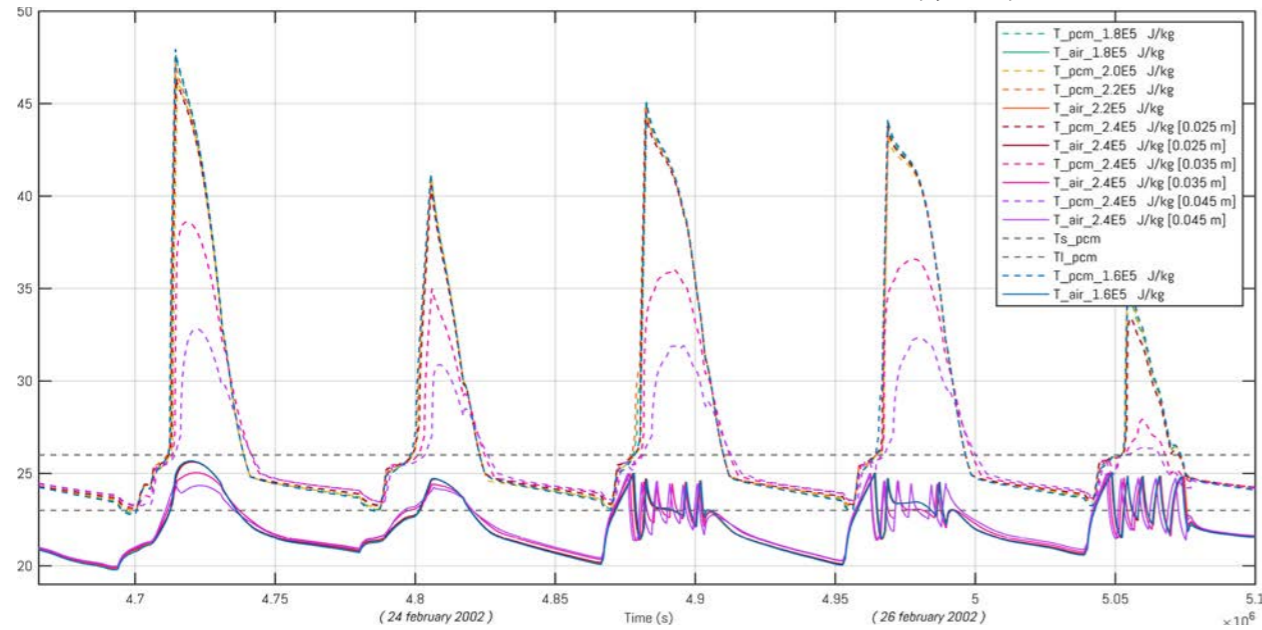
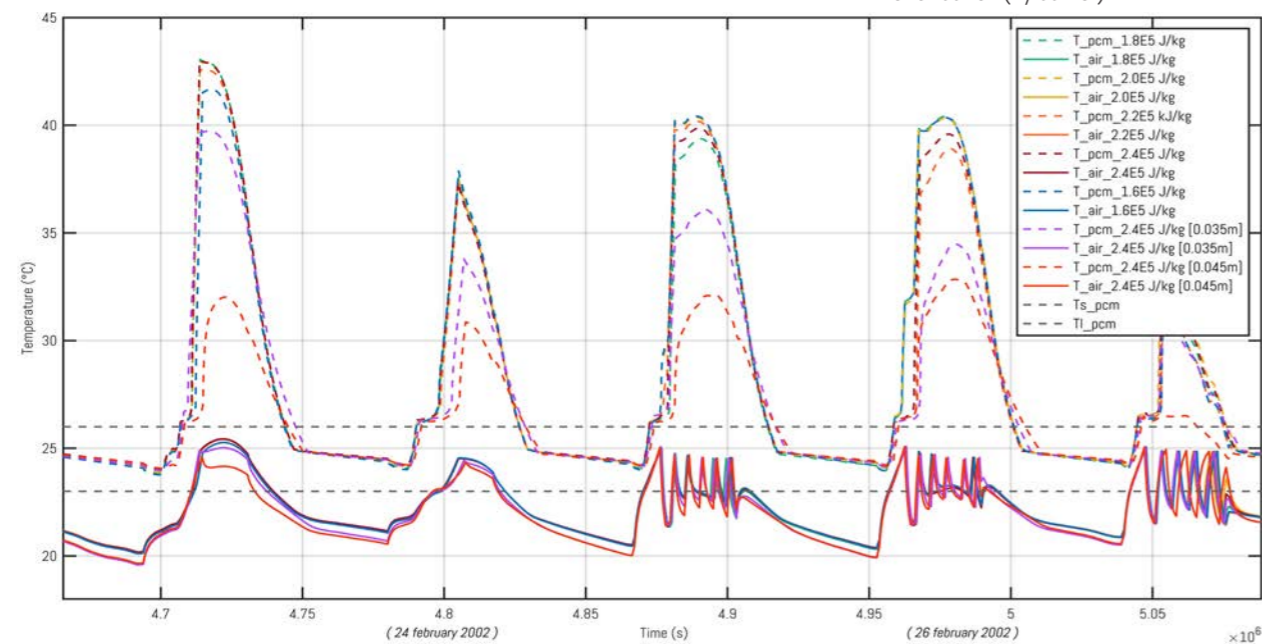


Figure 1.92
Graphs with results from the variation in the latent heat of fusion for the inorganic PCM in winter situation (By author)



6.14 MACRO: Melting temperature

Table 1.15 Overview energy usage and energy reduction considering various melting PCM temperatures

ID (#)	Melting temperature (°C)	Cooling energy usage (kWh)	Heating energy usage (kWh)	Cooling reduction (%)	Heating reduction (%)	Cooling reduction (kWh)	Heating reduction (kWh)	Yearly energy reduction (kWh)
24	20.00	657.90	135.43	41.88	58.85	474.10	193.67	667.76
25	21.00	639.30	108.92	43.52	66.90	492.70	220.18	712.88
26	22.00	605.88	92.71	46.48	71.83	526.12	236.39	762.52
27	23.00	566.55	89.46	49.95	72.82	565.45	239.64	805.09
28	24.00	517.66	92.67	54.27	71.84	614.34	236.43	850.77
29	25.00	465.95	93.52	58.84	71.58	666.05	235.58	901.64
30	26.00	444.46	116.98	60.74	64.45	687.54	212.12	899.66

The temperature graphs with the indoor air temperature show that a higher melting temperature gives better results in the extreme winter and summer situations, in summer the temperature is lower and more stable (Figure 1.93) and in winter the diurnal air temperature is higher and more stable (Figure 1.94). However, the total yearly energy reduction for the heating situation shows different results. A lower melting temperature of 23°C performance best for the heating season and a high melting temperature of 26°C for cooling, on yearly base a melting temperature of 25°C gives the highest energy reduction. This is mainly because of the difference in magnitude of the energy reduction for cooling and heating, more cooling energy is needed on yearly base. The plot of the PCM temperature and air temperature also shows a clear difference in summer situation, the PCM temperature with the 25°C melting temperature or higher stays almost at the same level. This indicates that the PCM absorbs all the heat from the adjacent air without transforming to a full liquid phase (Figure 1.93). In the end, this results in the lowest overall air temperature during the night and the most stable temperature during the day. The other melting temperatures do not stay long within the nucleation phase, the PCM melts too quick. In this specific design case, an application with two melting temperatures will only increase the performance of the system by 25.54 kWh (239.64 + 687.54 - 901.64 kWh), therefore the 25°C melting temperature seems most appropriate for the yearly application considering the energy reduction.

Figure 1.93
Graphs with results from the variation in the melting temperature in summer situation (By author)

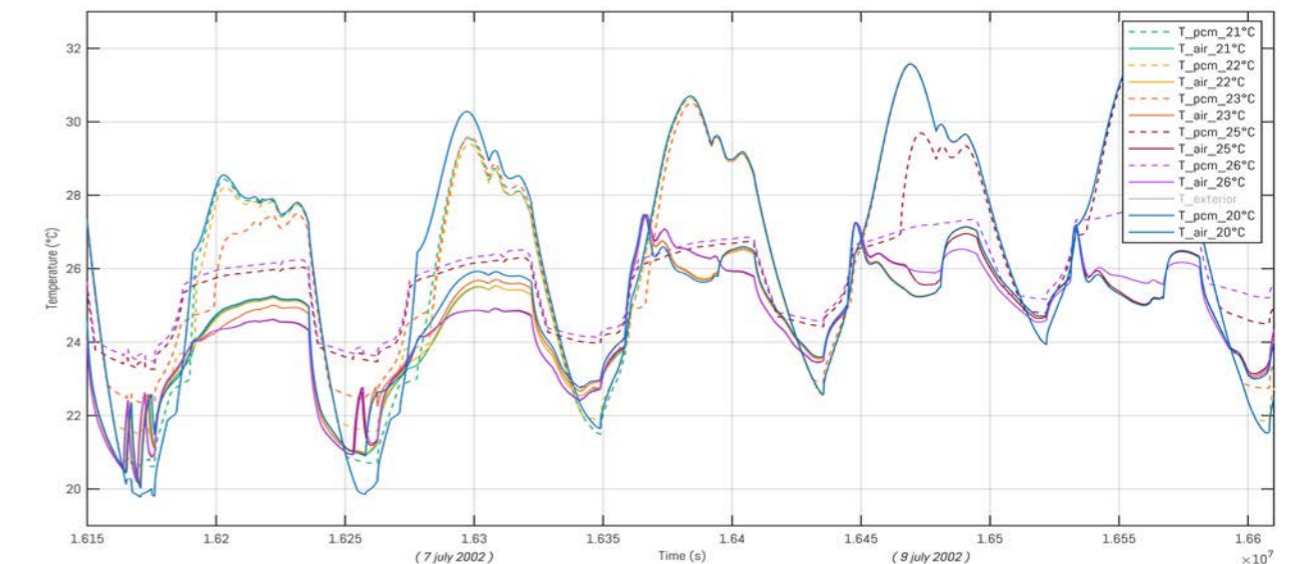
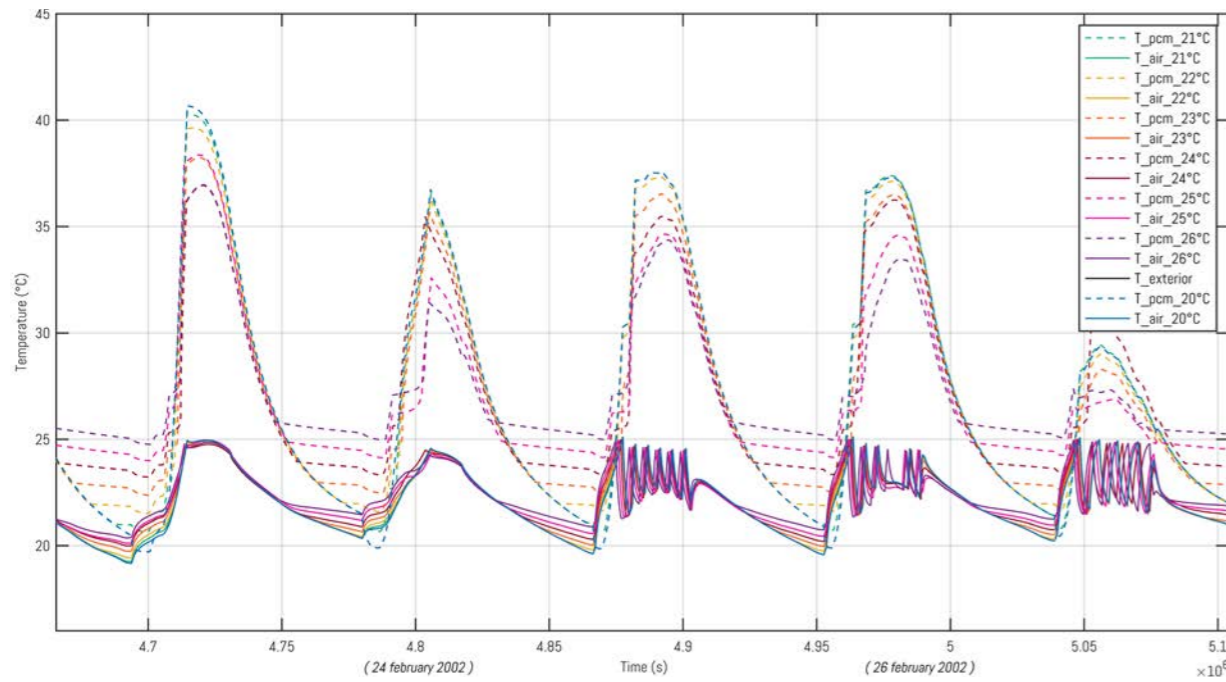


Figure 1.94
Graphs with results from the variation in the melting temperature in the extreme winter situation (By author)



6.1.5 MESO: Trombe wall to wall ratio (TWR)

Table 1.16 Overview energy usage and energy reduction considering various TWRs: PCM faces the room [TWR 1]

ID (#)	Trombe wall ratio 1 (%)	Cooling energy usage (kWh)	Heating energy usage (kWh)	Cooling reduction (%)	Heating reduction (%)	Cooling reduction (kWh)	Heating reduction (kWh)	Yearly energy reduction (kWh)
31	0.40	451.99	474.72	60.07	-44.25	680.01	-145.62	534.39
32	0.50	453.05	396.87	59.98	-20.59	678.95	-67.77	611.18
33	0.60	461.44	299.20	59.24	9.09	670.56	29.90	700.46
34	0.70	453.50	270.48	59.94	17.81	678.50	58.62	737.12
35	0.80	451.90	209.00	60.08	36.49	680.10	120.10	800.20
36	0.90	450.20	156.50	60.23	52.45	681.80	172.60	854.40

Table 1.17 Overview energy usage and energy reduction considering various TWRs: PCM facing the cavity [TWR 2]

ID (#)	Trombe wall ratio 2 (%)	Cooling energy usage (kWh)	Heating energy usage (kWh)	Cooling reduction (%)	Heating reduction (%)	Cooling reduction (kWh)	Heating reduction (kWh)	Yearly energy reduction (kWh)
37	0.40	343.42	764.97	69.66	-132.44	788.58	-435.87	352.71
38	0.50	363.30	610.00	67.91	-85.35	768.70	-280.90	487.80
39	0.60	377.62	474.48	66.64	-44.18	754.38	-145.38	609.00
40	0.70	383.74	343.46	66.10	-4.36	748.26	-14.36	733.90
41	0.80	415.27	233.81	63.32	28.95	716.73	95.29	812.02
42	0.90	451.90	156.50	60.08	52.45	680.10	172.60	852.70

Two Trombe wall to wall ratios (TWR) are simulated according to the rotation schedule of the latent heat storage unit, in each situation the volume of the PCM is kept the same. The first strategy (TWR 1) simulates the effect of the opening area when the PCM is facing the room, so during a summer day (charging from the room) and a winter night (discharging towards the room). The second strategy (TWR 2)

considers the effect of the opening area when the PCM faces the cavity, this relates to a summer night (discharging towards the cavity) and a winter day (charging from the sun). The results from the energy reduction from these two strategy clearly show that a higher Trombe wall ratio performs better considering the heating energy demand (Table 1.16 and Table 1.17). In this case the PCM is used on the one hand to absorb the direct sun radiation and release it to the interior during the night due to a larger surface area available (Figure 1.95). On the other hand the PCM works as extra insulation layer to prevent heat loss to the exterior. For the panels with a small TWR this energy is not released during the night to the interior, this results in a higher PCM temperature for this design. The total thickness of the PCM is too small, this is seen in the overheating effect. For this situation, a larger TWR results in a higher overall yearly energy reduction for cooling and heating combined.

Figure 1.95
Graphs with results from the variation in the TWR [1] in an extreme winter situation (By author)

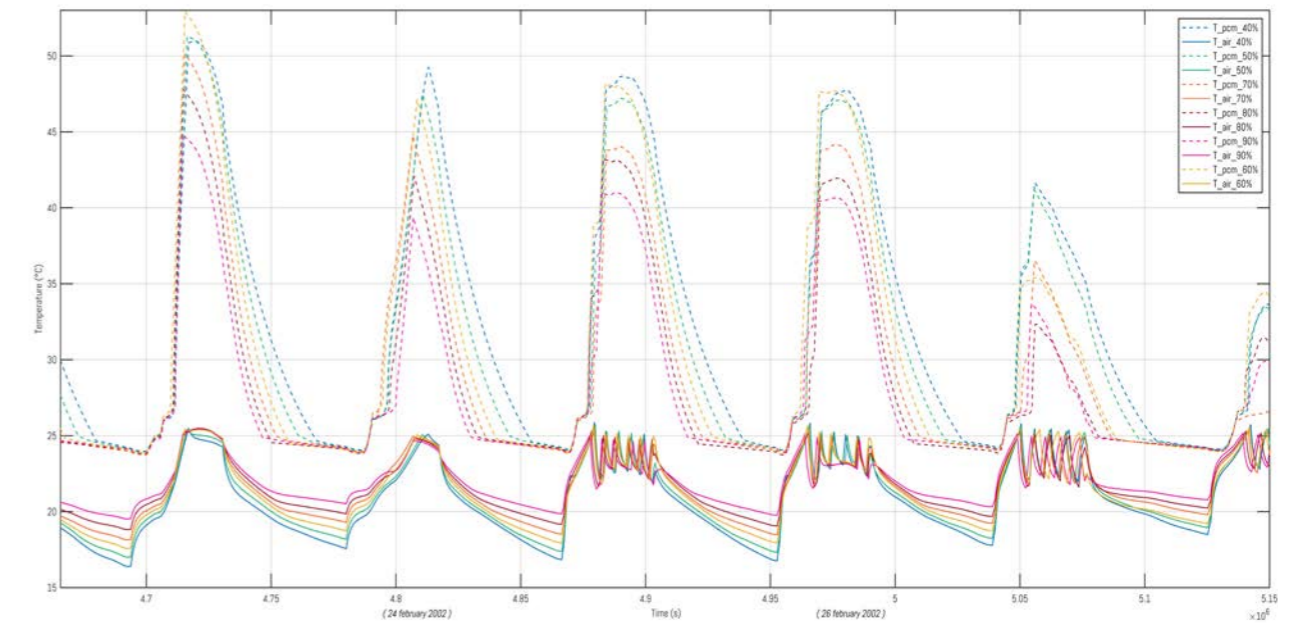
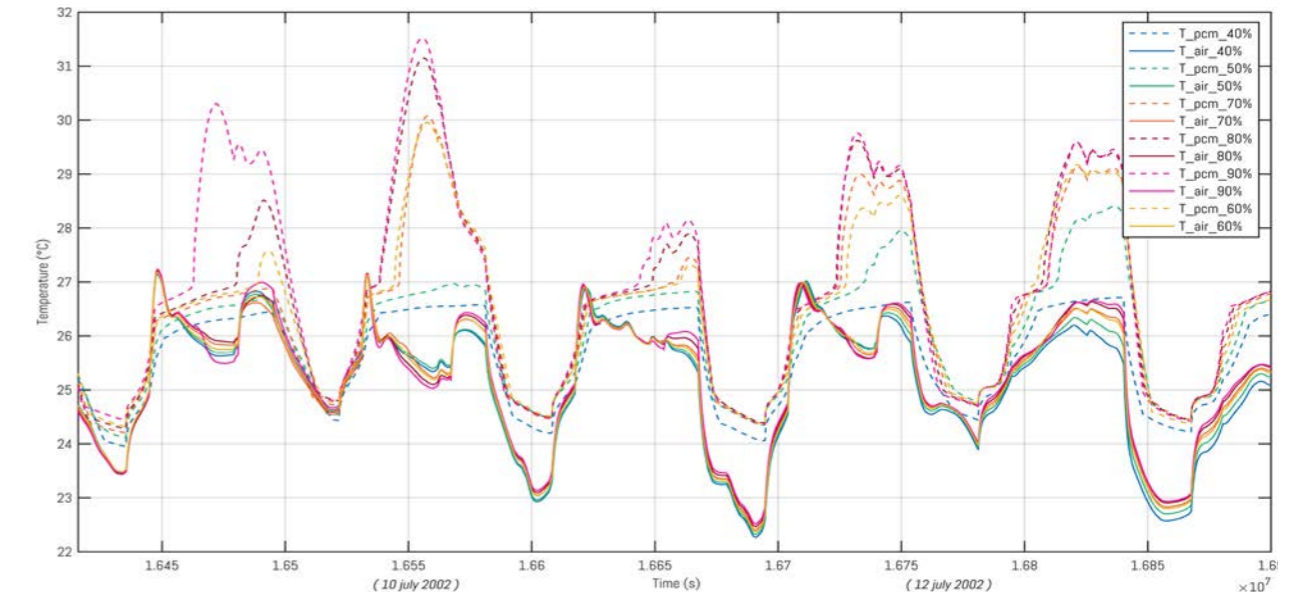


Figure 1.96
Graphs with results from the variation in the TWR [1] in an extreme summer situation (By author)

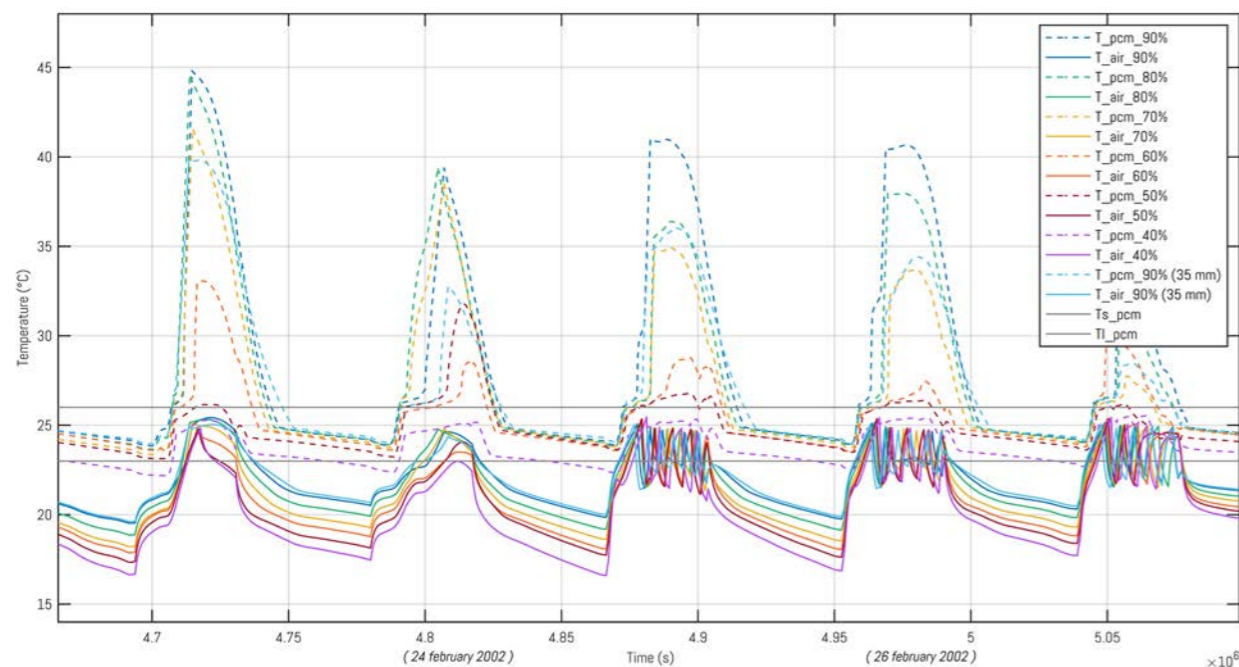


From the detailed graph it is shown that on the rather extreme summer days (Figure 1.96), a smaller panel ratio gives a lower and more stable air temperature within one diurnal cycle. For these ratios the PCM is activated effectively indicated by the horizontally developing PCM temperature for the 40% and 50% panel. The section thickness is larger due to the preserved panel volume, therefore the PCM does not fully liquefy. Only small deviations are observed in the cooling season when the PCM is facing the room (Table 1.16), in this case the PCM absorbs the heat from the interior but it also blocks the direct airflow towards the exterior, for heating these differences are much more significant.

The results from TWR 2 clearly show the effect on the heating and cooling energy demand, for the heating energy demand it is noticed that with a lower TWR less energy is released to the interior during the night and more heat seems to be lost resulting in a lower overall night temperature (Figure 1.97). Additionally, the direct sun radiation during the day is all absorbed and blocked by the PCM due to a higher TWR, so this strategy results in a negative performance. Therefore, the PCM needs to be fully closed during a winter night. On the other hand, a lower TWR in summer results in a higher air flow rate from the room towards the exterior, this reduces the PCM temperature and the air temperature and subsequently reduces the need for cooling as seen in Table 1.17.

In the end, the results clearly tell that a lower TWR results in a negative performance regarding the heating mode of the PCM in both the situations (absorbing from the exterior on a winter day and releasing towards the interior during night). The TWR during the cooling mode on the other hand does not make a lot of difference when the PCM absorbs the heat from the interior (TWR 1) and a lower TWR performs better for the situation when the PCM needs to cool the room during the night (TWR 2).

Figure 1.97
Graphs with results from the variation in the TWR [2] in an extreme winter situation (By author)



6.1.6 MESO: Multi-layered LHSU

Table 1.18 Overview energy usage and energy reduction considering the multi-layered strategy with descending melting temperatures

ID (#)	System layers -degrees (no.)	Cooling energy usage (kWh)	Heating energy usage (kWh)	Cooling reduction (%)	Heating reduction (%)	Cooling reduction (kWh)	Heating reduction (kWh)	Yearly energy reduction (kWh)	Melting temperature (°C)
27	1.00	566.55	89.46	49.95	72.82	565.45	239.64	805.09	23
43.1	1.00	465.95	93.52	58.84	71.58	666.05	235.58	901.64	25
44.1	2.00	471.90	113.80	58.31	65.42	660.10	215.30	875.40	25-21
45.1	3.00	459.20	116.42	59.43	64.62	672.80	212.68	885.48	25-23-21
30	1.00	444.46	116.98	60.74	64.45	687.54	212.12	899.66	26
46.1	1.00	470.47	148.65	58.44	54.83	661.53	180.45	841.98	28
47.1	2.00	486.72	138.69	57.00	57.86	645.28	190.41	835.69	28-24
48.1	3.00	481.81	165.60	57.44	49.68	650.19	163.50	813.69	28-26-24

Table 1.19 Overview energy usage and energy reduction considering the multi-layered strategy with ascending melting temperatures

ID (#)	System layers +degree (no.)	Cooling energy usage (kWh)	Heating energy usage (kWh)	Cooling reduction (%)	Heating reduction (%)	Cooling reduction (kWh)	Heating reduction (kWh)	Yearly energy reduction (kWh)	Melting temperature (°C)
43.2	1.00	638.27	106.81	43.62	67.54	493.73	222.29	716.02	21
27	1.00	566.55	89.46	49.95	72.82	565.45	239.64	805.09	23
44.2	2.00	494.43	115.87	56.32	64.79	637.57	213.23	850.80	21-25
45.2	3.00	487.63	109.23	56.92	66.81	644.37	219.87	864.24	21-23-25
46.2	1.00	509.78	92.55	54.97	71.88	622.22	236.55	858.77	24
30	1.00	444.46	116.98	60.74	64.45	687.54	212.12	899.66	26
47.2	2.00	490.49	146.61	56.66	55.45	641.51	182.49	824.00	24-28
48.2	3.00	455.43	149.20	59.77	54.66	676.57	179.90	856.47	24-26-28

The multi-layered system is also divided into two main strategies, the first one targets the effect of multiple layers with a descending melting temperature range. Here the inner most layer has a lower temperature compared to the layer on the outside. The second strategy is based on the opposite where an ascending melting temperature range is considered, the outer most layer has the lowest temperature compared to the inner layer as illustrated in Table 1.9 on page 94.

For the descending melting temperatures the results from Table 1.18 shows the highest performance for the one layered 25°C, a clear difference is observed between the two variants. For the cooling season the three layered 25°C system performs better, however here the differences are small. On extreme days the temperature graphs show that the 28°C descending temperatures show a better performance for the stability of the indoor air temperature (Figure 1.98), it is seen that on these extreme days the PCM stays within its transition zone, this is seen by the horizontal developing PCM temperature. The differences in the indoor air temperature are only seen on some extreme days, on the more typical day on the left the indoor air temperature is slightly higher for the 25°C system.

For the ascending melting temperatures it is seen that the one layered 24°C system performs significantly better for the heating season and the three layered system performs better for cooling. The graphs show only small deviations between the results from the indoor air temperature in winter (Figure 1.99). This is also noticed in the energy reduction and energy usage from Table 1.19, the 3 layered system improves the performance of the panel for the reduction in cooling energy but the differences are small. This three layered panel deteriorates the performance of the system considering the heating strategy.

Comparing the ascending and descending strategies it is noticed that the standard single layer 25°C system performs best for the yearly energy reduction. In general it can be seen that the multi-layering does not add much to the performance of the PCM panel, the investment in the more complex design seems therefore not beneficial considering the energy reduction.

Figure 1.98
Graphs with results from the multi-layering strategy with descending temperatures in summer situation (By author)

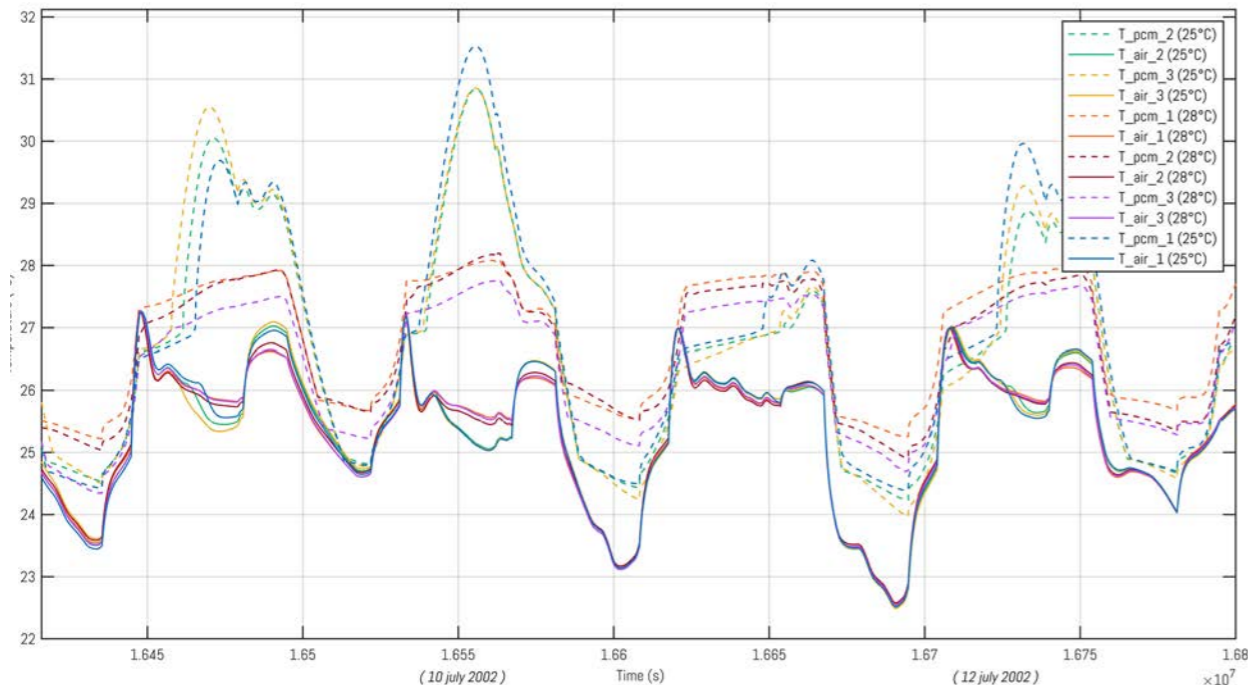
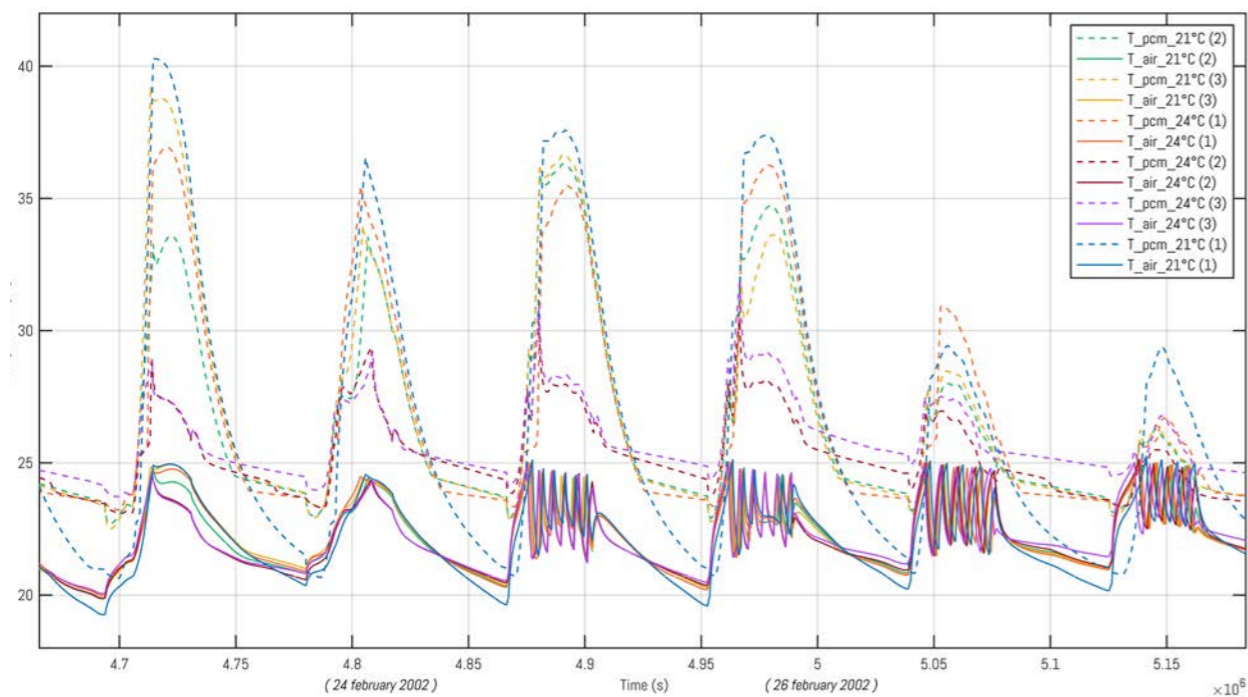


Figure 1.99
Graphs with results from the multi-layering strategy with ascending temperatures in winter situation (By author)



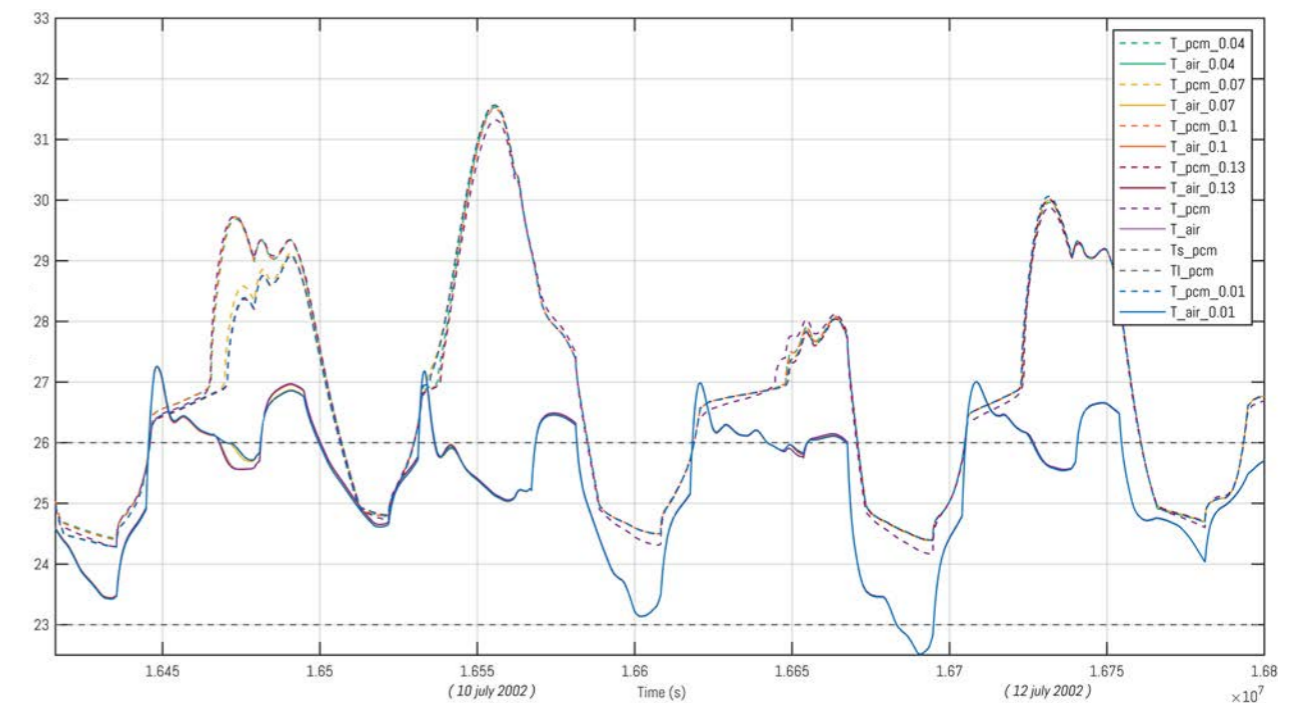
6.1.7 MESO: Cavity width

Table 1.20 Overview energy usage and energy reduction considering width of the cavity

ID (#)	Cavity width (m)	Cooling energy usage (kWh)	Heating energy usage (kWh)	Cooling reduction (%)	Heating reduction (%)	Cooling reduction (kWh)	Heating reduction (kWh)	Yearly energy reduction (kWh)
61	0.01	482.30	106.00	57.39	67.79	649.70	223.10	872.80
62	0.04	482.50	106.00	57.38	67.79	649.50	223.10	872.60
63	0.07	481.70	114.00	57.45	65.36	650.30	215.10	865.40
64	0.10	478.30	115.10	57.75	65.03	653.70	214.00	867.70
65	0.13	480.00	106.80	57.60	67.55	652.00	222.30	874.30
66	0.16	478.40	108.10	57.74	67.15	653.60	221.00	874.60

As mentioned before, the usable floor area is important for a cost-effective application of the PCM Trombe wall within office spaces, therefore the cavity width is also an highly important factor. The results from this strategy indicate the actual effect of the cavity on the energy usage of the room and the air temperature within the room. The cavity with a width of 13 centimetre or 16 centimetre gives the best results, interesting to see is the fact that the results are almost the same. So the cavity width does not really affect the performance of the system regarding the energy demand within the tested simulations, which is also noticed in the detailed temperature results (Figure 1.100), the graphs from the different parameters develop almost exactly the same. Therefore, the width of the cavity will be fixed on 4 centimetre within the detailed energy performance simulations, the one centimetre cavity can be considered too small considering the construction of the trombe wall.

Figure 1.100
Graphs with results from the variation in the width of the cavity for the extreme summer situation (By author)



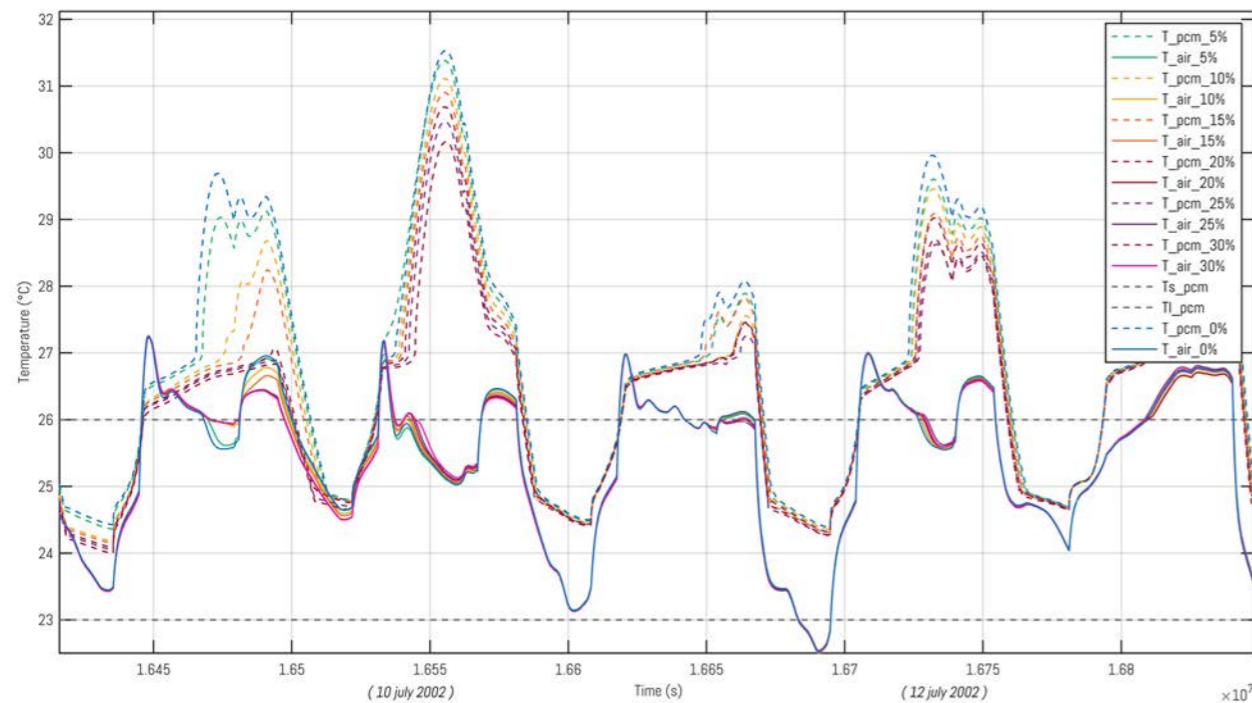
6.1.8 MESO: Surface area

Table 1.21 Overview energy usage and energy reduction considering increase in surface area

ID (#)	Panel area ratio (%)	Cooling energy usage (kWh)	Heating energy usage (kWh)	Cooling reduction (%)	Heating reduction (%)	Cooling reduction (kWh)	Heating reduction (kWh)	Yearly energy reduction (kWh)
49	1.05	476.00	105.80	57.95	67.85	656.00	223.30	879.30
50	1.10	470.70	114.00	58.42	65.36	661.30	215.10	876.40
51	1.15	468.60	113.40	58.60	65.54	663.40	215.70	879.10
52	1.20	463.40	113.00	59.06	65.66	668.60	216.10	884.70
53	1.25	458.80	106.00	59.47	67.79	673.20	223.10	896.30
54	1.30	453.90	115.60	59.90	64.87	678.10	213.50	891.60

The increase in surface area has a direct affinity with the convective heat transfer in the strategy from Section "6.1.9 MICRO: Convective heat transfer", the surface area increase within MATLAB will only increase the energy exchange by radiation between the construction surfaces of the room. Increasing this area will also affect the heat transfer coefficient depending on the design of the surface. Results show that only the increase in surface area without an increase in convective heat transfer coefficient improves the energy performance of the panel by just 20 kWh [896.30 - 876.40 kWh] for the yearly energy reduction (Table 1.21). In summer a more stable indoor climate is realized by using an increased surface area for the PCM panel, the purple/pink line in the summer situation (Figure 1.101) shows a more stable indoor air temperature, however the differences compared with the standard flat surface situation are small. The other days do not show large deviations, combining this strategy with the convective heat transfer will result in a higher differentiation for the performance of the system.

Figure 1.101
Graphs with results from the surface area increase for summer (top) and winter (bottom) situation (By author)



6.1.9 MICRO: Convective heat transfer

Table 1.22 Overview energy usage and energy reduction considering the convective heat transfer coefficient (W/m²/K)

ID (#)	Simulation value	Cooling energy usage (kWh)	Heating energy usage (kWh)	Cooling reduction (%)	Heating reduction (%)	Cooling reduction (kWh)	Heating reduction (kWh)	Yearly energy reduction (kWh)
55	2.00	495.67	78.70	56.21	76.09	636.33	250.40	886.74
56	2.50	486.00	101.94	57.07	69.02	646.00	227.16	873.16
57	3.00	455.50	122.16	59.76	62.88	676.50	206.94	883.44
58	3.50	438.34	158.56	61.28	51.82	693.66	170.54	864.20
59	4.00	420.78	181.13	62.83	44.96	711.22	147.97	859.19
60	4.50	418.51	207.80	63.03	36.86	713.49	121.30	834.79

The results for the increase in the convective heat transfer show a clear distinction between the yearly energy reduction and the separated heating or cooling energy reduction (Table 1.22). In winter the convective heat transfer needs to be as low as possible, a higher heat transfer in winter results in a shorter nucleation period as illustrated in Figure 1.102, therefore less energy is released. Besides this, the absorbed energy is released less quickly by the lower heat transfer coefficient, in this situation the PCM has a double function, on the one hand it absorbs the heat from the direct solar radiation and on the other hand it works as a more effective insulation layer. Therefore, less heat is lost to the exterior during the night and the absorbed heat can be released towards the interior space. The results from the simulation indicate that in both the extreme and the typical winter situation the air temperature of the room is increased using a low convective heat transfer (Figure 1.102). So two different situations for heating and cooling will give the highest performance.

Figure 1.102
Graphs with results from the variation the convective heat transfer coefficient for the extreme winter situation. (By author)

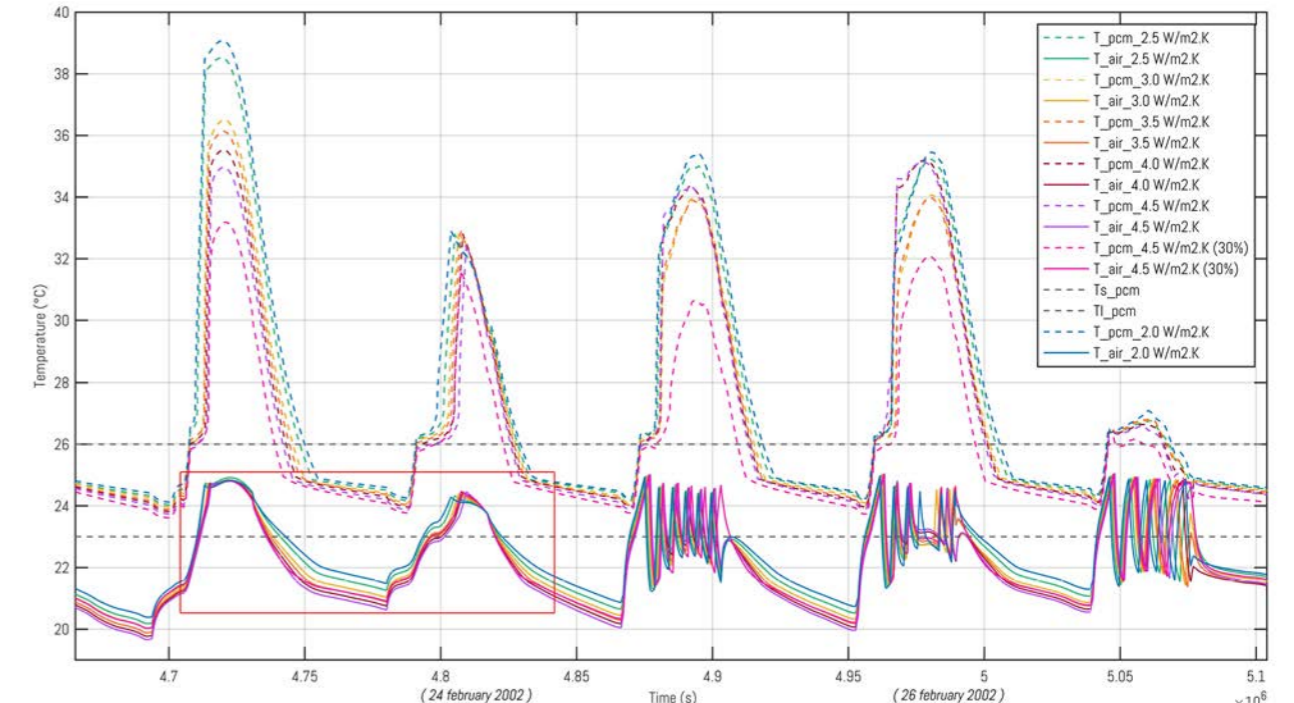
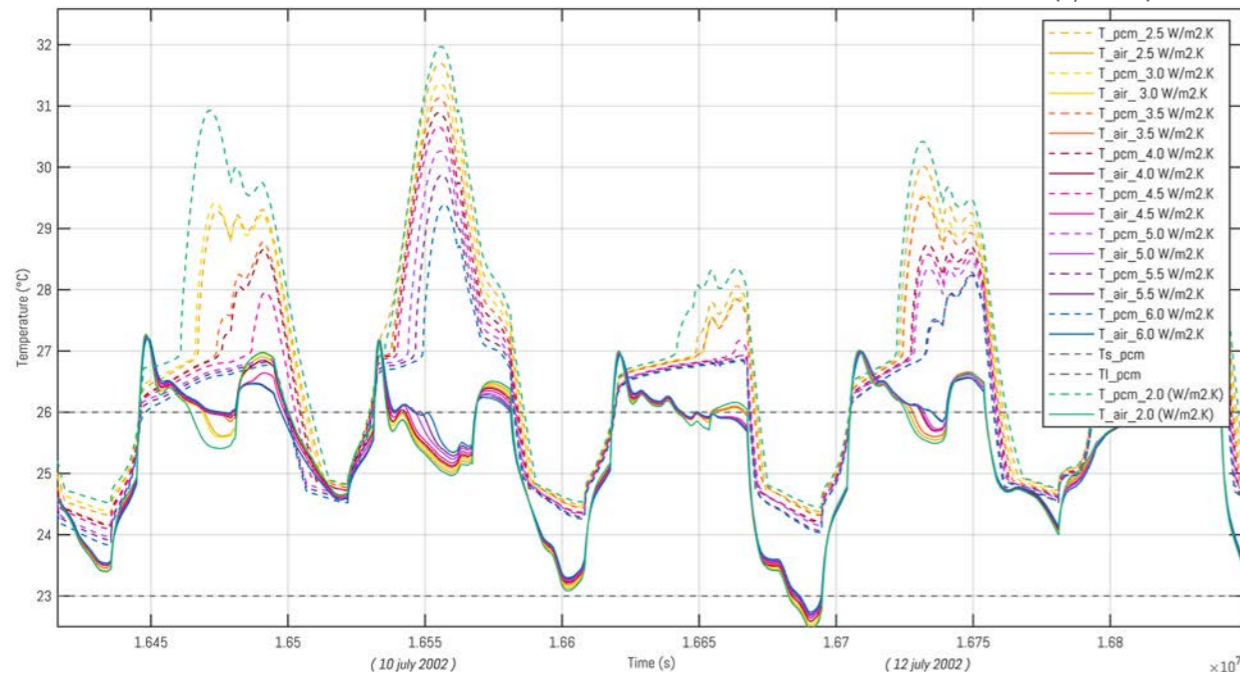


Figure 1.103
Graphs with results from the variation the convective heat transfer coefficient for the extreme summer situation (By author)



The temperature difference in the summer situation shows that a higher convective heat transfer results in a lower and more stable PCM temperature on extreme days (Figure 1.103), in this way the PCM stays in the transition phase for a longer period, during the night the PCM can release the heat more rapidly due to a higher exchange rate with the adjacent air. The effect of the convective heat transfer increases the performance of the PCM panel by 10.8% (636.33 / 713.49 kWh) for cooling, for heating the performance index (Table 1.22) shows a difference of 51.6% (121.30 / 250.40 kWh).

6.1.10 MICRO: Conductivity heat transfer

Table 1.23 Overview of the energy reduction considering the thermal conductivity (W/m.K) and the density (kg/m³)

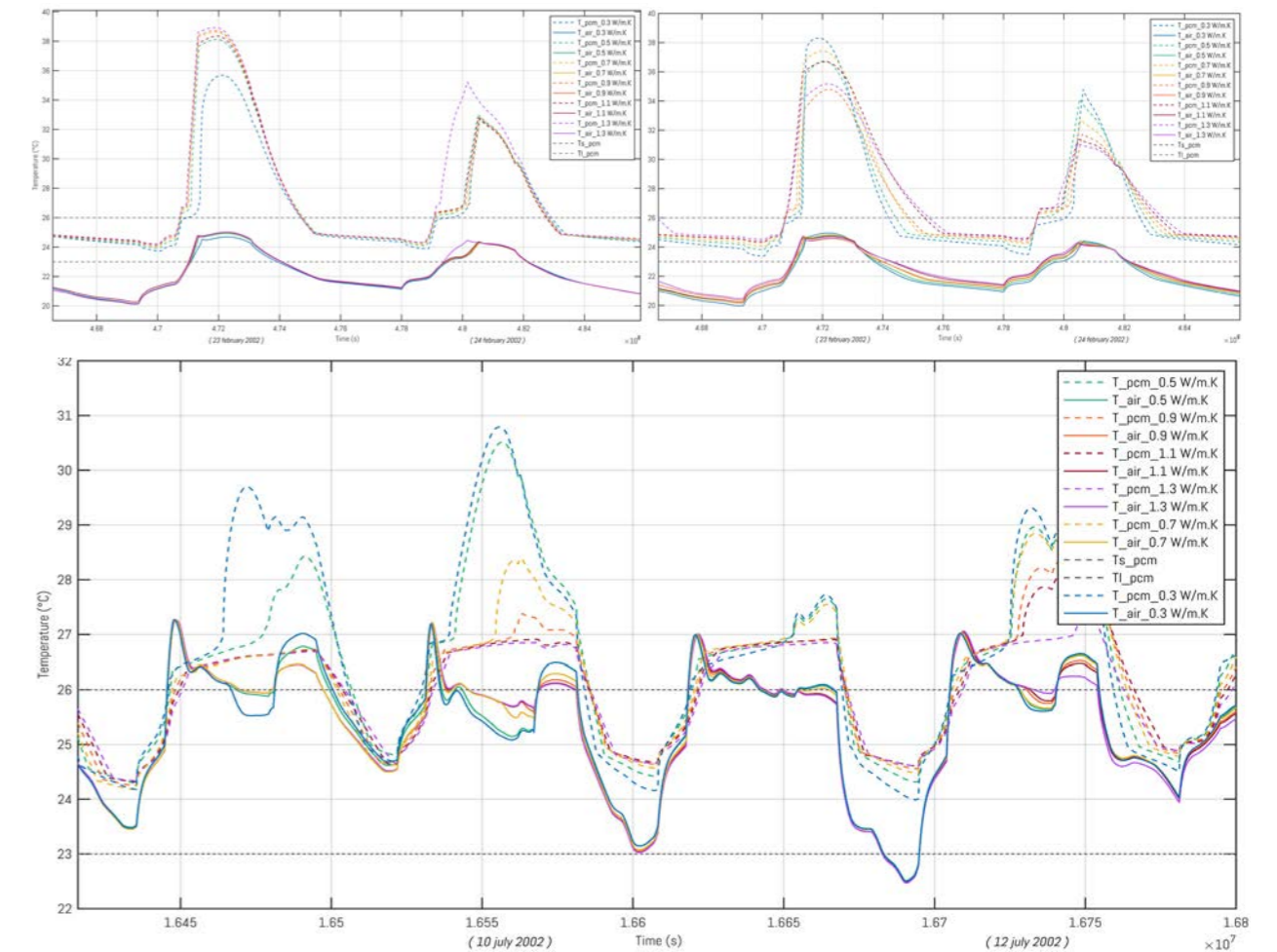
ID (#)	Thermal conductivity (W/m.K)	Cooling energy usage (kWh)	Heating energy usage (kWh)	Cooling reduction (%)	Heating reduction (%)	Cooling reduction (kWh)	Heating reduction (kWh)	Yearly energy reduction (kWh)	Material density (kg/m ³)
67	0.30	478.30	119.80	57.75	63.59	653.70	209.30	863.00	950.00
68	0.50	463.30	105.30	59.07	68.00	668.70	223.80	892.50	1250.00
69	0.70	451.40	88.38	60.13	73.15	680.60	240.72	921.32	1550.00
70	0.90	444.90	70.67	60.70	78.53	687.10	258.43	945.53	1850.00
71	1.10	438.70	60.29	61.24	81.68	693.30	268.81	962.11	2150.00
72	1.30	435.70	46.39	61.51	85.91	696.30	282.71	979.01	2450.00

Table 1.24 Overview energy usage and energy reduction considering the thermal conductivity (W/m.K)

ID (#)	Thermal conductivity (W/m.K)	Cooling energy usage (kWh)	Heating energy usage (kWh)	Cooling reduction (%)	Heating reduction (%)	Cooling reduction (kWh)	Heating reduction (kWh)	Yearly energy reduction (kWh)	Material density (kg/m ³)
67	0.30	485.70	105.90	57.09	67.82	646.30	223.20	869.50	1450.00
68	0.50	483.30	108.10	57.31	67.15	648.70	221.00	869.70	1450.00
69	0.70	481.20	106.60	57.49	67.61	650.80	222.50	873.30	1450.00
70	0.90	476.00	109.20	57.95	66.82	656.00	219.90	875.90	1450.00
71	1.10	471.70	106.80	58.33	67.55	660.30	222.30	882.60	1450.00
72	1.30	472.80	119.60	58.23	63.66	659.20	209.50	868.70	1450.00

Two main simulations are executed to indicate the effect of the thermal conductivity on the performance of the system. First the simulation is done with an increased material density and conductivity, the material properties overview ("APPENDIX D") shows that the an increased thermal conductivity mainly is accompanied by a higher density, the energy performance results are shown in Table 1.23. For both winter and summer application the best solution is the 1.3 W/m.K in combination with a higher volumetric heat capacity, this obviously performs better due to the increased heat capacity from the PCM. The differences in the performance index shows a total increase of 11,8% (863,00 / 979,01 kWh). A clear difference is observed for the materials with a higher density (950 kg/m³ and higher), this is mainly due to a higher total heat capacity of the material during the latent heat storage, the summer temperature distribution shows that only these variants stay within their nucleation phase (Figure 1.104: bottom). Besides this, the results for the heating situation indicate that the differences between the separate simulations become too small, no clear correlation is observed. Considering the results from the detailed graphs with the indoor air temperature and the PCM temperature in winter it can be noticed that a more stable indoor air temperature is created using the combined higher conductivity and higher density, a maximum difference of 1°C is observed (Figure 1.104: top). For the situation where only the conductivity is varied, the differentiation within the results is negligible (Figure 1.104: left).

Figure 1.104
Graphs with results in extreme winter from the variation the thermal conductivity (left), combined with density (right) and the extreme summer situation (bottom) (By author)



6.1.11 Results overview

The overview of the results gives an indication on the energy performance of the different variables by comparing them with the other simulated variables. The green and red expression (Table 1.25) show the variables with the highest impact, a larger thickness [1.3], the melting temperature [5.1], the variation in trombe wall ratio [6.1] and [7.1], the convective heat transfer [11.1] and a higher volumetric heat capacity [13.1] all have a large impact on the energy performance of the system (negative and positive). The trombe wall ratio is most important for the cooling season and the volumetric heat capacity for the heating season. These energy reduction results will be combined with the performance in the reduction in maximum power-load (kW) throughout the year for sizing the equipment, this will be used to highlight the differences between the two strategies for this specific design case. An overview with the actual difference in performance and the best performing input parameters will be given in Section "64 DESIGN GUIDELINE".

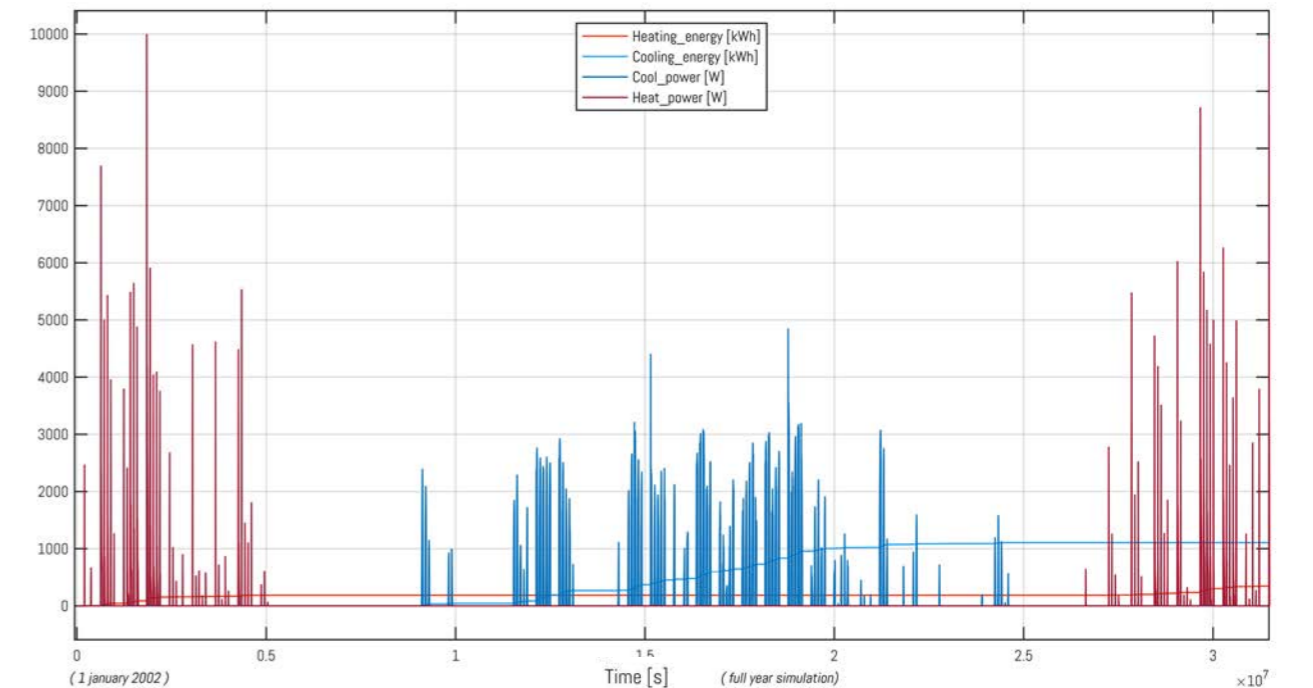
Table 1.25 Comparison overview showing the results from Design of Experiments (By author)

	INPUT		RESULTS				SIMULATION RESULT VALUES					
	ID (#)	Simulation value	Cooling reduction (%)	Heating reduction (%)	Cooling reduction (kWh)	Heating reduction (kWh)	Heating energy usage (kWh)	Heating energy usage (kWh)	Total panel volume (m³)	Latent storage capacity (kJ)	Panel surface area (m²)	
1.1	Panel thickness (m)	1.1	0.010	48.53	50.82	549.35	167.26	582.65	161.84	0.21	5.39E+07	20.65
		1.2	0.015	53.01	59.95	600.12	197.31	531.88	131.79	0.31	8.09E+07	20.65
		2.1	0.020	57.51	64.17	651.06	211.18	480.94	117.92	0.41	1.08E+08	20.65
		2.2	0.025	58.84	71.86	666.05	235.58	465.95	93.52	0.52	1.35E+08	20.65
		3.1	0.030	59.76	71.86	676.45	236.49	455.55	92.61	0.62	1.62E+08	20.65
		3.2	0.035	60.71	74.73	687.26	245.93	444.74	83.17	0.72	1.89E+08	20.65
		4.1	0.040	61.51	77.09	696.35	253.72	435.65	75.38	0.83	2.16E+08	20.65
		4.2	0.045	61.76	77.93	699.10	256.46	432.90	72.64	0.93	2.43E+08	20.65
		5.1	0.050	61.64	79.89	697.74	262.92	434.26	66.18	1.03	2.70E+08	20.65
		5.2	0.055	62.66	78.02	709.36	256.76	422.64	72.34	1.14	2.97E+08	20.65
2.1	Blind covering (°C)	6	0.060	80.37	80.37	707.51	284.49	424.49	64.61	1.24	3.23E+08	20.65
		7	20.00	60.50	50.19	684.88	165.19	447.12	163.91	0.52	1.35E+08	20.65
		8	21.00	60.68	60.66	686.94	199.64	445.06	129.46	0.52	1.35E+08	20.65
		9	22.00	58.84	71.58	666.05	235.58	465.95	93.52	0.52	1.35E+08	20.65
		10	23.00	48.74	75.01	551.76	246.86	580.24	82.24	0.52	1.35E+08	20.65
		11	24.00		75.99		250.08	829.40	79.02	0.52	1.35E+08	20.65
		12	25.00		77.16		253.95	3029.17	75.15	0.52	1.35E+08	20.65
		13	26.00		77.85		256.20	538.89	72.90	0.52	1.35E+08	20.65
		14	1.60E+05	52.47	57.72	593.92	189.96	538.08	139.14	0.52	7.02E+07	20.65
		15	1.80E+05	52.37	58.90	592.86	193.83	539.14	135.27	0.52	7.90E+07	20.65
3.1	Latent heat storage: organic (J/kg)	16	2.00E+05	52.94	63.58	599.32	209.24	532.68	119.86	0.52	8.78E+07	20.65
		17	2.20E+05	52.69	69.10	596.42	227.40	535.58	101.70	0.52	9.66E+07	20.65
		18	2.40E+05	53.02	68.58	600.15	225.69	531.85	103.41	0.52	1.05E+08	20.65
		19	1.60E+05	58.25	67.30	659.38	221.48	472.62	107.62	0.52	1.20E+08	20.65
		20	1.80E+05	58.84	71.58	666.05	235.58	465.95	93.52	0.52	1.35E+08	20.65
		21	2.00E+05	58.92	74.02	666.92	243.62	465.08	85.48	0.52	1.50E+08	20.65
		22	2.20E+05	59.45	78.67	673.01	258.90	458.99	70.20	0.52	1.65E+08	20.65
		23	2.40E+05	60.64	76.81	686.40	252.79	445.60	76.31	0.52	1.80E+08	20.65
		24	20.00	41.88	58.85	474.10	193.67	657.90	135.43	0.52	1.35E+08	20.65
		25	21.00	43.52	66.90	492.70	220.18	639.30	108.92	0.52	1.35E+08	20.65
5.1	Melting temperature (°C)	26	22.00	46.48	71.83	526.12	236.39	605.88	92.71	0.52	1.35E+08	20.65
		27	23.00	49.95	72.82	565.45	239.64	566.55	89.46	0.52	1.35E+08	20.65
		28	24.00	54.27	71.84	614.34	236.43	517.66	92.67	0.52	1.35E+08	20.65
		29	25.00	58.84	71.58	666.05	235.58	465.95	93.52	0.52	1.35E+08	20.65
		30	26.00	60.74	64.45	687.54	212.12	444.46	116.98	0.52	1.35E+08	20.65
		31	0.40	60.07	-44.25	680.01	-145.62	451.99	474.72	0.23	5.99E+07	9.18
		32	0.50	59.98	-20.59	678.95	-67.77	453.05	396.87	0.29	7.49E+07	11.47
		33	0.60	59.24	9.09	670.56	29.90	461.44	299.20	0.34	8.98E+07	13.77
		34	0.70	59.94	17.81	678.50	58.62	453.50	270.48	0.40	1.05E+08	16.06
		35	0.80	60.08	36.49	680.10	120.10	451.90	209.90	0.52	1.20E+08	18.36
6.1	Trombe wall ratio 1 (%)	36	0.90	60.23	52.45	681.80	172.60	450.20	156.50	0.52	1.35E+08	20.65
		37	0.40	69.66	-132.44	788.58	-435.87	343.42	764.97	0.52	1.35E+08	20.65
		38	0.50	67.91	-85.35	768.70	-280.90	363.30	610.00	0.52	1.35E+08	20.65
		39	0.60	66.64	-44.18	754.38	-145.38	377.62	474.48	0.52	1.35E+08	20.65
		40	0.70	66.10	-4.36	748.26	-14.36	383.74	343.46	0.52	1.35E+08	20.65
		41	0.80	63.32	28.96	716.73	95.29	415.27	233.81	0.52	1.35E+08	20.65
		42	0.90	60.08	52.45	680.10	172.60	451.90	156.50	0.52	1.35E+08	20.65
		43.1	1.00	58.84	71.58	666.05	235.58	465.95	93.52	0.52	1.35E+08	20.65
		44.1	2.00	58.31	65.42	660.10	215.30	471.90	113.80	0.52	1.35E+08	20.65
		45.1	3.00	59.43	64.62	672.80	212.68	459.20	116.42	0.52	1.35E+08	20.65
8.1	System layers degrees (no.)	46.1	1.00	58.44	54.83	661.53	180.45	470.47	148.65	0.52	1.35E+08	20.65
		47.1	2.00	57.00	57.86	645.28	190.41	486.72	138.69	0.52	1.35E+08	20.65
		48.1	3.00	57.44	49.68	650.19	163.50	481.81	165.60	0.52	1.35E+08	20.65
		43.2	1.00	43.62	67.54	493.73	222.29	638.27	106.81	0.52	1.35E+08	20.65
		44.2	2.00	56.32	64.79	637.57	213.23	494.43	115.87	0.52	1.35E+08	20.65
		45.2	3.00	56.92	66.81	644.37	219.87	487.63	109.23	0.52	1.35E+08	20.65
		46.2	1.00	54.97	71.88	622.22	236.55	509.78	92.55	0.52	1.35E+08	20.65
		47.2	2.00	56.66	55.45	641.51	182.49	490.49	146.61	0.52	1.35E+08	20.65
		48.2	3.00	59.77	54.66	676.57	179.90	455.43	149.20	0.52	1.35E+08	20.65
		49	1.05	57.95	67.85	656.00	223.30	476.00	105.80	0.52	1.35E+08	21.69
10.1	Panel area ratio (%)	50	1.10	58.42	65.36	661.30	215.10	470.70	114.00	0.52	1.35E+08	22.72
		51	1.15	58.60	65.54	663.40	215.70	468.60	113.40	0.52	1.35E+08	23.75
		52	1.20	59.06	65.66	668.60	216.10	463.40	113.00	0.52	1.35E+08	24.79
		53	1.25	59.47	67.70	673.20	223.10	458.80	106.00	0.52	1.35E+08	25.82
		54	1.30	59.90	64.87	678.10	213.50	453.90	115.60	0.52	1.35E+08	26.85
		55	2.00	56.21	76.09	636.33	250.40	495.67	78.70	0.52	1.35E+08	20.65
		56	2.50	57.07	69.02	646.00	227.16	486.00	101.94	0.52	1.35E+08	20.65
		57	3.00	59.76	62.88	676.50	206.94	455.50	122.16	0.52	1.35E+08	20.65
		58	3.50	61.28	51.82	693.66	170.54	438.34	158.56	0.52	1.35E+08	20.65
		59	4.00	62.83	44.96	713.22	147.97	425.78	181.33	0.52	1.35E+08	20.65
11.1	Convective heat transfer (W/m2K)	60	4.50	63.03	36.86	713.49	121.30	418.51	207.80	0.52	1.35E+08	20.65
		61	0.01 m	57.39	67.79	649.70	223.10	482.30	106.00	0.52	1.35E+08	20.65
		62	0.04 m	57.38	67.79	649.50	223.10	482.50	106.00	0.52	1.35E+08	20.65
		63	0.07 m	57.45	65.36	650.30	215.10	481.70	114.00	0.52	1.35E+08	20.65
		64	0.10 m	57.75	65.03	653.70	214.00	478.30	115.10	0.52	1.35E+08	20.65
		65	0.13 m	57.60	67.55	652.00	222.30	480.00	106.80	0.52	1.35E+08	20.65
		66	0.30 m	57.74	67.15	653.60	221.00	478.40	108.30	0.52	1.35E+08	20.65
		67	0.30 m	57.75	63.59	653.70	209.30	478.30	119.80	0.52	1.35E+08	20.65
		68	0.50	59.07	68.00	668.70	223.80	463.30	105.30	0.52	1.35E+08	20.65
		69	0.70	60.13	73.15	680.60	240.72	451.40	88.38	0.52	1.35E+08	20.65
13.1	Thermal conduction (W/m.K) + density	70	0.90	60.70	78.53	687.10	258.43	444.90	70.67	0.52	1.35E+08	20.65
		71	1.10	61.24	81.68	693.30	268.81	438.70	60.29	0.52	1.35E+08	20.65
		72	1.30	61.51	85.91	696.30	282.71	435.70	46.39	0.52	1.35E+08	20.65
		67	0.30	57.09	67.82	646.30	223.20	485.70	125.90	0.52	1.35E+08	20.65
		68	0.50	57.31	67.15	648.70	221.00	483.30	108.10	0.52	1.35E+08	20.65
		69	0.70	57.49	67.61	650.80	222.50	481.20	106.60	0.52	1.35E+08	20.65
		70	0.90	57.95	66.82	656.00	219.90	476.00	109.20	0.52	1.35E+08	20.65
		71	1.10	58.33	67.55	660.30	222.30	471.70	106.80	0.52	1.35E+08	20.65
		72	1.30	58.23	63.66	659.20	209.50	472.80	119.60	0.52	1.35E+08	20.65

6.2 ECONOMIC EVALUATION

The second important objective for this research study is the cost-effectiveness of the different optimization strategies, within this evaluation the results from the Design of Experiments will be compared with the benchmark situation. The reduction in heating and cooling power needed by the installations for conditioning the room will be used to indicate the actual performance. Reducing the heating and cooling power that is required will also reduce the size of the desired installation system, the size of these installations are determined according to the maximum power load possible within the building. The benchmark study shows that the maximum heating power needed on extreme winter days reaches up to 10 kW, for extreme summer days the cooling power shows a maximum of up to 5 kW (Figure 1.105). Normally the size of installations is calculate according to a reference extreme winter day with a delta temperature of 30°C, this temperature determines the difference between the outdoor and the indoor temperature (-10°C and 20°C). This dynamic calculation shows the actual peaks in power-load throughout the year according to the temperature-files from the NEN5060-2008 (B2).

Figure 1.105
Graphs with daily heating and cooling energy loads from the benchmark situation on yearly base (By author)



The objective of the optimization is to minimize the total cost of ownership of the system over a certain payback time. The system refers to the costs for the PCM panel and the heating and cooling installation together. The use of the PCM panel will reduce the need for installation which subsequently reduces the total cost of ownership of the total heating and cooling installation. Mathematically, the objective function is defined as the total Total Cost of Ownership (TCO) of the system, which considers the one time investment (C_{capex}) and the total lifetime operation costs (C_{opex}) shown in Equation (1.38). The total operation costs over a certain time in years (N) is determined according to the inflation rate and the interest rate, this determines the future value of money expressed in the present worth factor (PWF).

6.2.1 Benchmark calculation

The results from the power load simulations are used as input for the cost evaluation for a payback period of 10 years. First the cost analysis of the benchmark situation is executed, this benchmark situation is based on the standard office size with a ground source heat-pump (GSHP) for the heating and cooling installation. This heat pump has an Coefficient of Performance (COP) of 3. The investment costs per kW of installed installation is used to define the total capital cost for the system (C_{capital}), these costs are based on an indication from the Centre of Alternative Technology (CAT, 2019). The maximum power-load is defined according to the benchmark simulation (Figure 1.105) and multiplied by the cost indication per kW, for the total cost of ownership this number is multiplied by the total office area. For a ground source heat-pump the total investment cost are based on the investment for the heat-pump (€462,00/kW) and the investment for the aquifer and the boreholes (€577,00/kW) as seen in Table 1.26 (CAT, 2019).

The operation costs (C_{OPER}) of the system will differ according to the payback time, within the comparison this value will give the amount of energy saved by the PCM panel. The actual value of these operation costs after 10 years needs to be determined according to the Present Worth Factor (PWF), Equation (140). In the end the total cost of ownership (TCO) over the given period of time determines the sum of the operation costs and the capital costs, this final investment value will be compared with the TCO from the different design parameters from the Design of Experiments and in the end to the results from the optimization study.

$$TCO_{\text{SYSTEM}} = C_{\text{CAPEX}} + C_{\text{OPEX}} \cdot PWF \quad (1.38)$$

$$TCO_{\text{SYSTEM}} = C_{\text{CAPEX}} + (C_{\text{FUEL}} + C_{\text{MAIN}}) \cdot PWF \quad (1.39)$$

$$PWF = \frac{1+i}{r-i} \left[1 - \left(\frac{1+i}{1+r} \right)^N \right] \quad (140)$$

LCC	total life cycle cost	[€]
C_{CAPEX}	total one time investment	[€]
C_{OPEX}	total operation costs	[€]
C_{MAIN}	maintenance costs	[€]
C_{FUEL}	fuel energy costs	[€]
i	inflation rate	[%]
r	interest rate	
N	number of years (payback)	
PWF	present worth factor	

Table 1.26 Calculated from the total cost of ownership for the benchmark office situation

1 ANNUAL COSTS BENCHMARK OFFICE				
# Category	Parameter	Value	Unit	Reference
1.10 Equipment	COP (Coefficient Of Performance)	3		
	Heatpump	€462.00	/kW	(CAT, 2019)
	Boreholes	€577.00	/kW	(CAT, 2019)
1.20 Energy cost	Electricity price (office)	€0.085	/kWh	(RVO, 2018)
1.30 Office building	Office room	60	m ²	
1.40 Present worth factor	Inflation rate	2.00%		(CBS, 2017; ECB, 2018)
	Interest rate	0.25%		(ECB, 2018)
1 Office equipment costs				
# Category	Parameter	Value	Unit	Reference
	Maximum powerload	10	kW	
1.40 Equipment costs	Powerload	0.167	kW/m ²	
	Area heatpump costs	€77.00	/m ²	
	Area boreholes costs	€96.17	/m ²	
	Area installation costs	€0.00	/m ²	+
	Annual equipment costs	€173.17	/m ²	
1 Office operation costs				
# Category	Parameter	Value	Unit	Reference
	Payback time	10	years	
	Benchmark heating energy	329.10	kWh	
	Benchmark cooling energy	1132.00	kWh	
	Total office energy	1461.10	kWh	
1.50 Energy costs	Area energy demand	24.35	kWh/m ² /year	
	Area office energy (COP)	8.12	kWh/m ² /year	
	Energy costs	€0.69	/m ² /year	
	Yearly operation costs	€0.69	/m ² /year	
	Annual operation costs (over time)	€7.60	/m ²	
TOTAL COST OF OWNERSHIP (TCOO)		€10,845.88		
TCOO per square meter floor area		€180.76	/m ²	
TCOO per square meter façade		€401.70	/m ²	

6.2.2 Results Design of Experiments (DoE)

The TCO shows the total cost for the total system, including the operation costs over a period of 10 years and the equipment costs. The results will now be compared to the results from the simulations, the investment space (Table 1.27 on page 149) determines the difference between the TCO from the benchmark situation and the TCO from each of the design variants. This is a quick indication to show the actual reduction in costs from the heat-pump installations, this value can be used for the investment in

the design of the final PCM product. The dark red indication shows the design solutions with less potential for a cost-effective application, the TCO for these simulations is almost as high as the costs from the benchmark situation.

Important to notice is the differences in the performance of the PCM system for the total yearly energy reduction and the reduction in equipment costs. As mentioned before, the size of the equipment is determined according to the maximum power load within the room, based on the highest temperature difference between the interior and the exterior. In a temperate climate like the Netherlands this temperature difference is highest in winter due to the relatively low outdoor air temperature during the night on the more extreme days. So strategies which perform best for the reduction in cooling energy demand will not perform best in reducing the size of the installation, and for this specific situation the heating power is the highest in magnitude. This difference is clearly seen in the following design parameters:

- For the panel thickness [1.2] the difference in operation costs is relatively small but the reduction in peak loads is much higher which is beneficial for the TCO of the system, a this higher heat capacity significantly reduces the peaks;
- The organic PCMs [3.2] do not have a high enough volumetric heat capacity to reduce the peak power-loads within the simulated thickness (3,5 centimetre) due to a lower combination of the latent heat of fusion (kJ/kg) and the density of the product (kg/m³) compared to the salt-hydrates [4.2]. For the latter, a higher latent heat of fusion shows a significant increase in the reduction in the power-load;
- The melting temperature of the panel [5.2], a higher melting temperature is wanted for the energy reduction and a lower melting temperature when considering the economic results. This lower temperature targets more specifically on the heating season;
- The trombe-wall to wall ratios [6.2] and [7.2] clearly show the negative effect of the opening area one the maximum power load, one fixed thickness is used within the simulation. The insulation effect from the panel is negatively affected by this trombe wall ratio, which has a clear adverse effect on the maximum heating power-loads;
- For the ascending system layers [9.2] the single layered system performs better on the reduction of the equipment costs than on the total yearly energy reduction, this can be the result from the multi-layering strategy, the difference in temperature for the two layered strategy is too high.
- The panel area ratio [10.2] does not show a clear correlation with the reduction in power-load, the differences between the simulated values are relatively small. This strategy does not have a large impact;
- A low convective heat transfer [11.2] performs better for both energy and peak load reduction, this lower value results in better insulation performances accompanied with the energy absorption at the same time;
- The cavity width [12.2] shows small deviations within the power-load reduction, the 10 centimetre cavity width shows the best performance;
- An in-between thermal conductivity [13.2] shows the best performance, this shows an eventual balance between the insulating effect from a lower lambda value and the increased energy absorbing rate for a higher lambda value.

Table 1.27 Simulation results from the total cost of ownership for different design solutions (By author)

Parameter indication	SIMULATION RESULTS								ECONOMIC RESULTS			
	Simulation ID (#)	Simulation value	Simulation unit	Yearly energy demand (kWh)	Cool power (W)	Heat power (W)	Maximum power (kW)	Total operation cost	Total equipment cost	Total cost of ownership (TCOO)	Total investment space	Total cost of ownership per floor area
1.2 Panel thickness (m)	1.1	0.01 m		810.81	3590	10000	10.0	€252.98	€10,390.00	€10,642.98	€202.90	€177.38 /m ²
	2.1	0.02 m		635.39	3422	10000	10.0	€198.25	€10,390.00	€10,588.25	€257.63	€176.47 /m ²
	3.1	0.03 m		570.90	3214	8982	9.0	€178.13	€9,332.01	€9,510.14	€1,335.74	€158.50 /m ²
	4.1	0.04 m		550.91	3111	7630	7.6	€171.89	€7,927.35	€8,099.24	€2,746.64	€134.99 /m ²
	5.1	0.05 m		523.78	3024	6962	7.0	€163.43	€7,233.25	€7,396.67	€3,449.21	€123.28 /m ²
	6	0.06 m		515.07	2946	5828	5.8	€160.71	€6,055.53	€6,216.24	€4,629.64	€103.60 /m ²
3.2 Latent heat storage: organic (kJ/kg)	14	1.60E+05 J/kg		653.21	3287	10000	10.0	€203.81	€10,390.00	€10,593.81	€252.07	€176.56 /m ²
	15	1.80E+05 J/kg		642.91	3278	10000	10.0	€200.60	€10,390.00	€10,590.60	€255.28	€176.51 /m ²
	16	2.00E+05 J/kg		631.50	3284	10000	10.0	€197.03	€10,390.00	€10,587.03	€258.85	€176.45 /m ²
	17	2.20E+05 J/kg		631.31	3278	10000	10.0	€196.98	€10,390.00	€10,586.98	€258.90	€176.45 /m ²
4.2 Latent heat storage: inorganic (kJ/kg)	18	2.40E+05 J/kg		623.20	3287	10000	10.0	€194.45	€10,390.00	€10,584.45	€261.43	€176.41 /m ²
	19	1.60E+05 J/kg		572.58	3174	8690	8.7	€178.65	€9,028.69	€9,207.34	€1,638.54	€153.46 /m ²
	20	1.80E+05 J/kg		572.89	3187	9276	9.3	€178.75	€9,638.23	€9,816.98	€1,028.90	€163.62 /m ²
	21	2.00E+05 J/kg		559.03	3168	8209	8.2	€174.43	€8,529.01	€8,703.43	€2,142.45	€145.06 /m ²
5.2 Melting temperature (°C)	22	2.20E+05 J/kg		542.78	3163	7822	7.8	€169.35	€8,126.78	€8,296.13	€2,549.75	€138.27 /m ²
	23	2.40E+05 J/kg		524.96	3163	6250	6.2	€163.79	€6,493.56	€6,657.35	€4,188.53	€110.96 /m ²
	24	20 °C		742.03	3211	6604	6.6	€231.52	€6,861.43	€7,092.95	€3,752.93	€118.22 /m ²
	25	21 °C		702.88	3211	6445	6.4	€219.31	€6,696.78	€6,916.09	€3,929.79	€115.27 /m ²
	26	22 °C		664.01	3211	6959	7.0	€207.18	€7,229.96	€7,437.14	€3,408.74	€123.95 /m ²
	27	23 °C		617.80	3211	6149	6.1	€192.76	€6,389.21	€6,581.97	€4,263.91	€109.70 /m ²
	28	24 °C		584.13	3210	6986	7.0	€182.25	€7,258.17	€7,440.42	€3,405.46	€124.01 /m ²
6.2 Trombe wall ratio 1 (%)	29	25 °C		572.89	3187	9276	9.3	€178.75	€9,638.23	€9,816.98	€1,028.90	€163.62 /m ²
	30	26 °C		570.08	2488	9405	9.4	€177.87	€9,772.12	€9,949.99	€895.89	€165.83 /m ²
	31	40 %		977.72	3478	10000	10.0	€305.06	€10,390.00	€10,695.06	€150.82	€178.25 /m ²
	32	50 %		882.83	3423	10000	10.0	€275.45	€10,390.00	€10,665.45	€180.43	€177.76 /m ²
	33	60 %		786.99	3384	10000	10.0	€245.55	€10,390.00	€10,635.55	€210.33	€177.26 /m ²
	34	70 %		689.25	3322	10000	10.0	€215.06	€10,390.00	€10,605.06	€240.82	€176.75 /m ²
7.2 Trombe wall ratio 2 (%)	35	80 %		631.67	3246	10000	10.0	€197.09	€10,390.00	€10,587.09	€258.79	€176.45 /m ²
	36	90 %		572.89	3187	9276	9.3	€178.75	€9,638.23	€9,816.98	€1,028.90	€163.62 /m ²
	37	40 %		1049.60	3472	10000	10.0	€327.49	€10,390.00	€10,717.49	€128.39	€178.62 /m ²
	38	50 %		935.34	3399	10000	10.0	€291.84	€10,390.00	€10,681.84	€164.04	€178.03 /m ²
	39	60 %		839.98	3341	10000	10.0	€262.08	€10,390.00	€10,652.08	€193.80	€177.53 /m ²
8.2 System layers -degrees (no.)	40	70 %		723.94	3277	10000	10.0	€225.88	€10,390.00	€10,615.88	€230.00	€176.93 /m ²
	41	80 %		617.02	3217	10000	10.0	€192.52	€10,390.00	€10,582.52	€263.36	€176.38 /m ²
	42	90 %		572.89	3187	9276	9.3	€178.75	€9,638.23	€9,816.98	€1,028.90	€163.62 /m ²
	43.1	1 (25°C)		572.89	3187	9276	9.3	€178.75	€9,638.23	€9,816.98	€1,028.90	€163.62 /m ²
	44.1	2 (25-21°C)		575.44	3174	8830	8.8	€179.55	€9,174.15	€9,353.70	€1,492.18	€155.89 /m ²
9.2 System layers +degrees (no.)	45.1	3 (25-23-21°C)		585.06	3186	8158	8.2	€182.55	€8,476.21	€8,658.75	€2,187.13	€144.31 /m ²
	46.1	1 (28°C)		639.98	2515	10000	10.0	€199.68	€10,390.00	€10,589.68	€256.20	€176.49 /m ²
	47.1	2 (28-24°C)		632.19	2625	10000	10.0	€197.25	€10,390.00	€10,587.25	€258.63	€176.45 /m ²
	48.1	3 (28-26-24°C)		622.38	2663	9679	9.7	€194.19	€10,056.80	€10,250.99	€594.89	€170.85 /m ²
	43.2	1 (21°C)		702.90	3203	6445	6.4	€219.31	€6,696.78	€6,915.67	€3,930.21	€115.26 /m ²
10.2 Panel area ratio (%)	44.2	2 (21-25°C)		740.60	3103	8335	8.3	€231.08	€8,660.07	€8,891.14	€1,954.74	€148.19 /m ²
	45.2	3 (21-23-25°C)		751.80	3104	7721	7.7	€234.57	€8,022.12	€8,256.69	€2,589.19	€137.61 /m ²
	46.2	1 (24°C)		584.10	3210	6986	7.0	€182.25	€7,258.17	€7,440.70	€3,405.18	€124.01 /m ²
	47.2	2 (24-28°C)		611.20	3199	6514	6.5	€190.70	€6,768.05	€6,958.75	€3,887.13	€115.98 /m ²
	48.2	3 (24-26-28°C)		627.40	3205	7266	7.3	€195.76	€7,549.37	€7,745.13	€3,100.75	€129.09 /m ²
11.2 Convective heat transfer (W/m2K)	49	105 %		557.70	3189	9278	9.3	€174.01	€9,639.51	€9,813.51	€1,032.37	€163.56 /m ²
	50	110 %		552.44	3186	8583	8.6	€172.37	€8,917.24	€9,089.61	€1,756.27	€151.49 /m ²
	51	115 %		563.61	3201	9720	9.7	€175.85	€10,099.03	€10,274.88	€571.00	€171.25 /m ²
	52	120 %		548.18	3212	8510	8.5	€171.04	€8,842.15	€9,013.19	€1,832.69	€150.22 /m ²
	53	125 %		553.59	3219	9134	9.1	€172.73	€9,490.02	€9,662.75	€1,183.13	€161.05 /m ²
	54	130 %		543.73	3227	8674	8.7	€169.65	€9,012.43	€9,182.08	€1,663.80	€153.03 /m ²
12.2 Cavity width (m)	55	2 W/m ² K		539.38	3109	5841	5.8	€168.29	€6,068.54	€6,236.83	€4,609.05	€103.95 /m ²
	56	2.5 W/m ² K		551.54	3167	7523	7.5	€172.09	€7,816.74	€7,988.83	€2,857.05	€133.15 /m ²
	57	3 W/m ² K		572.10	3204	8889	8.9	€178.50	€9,235.38	€9,413.88	€1,432.00	€156.90 /m ²
	58	3.5 W/m ² K		588.42	3244	9269	9.3	€183.59	€9,630.29	€9,813.88	€1,032.00	€163.56 /m ²
	59	4 W/m ² K		609.70	3274	10000	10.0	€190.23	€10,390.00	€10,580.23	€265.65	€176.34 /m ²
13.2 Thermal conduction (W/m.K)	60	4.5 W/m ² K		642.44	3310	10000	10.0	€200.45	€10,390.00	€10,590.45	€255.43	€176.51 /m ²
	61	0.01 m		570.07	3165	9220	9.2	€177.87	€9,579.83	€9,757.70	€1,088.18	€162.63 /m ²
	62	0.04 m		572.89	3187	9276	9.3	€178.75	€9,638.23	€9,816.98	€1,028.90	€163.62 /m ²
	63	0.07 m		571.23	3173	9041	9.0	€178.23	€9,393.99	€9,572.22	€1,273.66	€159.54 /m ²
	64	0.1 m		551.23	3159	7630	7.6	€171.99	€7,927.22	€8,099.21	€2,746.67	€134.99 /m ²
	65	0.13 m		550.66	3170	8207	8.2	€171.81	€8,527.39	€8,699.20	€2,146.68	€144.99 /m ²
13.2 Thermal conduction (W/m.K)	66	0.16 m		564.21	3166	9409	9.4	€176.04	€9,775.49	€9,951.53	€894.35	€165.86 /m ²
	67	0.3 W/m.K		569.18	3153	8085	8.1	€177.59	€8,400.54	€8,578.13	€2,267.75	€142.97 /m ²
	68	0.5 W/m.K		574.51	3160	9122	9.1	€179.25	€9,477.34	€9,656.60	€1,189.29	€160.94 /m ²
	69	0.7 W/m.K		556.90	3166	8250	8.2	€173.76	€8,571.68	€8,745.44	€2,100.44	€145.76 /m ²
	70	0.9 W/m.K		546.92	3197	7558	7.6	€170.65	€7,852.30	€8,022.95	€2,822.93	€133.72 /m ²
	71	1.1 W/m.K		545.38	3179	7931	7.9	€170.16	€8,240.76	€8,410.93	€2,434.95	€140.18 /m ²
72	1.3 W/m.K		542.73	3203	8952	9.0	€169.34	€9,300.64	€9,469.98	€1,375.90	€157.83 /m ²	

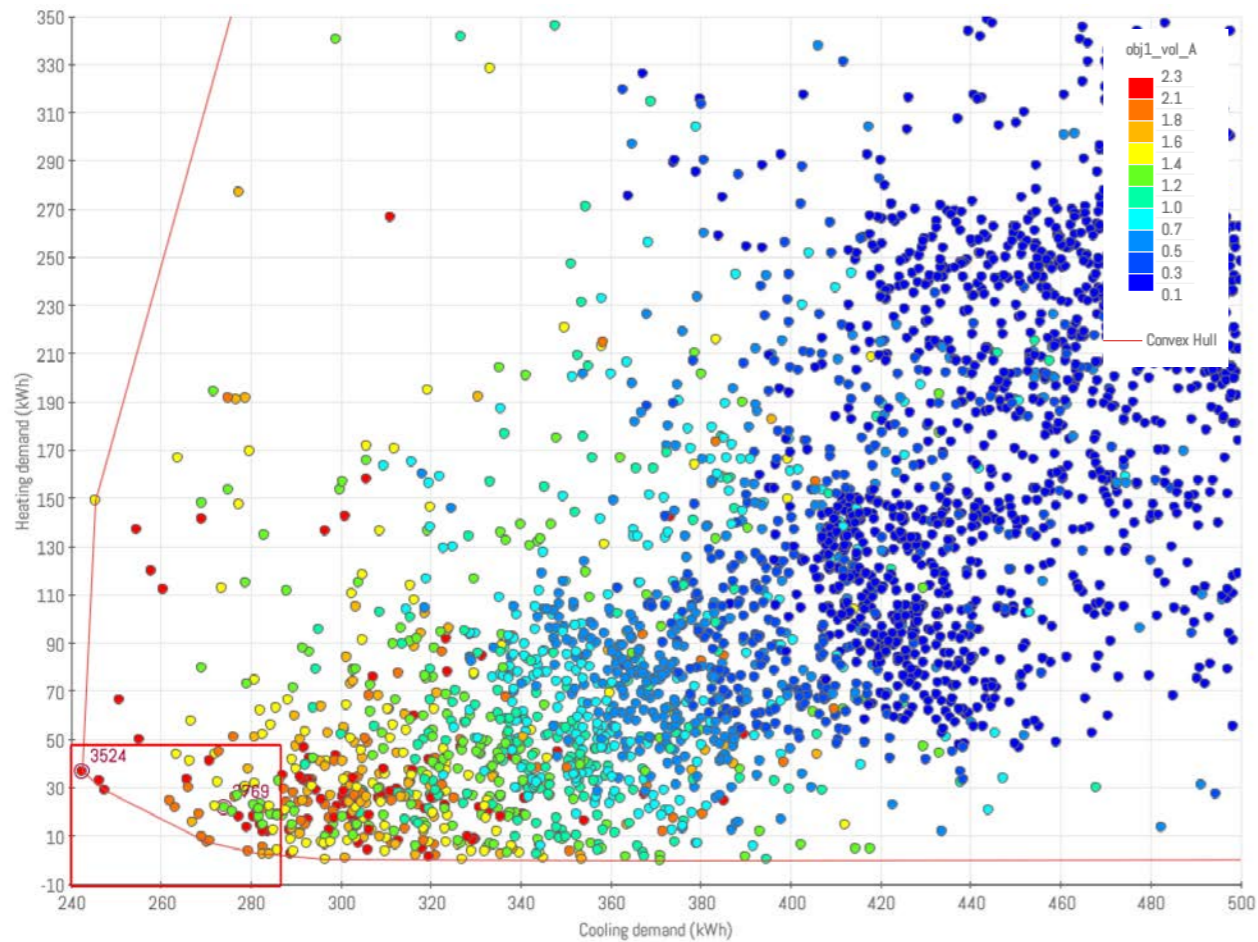
6.3 OPTIMIZATION EVALUATION

Four different design optimization strategies are adopted to reduce the overall heating and cooling energy and increase the cost-effectiveness, first a combined all-season optimization is done to point out the difference between the three, a correlation matrix will be shown for each optimization together with the actual results from the energy performance. The matrix defines the correlation between the different input and output variables to give an overview of the interaction between the two. After this, both the heating and cooling energy demand are optimized separately to evaluate the maximum energy reduction possible for both the strategies. In the end, a combined multi-objective economic optimization will be shown.

6.3.1 ONE: Combined optimization

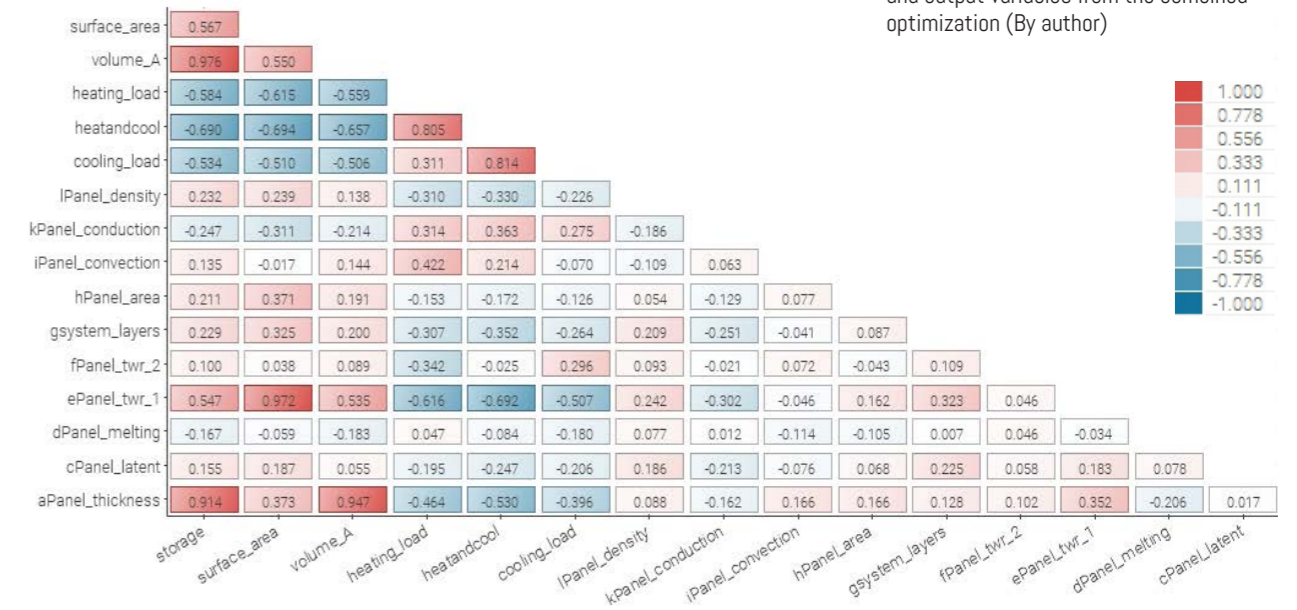
For the combined heating and cooling optimization 4000 iterations are executed, the convergence shows that around 4% of the designs (161 designs) lay within a range of 50kWh from the most optimal designs. For the combined optimization the scattered overview chart in Figure 1.106 shows that the design converges relatively quick to an optimum design for the reduction in heating load (Y-axis), this indicates that the system is easily optimized for heating. This can be expected due to the difference in magnitude between the heating and cooling load, the most optimal design are shown by the red frame (Figure 1.106), the results from these designs are illustrated more detailed in "APPENDIX E".

Figure 1.106
Scattered chart showing the correlation between the heat demand, the cooling demand and the panel volume from the combined optimization (By author)



The Pearson matrix illustrates the correlation between the input and output variables, a clear correlation is observed between the energy performance and the volume (Volume_A), the surface area (hPanel_area) and the opening area when facing the room (fPanel_twr_1). After that the correlation is the highest for the convective heat transfer (iPanel_convection), the opening area when facing the cavity (fPanel_twr_2). The surface area does not affect the volume as seen in Figure 1.107, but only the convective heat transfer between the adjacent fluid and the wall and the radiation.

Figure 1.107
Pearson correlation matrix indicating the interaction between the different input and output variables from the combined optimization (By author)



When evaluating the results more in detail ("APPENDIX E") it is seen that the most optimum designs are based on a combination of the following properties:

- A large surface area (125% - 130%);
- A high melting temperature (24,5 - 26,0 °C)
- A small trombe wall ratio when the panel faces the cavity (48% - 78%);
- A large trombe wall ratio when the panel faces the room (100%);
- A high latent heat of fusion (215 kJ/kg - 240 kJ/kg) increases the heat capacity;
- The use of a multiple layered system (3 layers), the different melting temperatures can target both seasons.
- A normal to high convective heat transfer (3.5 W/m²K - 6.5 W/m²K), this reduces mainly the cooling energy demand;
- A low thermal conductivity (0.1 W/m.K- 0.4 W/m.K);
- A standard density value for salt-hydrates (1350 kg/m³ - 1450 kg/m³)
- A large thickness (5,75 cm - 10 cm)

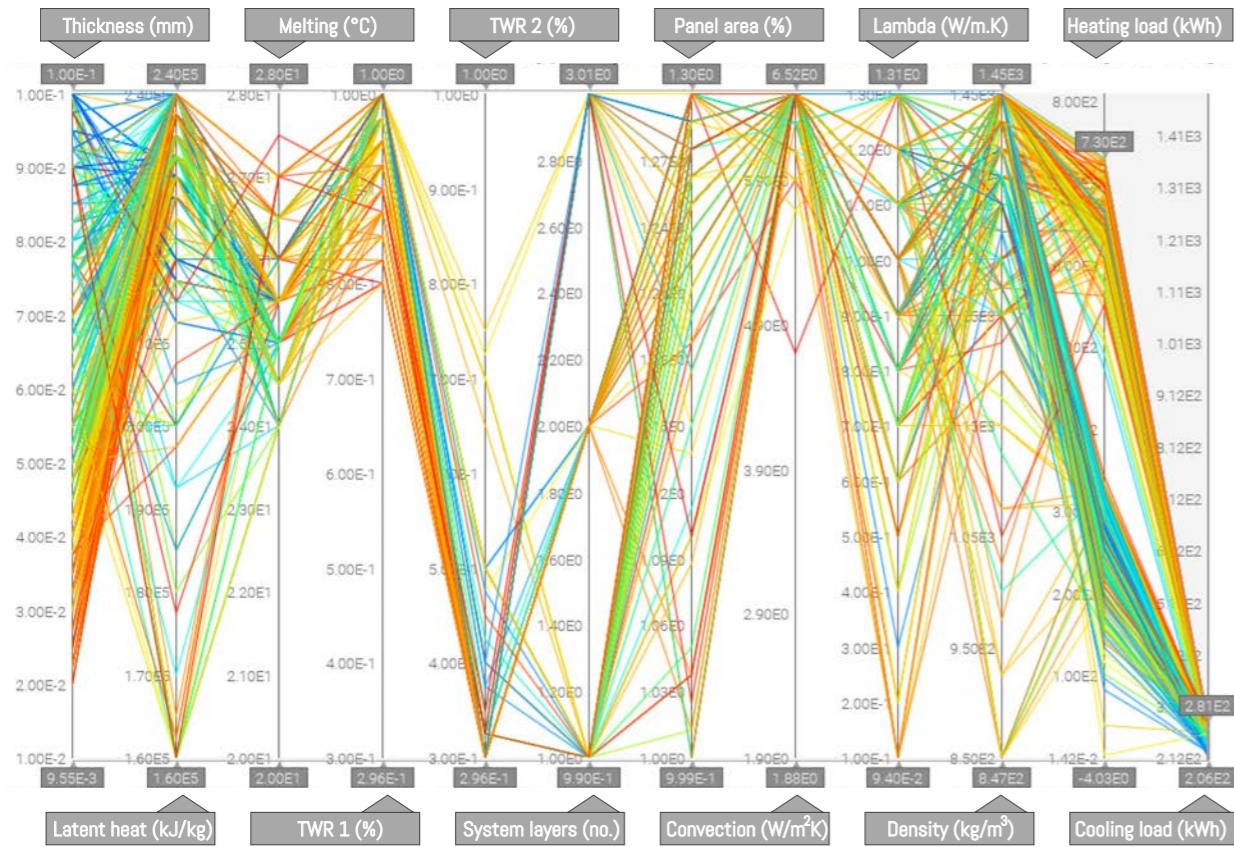
The optimization showed a significant reduction in the total heating and cooling energy demand compared to the results from the Design of Experiments, the maximum total yearly energy reduction was 979 kWh and for the optimization the most optimal design shows a total combined energy demand of 276 kWh, this accounts for a total energy reduction of 1185 kWh compared to the benchmark. The two most optimum design (#3776 and #3899) have a low volume combined with a large energy reduction.

6.3.2 TWO: Cooling optimization

For the cooling optimization in total 4000 iterations are employed and 8,6% of the designs (345 designs) converged towards the optimal value within a range of 50 kWh. When evaluating the results from the separately employed optimization for cooling ("APPENDIX F") it can be noticed that the differences in energy performance are not that large, for the optimized cooling design a minimum energy demand of 217,45kWh is obtained by the quasi-optimal design (#1076), which has a low volume and a high energy reduction. However, the heating load for the optimum designs is significantly higher. The total heating load for the optimal designs lays within a range of 230 kWh and 300 kWh. The following differentiation in design strategy is observed for the cooling optimization:

- A higher thermal conductivity (0.9 W/m.K- 1.3 W/m.K), in this way the heat can be transferred more quickly to the exterior, this results in a smaller insulation effect from the panel;
- A higher convective heat transfer is wanted (6.5 W/m²K), the heat is released and absorbed in a higher rate by the panel in summer situation;
- The results show that only one system layer gives the best results (1 layer), one optimal melting temperature value can be chosen to target only the cooling situation.
- A small trombe wall rate when the panel faces the cavity (30% - 40%), more direct ventilation is allowed during the night and the PCM can discharge more effectively;
- A large surface area (130%), this also increases the rate of heat transfer from the panel, in this way more heat can be transferred to the exterior;
- And a large thickness is required to get to the optimal cooling reduction (7,5 centimetre - 10 centimetre) with a total volume of 1.72 m³.

Figure 1.108
Correlation of different variables with the cooling energy demand reduction (By author)



The graph in Figure 1.108 clearly shows the importance from the different input variables, the variables with the more dense distribution of the lines tend to converge to one optimal input parameter. The distributed lines indicate the variables with less importance for the cooling performance. It can be observed that for a smaller panel thickness (indicated with the red/orange lines) a high convective heat transfer and latent heat storage, a small opening size when facing the room, a large opening size when facing the cavity and a large panel area are needed to increase the efficiency of the thin layered PCM.

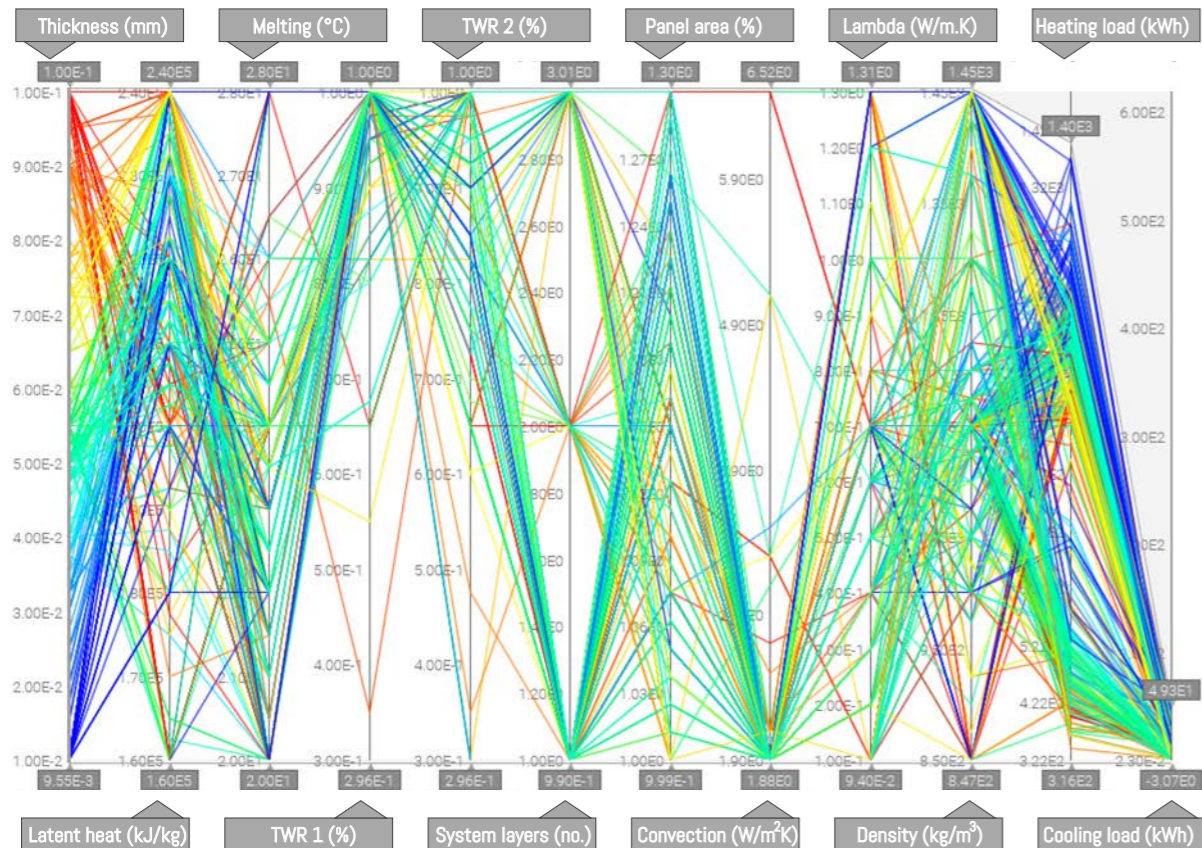
6.3.3 THREE: Heating optimization

For the heating optimization 1200 iterations are carried out, the results converge relatively quick towards an optimum and 26% of design lay within a range of 50 kWh from the most optimal. The optimum from this optimization is almost 0 kWh, multiple designs show this optimum value ("APPENDIX G"). So the heating energy can be completely provided by the PCM. This value results in a cooling load between 450 kWh and 1100 kWh so these strategies clearly show negative effects on the performance of the PCM panel for application in both seasons. The following differentiations in the results are observed comparing them to the combined optimization strategy:

- A lower PCM melting temperature (22°C -24°C), this value targets the lower indoor air temperature better;
- Mainly low values for the thermal conductivity (0.1 W/m.K - 0.7 W/m.K), this increases the insulating effect from the panel, as mentioned before;
- A lower convective heat transfer coefficient (1.9 W/m²K - 3.1 W/m²K), in this way the panel also insulates more effectively, the heat is released in a lower rate which reduce the heat loss to the exterior;
- A large trombe wall ratio when the panel faces the cavity and discharges to the room (87.5% - 100%), this reduces the amount of heat lost to the exterior and increases the amount of energy released to the interior;
- The application of single or multiple layers can both be adopted (1-3 layers), also no high impact was observed within the detailed observation in Section "6.1.6 MESO: Multi-layered LHSU" on page 137.
- A smaller thickness is needed for the heating season compared to the cooling season (5 centimetre - 7,75 centimetre);
- Different values for the panel area ratio are possible, no direct correlation is seen between the reduction in heating energy and the increased surface area.

The parallel chart (Figure 1.105) shows the overall trend from the different input parameters from the most optimal designs. Designs with a small thickness, indicated with the blue lines, show a trend towards a high panel area, a low convective heat transfer, a lower melting temperature, a high latent heat of fusion and small opening areas when facing the room and facing the cavity. The panel needs to charge efficiently for heating during the day (when facing the cavity) and during the night the heat needs to be released to interior by the largest area possible to heat the room. The values for the material density and the thermal conductivity are rather well distributed along the axes, these values seem less important for the performance regarding heating, this shows the same trend as the results from the more detailed table in ("APPENDIX G").

Figure 1.109
Correlation of different variables with the heating energy demand reduction (By author)



6.34 FOUR: Total cost of ownership (TCO) optimization

The TCO optimization is carried out by means of three main design objectives to reduce the total cost of ownership (TCO) [€], in general this is the sum of the capital expenditures [€] and the operation expenditures over a period of ten years [€]. Therefore this optimization focuses on the reduction of the heating and cooling energy demand [kWh], the heating power load [kW] and the volume of the PCM panel [m³]. These objectives reduce at the same time the costs for energy, the installation equipment and the volume of the product. The most important objective from the three is the reduction of the equipment, the highest performing design is the one with an equivalent power load for heating and cooling. For this optimization study 4000 iterations are used to converge to the quasi-optimal design, for this optimization not one optimal design can be found. The results show that a higher performing system for the heating and cooling power load in most cases also needs a larger volume.

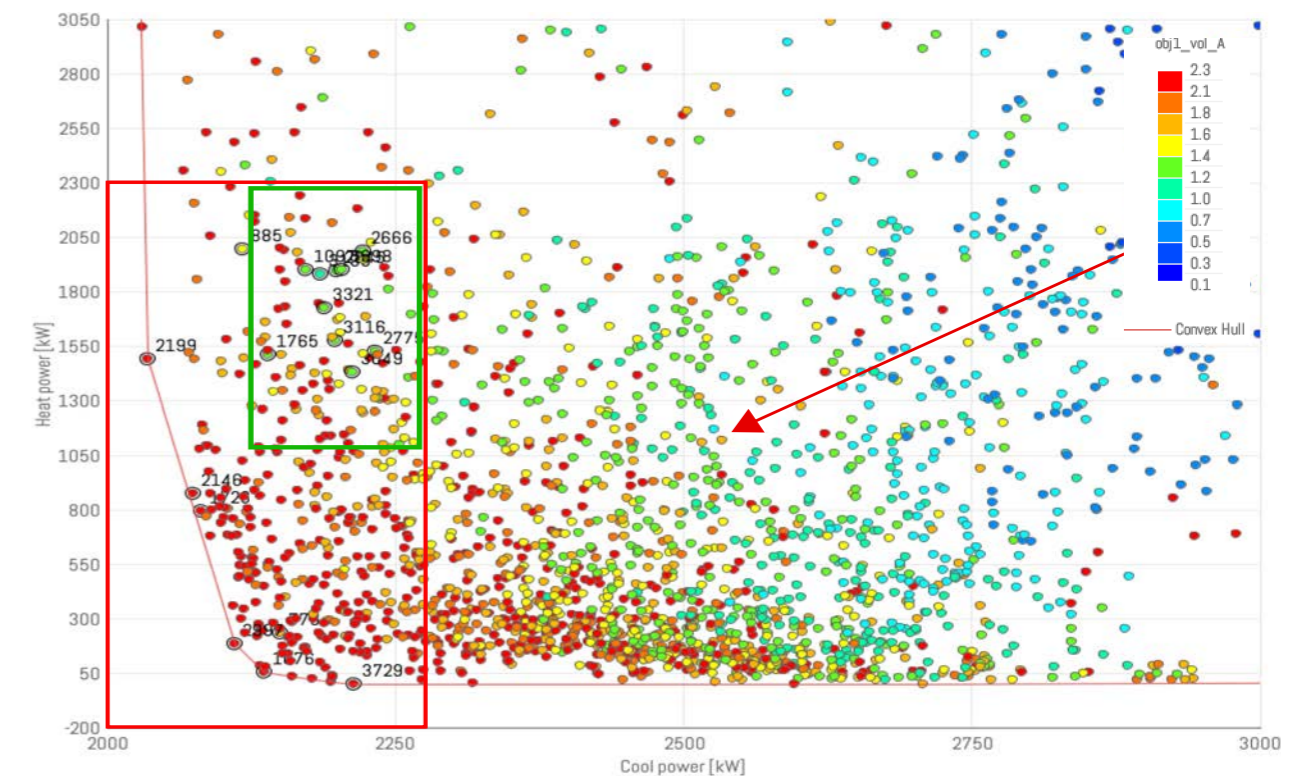
The scattered chart (Figure 1.110) shows the lowest overall power load illustrated in the left corner of the Pareto front, however the heating power is not equal to the cooling power at this point. The design that converges most to this point is illustrated at the left side in the red box (Design #2199), this design has a maximum heat power of 1488.25 kW and a maximum cool power of 2034.76 kW.

A clear correlation is seen (Red arrow) between the heat and cool power and the volume of the panel, the colour indication defines the volume [m³] of the design variables, so three objectives area seen (Figure 1.110). It is clearly shown that all the designs on the Pareto front contain a high volume, the total volume from the optimal design is 2.29 m³ with a panel thickness of 0.1 meter as illustrated in "APPENDIX E". Some of the designs are marked within this chart, some of these designs show a combination of a low

volume and a low heat and cool power, this combination is desired to reduce the TCO. These designs will be evaluated more in detail to indicate the difference for the input and output variables, the red box (Figure 1.110) shows the designs with a low maximum heat power and cool power, all below [2.300 W]. The green indication gives the combination of a low volume combined with a low power. The bubble chart and the table illustrated in "APPENDIX E" show the results from the marked design from Figure 1.110. From the results it is shown that almost all the designs need a three layered system to optimize the performance for all the objectives combined, there is one design [3321] shown with a combination of a low volume using just one layer. The following is observed within the detailed results:

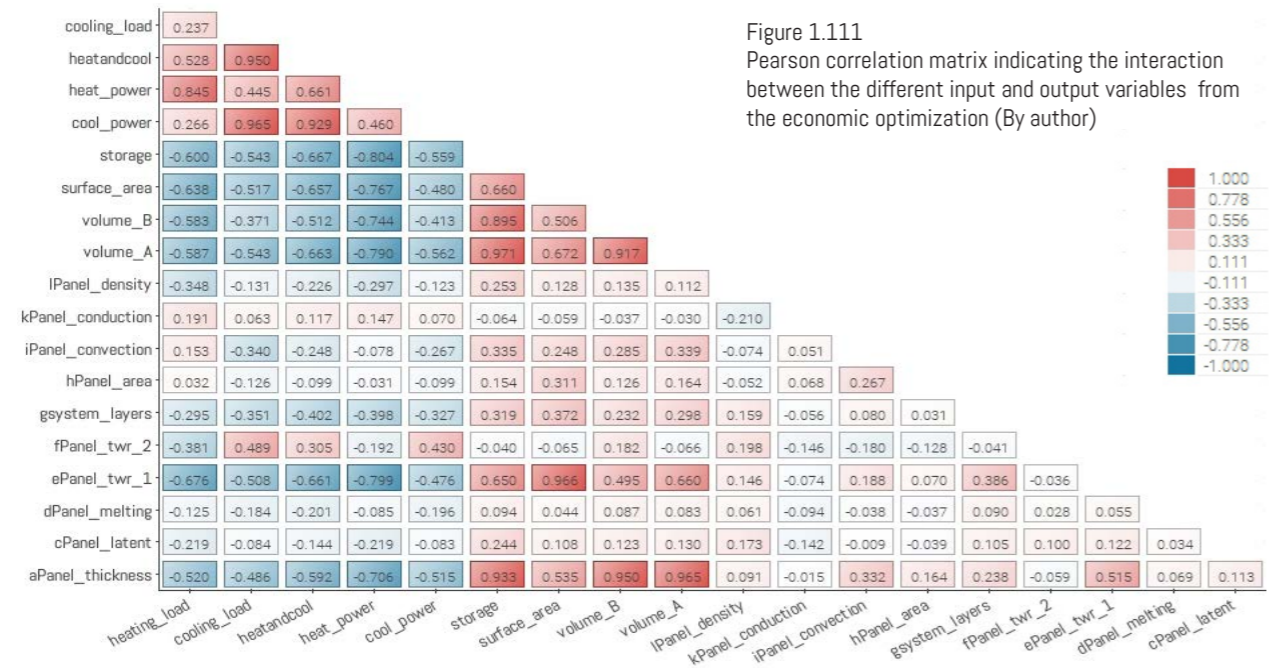
- All the design show a combination of an increased surface area with an increased convective heat transfer for the surface;
- The melting temperature for the most optimal designs ranges from 25°C up to 27°C, this indicates that the melting temperature for the overall optimization needs to be higher than the melting temperature from the economic evaluation from the Design of Experiments shown in Section "6.2.2 Results Design of Experiments (DoE)", this new melting temperature takes into account both the reduction in cooling an heating power-load;
- Also a high density product is desired when the volume needs to be reduced, in this way a higher volumetric heat capacity is obtained which reduces the possibility for overheating and increases the energy absorbed by the panel.

Figure 1.110
Scattered diagram showing the correlation between the heating and cooling power and the volume (top), Pearson correlation matrix indicating the interaction between the different input and output variables (bottom) (By author)



The correlation chart shows that almost all variables with a high correlation with the heating load or heating power also have a high correlation with the cooling load and power. However when looking more

in detail on the results from this chart it can be noticed that for instance the surface area of the panel has more influence on the results from the heating power than from the cooling power. TWR 2 has a much higher correlation with the cooling energy demand and the cooling power load compared to energy and power-load from heating.



As said, the optimization is done according to three main objectives to increase the accuracy of the optimization, more objectives would be difficult for the optimization algorithms, therefore a detailed simulation is done to reduce the latent heat and thickness by varying the adjacent simulation values from the optimal design [3321], the results are shown in Table 1.28. The detailed result showed that the costs for the PCM could be reduced by using a lower latent heat of fusion for the panel, this increases the total heating power-load significantly but it also reduces the price of the PCM. This outweighs the increased performance of the system, therefore the most optimal cost-effective design for this design case is the 6 centimetre panel with a latent heat of fusion of 180 kJ/kg [#3321.5] and the for design 3321 defined input variables in "APPENDIX H". The investment space per panel area (no pcm) shows the amount of Euro per square meter of Trombe wall available after subtracting the actual PCM price according to the volume and the quality (kJ/kg). The price is assumed to be doubled for the PCM with a latent heat of fusion of 225 kJ/kg according to the price indication for the high quality (HC) PCM from Rubitherm ("APPENDIX C"), linear interpolation is used to give a price indication for the other values for the heat of fusion.

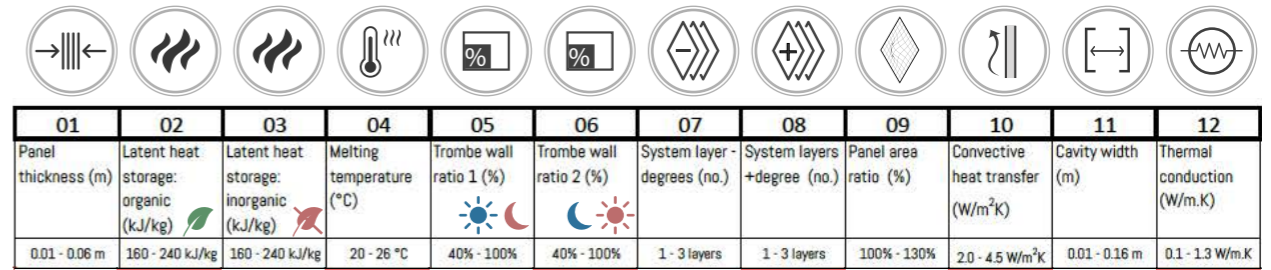
Table 1.28 Detailed optimization results from the economic optimization study for a 60 m² office room (By author)

ID (#)	SIMULATION RESULTS					ECONOMIC RESULTS					INVESTMENT SPACE		
	Adjacent simulation value for optimization	Yearly energy demand (kWh)	Cool power (W)	Heat power (W)	Maximum power (kW)	Total operation cost	Total equipment cost	Total cost of ownership (TCOO)	Total investment space	PCM panel price indication	Investment space per panel area	Design investment space	Investment space per panel area (no pcm)
3321.1	0.06 m (225 kJ/kg)	341.74	2188	1725	2.2	€106.63	€2,273.78	€2,380.41	€8,465.47	€5,974.98	€388.28 /m ²	€2,490.50	€114.23 /m ²
3321.2	0.05 m	366.59	2380	2282	2.4	€114.38	€2,473.24	€2,587.62	€8,258.27	€4,979.15	€378.78 /m ²	€3,279.12	€150.40 /m ²
3321.3	0.04 m	387.96	2527	3892	3.9	€121.05	€4,043.79	€4,164.83	€6,681.05	€3,983.32	€306.43 /m ²	€2,697.73	€123.73 /m ²
3321.4	0.06 m (200 kJ/kg)	357.57	2210	2144	2.2	€111.57	€2,295.88	€2,407.44	€8,438.44	€4,779.98	€387.04 /m ²	€3,658.46	€167.80 /m ²
3321.5	0.06 m (180 kJ/kg)	361.56	2223	2866	2.9	€112.81	€2,977.67	€3,090.48	€7,755.40	€3,584.99	€355.71 /m ²	€4,170.41	€191.28 /m ²
3321.6	0.05 m (180 kJ/kg)	377.65	2429	3643	3.6	€117.83	€3,784.66	€3,902.49	€6,943.39	€2,987.49	€318.47 /m ²	€3,955.90	€181.44 /m ²

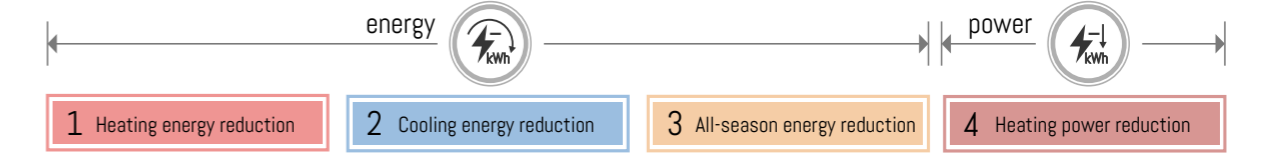
64 DESIGN GUIDELINE

This section includes a design guideline which is illustrated in Figure 1.113, this guideline is developed for experts to give a clear overview on the impact of each simulated parameter on four design categories (Heating energy, cooling energy, all-season energy reduction and heating power reduction). First a comprehensive explanation will be given regarding the working principle of this design guideline, in the end all the different segments are combined into one extensive concluding graph. The overview can be used to get a quick indication of the deviation in the best performing parameters for each design category on the one hand and the difference in impact on the energy and power reduction on the other hand, the actual values are given within the results of the previously shown sections in this report.

Twelve different input parameters are simulated, these parameters are shown below. Each of these parameters contains its own input range which is determined according to a detailed literature study. All these parameters are shown in the illustration below. The input variable for the latent heat storage is divided into organic [02] and inorganic [03] compounds with a different conductivity (org: 0.2 W/m.K ; inorg: 0.6 W/m.K) and density (org: 850 kg/m³; inorg: 1450 kg/m³). The Trombe wall ratio (TWR) determines the ratio of the trombe wall in relation to the south facade divided in two situation, TWR 1 [05] shows the results for the summer day ☀ and winter night 🌙 and TWR 2 [06] for a summer night 🌙 and a winter day ☀. The system layers are used to simulate different design situation with multiple layers, also here two situation are used. First the multiple layers with an ascending [07] melting temperature range (i.e.: 21-23-25°C) is used and secondly a descending [08] strategy is adopted (i.e.: 25-23-21°C). The other parameters speak more some for themselves and are related to the properties of the Trombe wall design.

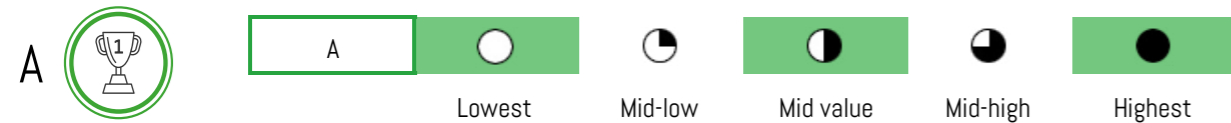


Each input parameter is simulated within 4 different categories to indicate the performance of each parameter within the different climatic situations. Here the first three categories point out the results for the yearly energy performance, the results are compared to a benchmark situation using a standard office size of 60m² including a double glazed south facade with a window to wall ratio (WWR) of 85% and a sun screen. The fourth category shows the performance of each variable for the peak load reduction in the heating situation. This research study is based on a temperate climate with a high diurnal temperature swing in the heating season, therefore this season is decisive for sizing the installation equipment. Important to notice is the difference in impact on the heating energy and the peak load reduction, some parameters have a high impact on the power load reduction and a low impact on the energy or vice versa.



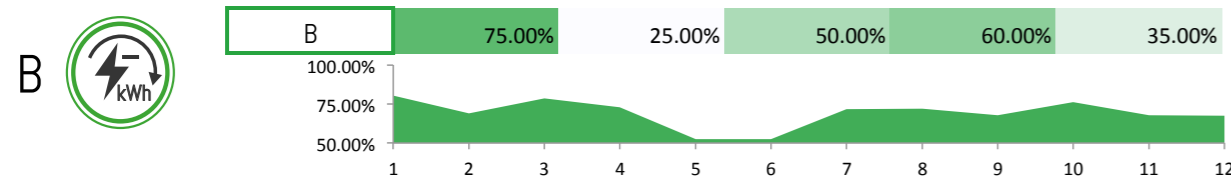
Best performing parameter value

The overview shows the best performing parameter for each case [A1 - A3] using indicators for the lowest to the highest input parameters. For instance, a low indicator is equivalent to a low input parameter from the simulation. The best performing parameters also correspond with the results from each optimization for the different design categories. These indicators can be used to identify the difference in input parameter between the different categories as mentioned before, for instance a low convective heat transfer is needed in winter and a high value is required in summer. Therefore an adaptive design is needed to increase the performance of the system in both situations.



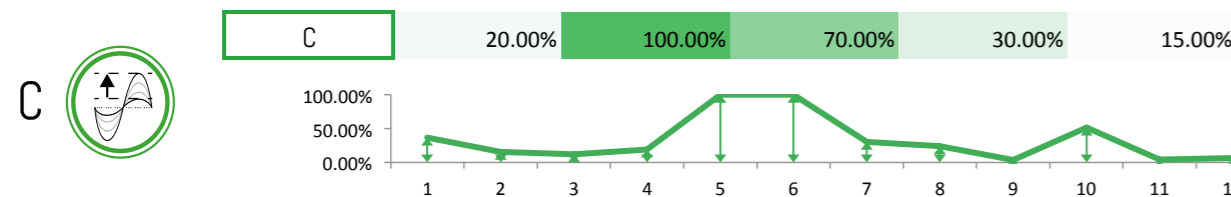
Energy reduction performance

The second overview [B1 - B3] shows the percentile impact of each variable on the energy reduction for heating, cooling and the combined heating and cooling performance by using the filled area graphs, a higher reduction is positive. In horizontal direction this graph gives insight in the differences in results for the energy and power reduction between the twelve input variables. In vertical direction the impact of each variable can be compared between the seasons to point out the performance for each situation. In this way all the different parameters can be compared on the actual reduction in energy.



Range of dataset

The line graphs [C1 - C3] illustrate the range in the results from each variable, this indicates the actual difference between the lowest and the highest resulting value from each parameter. When a high range is shown, the difference in result between the lowest and the highest performing value is also high. A low value indicates that this range is also low and the impact of the variation within the input variable is negligible. With these three elements a clear overview is given on the impact and the performance regarding the energy reduction, a mutual comparison can be done between the different categories and between the various input variables to get a clear indication on the performance of variables for different simulations.



Power-load reduction

For the reduction in power-load only the heating power is included in the guideline overview, this power-load indicates the reduction in peak-loads to reduce the size installation equipment. The impact on the cooling power is too small due to relatively low power-loads for cooling, the simulated temperate climate has a a lower diurnal temperature swing in the summer season between day and night. Therefore, the size of the equipments is determined according to the heating (winter) season. Comparing the results from the combined energy reduction [A3-C3] to the results from the reduction in power-load [A4-C4] a clear difference is observed, the impact on the performance in energy or power-load differs for each input parameter. The trombe wall ratio for instance has a positive effect on the overall energy reduction but a negative effect on the power-load reduction. The convective heat transfer on the other hand does not really affect tot total energy reduction, but it has a large impact on the power-load reduction (indicated by the lined graphs).

Summarized result overview

The results from the design guideline are combined in one summarized overview to indicate the performance of each variable on all the different categories. The "Energy and Power" summary overview (Figure 1.112) shows a combination of the impact on the heating an cooling energy demand and the maximum heating power load, the parameters with the largest impact on the combined situation contain the high values [D4]. Here it can be noticed that the parameters with the highest positive impact are the panel thickness, the latent heat of fusion, the trombe wall ratio, the system layers and the convective heat transfer. The values for the best performing parameters [A.4] are based on the final input parameters for the optimal design [#3321] from the economic optimization from Section "6.34 FOUR: Total cost of ownership (TCO) optimization".

Figure 1.112 Summarized overview of the combined results for heating and cooling energy reduction and heating power load reduction (By author)

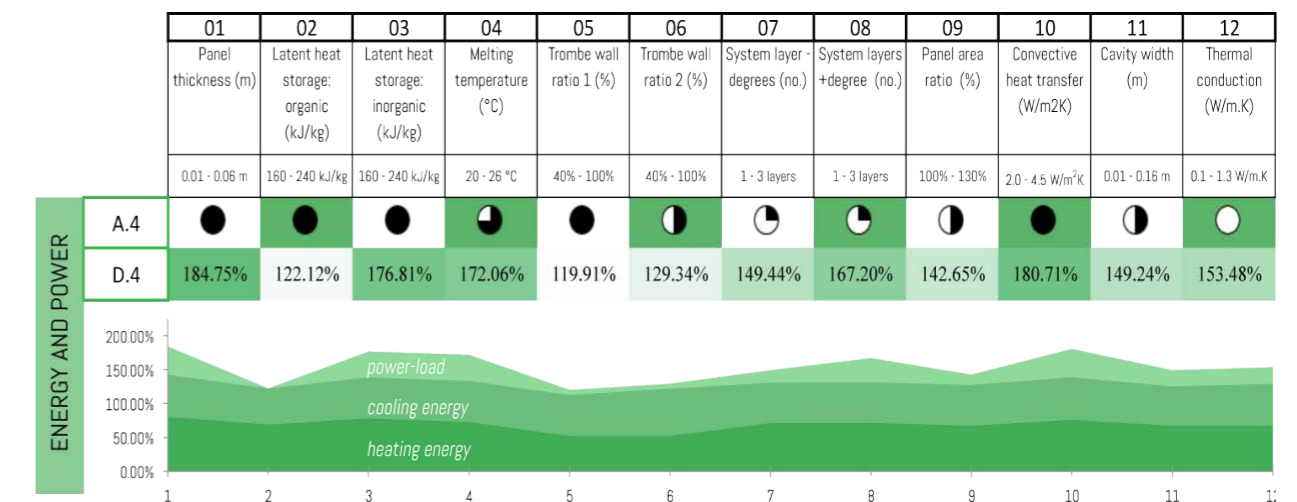
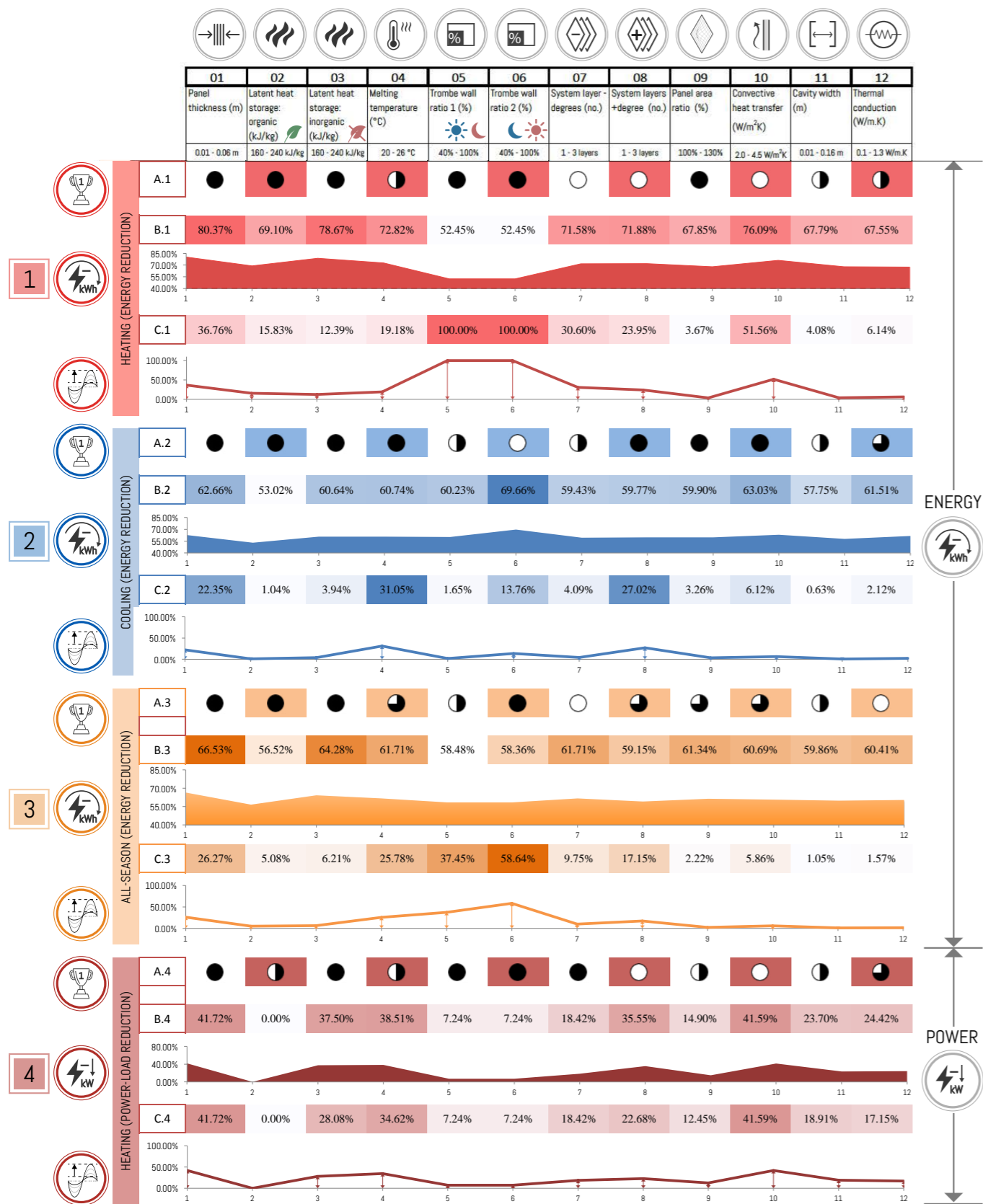
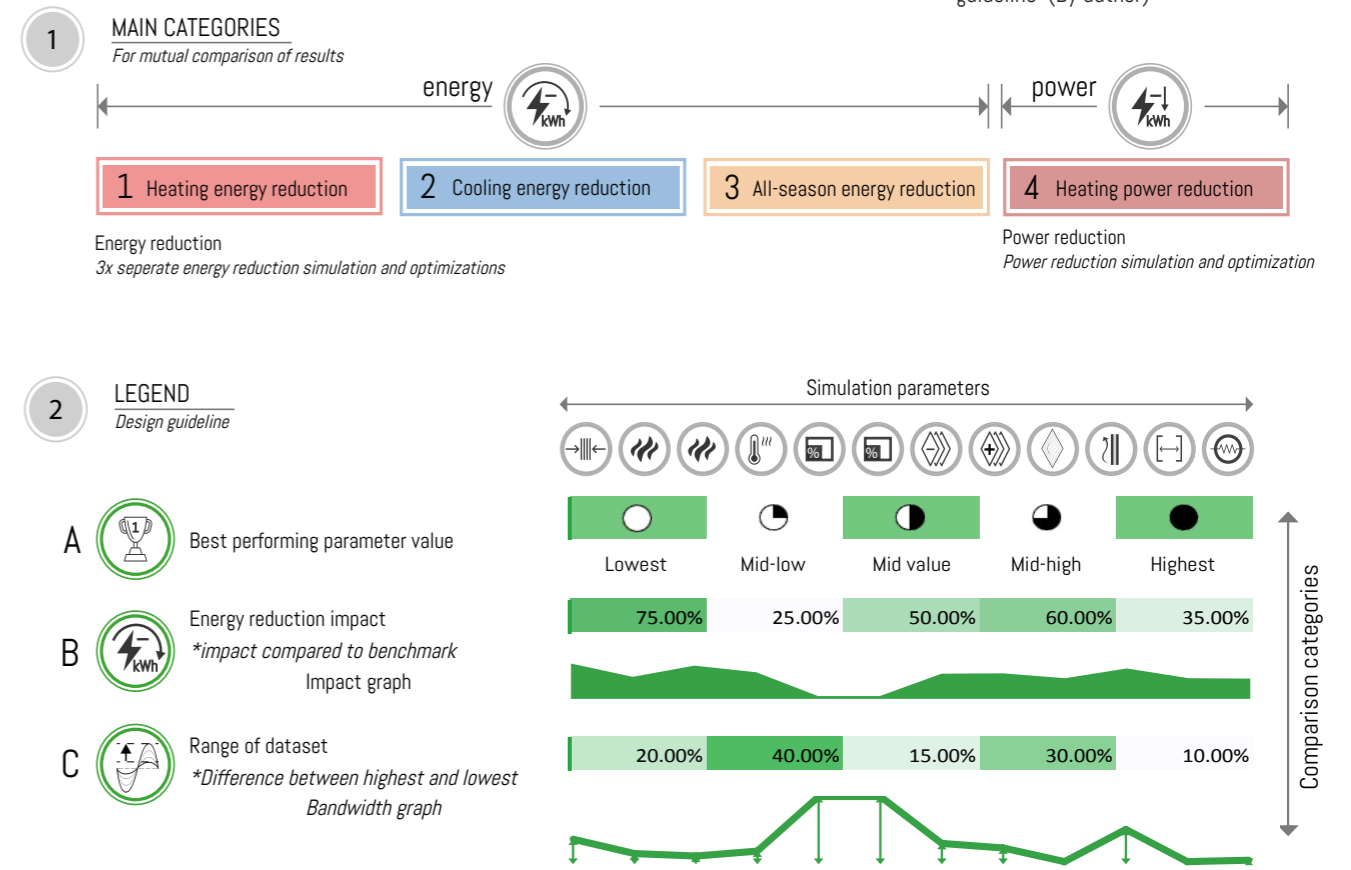


Figure 1.113
Design guideline showing the impact and the performance of each parameter (By author)



*Detailed results on the actual energy and power performance are shown in Section "6.1 THERMODYNAMIC EVALUATION", "6.2 ECONOMIC EVALUATION" and "6.3 OPTIMIZATION EVALUATION".

Figure 1.114
Legend and quick guide for the design guideline (By author)



Example case


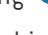

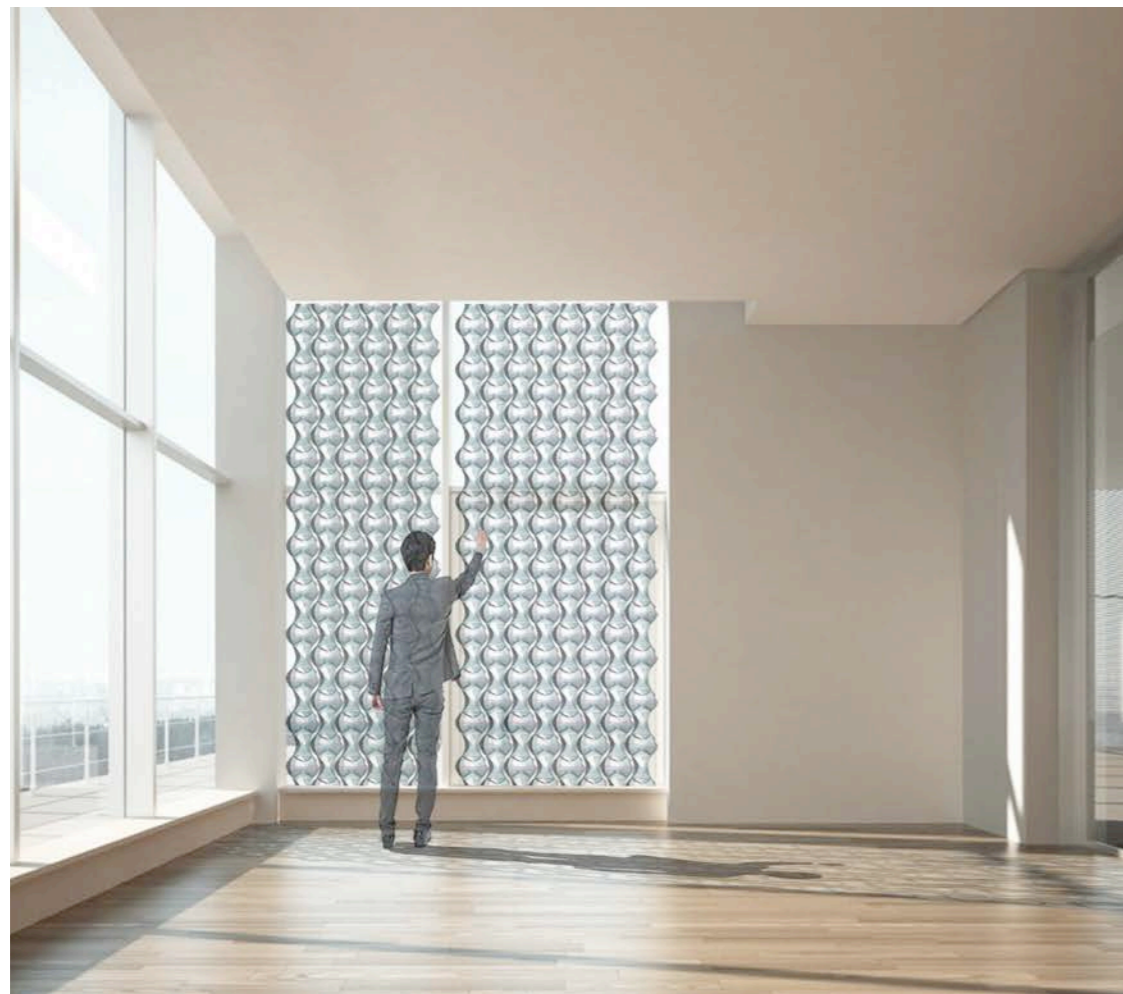
One brief example case will be given to indicate the working principle and the usage of the design guideline. Important for the design with the PCM trombe wall are first the most important design requirements from the design case. If for instance the impact on the usable floor area is important to the designer than different parameters affect this requirement, here for instance a low cavity width and thickness is wanted to reduce the overall dimensions of the system. Another important parameter in this situation is the opening area, it can be noticed from the design guideline that the input value for the heating and cooling situation are different , this means that an adaptive design performs better. This adaptive design requires for instance a design strategy to allow for different opening areas, this can increase the impact on the usable floor area. Moreover, it can be observed that the impact of the opening area is positive for the cooling situation, here a peak is seen for the night cooling . However, for the heating situation a negative performance is seen for both day and night , the highest performing parameter (TWR 100%) already shows a low performance compared to the other variables. When reducing this trombe wall ratio the performance reduces even more. In this way, an adaptive design is actually required to increase the efficiency when designing for both seasons. The cavity width on the other hand has a low range within the dataset, this indicates that this variable does not increase the performance and therefore the dimension of the system can be reduced. In this way different important project requirements can be assessed using the design guideline.

Figure 1.115
Illustration of the implementation of the design solution directly behind the curtain wall, situated within an office space (By author)



7. DESIGN PHASE

The results from the simulation and optimization phase, together with the knowledge from the background analysis, are used to define the design requirements for the application of a PCM Trombe wall within an office space in The Netherlands. Some additional requirements are included to allow for instance for maintenance and to reduce the impact on the usable floor area of the room. A summarized overview will be given regarding all the requirements for the design, this overview will be the input for the design phase.

The elaboration of the design is divided into three parts, first the general working principle with the different design typologies, the configuration and the material choices are shown, after that a technical description will be given on the implementation of different existing products and the connection with the surrounding building. In the end, the design will be evaluated on costs to indicate the actual total cost of ownership (TCO) of the system according to the needs and the design requirements.

TROMBE WALL PROPERTIES



Panel thickness
6 cm



Latent heat of fusion
180 kJ/kg



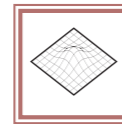
Various Trombe wall ratios



Melting temperature
25°C



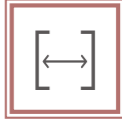
Varying convective heat transfer



Increased surface area



Panel layering
1 layered



Small cavity width



Thermal conductivity
0.1 W/m.K



Cascading strategy



Panel translucency

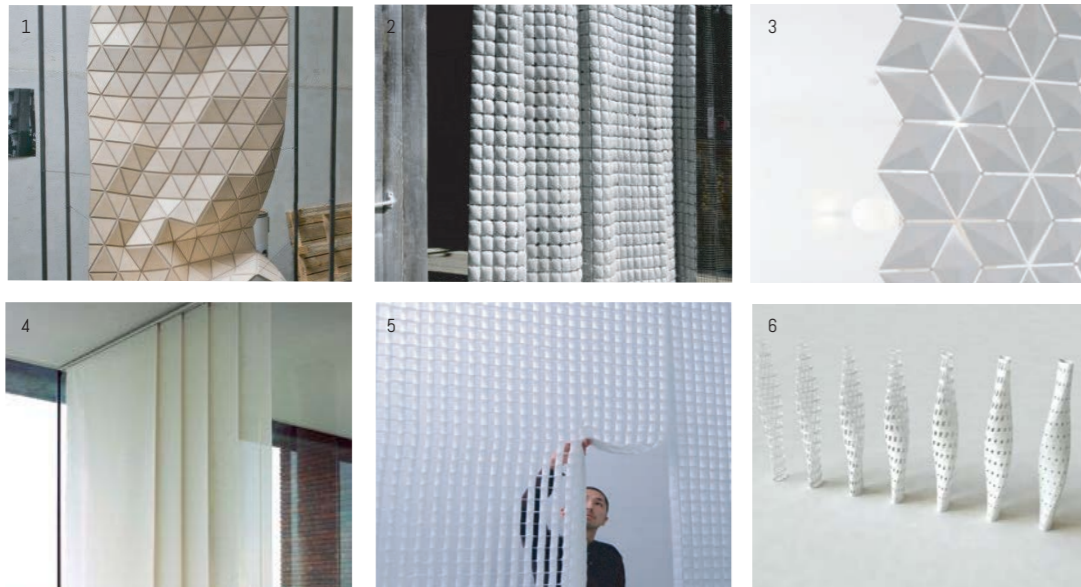


Easy maintenance

ADJUSTABILITY



! Active energy storage volume needs to be preserved

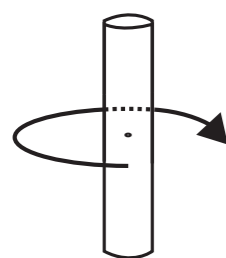


- 1) Woodskin: The Flexible Timber Skin [digital image]. Retrieved from: <https://selfieus.com/media/1450288372395560904>
- 2) Memux (2006). Concrete tiles curtain [digital image]. Retrieved from: <http://not-for-them.blogspot.com/2008/12/concrete-tiles-curtain.html>
- 3) Blooming (2014). Decorative room divider [digital image]. Retrieved from: <https://www.blooming.com/showcase/>, by
- 4) Benedetti (n.d.) Paneelgordijnen [digital image]. Retrieved from: <https://www.benedetti.be/paneelgordijnen.htm>
- 5) Designboom (2011). Student design awards [digital image]. Retrieved from: <https://www.designboom.com/design/design-for-asia-student-award-2011/>
- 6) Lu yen-cheng (2013). Rotate tower [digital image]. Retrieved from: <https://www.grasshopper3d.com/photo/rotate-tower/next?context=user>

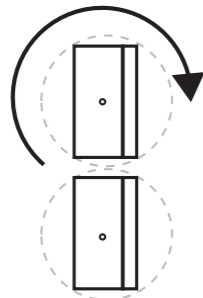
ORIENTATION



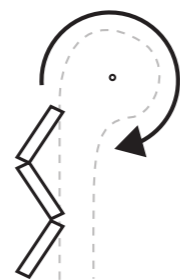
! More discharge in summer night, more direct daylight on winter day



vertical rotation



horizontal rotation



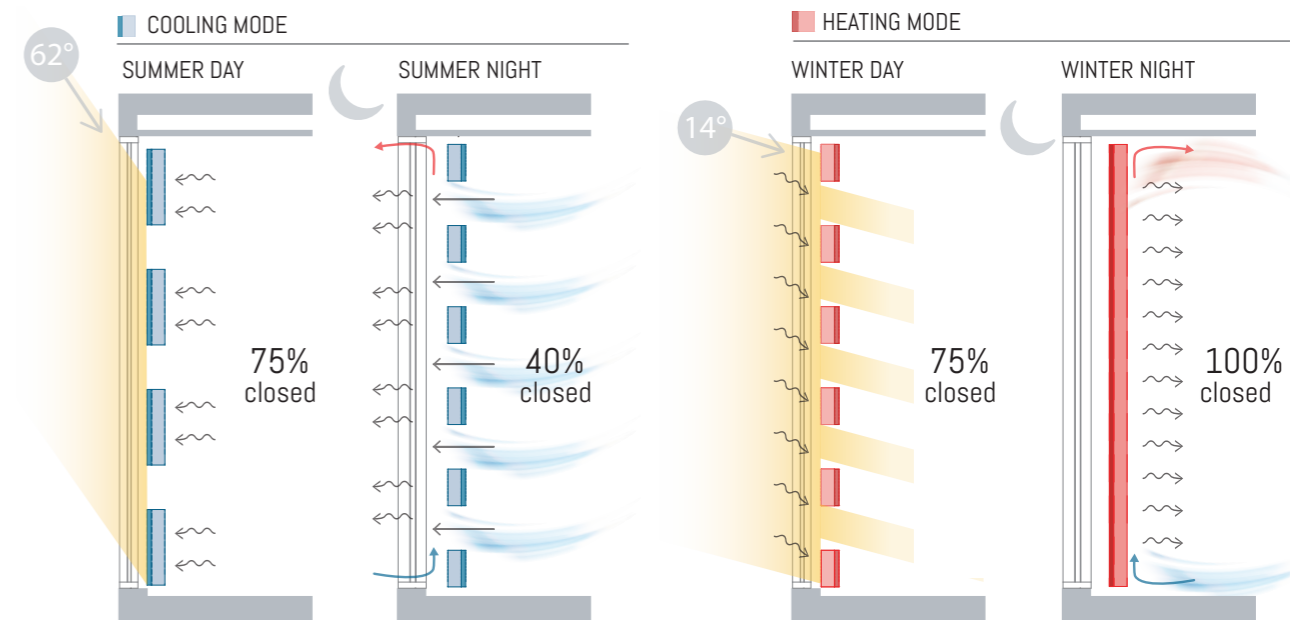
double railsystem

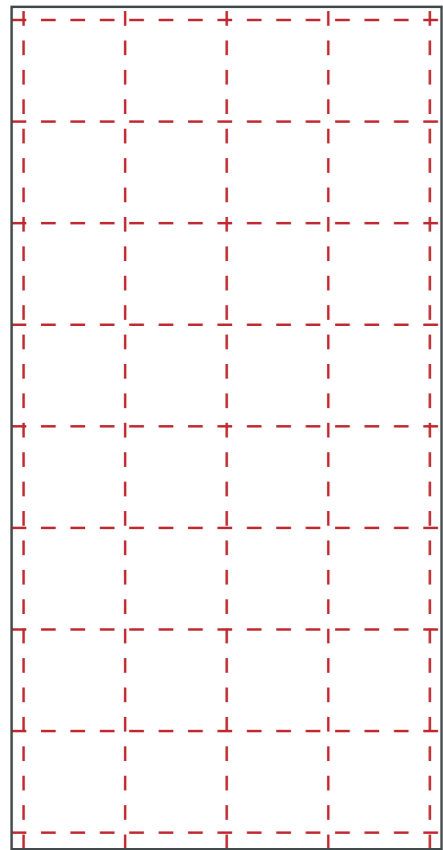


7.6.1 Design requirements

All the results from the literature study together with the results from the different simulation and optimization strategies are used to make the transition towards an actual integrated product. The main objective of this research study is create an optimal design regarding the thermodynamic performance and the cost-effectiveness of the system. The ideal thermophysical parameters, obtained from the simulation and optimization, are shown in the trombe wall properties on the left. These properties will be the base for the design of the product. Additionally, some basic design requirements are defined according to the purpose of the system and the functionality of the office space. The following requirements will be used as starting point for the design:

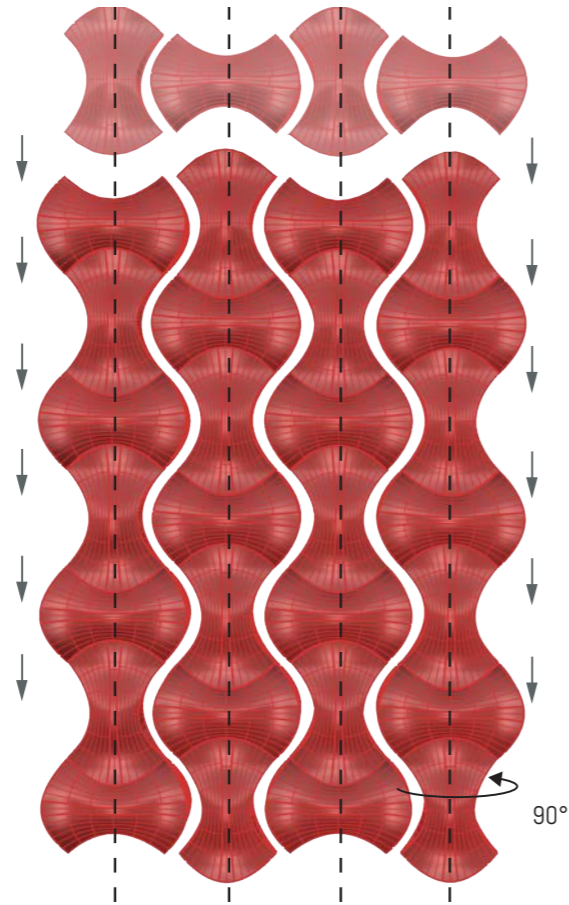
- Fixed system, the system will be fixed within the reveal of the curtain wall to increase the amount of usable space. A simple unlocking mechanism must be included to allow for maintenance and window cleaning, the system must be manual operable to reach for the window;
- Adjustable system, the opening percentage will be automatically variable. The values for the opening percentage are shown in the cooling and heating mode diagram. The detailed study showed that the energy and cooling power influence of the opening area on a summer day is relatively small. Here the opening will be 75%, this value differs from the most optimal design due to the limitation in the simulation. The TWR for the summer day and the winter night where directly connected, results showed that this parameter mainly affects the heating energy demand;
- Rotatable system, the system needs to rotate to either orient the PCM towards the room or the cavity according to the diagram shown below;
- The system only needs to rotate outside the working hours. A slow mechanism will be implemented to create a save product and working environment;
- A cascading strategy improves the design of the panel, it reduces the possibility of internal convection and an irregular melting pattern;
- A small cavity width reduces the amount of usable space lost, in this way the PCM can be integrated within the window reveal.





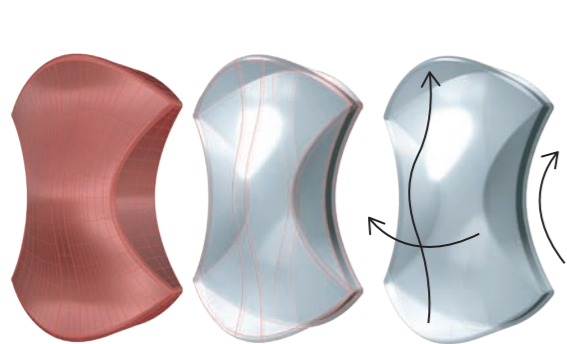
1 Small segment division

The trombe wall element will be divided in smaller segments to create a more compact rotation within the system, this reduces the impact on the usable floor area.



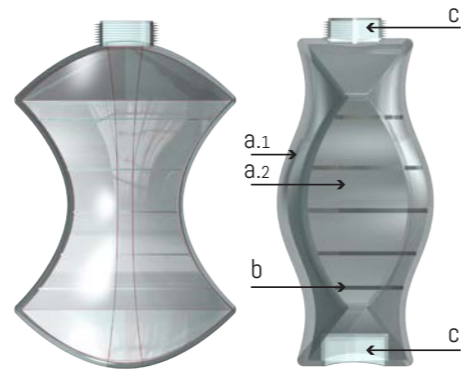
2 Vertical elements

Modules are stacked in vertical direction to allow for a modular height, this vertical alignment increases also the structural stability. The modules can be rotated 90 degrees to orient the module according to the configuration scheme for the different seasons.



3 Double curvature

The module is morphed in two directions to create a smooth surface with different heat transfer coefficients within the different configurations of the seasons. A large surface area increase is adopted for the summer situation (side and front). In the winter situation the system is closed, in this way only a small increased



4 Module typology

This double curvature is created using the PMMA container material, which is produced using the injection moulding technique. On the back of the module an insulated segment will be implemented, this part will be filled with aerogel insulation (a.1) and PCM (a.2). Internal segments (b) are added to reduce the internal convection and a cap (c) is introduced for filling the module and for stiffness of the total

7.6.2 Materials and products

An analysis will be shown on the material choice and products implemented in the design, this to create a fully integrated design that fits within the cost-effective optimization. The design process is based on the alternation between a study on existing products and materials and an in-depth analysis on the available materials for this specific application. The latter is employed using CES Analysis, a comprehensive database of materials and production processes (CES Edupack, 2019), comparing several materials and processes for the production of the container.

To allow for enough daylight and for visible access to the exterior, the container of the PCM will be transparent. Important for this encapsulation is the ability of the material to transmit both the wavelengths for visible light and the Infrared Light (IR), in this way the PCM can absorb most of the energy radiated from the sun. The infrared spectrum ranges from 780 nm up to 1000 nm, a detailed optical measurement from Hitachi, Ltd. (n.d.) indicates that Polymethyl methacrylate (PMMA), Polyvinyl chloride (PVC), Polyethylene terephthalate (PET) and Polycarbonate (PC) are plastic materials that transmit all the wavelengths within this spectrum. This measurement showed that PMMA has the highest light transmittance, changing the plate thickness up to 10 mm does not affect this transmittance (Hitachi, Ltd., n.d.). An analysis is done to indicate which of these materials is low in cost and has a high overall specific strength to be durable for impact ("APPENDIX I"), a selection filter is used to define materials that are durable for UV-radiation, fresh water and salt water. The results showed that here PMMA has a combination of a relatively high specific strength and is low in costs compared to the other possible materials, this material will be included in the design.

The design requirements showed that the system requires the ability to orient towards two sides, to have various opening ratios, to allow for maintenance and window cleaning and to have a low impact on the usable space. Therefore at least two mechanism needed to be integrated, a vertical rotation mechanism is implemented to allow for both the orientation of the panel and the various opening percentages.

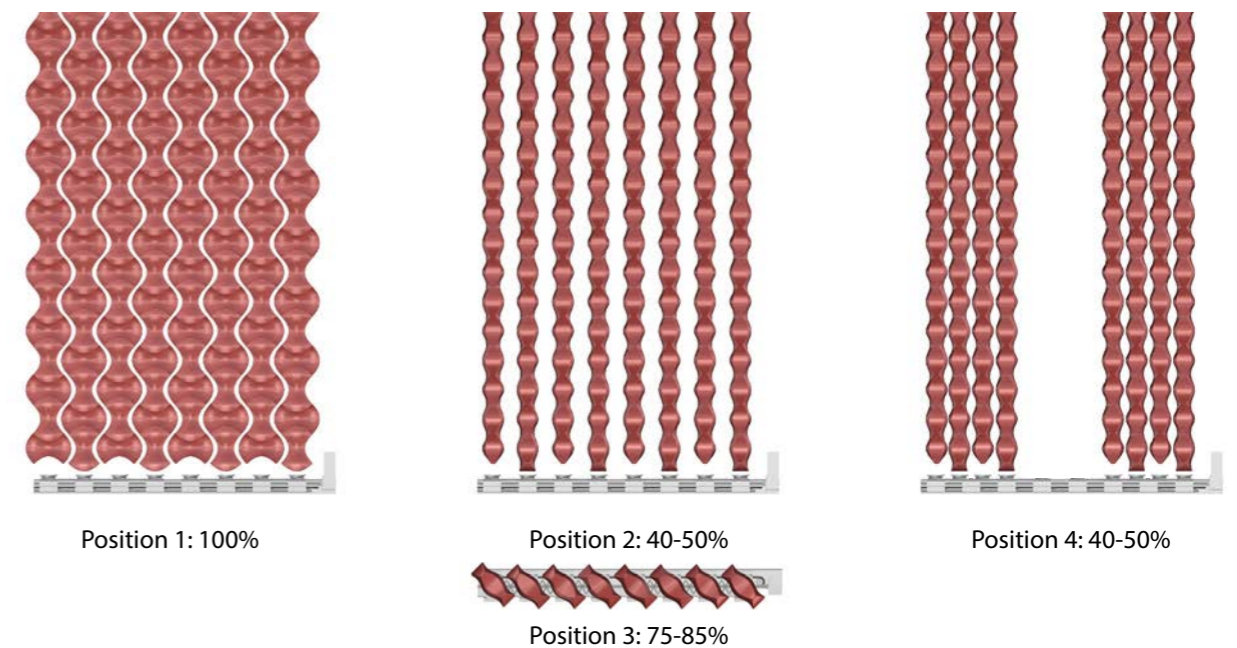
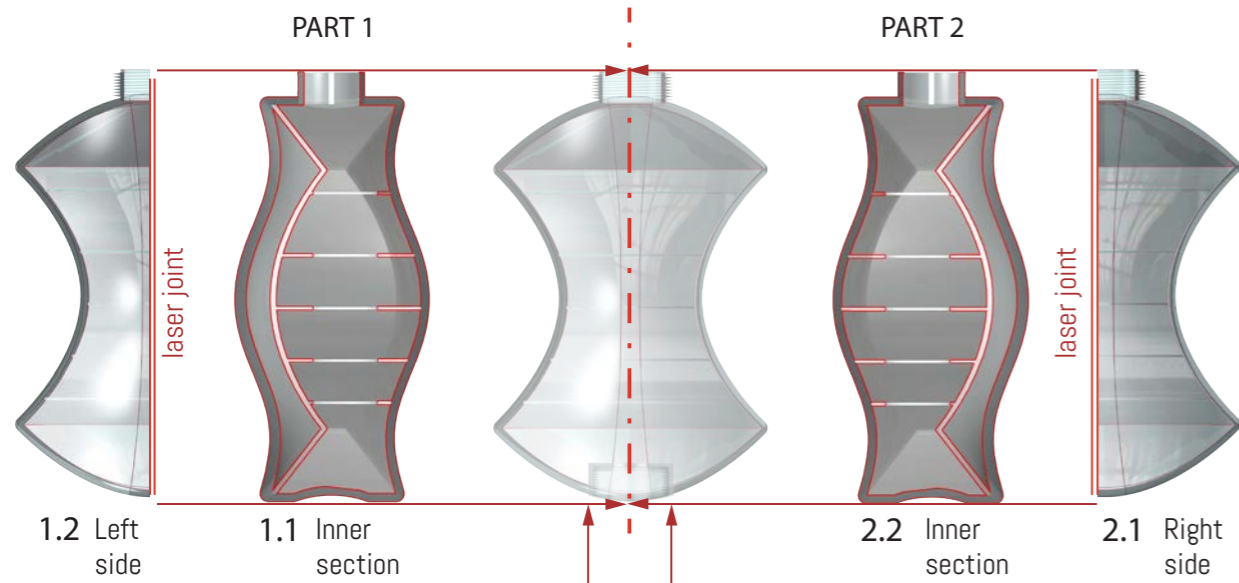


Figure 1.116
Diagrammatic principle of PCM panel design, scale 1:20 (By author)

7.6.3 Module production & assembly

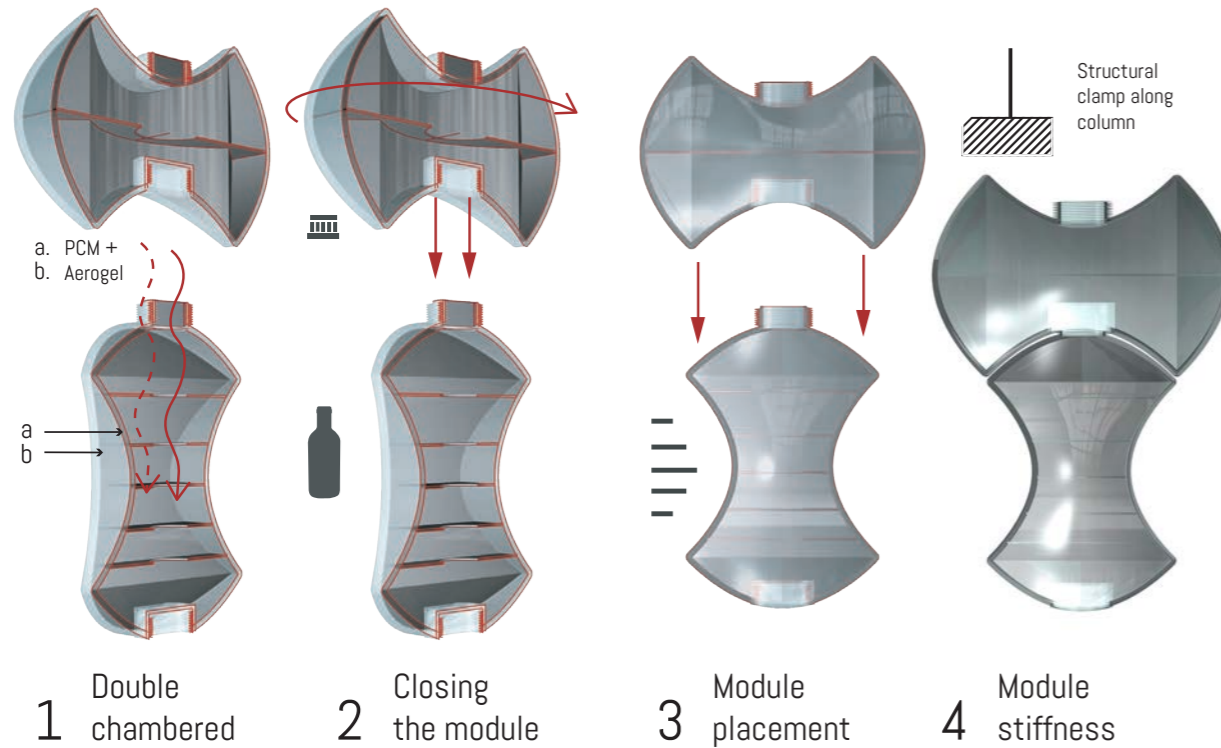


Part 1 & 2

These parts are identical to each other, the module is cut in two at the middle. The outer skin of the module is tapered towards the side to effectively remove the mould. The inner parts are all straight according to the direction in which the mould will be removed, no curves are used.

Part 3

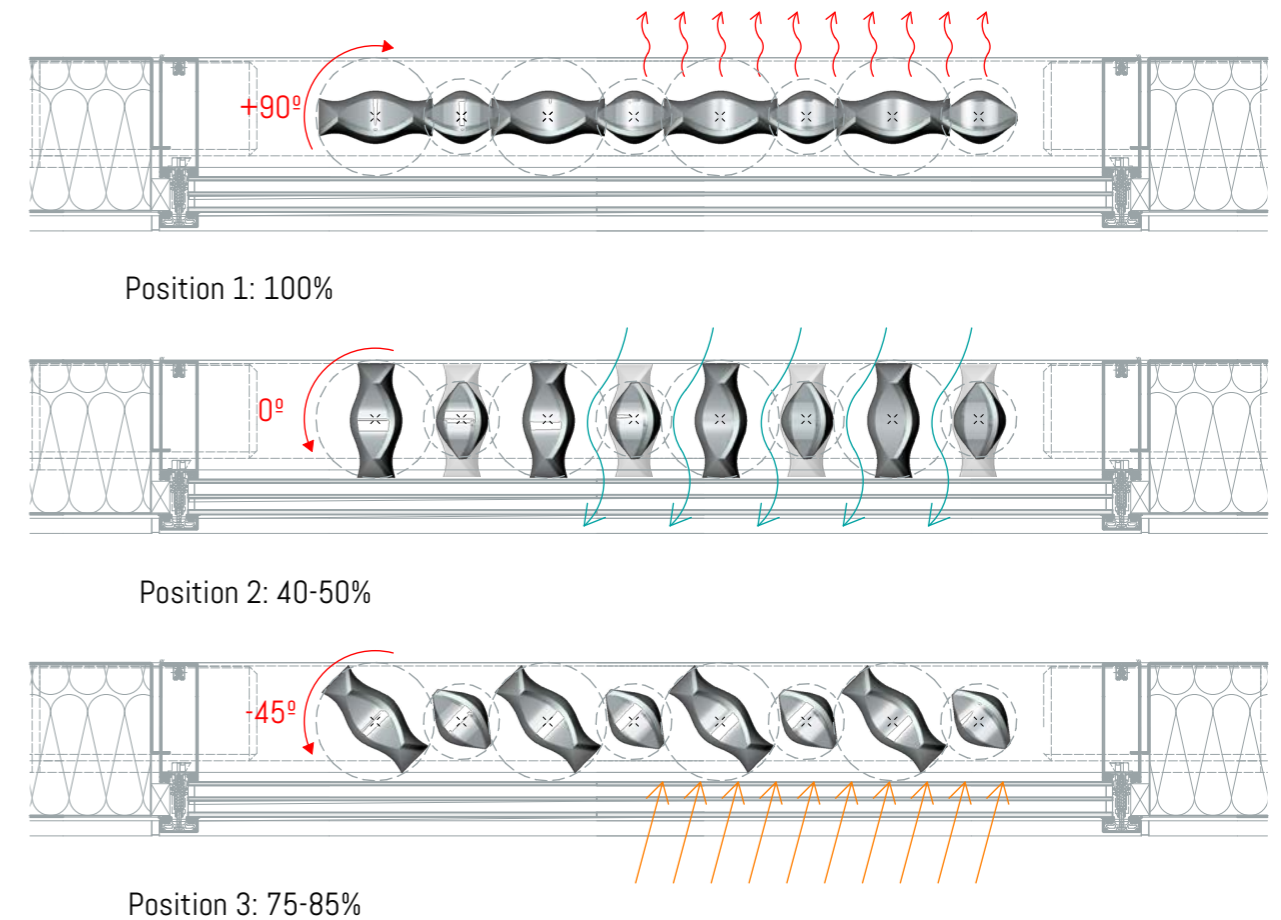
The 'cap' will be included in the bottom part will be placed at the end. The cap overlaps with the module. All the seems will (—) be watertight connected u laser welding combined with a coating at the joints. this way a transparant and colourless connection c created.



All the modules are double chambered (1.1 inner section), these two chambers allow for the phase change material and the aerogel, the chambers are filled from the top using the cap which is split in two. The top module is placed on the lower one by rotating it on top, the threat connects the two seperate elements creating one stiff column. In this way the cap has a double function, structural stiffness and the filling of the modules.

The element is designed in such a way that it can be integrated within the reveal of the window, in this way the element does not affect the space of the room. A linear guiding rail is introduced to fully open the system, illustrated in the detailed overview in Figure 1.118 on page 170. The different opening position are shown in the diagrammatic overview in Figure 1.116.

Figure 1.117
Diagrammatic principle of PCM panel design, scale 1:10 (By author)



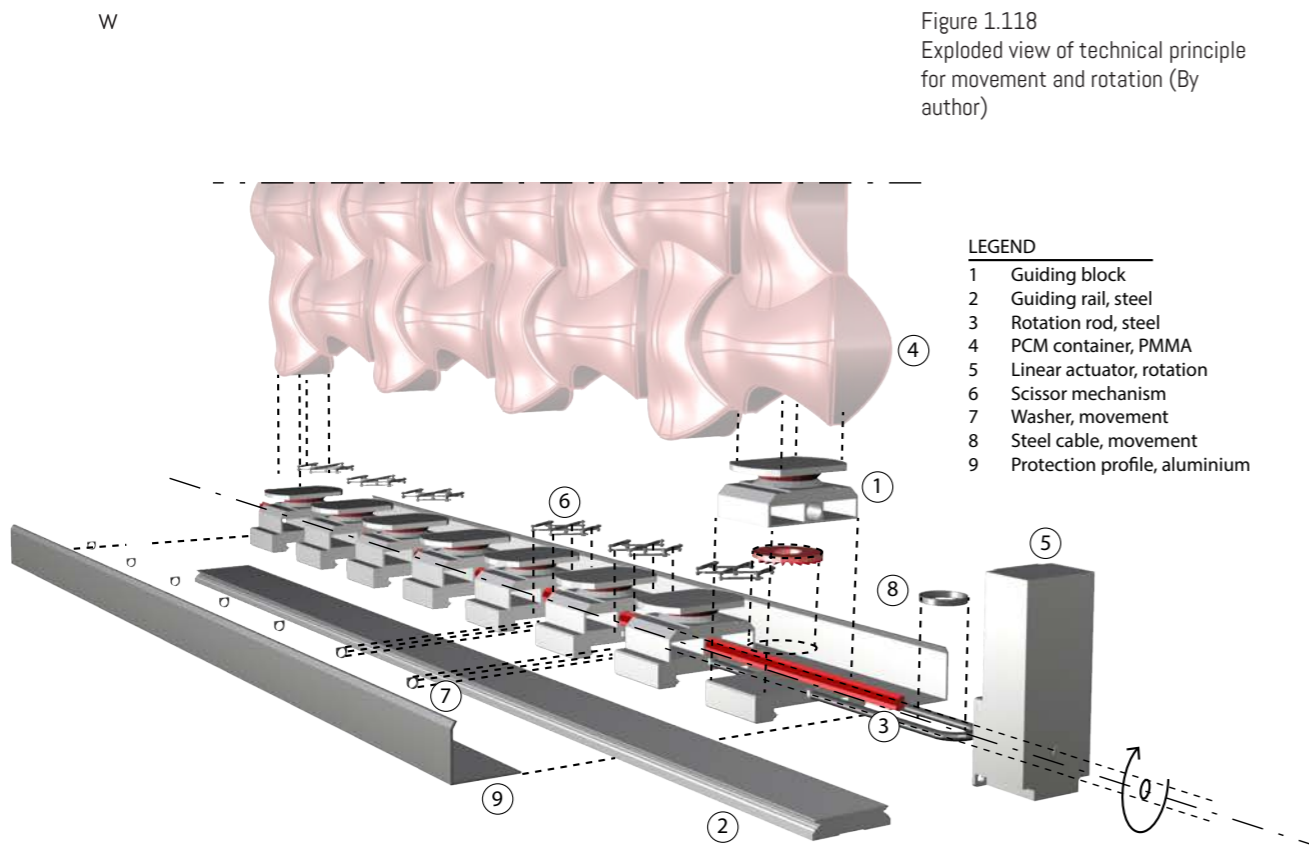
The PCM system, related to one window segment, is divided into eight separate containers to allow for a compact rotation within the reveal of the window frame. The number of elements and the size can be varied according to the application. The surface of the container is increased by creating a smooth and wavy surface on both the axes as seen on the previous page. When the panel is in the first position (Figure 1.117), the PCM is only on one side in direct contact with the adjacent air because the back is covered with insulation. In this position the PCM is in heating mode and releases the energy to the interior. When the system is rotated to the second position, the surface area in direct contact with the air flow is also increased, this increases the heat transfer between the two which is requested. The third position on the one hand allows for direct ventilation with the exterior and a view to the outside, on the other hand it absorbs as much solar radiation as possible. And the last position can be operated manually, in this position the PCM slats can be moved aside to give visible access to the exterior and to allow for maintenance (Figure 1.116). The difficult part is to allow both for rotation and for movement within the same axes, this same principle is integrated within a standard vertical blind system. The exploded illustration (Figure 1.118) shows the technical integration of the different parts in the bottom rail element, this element will be placed within the window frame. The guide block [1], situated on the guiding rail [2], moves over a steel rod [3]

which can be rotated. This steel rod is based on a star section to drive the small rotation wheel within the guiding block, in this way the box can still slide over the rod while allowing for rotation at the same time. A more detailed section is shown in the details in Section "7.64 Technical detail" on page 172. The PCM container [4] is fixed on top of the rotation block and rotates vertically, this rotation is motorized by the actuator [5] placed at the end of the steel rod.

A scissor mechanism [6] is placed between the guide blocks to keep the predefined distance between the separate blocks, several washers [7] are connected to the movement cable [8] at the front of each block. By rotating this cable the guiding blocks can be moved towards one side, when moving the other way around the blocks are brought back in position by the scissor mechanism.

The protection profile [9] covers the system up to protect the system from external factors. All the element integrated within this design are based on existing products, some additional changes are made to some elements to be suitable for this specific application. These changes are mainly based on the automated rotation parts within the guiding block. A more detailed elaboration on the technical implementation is shown in Section "7.64 Technical detail" on page 172.

Figure 1.118
Exploded view of technical principle for movement and rotation (By author)



An assumption is made for the costs of the different parts integrated in the system to define whether this design is actually cost-effective. These costs are based on references varying from a detailed price indication from product sellers to quick estimations from online product resellers for consumers. The latter gives a first estimation, however for large scale production the prices will differ. The detailed overview from all the costs are shown in "APPENDIX J" on page 207. It is seen that the cost of the system are relatively high due to the high PCM price, the price of the aerogel insulation and the linear guiding system Table 1.29. The guiding system is only needed for maintenance and can be omitted from the design if a more simple design is needed. The PCM and aerogel materials are relatively expensive, however a drop in the price is expected according to information from the producers and to literature. A more simple design can

reduce the price by creating a non-sliding system which can only rotate. The major prices for the materials estimation in "APPENDIX J" on page 207 are based on an large office of 350 m². The production prices are determined according to the CES analysis, here the material costs are subtracted from the production estimation, CES takes into account a standard value of €6.77/kg of material which does not relate to the exact material price. The results in Table 1.29 show that the PCM system is only beneficial when considering the comparison for new buildings, a lower capital cost (1.1) is obtained compared to the heat pump (2.1) and also a significantly lower operation cost is seen (1.2 and 2.2). For renovation investment the system is not beneficial considering the reduction in operation costs and the investment needed, however when installation equipment is needed a lower total cost of ownership is obtained compared to a heat-pump.

Table 1.29 Price estimation and comparison from the design of the PCM Trombe wall for a 60 m² office room

	INPUT		COST RESULTS	
	Description	Note	Value Unit	Value Unit
COMPARISON NEW BUILDING INVESTMENT	1.1 Capital costs: PCM panel (60 m ²)	required installation included	€9,143.79	€152.40 /m ²
	1.2 Operation costs: PCM panel	additional heatpump operation costs	€21.33 /year	€0.36 /m ² /year
COMPARISON RENOVATION INVESTMENT	2.1 Capital costs: Heatpump (60 m ²)	installation (10 kW) and boreholes costs	€10,390.00	€173.17 /m ²
	2.2 Operation costs: Heatpump	COP 3 (coefficient of performance)	€86.20 /year	€1.44 /m ² /year
COMPARISON RENOVATION INVESTMENT	3.1 Operation costs: PCM panel	additional boiler operation costs	€62.08 /year	€1.03 /m ² /year
	4.1 Operation costs: Boiler (HR 107)	97% boiler efficiency	€31.99 /year	€0.53 /m ² /year
	Compressioncooling	COP 1.5 (coefficient of performance)	€151.72 /year	€2.53 /m ² /year
	Total savings		€121.64 /year	€2.03 /m²/year
	Total payback time		50.69 years	
	Total payback time	after energy investment allowance	21.22 years	
	Total final profit (over 10 years)	The different project cost and investment cost for comparison new building investment	€1,960.60	€80.71 /m ² façade office
	Energy investment allowance	EIA Energylist code 210405 [W]	€3,584.99	€32.68 /m ² office

In the Netherlands the Energy-list and Environment-list 2019 (Energie lijst en Milieulijst 2019) defines several investment grants for sustainable enhancement techniques when improving the energy performance of office buildings and other business related buildings. These grants are defined in the Energy-investment Allowance (EIA) from the government of the Netherlands (RVO, 2019), for the year 2019 a budget of € 147 billion will be invested in sustainable techniques. This regulation on average creates a profit of 11% on energy efficient investments. Materials which are intended for the application to reduce the energy demand for heating or cooling of spaces and which are based on latent heat storage, with a minimum latent heat of fusion of 100 kJ/kg, will be subsidised by the government according to the EIA. The maximum investment for the deduction of latent heat storage material amounts € 10/kg of material, this is prescribed the EIA Energylist code 210405 [W] (RVO, 2019). This means that the price of the system can be reduced substantially which makes it even more interesting for investors, the price can be reduced by around € 3.585 which reduces the total payback time significantly (Table 1.29). It seems that the government is highly interested in the use of passive heating and cooling strategies to reduce the need for installation equipment of buildings and the related embodied energy. However within the calculation of this specific design case this will not be included to showcase the possibilities without the use of subsidies. For the application in the Netherlands, these investment allowances can reduce the cost of sustainable technologies significantly to make them beneficial for investors.

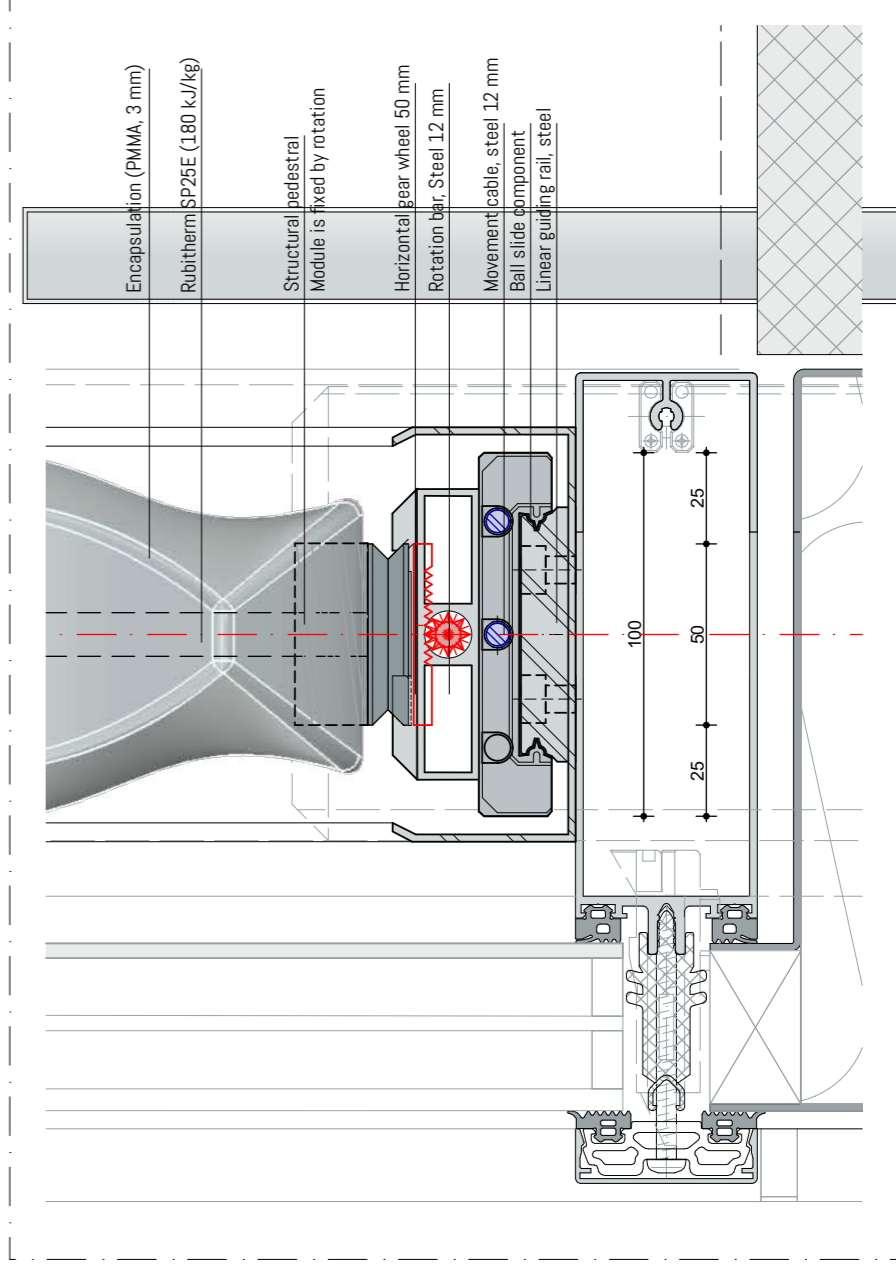
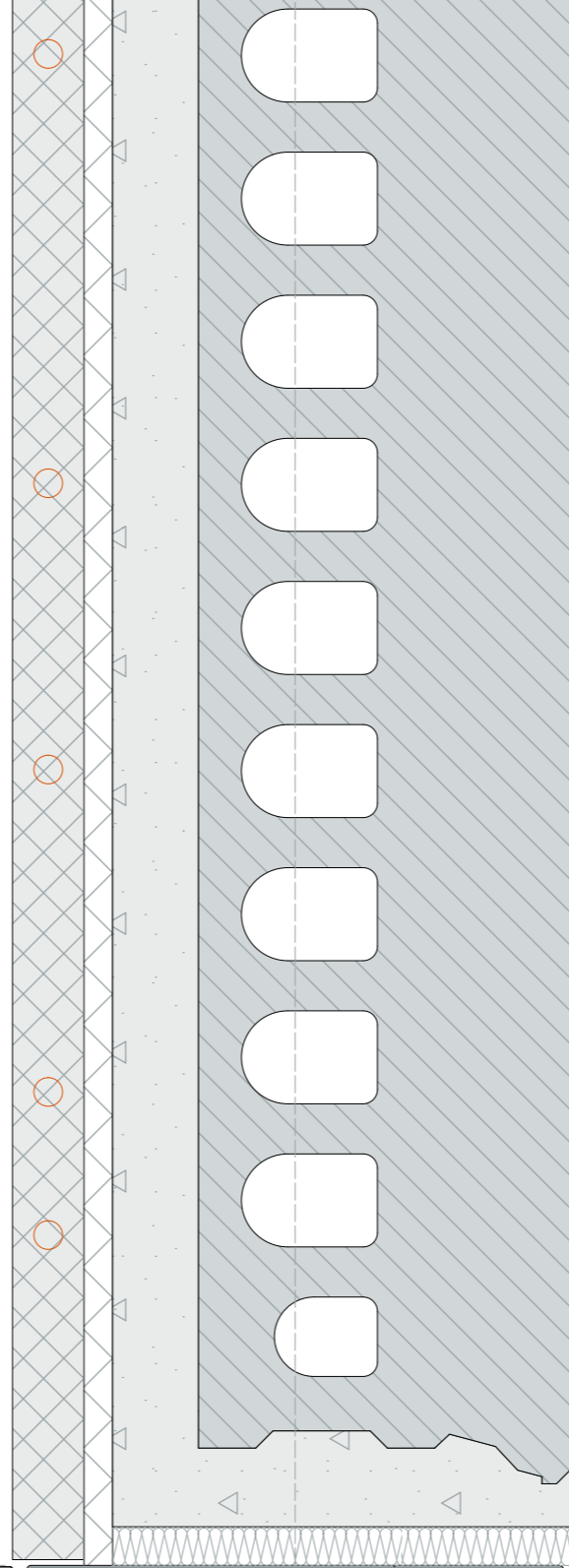
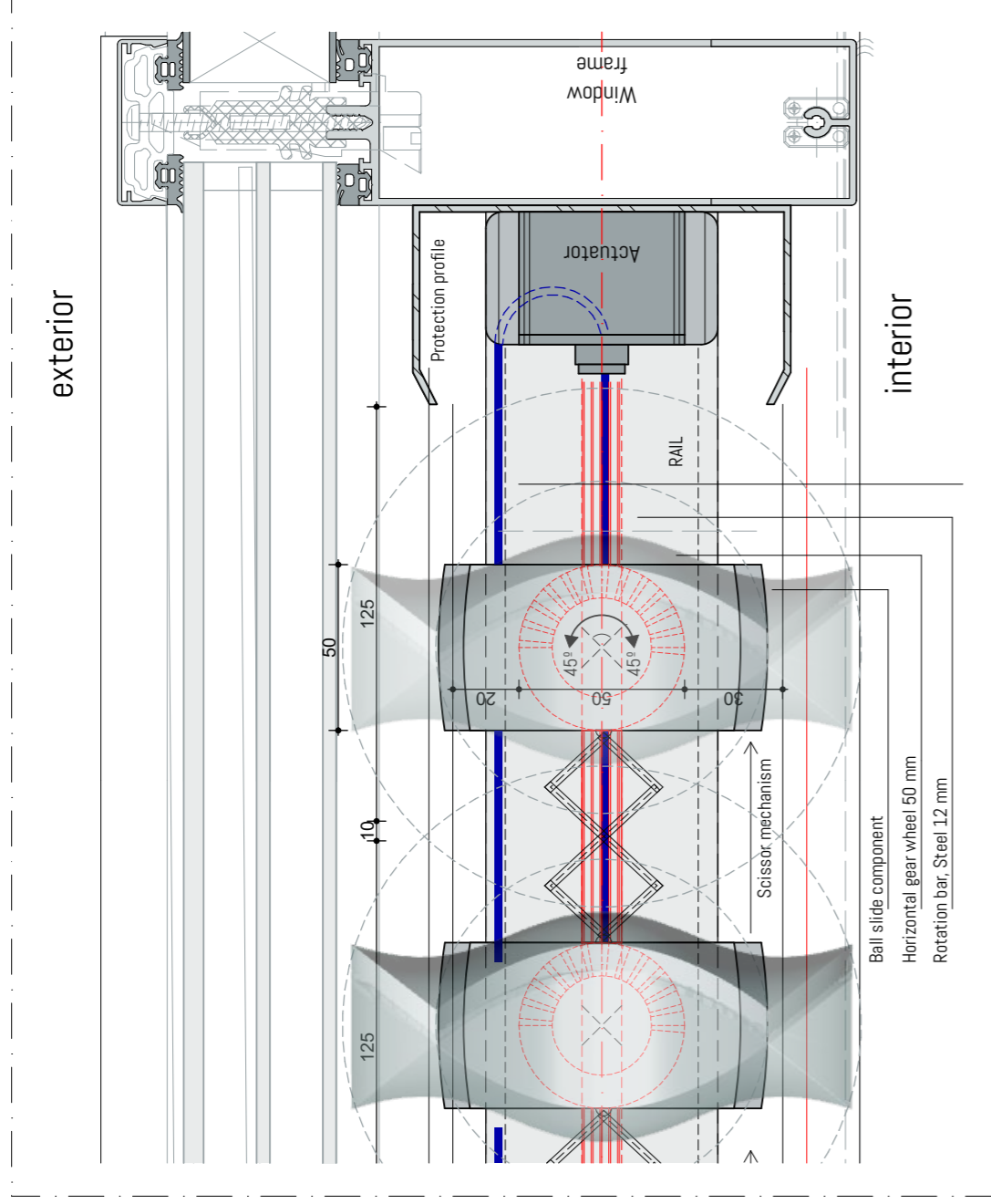
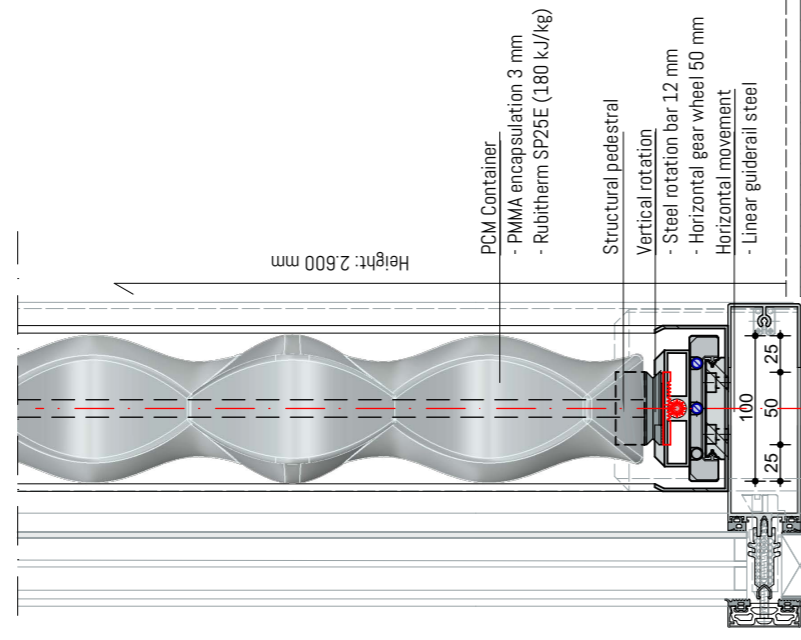
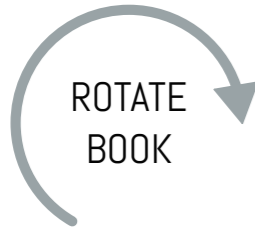


Figure 1.119
Illustration of configuration of the design
modules for integration within an office
typology (By author)



8. SYNTHESIS

Within the synthesis all the results from this research study are drawn together to point-out the contribution in designing with PCMs in the built environment. First, a general conclusion is shown on the main parts of this research study, after that some recommendations are given for possible future research topics and interesting directions. The discussion reflects on the research methodology and the different choices made during the process to indicate the value of the results from this study. Some limitations are shown according to the simulation methodology, the assumptions made within this study and the obtained results.

8.1 DISCUSSION

On the one hand this study includes the effect of each parameter on the yearly performance of the PCM, however on the other hand a drawback from this simulation and optimization method is that the actual influence of the shape of the product is neglected to reduce the simulation time needed. In this way, the performance of the system can turn out positive while in the real design the performance appears to be less due to negative effects from for instance shape on the heat transfer rate for fluid dynamics or the sun radiation. Within this study a broad focus is adopted, combining the impact of the PCM on energy performance and the cost-effectiveness, including the actual PCM costs and the installation equipment. Most of the studies from the literature analysis mainly focused on the detailed performance of the PCM regarding internal thermodynamics and air temperatures. With this wide view the overall impact and performance of the PCM on each season is deeply examined and the cost-effectiveness of this material is assessed. The actual cost-effectiveness, as stated in the main question, is depended on the elaboration of the final product. The application of the PCM itself seems cost-effective, however the design investment cost must not be exceeded.

For the cost-effective calculation now just one case is studied using a heat-pump installation for both heating and cooling, in this way the reduction in peak-loads for heating also takes into account the overall costs for the cooling installation. The results will differ from this case when a separate heating and cooling installation is accounted for, in this way only the costs for the heating installation are reduced. However, this relatively new adopted installation equipment has a high coefficient of performance, comparing this to more standard boiler installations the efficiency is much higher. Moreover, another important issue for the costs is the scale of production, the PCM price accounted for in this study (Rubitherm SPE25E€; 1,89 / kg) is based on a production scale of 10.000 kg, comparing this to the actual amount needed this price refers to an office space of 350 m². Increasing the application to large-scale production would also reduce the price significantly, small application in for instance single offices seems not be beneficial.

Within this study the PCM Trombe wall is optimized for one specific reference year according to the NEN5060-B2 (2008), when the PCM panel is implemented into a real design case the temperatures for these cases can vary a lot. When on extreme periods the actual temperature exceeds the temperature from this reference year also the peak loads within the room are higher. The installation equipment is based on the maximum peak loads for this reference year, this installation will therefore not be sufficient enough and comfort temperature may be exceeded. This makes the performance of the system unpredictable in comparison with mechanical auxiliary systems, this needs to be taken for granted by the user/owner of the building when integrating these type of passive solutions. The number of temperature exceeding days will be higher compared to a mechanical solutions. However, this is only the case for very few situations when these temperatures are actually surpassed. Additionally, the more save choice would always be the traditional implementation of mechanical devices compared to the more complex and unreliable use of passive solutions.

A huge benefit from this type of passive systems is the growing demand for sustainable and environmental friendly offices, the current corporate branding is based on sustainable strategies to be competitive with concurrence. This is the new business approach of corporate businesses, the reduction in installation equipment also reduces the impact on the environment.

8.2 CONCLUSION: FINAL

This research aimed to first identify the most important parameters to optimize a PCM trombe wall for year round application in an office building, located in a temperate climate, to then create an thermodynamically and cost-effectively optimized passive heating and cooling system. The main research question addressed within this study is: *"What is most cost-effective and thermodynamic optimized design for a passive trombe wall based on latent heat storage for year round application in an office building in Amsterdam, the Netherlands?"*

The information from the literature study showed the important requirements for designing with PCM within the built environment such as the important properties for each compound and the associated thermophysical limitations. The inclusion of PCM within a Trombe wall showed great potential due to an effective use of the solar energy available and the integration of different ventilation strategies. This is needed to cool or discharge the PCM Trombe wall efficiently, in this way the PCM can have a full charge and discharge cycle. A key factor for designing with PCM is the possibility for overheating of the material, this can lead to phase segregation which affects the long-term stability of the product. The maximum operation temperature of the salt-hydrate PCMs is around 45°C. Incongruent melting and internal convection are other important factors that affect the performance of the PCM, several techniques such as cascading or container rotation can be adopted to reduce these phenomenons. And lastly, when designing a trombe wall the south facade is mainly used to increase the efficiency, design strategies should be adopted to increase the transmittance of daylight and increase the view to the exterior.

Ten main enhancement techniques are adopted from the literature study, these techniques are directly related to the properties of the wall and the performance of the system. Some assumptions are made for this research study, the results needed for this study are based on yearly simulations, a simplified 2D simulation setup is required to reduce the overall simulation time. Some negative effects of shape on the convective heat transfer, the self-shading and the internal convection is not accounted for, this can reduce the efficiency of the system due to a bad design.

The enhancement techniques used within this study are first the increased layer thickness and the latent heat of fusion to improve the overall thermal capacity of the wall. The convective heat transfer, thermal conductivity, the trombe-wall to wall ratio and the increase surface area are introduced to assess the influence of the heat transfer rate on the performance of the wall the PCM Trombe wall. The melting temperature and the multi-layering strategy are used to define at what scale different melting temperatures affect the performance for each target season.

This actual simulation and optimization study is based on a quantitative and qualitative analysis on creating a cost-effective application and giving insight in the performance of various optimization parameters. It can be concluded that three important strategies significantly affect the total cost of ownership of the installation system, these are a combination of the reduction in the maximum power-load during the heating season, the yearly energy reduction and the price and volume of the PCM product. The results indicate that the most important factor is the reduction in power-load, this reduces the actual size and costs of the equipment needed to heat or cool the building. This reduction in cost can be used as investment for the realization of the PCM Trombe wall. The overall results showed some major differences in the performance of the wall for the different applications (heating, cooling, all-season). The thermal conduction, the cavity width and the panel area ratio showed no major influence on the performance in energy reduction.

However, these parameters did have a significant impact on the performance for the power-load reduction.

Four optimizations are done regarding the reduction in heating, cooling, all-season energy and the overall costs of the system. This study points out the main differences in the final design for each case. For heating the most optimal situation reduction showed that all heating needed (100%) can be realized by just the PCM Trombe wall. The PCM needs to be designed with a double function, on the one hand the insulation factor needs to be high. On the other hand, the PCM needs to absorb as much energy from the sun and all this energy needs to be released to the interior, so the full south facade is needed to accomplish this. For cooling up to 81.2% of the energy can be reduced compared to the benchmark study, this is realized by using a high convective heat transfer to release the heat quickly and a low TWR to allow for enough ventilation within the discharging mode. Lastly, for the all-season energy demand up to 81% can be reduced by optimizing the parameters. In all situations a high heat capacity of the PCM is required to allow for a higher density, this also increases the price of the PCM. The economic optimization showed for the most optimal design a total heating and cooling reduction of 75,3% can be realised by a standard quality PCM. This design [3321.5] also showed a significant reduction in the maximum heating and cooling power-load. This all combined gives a total investment space of over €7.755 for the PCM Trombe wall, by subtracting the PCM costs this results in an extra investment of €191.28/m² of panel. A higher reduction in energy and power-load gives an increase in the volume and quality of the PCM, which subsequently reduces the final investment space.

The results in the combined energy and power overview (Figure 1.114) show that the most important parameters for a cost-effective application are the thickness, the latent heat of fusion, the convective heat transfer, the use of multiple layers and the melting temperature of the PCM. These parameters have the highest impact on both the heating and cooling reduction, the price of the pcm and the heating power-load reduction.

Some major differences are observed between the simulation on the energy reduction and the cost-effective optimization. The results show that a higher section thickness does not add much to the performance on the indoor air temperature and the energy reduction. However, to reduce the peak-load effectively a higher volume is needed, this significantly reduces the total costs for the system. This indicates that, for this design location, a higher thickness is only needed for the winter situation to reduce both the overheating effect and the maximum power-loads.

For the design of the PCM Trombe wall some compromises need to be made to create one integrated design solution. Choosing different PCMs with different melting temperatures, thicknesses and different surface geometries would not be beneficial considering the performance improvement and the extra investment cost needed. Therefore the most dominant overall design solution is based on the most extreme environmental conditions, the optimization showed that a combination of a low overall energy demand and a low maximum power-load is obtained by a higher convective heat transfer and a higher melting temperature which is not for just the reduction in power-load. The results from the separate simulations and optimizations showed different results compared to this most optimal solution. So for designing with PCM the most important considerations are based on the most dominant external conditions. These quasi-optimal solutions for this design case, located in Amsterdam, The Netherlands contains the following parameters:

- A large section PCM thickness and volume (0.045 - 0.1 m);
- A high PCM melting temperature (25-26 °C);

- An increased convective heat transfer rate to increase the amount of heat released in the discharging mode (3.0 - 6.5 W/m².K);
- An increased surface area of the panel to increase the heat absorption rate specifically in summer situation, in this way the heat transfer is increased. In winter a smaller increase in heat transfer is wanted;
- A high insulation value by reducing the thermal conductivity, this reduces the peak-loads (0.1 - 0.5 W/m.K);
- A smaller trombe-wall to wall ratio during summer nights to increase the ventilation rate (40% - 50%);
- A higher trombe-wall to wall ratio during winter nights and days to increase the amount of heat absorbed and released to the interior and reduce the amount of heat lost to the exterior (75% - 100%)
- The use of multiple layers is dominated within the optimization results, also one layered systems are seen. These are lower in production costs which is needed considering the low impact of this variable. (1 layered)

The results indicate that the PCM Trombe wall targets both the cooling energy reduction and the maximum heating power-load reduction within one combined design solution. The main findings show that not only the indoor air temperature and the energy reduction are important for designing with PCMs, the reduction in peak-loads are as important. Of-course, the trends of the results are comparable due to the same target conditions, however some parameters showed more importance for different applications.

8.2.1 Future research directions

According to the results from this study some recommendations for future research directions have emerged, the results together with the simulation model from this study can be used for this work.

- This study focused mainly on the search to a quasi-optimal solution for yearly application in one specific climate, it can be interesting to search for the optimal solutions for different climate classifications and building typologies to create an overall design guideline for the implementation of PCMs in each region of the world. This to point-out the actual cost-effectiveness for each situation and the differences for each application.
- Besides this, the results are all based on a numerical study, no experiments are included to validate and verify the results. A new study could focus mainly on the experimental phase to show the effect of each parameter on the temperature distribution within the panel or the effect on the room air temperature.
- Another directions can be the geometrical effect on the actual cost-effectiveness considering the overall energy reduction, the peak-load reduction and the panel investment costs using for instance an Computational Fluid Dynamic (CFD) analysis together with an yearly analysis.
- Another interesting direction is the comparison of different application typologies, such as in the floor, the ceiling and in a trombe wall, to compare the differences in cost-effectiveness. Also taking into account the view to the outside and the daylight transmittance for energy usage of light within the room.

9. REFERENCES

- Abbassi, F., & Dehmani, L. (2015). Experimental and numerical study on thermal performance of an unvented Trombe wall associated with internal thermal fins. *Energy and buildings*, 105, 119–128.
- Alawadhi, E. M. (2012). Using phase change materials in window shutter to reduce the solar heat gain. *Energy and buildings*, 47, 421–429.
- Banggood. (2019, n.d.). Machifit 15st 600mm optische asgeleider Lagerhuizen Lineaire railssteunenset. Retrieved May 15, 2019, from banggood.com: https://www.banggood.com/nl/Machifit-15pcs-600mm-Optical-Axis-Guide-Bearing-Housings-Linear-Rail-Shaft-Support-Set-p-1392743.html?rmmds=search&cur_warehouse=CN
- Behbahani, P. M., Kazerouni, R. B., & Davar, H. (2014). Optimization Of Air Channel Geometry On Trombe Wall For Transmitting Excessive Heat. *Indian Journal of Fundamental and Applied Life Sciences*, 4, 877–889.
- Bland, A., Khzouz, M., Statheros, T., & Gkanas, E. I. (2017). PCMs for Residential Building Applications: A Short Review Focused on Disadvantages and Proposals for Future Development. *Buildings*, 7, Article 78.
- Bokel, R. (2017). *Building Physics Energy: Non-stationary room heat balances (lecture reader)*. Retrieved Januari 14, 2019, from brightspace.tudelft.nl: <https://brightspace.tudelft.nl/d21/le/content/49526/Home>
- Bony, J., & Citherlet, S. (2007). Numerical model and experimental validation of heat storage with phase change materials. *Energy and Buildings*, Volume 39, 1065–1072.
- Bourne, S., & Novoselac, A. (2015). Compact PCM-based thermal stores for shifting peak cooling loads. *BUILD SIMUL*, Volume 8 (6), 673–688.
- Bouwbesluit. (2018). Afdeling 5.1. Energiezuinigheid, nieuwbouw. Retrieved 12 20, 2018, from bouwbesluitonline.nl: <https://www.bouwbesluitonline.nl/Inhoud/docs/wet/bb2012/hfd5/afd5-1#art5.3>
- Brand, S. (1995). *How buildings learn: What happens after they're built*. London: The penguin group.
- Carli, M. D., Bernardi, A., Cultrera, M., Santa, G. D., Bella, A. D., Emmi, G., et al. (2018). A Database for Climatic Conditions around Europe for Promoting GSHP Solutions. *Geosciences*, 8, Article 71.

CAT. (2019, Februari). Heat Pumps. Retrieved April 04, 2019, from Centre for alternative technology: <https://www.cat.org.uk/info-resources/free-information-service/energy/heat-pumps/>

CBS. (2017, Januari 09). Average inflation 2016 lowest in nearly 30 years. Retrieved from CBS: <https://www.cbs.nl/en-gb/news/2017/01/average-inflation-2016-lowest-in-nearly-30-years>

CEN. (2007). NEN-EN 15251:2007 (en). Brussels: European committee for standardization.

CES Edupack. (2019). CES Edupack. Retrieved Februari 08, 2019, from grantadesign.com: <http://www.grantadesign.com/education/edupack/>

Climate Consultant 6.0. (2018, July 05). Climate Consultant Download Page. Retrieved November 18, 2018, from energy-design-tools.aud.ucla.edu: <http://www.energy-design-tools.aud.ucla.edu/climate-consultant/request-climate-consultant.php>

Climator. (2017). Product data sheets. Retrieved 12 03, 2018, from climator.com: <https://www.climator.com/en/pcm-climsel/product-data-sheets>

Conrad. (2019, n.d.). Buismotor e-ast ER1060-20 60. Retrieved May 17, 2019, from conrad.nl: https://www.conrad.nl/p/buismotor-e-ast-er1060-20-60-mm-45-kg-156-w-20-nm-1081358?WT.mc_id=gshop&gclid=Cj0KQCjwNmBRD0ARIsAJYs6o2g9pWnb-LatRKsrNRlbtXZSLdTvTTGoSc13HjRAZ5z6UYUyxwFy-BkaAgmLEALw_wcB&tid=933477491_48124233073_pla-457453266174_pla-1081358&WT.srch=1&vst=true&insert_kz=8j

Corasaniti, S., Manni, L., Russo, F., & Gori, F. (2017). Numerical simulation of modified Trombe-Michel Walls with exergy and energy analysis. *International Communications in Heat and Mass Transfer*, 88, 269–276.

Cupkova, D., & Azel, N. (2015). Mass Regimes: Geometric Actuation of Thermal Behavior. *international journal of architectural computing*, 13 (2), 169-193.

Cupkova, D., & Promopatum, P. (2017). Modulating Thermal Mass Behavior Through Surface Figuration. *ACADIA 2017: Disciplines & Disruption* (pp. 202-211). Cambridge: Massachusetts Institute of Technology.

Dabaieh, M., & Elbably, A. (2015). Ventilated Trombe wall as a passive solar heating and cooling retrofitting approach; a low-tech design for off-grid settlements in semi-arid climates. *Solar Energy*, 122, 820-833.

David, D., Kuznik, F., & Roux, J.-J. (2011). Numerical study of the influence of the convective heat transfer on the dynamical behaviour of a phase change material wall. *Applied Thermal Engineering*, 31, 3117e3124.

Designbuilder. (n.d., n.d.). Natural ventilation modelling. Retrieved from designbuilder.co.uk: https://designbuilder.co.uk/helpv1/Content/_Natural_ventilation_modelling.htm

Diaconu, B. M., & Cruceru, M. (2010). Novel concept of composite phase change material wall system for year-round thermal energy savings. *Energy and buildings*, 42, 1759–1772.

Duffie, J. A., & Beckman, W. A. (2013). Chapter 14 Building Heating: Passive and Hybrid Methods. In J. A. Duffie, & W. A. Beckman, *Solar Engineering of Thermal Processes* (pp. 544-574). Hoboken, New Jersey: John Wiley & Sons, Incorporated.

ECB. (2018, September 13). Monetary policy decisions . Retrieved from ECB.europa: <https://www.ecb.europa.eu/press/pr/date/2018/html/ecb.mp180913.en.html>

Ellis, B. (2007, Januari). Life Cycle Cost. Retrieved November 22, 2018, from researchgate.net: https://www.researchgate.net/publication/235636259_Life_Cycle_Cost

EngineeringToolBox. (2003). Metabolic Heat Gain from Persons. Retrieved 12 18, 2018, from engineeringtoolbox.com: https://www.engineeringtoolbox.com/metabolic-heat-persons-d_706.html

ESTECO SpA. (2018). modeFRONTIER User Guide. Trieste: Esteco SpA.

European Commission (EC). (2018, May). Energy efficiency - Buildings. Retrieved November 21, 2018, from europa.eu: <https://ec.europa.eu/energy/en/topics/energy-efficiency/buildings>

European Commission. (2018, November 28). The Commission calls for a climate neutral Europe by 2050.

Retrieved November 30, 2018, from europa.eu: http://europa.eu/rapid/press-release_IP-18-6543_en.htm

Eurostat. (2018, October 23). Electricity prices for non-household consumers. Retrieved from eurostat.ec.europa: https://ec.europa.eu/eurostat/statistics-explained/index.php/Electricity_price_statistics

Evolaa, G., Marletta, L., & Sicurella, F. (2014). Simulation of a ventilated cavity to enhance the effectiveness of PCM wallboards for summer thermal comfort in buildings. *Energy and buildings*, 17, 480–489 .

Ezra, M., Kozak, Y., Dubovsky, V., & Ziskind, G. (2016). Analysis and optimization of melting temperature span for a multiple-PCM latent heat thermal energy storage unit. *Applied Thermal Engineering*, 93, 315-329.

GlassX. (2017, October). Introducing GlassX – the world’s first Thermodynamic Glazing system. Retrieved December 03, 2018, from glassxpcm.com: <https://www.glassxpcm.com/how-glassx-works/>

Global-e-systems. (n.d.). Products. Retrieved December 12, 2018, from global-e-systems: <https://www.global-e-systems.com/en/products/>

Gracia, A. d., & Cabeza, L. (2015). Phase change materials and thermal energy storage for buildings. *Energy and Buildings*, Volume 103, 414-419.

Guarino, F., Dermardiros, V., Chen, Y., Raob, J., Athienitis, A., Celluraa, M., et al. (2015). PCM thermal energy storage in buildings: experimental study and applications. *Energy Procedia*, Volume 70, 219-228.

Halawa, E., & Saman, W. (2011). Thermal performance analysis of a phase change thermal storage unit for space heating. *Renewable Energy*, 36, 259-264.

Hasan, A. (1999). Optimizing insulation thickness for buildings using life cycle cost. *Applied energy*, 63, 115-124.

Herwig, H. (2016). What Exactly is the Nusselt Number in Convective Heat Transfer Problems and are There Alternatives? *Entropy*, 18, Article 198.

Hitachi, Ltd. (n.d., n.d.). Measurement of Optical Characteristic of Plastic by UH4150 Spectrophotometer. Retrieved from hitachi-hightech.com: https://www.hitachi-hightech.com/products/images/8414/uh4150_data1_e.pdf

Holman, J. P. (1986). *Heat Transfer*, sixth edition (Vol. 1). Singapore: Mc Graw-Hill Book Co.

Hu, Z., He, W., Jia, J., & Zhang, S. (2017). A review on the application of Trombe wall system in buildings. *Renewable and Sustainable Energy Reviews*, Volume 17, 976–987.

IGU. (2012). Natural Gas Conversion Guide. Retrieved Januari 29, 2019, from agnatural.pt: http://agnatural.pt/documentos/ver/natural-gas-conversion-guide_cb4f0ccd80ccaf88ca5ec336a38600867db5aaf1.pdf

Ismail, K., Henríquez, J., & Silva, T. d. (2003). A parametric study on ice formation inside a spherical capsule. *International Journal of Thermal Sciences*, 42, 881–887.

Itard, L. (2012). Energy in the Built Environment. In E. v. Bueren, H. v. Bohemen, L. Itard, & H. Visscher, *Sustainable Urban Environments: An Ecosystem Approach* (pp. 113-176). Dordrecht: Springer Science + Business Media B.V.

Izquierdo-Barrientos, M., Belmonte, J., Rodríguez-Sánchez, D., Molina, A., & Almendros-Ibáñez, J. (2012). A numerical study of external building walls containing phase change materials (PCM). *Applied Thermal Engineering*, 47, 73-85.

Jaber, S., & Ajib, S. (2011). Optimum design of Trombe wall system in mediterranean region. *Solar Energy*, 85, 1891–1898.

Jegadheeswaran, S., & Pohekar, S. (2009). Performance enhancement in latent heat thermal storage system: A review. *Renewable and Sustainable Energy Reviews*, Volume 13, 2225–2244.

Kalnæs, S., & Jelle, B. (2015). Phase change materials and products for building applications: A state-of-the-art review and future research opportunities. *Energy and Buildings*, Volume 94, 150-176.

Kamkari, B., Shokouhmand, H., & Bruno, F. (2014). Experimental investigation of the effect of inclination angle on convection-driven melting of phase change material in a rectangular enclosure. *International Journal of Heat and Mass Transfer* , 72, 186-200.

Kashyap, U., Das, K., & Debnath, B. K. (2018). Effect of surface modification of a rectangular vortex generator on heat transfer rate from a surface to fluid. *International Journal of Thermal Sciences* , 127, 61-78.

Khannaa, S., Reddy, K., & Mallick, T. K. (2018). Optimization of finned solar photovoltaic phase change material (finned pv pcm) system. *International Journal of Thermal Sciences* , 130, 313-322.

Kharbouch, Y., Mimet, A., Ganaoui, M. E., & Ouhaine, L. (2018). Thermal energy and economic analysis of a PCM-enhanced household envelope considering different climate zones in Morocco. *International Journal of Sustainable Energy* , 37, 515-532.

Khudhair, A., & Farid, M. (2004). A review on energy conservation in building applications with thermal storage by latent heat using phase change materials. *Energy Conversion and Management* , Volume 45 (2), 263-275.

Konuklu, Y., Ostry, M., Paksoy, H., & Charvat, P. (2015). Review on using microencapsulated phase change materials (PCM) in building applications. *Energy and Buildings* , 106, 134-155.

Koo, B., Lee, K., An, Y., & Lee, K. (2018). Solar Heat Gain Reduction of Ventilated Double Skin Windows without a Shading Device. *Sustainability* , 10, Article 64.

Kosny, J., Shukla, N., & Fallahi, A. (2013). Cost Analysis of Simple Phase Change Material-Enhanced Building Envelopes in Southern U.S. Climates. Cambridge: Fraunhofer CSE.

Kumar, A., & Buddhi, D. (2013). Thermal Management Components and their Significance in Energy Efficient/Green Buildings in India: A Review. *Journal of Pure and Applied Science & Technology* , Volume 3 (1), 60-73.

KWA Bedrijfsadviseurs B.V. (2011, Januari 19). Het elektrisch energieverbruik van koelinstallaties in Nederland en de aanwezige hoeveelheid koudemiddelen per sector. Retrieved Januari 29, 2019, from rvo.nl: https://www.rvo.nl/sites/default/files/Het_elektrisch_energieverbruik_van_koelinstallaties_in_nederland_januari_2011.pdf

Lara, C. C., Tenpierik, M., Spoel, W. v., & Turrin, M. (2015). Thermal Simulations: DoubleFace Project. 3TU Federatie.

Latouche, P.-É. (2007, April). The Kelbaugh House. Retrieved December 03, 2018, from cca.qc.ca: <https://www.cca.qc.ca/en/issues/19/the-planet-is-the-client/33741/the-kelbaugh-house>

Manzan, M., & Clarich, A. (2017). FAST energy and daylight optimization of an office with fixed and movable shading devices. *Building and Environment* , 113, 175-184.

Mathworks. (2019). Simulink: Simulation and Model Based Design. Retrieved Januari 16, 2019, from mathworks.com: <https://nl.mathworks.com/products/simulink.html>

Medici, P. (2017). 45 The Trombe Wall during the 1970s: technological device or architectural space? *Spool* , Volume 04, 45-60.

Melero, S., Morgado, I., Neila, F., & Acha, C. (2011). Passive evaporative cooling by porous ceramic elements integrated in a trombe wall. 27th International Conference on Passive and Low Energy Architecture. Volume 2, pp. 267-272. Louvain-la-Neuve: Presses Universitaires- de Louvain.

Menezes, A., Cripps, A., Buswell, R., Wright, J., & Bouchlaghem, D. (2014). Estimating the energy consumption and power demand of small power equipment in office buildings. *Energy and Buildings* , 75, 199-209.

Microtek. (2018, July 30). Micronal®. Retrieved December 05, 2018, from Microteklabs.com: <https://www.microteklabs.com/micronal>

Milián, Y., Gutiérrez, A., Grágeda, M., & Ushak, S. (2017). A review on encapsulation techniques for inorganic phase change materials and the influence on their thermophysical properties. *Renewable and Sustainable*

Energy Reviews , 73, 983-999.

Miyazaki, T., Akisawa, A., & Kashiwagi, T. (2006). The effects of solar chimneys on thermal load mitigation of office buildings under the Japanese climate. *Renewable Energy* , Volume 31, 987-1010.

Mosaffa, A., Farshi, L. G., Ferreira, C. I., & Rosen, M. (2014). Energy and exergy evaluation of a multiple-PCM thermal storage unit for free cooling applications. *Renewable Energy* , 68, 452-458.

NEN. (2008). Hygrothermal performance of buildings - Climatic reference data. Delft: Nederlands Normalisatie-instituut.

Nguyen, A., Reiter, S., & Rigo, P. (2014). A review on simulation-based optimization methods applied to building performance analysis. *Applied Energy* , 113, 1043-1058.

Oeffelen, E. H.-v., Spiekman, M., & Bulavskaya, T. (2013). Energielabels en het gemeten energiegebruik van utiliteitsgebouwen. Delft: TNO.

Pomianowski, M., Heiselberg, P., & Zhang, Y. (2013). Review of thermal energy storage technologies based on PCM application in buildings. *Energy and Buildings* , 67, 56-69.

PureTemp. (2018). PCM products. Retrieved December 05, 2018, from puretemp.com: <https://store.puretemp.com/#/puretemp>

Qureshi, W., Nair, N., & Farid, M. (2011). Impact of energy storage in buildings on electricity demand side management. *Energy Conversion and Management* , Volume 52, 2110-2120.

Rabani, M., Kalantar, V., Dehghan, A., & FaghihSchool, A. (2015). Empirical investigation of the cooling performance of a new designed Trombe wall in combination with solar chimney and water spraying system. *Energy and Building* , Volume 102, 45-57.

Riffat, S., Mempo, B., & Fang, W. (2013). Phase change material developments: a review. *International Journal of Ambient Energy* , Volume 36 (3), 102-115.

Rijksoverheid. (2018, December 21). Kamerbrief over aanbidding ontwerp-Klimaatakkoord . Retrieved Januari 04, 2019, from rijksoverheid.nl: <https://www.rijksoverheid.nl/onderwerpen/klimaatverandering/documenten/kamerstukken/2018/12/21/kamerbrief-over-aanbidding-ontwerp-klimaatakkoord>

RS Components. (2019, n.d.). SKF Linear Guide Carriage LLTHZ 15 S6, LLTHZ . Retrieved May 15, 2019, from rs-online.com: <https://nl.rs-online.com/web/p/linear-guides-guide-blocks-carriages/1849763/>

Rubitherm. (2018). Macroencapsulation - Cooling accumulators. Retrieved 12 03, 2018, from rubitherm.eu: <https://www.rubitherm.eu/en/index.php/productcategory/makroverkaspelung-kuehlakkus>

Rubitherm. (2019). PCM RT-LINE: Wide-ranging organic PCM for your application. Retrieved Januari 28, 2019, from rubitherm.eu: <https://www.rubitherm.eu/en/index.php/productcategory/organische-pcm-rt>

RVO. (2019, n.d.). Energielijst en milieulijst 2019. Retrieved 05 17, 2019, from rvo.nl: <https://www.rvo.nl/subsidies-regelingen/milieulijst-en-energielijst/huidig-jaar/2019>

RVO. (2018). Energieprijzen. Retrieved Januari 29, 2019, from energiecijfers.databank.nl: <https://energiecijfers.databank.nl/dashboard/Energieprijzen>

RVO. (2019, May 10). Faseovergangsmateriaal [W]. Retrieved May 17, 2019, from rvo.nl: <https://www.rvo.nl/subsidies-regelingen/milieulijst-en-energielijst/eia/faseovergangsmateriaal-w-0>

S3i Group. (2019, n.d.). 7x7 Stainless Steel Wire Rope . Retrieved May 15, 2019, from s3i.co.uk: <https://www.s3i.co.uk/7x7.php>

Saadatian, O., Sopian, K., Lim, C., Asim, N., & Sulaiman, M. (2012). Trombe walls: A review of opportunities and challenges in research and development. *Renewable and Sustainable Energy Reviews* , Volume 16, 6340-6351.

Saadatian, Sulaiman, Asim, & Sopian. (2012). Trombe walls: A review of opportunities and challenges in research and development . *Renewable and Sustainable Energy Reviews* , Volume 16 (8), 6340-6351.

Salunkhe, P., & Shembekar, P. (2012). A review on effect of phase change material encapsulation on the thermal performance of a system. *Renewable and Sustainable Energy Reviews*, Volume 16 (8), 5603–5616.

Sarbu, I., & Sebarchievici, C. (2018). A Comprehensive Review of Thermal Energy Storage. *Sustainability*, Volume 10 (191).

Sargent, R. G. (2011). Verification and validation of simulation models. *Proceedings of the 2011 Winter Simulation Conference* (pp. 183-198). Baltimore, USA: IEEE Xplore.

Schlesinger, Crosbie, Gagne, Innis, Lalwani, Loch, et al. (1979). Terminology for model credibility. *Simulation*, 32 (3), 103-104.

Seeniraj, R., & Narasimhan, N. L. (2008). Performance enhancement of a solar dynamic LHTS module having both fins and multiple PCMs. *Solar Energy*, 82, 535-542.

Shen, Lassue, Zalewski, & Huang. (2007). Numerical Study of Classical and Composite Solar Walls by TRNSYS. *Journal of Thermal Science*, Volume 16 (1), 46–55.

Sipma, J. (2016, Januari 18). Nieuwe benchmark energieverbruik utiliteitsgebouwen en industriële sectoren. Retrieved Januari 29, 2019, from [energievastgoed.nl: http://www.energievastgoed.nl/wp-content/uploads/downloads/2016/01/nieuwe_benchmark_energieverbruik_utiliteit_sipma.pdf](http://www.energievastgoed.nl/wp-content/uploads/downloads/2016/01/nieuwe_benchmark_energieverbruik_utiliteit_sipma.pdf)

Souayfane, F., Fardoun, F., & Biwoleb, P. (2016). Phase change materials (PCM) for cooling applications in buildings: A review. *Energy and Buildings*, 129, 396–431.

Spoel, W. v. (2017). “Playing with heat balances” An introduction to numerical modelling of heat transfer problems [Lecture notes]. Delft: Delft University of Technology.

Srikanth, R., Nemani, P., & Balaji, C. (2015). Multi-objective geometric optimization of a PCM based matrix type composite heat sink. *Applied Energy*, Volume 156, 703–714.

Straube, J. (2011, December 12). BSD-011: Thermal Control in Buildings. Retrieved November 24, 2018, from [buildingscience.com: https://buildingscience.com/file/5734/download?token=p4gsosRD](https://buildingscience.com/file/5734/download?token=p4gsosRD)

Stritih, U. (2004). An experimental study of enhanced heat transfer in rectangular PCM thermal storage. *International Journal of Heat and Mass Transfer*, 47, 2841–2847.

Sun, W., Ji, J., Luo, C., & He, W. (2011). Performance of PV-Trombe wall in winter correlated with south façade design. *Applied Energy*, Volume 88 (1), 224-231.

Sun, Y., Wang, S., Xiao, F., & Gao, D. (2013). Peak load shifting control using different cold thermal energy storage facilities in commercial buildings: A review. *Energy Conversion and Management*, 71, 101–114.

Tenpierik, M., Watez, Y., Turrin, M., Cosmatu, T., & Tsafou, S. (2018). Double Face 2.0: A lightweight, adjustable, translucent Trombe wall. *Journal of Architecture and the Built Environment (online)*, 5 (2).

Torcellini, P., & Pless, S. (2004). *Trombe Walls in Low-Energy Buildings: Practical Experiences*. Denver: National Renewable Energy Laboratory.

Unen, J. v. (2018). *The Energy and Comfort Performance of a Lightweight Translucent Adaptable Trombe Wall in Different Buildings and Climates*. Delft University of Technology. Delft: Delft University of Technology.

Uysal, & Tung. (1991). Passive Solar Heating of Buildings Using a Fluidized Bed Plus Trombe Wall System. *Applied Energy*, Volume 38 (3), 199-213.

Veen, R. v., & Hakvoort, R. (2016). The electricity balancing market: Exploring the design challenge. *Utilities Policy*, Volume 43, 186-194.

Veerappan, M., Kalaiselvam, S., Iniyan, S., & Goic, R. (2009). Phase change characteristic study of spherical PCMs in solar energy storage. *Solar Energy*, 83, 1245–1252.

Wang, J., Chen, G., & Jiang, H. (1999). Theoretical Study On A Novel Phase Change Process. *INTERNATIONAL JOURNAL OF ENERGY RESEARCH*, 23, 287—294.

Wang, Q., & Zhao, C. (2015). Parametric investigations of using a PCM curtain for energy efficient buildings. *Energy and buildings*, 94, 33–42.

Wang, Tian, & Ding. (2013). Investigation on the influencing factors of energy consumption and thermal comfort for a passive solar house with water thermal storage wall. *Energy and Buildings*, Volume 64 (September), 218–223.

Watez, Y., Cosmatu, T., Tenpierik, M., Turrin, M., & Heinzelmann, F. (2017). Renewed Trombe wall passively reduces energy consumption. *Design to Thrive: Proceedings of the 33rd PLEA International Conference* (pp. 4405-4412). Edinburgh: Network for Comfort and Energy Use in Buildings (NCEUB).

Webb, B. W., & Viskanta, R. (1986). Natural-convection-dominated melting heat transfer in an inclined rectangular enclosure. *Int. J. Heat Mass Transfer*, 29, 183-192.

Weinlaeder, H., Koerner, W., & Heidenfelder, M. (2011). Monitoring results of an interior sun protection system with integrated latent heat storage. *Energy and buildings*, 43, 2468–2475.

Wit, K. d. (2018, February 1). Number of square meters of office space per employee. Retrieved December 18, 2018, from [flexas.com: https://www.flexas.com/be-en/blog/number-of-square-meters-of-office-space-per-employee](https://www.flexas.com/be-en/blog/number-of-square-meters-of-office-space-per-employee)

Zamora, B., & Kaiser, A. S. (2009). Thermal and dynamic optimization of the convective flow in Trombe Wall shaped channels by numerical investigation. *Heat Mass Transfer*, 45, 1393–1407.

Zhang, X., Li, X., Zhou, Y., Hai, C., Shen, Y., Ren, X., et al. (2018). Enhanced thermal conductivity in a hydrated salt PCM system with reduced graphene oxide aqueous dispersion. *RSC Advances*, 1022-1029.

Zhang, Y., Chen, Z., Wang, Q., & Wu, Q. (1993). Melting in an Enclosure with Discrete Heating at a Constant Rate. *Experimental Thermal and Fluid Science*, 6, 196-201.

Zivkovic, B., & Fujii, I. (2001). An Analysis Of Isothermal Phase Change Of Phase Change Material Within Rectangular And Cylindrical Containers. *Solar Energy*, 70, 51–61.

Zukowski, M. (2007). Experimental study of short term thermal energy storage unit based on enclosed phase change material in polyethylene film bag. *Energy Conversion and Management*, 48, 166–173.

APPENDICES

APPENDIX A

Indoor design temperatures for buildings with HVAC: NEN-15251:2007 (E)

Table A.2 — Examples of recommended design values of the indoor temperature for design of buildings and HVAC systems

Type of building/ space	Category	Operative temperature °C	
		Minimum for heating (winter season), ~ 1,0 clo	Maximum for cooling (summer season), ~ 0,5 clo
Residential buildings: living spaces (bed rooms, drawing room, kitchen etc) Sedentary ~ 1,2 met	I	21,0	25,5
	II	20,0	26,0
	III	18,0	27,0
Residential buildings: other spaces: storages, halls, etc) Standing-walking ~ 1,6 met	I	18,0	
	II	16,0	
	III	14,0	
Single office (cellular office) Sedentary ~ 1,2 met	I	21,0	25,5
	II	20,0	26,0
	III	19,0	27,0
Landscaped office (open plan office) Sedentary ~ 1,2 met	I	21,0	25,5
	II	20,0	26,0
	III	19,0	27,0
Conference room Sedentary ~ 1,2 met	I	21,0	25,5
	II	20,0	26,0
	III	19,0	27,0
Auditorium Sedentary ~ 1,2 met	I	21,0	25,5
	II	20,0	26,0
	III	19,0	27,0
Cafeteria/Restaurant Sedentary ~ 1,2 met	I	21,0	25,5
	II	20,0	26,0
	III	19,0	27,0
Classroom Sedentary ~ 1,2 met	I	21,0	25,0
	II	20,0	26,0
	III	19,0	27,0
Kindergarten Standing/walking ~ 1,4 met	I	19,0	24,5
	II	17,5	25,5
	III	16,5	26,0
Department store Standing-walking ~ 1,6 met	I	17,5	24,0
	II	16,0	25,0
	III	15,0	26,0

Table A.1 — Examples of recommended categories for design of mechanical heated and cooled buildings

Category	Thermal state of the body as a whole	
	PPD %	Predicted Mean Vote
I	< 6	-0,2 < PMV < + 0,2
II	< 10	-0,5 < PMV < + 0,5
III	< 15	-0,7 < PMV < + 0,7
IV	> 15	PMV < -0,7; or +0,7 < PMV

A.3 Recommended indoor temperatures for energy calculations

Table A.3 — Temperature ranges for hourly calculation of cooling and heating energy in three categories of indoor environment

Type of building or space	Category	Temperature range for heating, °C	Temperature range for cooling, °C
		Clothing ~ 1,0 clo	Clothing ~ 0,5 clo
Residential buildings, living spaces (bed room's living rooms etc.) Sedentary activity ~1,2 met	I	21,0 - 25,0	23,5 - 25,5
	II	20,0-25,0	23,0 - 26,0
	III	18,0- 25,0	22,0 - 27,0
Residential buildings, other spaces (kitchens, storages etc.) Standing-walking activity ~1,5 met	I	18,0-25,0	
	II	16,0-25,0	
	III	14,0-25,0	
Offices and spaces with similar activity (single offices, open plan offices, conference rooms, auditorium, cafeteria, restaurants, class rooms, Sedentary activity ~1,2 met	I	21,0 – 23,0	23,5 - 25,5
	II	20,0 – 24,0	23,0 - 26,0
	III	19,0 – 25,0	22,0 - 27,0
Kindergarten Standing-walking activity ~1,4 met	I	19,0 – 21,0	22,5 - 24,5
	II	17,5 – 22,5	21,5 – 25,5
	III	16,5 – 23,5	21,0 - 26,0
Department store Standing-walking activity ~1,6 met	I	17,5 – 20,5	22,0 - 24,0
	II	16,0 – 22,0	21,0– 25,0
	III	15,0 – 23,0	20,0 - 26,0

APPENDIX B

Types of PCM's integrated into walls

Table 1. Thermal properties of paraffin suitable for building walls

PCM	Melting Temperature (°C)	Heat of fusion (kJ/kg)	Thermal conductivity (w/m·k)	Density (kg/m³)	References
n-Heptadecane	19	240	0.21		[9]
Paraffin C17	21.7	213		817(liquid)754(solid)	[10]
Paraffin C13-C24	22-24	189	0.21(liquid)	760(liquid)900(solid)	[11-13]
Micronalr DS5001	26	245			[14]
Paraffin: RT-27	28	179	0.2	800	[15]
Paraffin RT-18	15-19	134	0.2	756	[16]
Paraffin C18	28	244	0.148(liquid)		[13,17]
n-octadecane	28	179	0.2	750(liquid)870(solid)	[18]

Table 2. Thermal properties of fatty acids suitable for building walls

PCM	Melting Temperature (°C)	Heat of fusion (kJ/kg)	Thermal conductivity (w/m·k)	Density (kg/m³)	References
Capric acid	30.2	142.7	0.2(liquid)0.12(solid)	815(liquid)752(solid)	[19]
CA and 1-dodecanol (CADE)	26.5	126.9	0.2 (liquid)0.12(solid)	817(liquid)754(solid)	[19]
Capric acid and palmitic acid	26.2	177	2.2	784	[20]
Capric acid	30	142.7		815(liquid)752(solid)	[21]
CA and 1-dodecanol (CADE)	27	126.9		817(liquid)754(solid)	[22]
MeP+ MeS	23-26.5	180			[23]
Butyl Stearate-Palmitate	17-20	137.8			[24]
Eutectic capric-myristic	21.7	155			[25]
Eutectic capric-stearic	24.7	179			[26]
Non-eutectic capric- lauric	19.2-20.3	144-150			[27]
Glycerin	17.9	198.7			[10]

Table 3 Thermal properties of hydrated salts suitable for building walls

PCM	Melting Temperature (°C)	Heat of fusion (kJ/kg)	Thermal conductivity (w/m·k)	Density (kg/m³)	References
Hydrated salt	29	175	1.0	1490	[28]
CaCl2·6H2O	29	187.49	0.54(liquid)1.09(solid)	560(liquid)1800(solid)	[29]
Mn(NO3)2·6H2O+MnCl2·4H2O	27	125.9	0.6	1700	[30]
hydrated salts [water+CaCl2+ KCl + additives]					[31]
CaCl2·6H2O	29.9	187	0.53(liquid)1.09(solid)	1710(liquid)1530(solid)	[32]
Hydrated salt	31.4	149.9			[33]
Hydrated salt	25-34	140			[34]
SP25A8 hydrate salt	26	180	0.6	1380	[15]
sodium sulfate decahydrate	32.5	180	0.6	1600	[35]
Eutectic salt	32	216			[36]
Sodium thiosulfate pentahydrate	40-48	210			[37]
S27	27	190	0.48(liquid)0.79(solid)		[38]
L30	30	270	1.02(liquid)0.56(solid)		[38]

APPENDIX C

PCM price indication obtained from private contact



Rubitherm Technologies GmbH
Imhoffweg 6
12307 Berlin
www.rubitherm.com
Tel: +49 30 71 09 622-0
Fax: +49 30 71 09 622-22
OFFER

TU Delft
Kees Jan Hendriks
Postbus 5024
2600 GA Delft
NIEDERLANDE

Number : 20180000687
Date : 18.12.2018
Customer : 20068
VAT-ID : NL 001569569B01

Pos.	Part-ID / Description	Quantity	U-Price	UQ	Ex-Price	S
We thank you for your interest in Rubitherm products and can offer as follows:						
1	16010015 RUBITHERM RT 15 HS-code: 27129031	500 kg	6,02		3.010,00	1
2	16010018 RUBITHERM RT 18 HS-code: 27129031	500 kg	6,15		3.075,00	1
3	16010020 RUBITHERM RT 21 HS-code: 27129031	500 kg	6,41		3.205,00	1
4	16010025 RUBITHERM RT 25 HS-code: 27122090	500 kg	6,63		3.315,00	1
5	16010031 RUBITHERM RT 31 HS-code: 27122010	500 kg	6,62		3.310,00	1
6	16010018 HC RUBITHERM RT 18 HC HS-code: 29011000	500 kg	10,18		5.090,00	1
7	16010021 HC RUBITHERM RT21 HC	500 kg	11,83		5.915,00	1
8	16010028 HC RUBITHERM RT28 HC HS-code: 29011000	500 kg	10,18		5.090,00	1
9	16060015 RUBITHERM SP15 HS Code: 29152900	500 kg	3,48		1.740,00	1
10	16060021 RUBITHERM SP21E HS-code: 28272000	500 kg	3,44		1.720,00	1
11	16060024 RUBITHERM SP24E	500 kg	3,31		1.655,00	1
12	16060025 RUBITHERM SP25E HS-code: 28272000	500 kg	3,19		1.595,00	1
13	16060026 RUBITHERM SP26E	500 kg	3,18		1.590,00	1
14	16060029 RUBITHERM SP 29Eu HS-code: 28272000	500 kg	3,28		1.640,00	1
amount carried forward			EUR		41.950,00	

Pos.	Part-ID/ Description	Quantity	U-Price	UQ	Ex-Price	S
					41.950,00	
15	16060031 RUBITHERM SP31 HS-code: 29152900	500 Kg	4,22		2.110,00	1
16	16070026 accumulator R1 (170x85x25) filled with RT or SP	1 St	5,95		5,95	1
17	16070026 accumulator R1 (170x85x25) filled with RT HC	1 St	10,95		10,95	1
18	16070027 accumulator R2 (210x130x25) filled with RT or SP	1 St	10,95		10,95	1
19	16070027 accumulator R2 (210x130x25) filled with RT HC	1 St	15,95		15,95	1
20	16070028 accumulator R3 (320x290x25mm) filled with RT or SP	1 St	15,95		15,95	1
21	16070028 accumulator R3 (320x290x25mm) filled with RT HC	1 St	25,95		25,95	1
22	16070211 aluminium compound bag filled with: max 1Kg RT/SP (max. size 34x34 cm)	1 St	15,00		15,00	1
23	16070210 polymer bag (max. size 130x290mm)	1 St	15,00		15,00	1

The prices are valid till 21st December 2018.

By ordering our material you declare to accept and be bound by the conditions stated below.

Orders with a product value <150,00EUR carry a 42,00EUR minimum order surcharge

Delivery terms: ex works Germany, Customer takes care of the transport.

amount carried forward EUR 44.175,70

Pos.	Part-ID/ Description	Quantity	U-Price	UQ	Ex-Price	S
					44.175,70	

**We've moved! Since April 4th, 2018 we are located at our new company adress:
 Rubitherm Technologies GmbH, Imhoffweg 6, 12307 Berlin.**

Our VAT-ID: DE 230027919

Netto VAT.1	VAT	%	Netto VAT. 2	VAT	%	Netto VAT. 0	Total Amount
44.175,70						EUR	44.175,70

30 Tage netto

Rubitherm Technologies GmbH, Imhoffweg 6, 12307 Berlin
 CEO: Thomas Braun, Lutz Klinkner
 Comm. Reg no.: Berlin-Charlottenburg, HRB 86322 B

Hypo-Vereinsbank, acc. No.: 572 64 17, bank code: 700 202 70
 IBAN: DE12 7002 0270 0005 7264 17 SWIFT: HYVEDEMMXXX
 VAT ID: DE 230 027 919

APPENDIX D

Overview showing the properties of the different PCM types available on the market

PCM	Type	Supplier (if known)	T _{melting} [C]	T _{max} [C]	IMPORTANT PROPERTIES										
					Density [kg/m ³]	Latent heat of fusion [kJ/kg]	Specific heat [kJ/kg.K]	Thermal conductivity [W/m.K]	Heat Capacity [kJ/m ² .K]	Flammability	Price [€/kg]	Price [€/dm ³]	Price [€/KJ]	Special notes	Reference
SP21E	Inorganic	Rubitherm GmbH	21	45	1450	170	2	0.6	2900	no	€2,14	€3,10	€1,07	mail contact	www.rubitherm.de
SP24E	Inorganic	Rubitherm GmbH	24	45	1450	180	2	0.6	2900	no	€2,01	€2,91	€1,01	mail contact	www.rubitherm.de
SP25E	Inorganic	Rubitherm GmbH	25	45	1450	180	2	0.6	2900	no	€1,89	€2,74	€0,95	mail contact	www.rubitherm.de
SP26E	Inorganic	Rubitherm GmbH	26	45	1450	180	2	0.6	2900	no	€1,88	€2,73	€0,94	mail contact	www.rubitherm.de
RT 21	Organic	Rubitherm GmbH	21	40	825	160	2	0.2	1650	low	€4,48	€3,70	€2,24	mail contact	www.rubitherm.de
RT 21 HC	Organic	Rubitherm GmbH	21	45	730	190	2	0.2	1460	low	€9,32	€6,80	€4,66	mail contact	www.rubitherm.de
RT 22 HC	Organic	Rubitherm GmbH	22	40	825	190	2	0.2	1650	low	€9,32	€7,69	€4,66	mail contact	www.rubitherm.de
RT 24	Organic	Rubitherm GmbH	24	55	825	160	2	0.2	1650	low	€4,67	€3,85	€2,34	mail contact	www.rubitherm.de
RT 25	Organic	Rubitherm GmbH	25	60	825	170	2	0.2	1650	low	€4,67	€3,85	€2,34	mail contact	www.rubitherm.de
RT 25 HC	Organic	Rubitherm GmbH	25	65	825	210	2	0.2	1650	low	€9,11	€7,52	€4,56	mail contact	www.rubitherm.de
RT 27	Organic	Rubitherm GmbH	27	50	825	179	2	0.2	1650	low	€9,11	€7,52	€4,56	mail contact	www.rubitherm.de
RT 28 HC	Organic	Rubitherm GmbH	28	50	825	250	2	0.2	1650	low	€9,11	€7,52	€4,56	mail contact	www.rubitherm.de
S19	Inorganic	PlusCE	19	33	1520	160	1.9	0.43	2888	no	€2,50	€3,80	€1,32	mail contact	www.pcmproducts.net
S21	Inorganic	PlusCE	21	45	1530	170	2.2	0.54	3366	no	€2,00	€3,06	€0,91	mail contact	www.pcmproducts.net
S22	Inorganic	PlusCE	22	40	1530	175	2.2	0.54	3366	no	€2,00	€3,06	€0,91	mail contact	www.pcmproducts.net
S23	Inorganic	PlusCE	23	33	1530	175	2.2	0.54	3366	no	€1,75	€2,68	€0,80	mail contact	www.pcmproducts.net
S24	Inorganic	PlusCE	24	33	1530	180	2.2	0.54	3366	no	€1,50	€2,30	€0,68	mail contact	www.pcmproducts.net
S25	Inorganic	PlusCE	25	33	1530	180	2.2	0.54	3366	no	€1,50	€2,30	€0,68	mail contact	www.pcmproducts.net
A22	Organic	PlusCE	22	60	785	145	2.2	0.18	1743	low	€6,00	€5,10	€2,79	mail contact	www.frees.com
A22H	Organic	PlusCE	22	60	820	216	2.9	0.18	2337	low	€5,50	€4,68	€2,62	mail contact	www.frees.com
A23	Organic	PlusCE	23	33	785	145	2.2	0.18	1743	low	€6,00	€5,10	€2,79	mail contact	www.frees.com
A24	Organic	PlusCE	24	33	790	145	2.2	0.18	1754	low	€6,00	€5,11	€2,79	mail contact	www.frees.com
A25	Organic	PlusCE	25	33	785	150	2.3	0.18	1774	low	€4,00	€5,52	€1,11	mail contact	www.dimator.com
A25H	Organic	PlusCE	25	33	810	226	2.2	0.18	1742	low	€4,00	€5,52	€1,11	mail contact	www.dimator.com
A26	Organic	PlusCE	26	33	790	150	2.2	0.21	1754	low	€4,00	€5,52	€1,11	mail contact	www.dimator.com
A28	Organic	PlusCE	28	33	789	155	2.2	0.21	1752	low	€4,00	€5,52	€1,11	mail contact	www.dimator.com
Crodatherm 19	Bio-based (100%)	Crodatherm	19	33	850	205	2.2	0.20	1828	no	€6,00	€5,10	€2,79	mail contact	www.frees.com
Crodatherm 21	Bio-based (100%)	Crodatherm	21	33	850	215	2.1	0.17	1785	no	€5,50	€4,68	€2,62	mail contact	www.frees.com
Crodatherm 24W	Bio-based (100%)	Crodatherm	24	33	843	207	2.1	0.23	1728	no	€6,00	€5,11	€2,79	mail contact	www.frees.com
Crodatherm 29	Bio-based (100%)	Crodatherm	29	33	851	223	1.9	0.19	1574	no	€6,00	€5,11	€2,79	mail contact	www.frees.com
PCMH22P	Inorganic	SAVENRG	22	33	1540	185	2.3	0.85	3479	no	€4,00	€5,52	€1,11	mail contact	www.puretemp.com
PCMH524P	Inorganic	SAVENRG	24	33	1540	185	2.3	0.85	3479	no	€4,00	€5,52	€1,11	mail contact	www.puretemp.com
Climsel C21	Inorganic	Climator	21	33	1380	112	3.6	0.84	4968	no	€4,00	€5,52	€1,11	mail contact	www.puretemp.com
Climsel C24	Inorganic	Climator	24	33	1380	151.3	3.6	0.6	4968	no	€4,00	€5,52	€1,11	mail contact	www.puretemp.com
Climsel C28	Inorganic	Climator	28	33	1420	162.3	3.6	0.6	5112	no	€4,00	€5,52	€1,11	mail contact	www.puretemp.com
PureTemp 20	Organic	PureTemp	20	33	860	180	2.59	0.22	2227	low	€6,00	€5,10	€2,79	mail contact	www.puretemp.com
PureTemp 23	Organic	PureTemp	23	33	830	203	1.84	0.18	1527	low	€6,00	€5,10	€2,79	mail contact	www.puretemp.com
PureTemp 24	Organic	PureTemp	24	33	860	185	2.85	0.21	2451	low	€6,00	€5,10	€2,79	mail contact	www.puretemp.com
PureTemp 25	Organic	PureTemp	25	33	860	185	1.99	0.18	1711	low	€6,00	€5,10	€2,79	mail contact	www.puretemp.com
PureTemp 27	Organic	PureTemp	27	33	860	200	2.46	0.21	2116	low	€6,00	€5,10	€2,79	mail contact	www.puretemp.com
PureTemp 28	Organic	PureTemp	29	33	860	205	2.34	0.21	2012	low	€6,00	€5,10	€2,79	mail contact	www.puretemp.com

Overview showing the results from the benchmark situations, first table showing the input values for each benchmark situation. The first two simulations do not contain values for the different parameters, in these situations no PCM panel is included.

BENCHMARK INPUT VALUES													
ID (#)	Simulation	Panel thickness (m)	Blind covering temperature (°C)	Latent heat storage (kJ/kg)	Melting temperature (°C)	Trombe wall ratio 1 (%)	Trombe wall ratio 2 (%)	System layers (no.)	Panel area ratio (%)	Convective heat transfer (W/m²K)	Total cavity width (m)	Thermal conduction (W/m.K)	Material density (kg/m³)
0.1	No sunscreen	0.000	-	0.00	0.00	0.00	0.00	0.00	0.00	0.00	0.00	0.00	0.00
0.2	With sunscreen	0.000	22.00	0.00	0.00	0.00	0.00	0.00	0.00	0.00	0.00	0.00	0.00
0.3	Concrete trombe	0.100	22.00	0.00	25.00	0.90	0.90	1.00	1.00	2.70	0.04	0.60	1450.00
0.4	PCM trombe	0.025	22.00	180000.00	25.00	0.90	0.90	1.00	1.00	2.70	0.04	0.60	1450.00

This table shows the benchmark results for the heating and cooling energy demand and the heating and cooling energy reduction from the concrete trombe wall and the standard pcm trombe wall.

ID (#)	Simulation	RESULTS				BENCHMARK RESULTS					
		Cooling reduction (%)	Heating reduction (%)	Cooling reduction (kWh)	Heating reduction (kWh)	Cooling energy usage (kWh)	Heating energy usage (kWh)	Total panel volume (m³)	Latent storage capacity (kJ)	Panel surface area (m²)	Opening area (%)
0.1	No sunscreen	-	-	-	-	4958.30	2926.70	-	-	-	-
0.2	With sunscreen	-	-	-	-	1132.00	329.10	-	-	-	-
0.3	Concrete trombe	22.26	36.80	252.00	121.10	880.00	208.00	2.08	-	20.65	0.90
0.4	PCM trombe	58.84	71.58	666.05	235.58	465.95	93.52	0.52	1.35E+08	20.65	0.90

General overview with the input values from the Design of Experiments for the detailed thermodynamic analysis

	SIMULATION INPUT VALUES													
	ID (#)	Simulation value	Panel thickness (m)	Blind covering temperature (°C)	Latent heat storage (kJ/kg)	Melting temperature (°C)	Trombe wall ratio 1 (%)	Trombe wall ratio 2 (%)	System layers (no.)	Panel area ratio (%)	Convective heat transfer (W/m²K)	Total cavity width (m)	Thermal conduction (W/m.K)	Material density (kg/m³)
1.1	Panel thickness (m)	1.1	0.010	0.010	22.00	180000.00	25.00	0.90	0.90	1.00	1.00	2.70	0.60	1450.00
		1.2	0.015	0.015	22.00	180000.00	25.00	0.90	0.90	1.00	1.00	2.70	0.60	1450.00
		2.1	0.020	0.020	22.00	180000.00	25.00	0.90	0.90	1.00	1.00	2.70	0.60	1450.00
		2.2	0.025	0.025	22.00	180000.00	25.00	0.90	0.90	1.00	1.00	2.70	0.60	1450.00
		3.1	0.030	0.030	22.00	180000.00	25.00	0.90	0.90	1.00	1.00	2.70	0.60	1450.00
		3.2	0.035	0.035	22.00	180000.00	25.00	0.90	0.90	1.00	1.00	2.70	0.60	1450.00
		4.1	0.040	0.040	22.00	180000.00	25.00	0.90	0.90	1.00	1.00	2.70	0.60	1450.00
		4.2	0.045	0.045	22.00	180000.00	25.00	0.90	0.90	1.00	1.00	2.70	0.60	1450.00
		5.1	0.050	0.050	22.00	180000.00	25.00	0.90	0.90	1.00	1.00	2.70	0.60	1450.00
		5.2	0.055	0.055	22.00	180000.00	25.00	0.90	0.90	1.00	1.00	2.70	0.60	1450.00
3.1	Latent heat storage: organic (J/kg)	6	0.060	0.060	22.00	180000.00	25.00	0.90	0.90	1.00	1.00	2.70	0.60	1450.00
		14	1.60E+05	0.025	22.00	160000.00	25.00	0.90	0.90	1.00	1.00	2.70	0.60	850.00
		15	1.80E+05	0.025	22.00	180000.00	25.00	0.90	0.90	1.00	1.00	2.70	0.60	850.00
		16	2.00E+05	0.025	22.00	200000.00	25.00	0.90	0.90	1.00	1.00	2.70	0.60	850.00
4.1	Latent heat storage: inorganic (J/kg)	17	2.20E+05	0.025	22.00	220000.00	25.00	0.90	0.90	1.00	1.00	2.70	0.60	850.00
		18	2.40E+05	0.025	22.00	240000.00	25.00	0.90	0.90	1.00	1.00	2.70	0.60	850.00
		19	1.60E+05	0.025	22.00	160000.00	25.00	0.90	0.90	1.00	1.00	2.70	0.60	1450.00
		20	1.80E+05	0.025	22.00	180000.00	25.00	0.90	0.90	1.00	1.00	2.70	0.60	1450.00
5.1	Melting temperature (°C)	21	2.00E+05	0.025	22.00	200000.00	25.00	0.90	0.90	1.00	1.00	2.70	0.60	1450.00
		22	2.20E+05	0.025	22.00	220000.00	25.00	0.90	0.90	1.00	1.00	2.70	0.60	1450.00
		23	2.40E+05	0.025	22.00	240000.00	25.00	0.90	0.90	1.00	1.00	2.70	0.60	1450.00
		24	20.00	0.025	22.00	180000.00	20.00	0.90	0.90	1.00	1.00	2.70	0.60	1450.00
6.1	Trombe wall ratio 1 (%)	25	21.00	0.025	22.00	180000.00	21.00	0.90	0.90	1.00	1.00	2.70	0.60	1450.00
		26	22.00	0.025	22.00	180000.00	22.00	0.90	0.90	1.00	1.00	2.70	0.60	1450.00
		27	23.00	0.025	22.00	180000.00	23.00	0.90	0.90	1.00	1.00	2.70	0.60	1450.00
		28	24.00	0.025	22.00	180000.00	24.00	0.90	0.90	1.00	1.00	2.70	0.60	1450.00
7.1	Trombe wall ratio 2 (%)	29	25.00	0.025	22.00	180000.00	25.00	0.90	0.90	1.00	1.00	2.70	0.60	1450.00
		30	26.00	0.025	22.00	180000.00	26.00	0.90	0.90	1.00	1.00	2.70	0.60	1450.00
		31	0.40	0.025	22.00	180000.00	25.00	0.90	0.90	1.00	1.00	2.70	0.60	1450.00
		32	0.50	0.025	22.00	180000.00	25.00	0.50	0.90	1.00	1.00	2.70	0.60	1450.00
8.1	System layers degrees (no.)	33	0.60	0.025	22.00	180000.00	25.00	0.60	0.90	1.00	1.00	2.70	0.60	1450.00
		34	0.70	0.025	22.00	180000.00	25.00	0.70	0.90	1.00	1.00	2.70	0.60	1450.00
		35	0.80	0.025	22.00	180000.00	25.00	0.80	0.90	1.00	1.00	2.70	0.60	1450.00
		36	0.90	0.025	22.00	180000.00	25.00	0.90	0.90	1.00	1.00	2.70	0.60	1450.00
9.1	System layers +degree (no.)	37	0.40	0.025	22.00	180000.00	25.00	0.40	0.90	1.00	1.00	2.70	0.60	1450.00
		38	0.50	0.025	22.00	180000.00	25.00	0.50	0.90	1.00	1.00	2.70	0.60	1450.00
		39	0.60	0.025	22.00	180000.00	25.00	0.60	0.90	1.00	1.00	2.70	0.60	1450.00
		40	0.70	0.025	22.00	180000.00	25.00	0.70	0.90	1.00	1.00	2.70	0.60	1450.00
10.1	Panel area ratio (%)	41	0.80	0.025	22.00	180000.00	25.00	0.80	0.90	1.00	1.00	2.70	0.60	1450.00
		42	0.90	0.025	22.00	180000.00	25.00	0.90	0.90	1.00	1.00	2.70	0.60	1450.00
		43.1	1.00	0.025	22.00	180000.00	25	0.90	0.90	1.00	1.00	2.70	0.60	1450.00
		44.1	2.00	0.025	22.00	180000.00	25-21	0.90	0.90	2.00	1.00	2.70	0.60	1450.00
11.1	Convective heat transfer (W/m²K)	45.1	3.00	0.025	22.00	180000.00	25-23-21	0.90	0.90	3.00	1.00	2.70	0.60	1450.00
		46.1	1.00	0.025	22.00	180000.00	28	0.90	0.90	1.00	1.00	2.70	0.60	1450.00
		47.1	2.00	0.025	22.00	180000.00	28-24	0.90	0.90	2.00	1.00	2.70	0.60	1450.00
		48.1	3.00	0.025	22.00	180000.00	28-26-24	0.90	0.90	3.00	1.00	2.70	0.60	1450.00
12.1	Cavity width (m)	43.2	1.00	0.025	22.00	180000.00	21	0.90	0.90	1.00	1.00	2.70	0.60	1450.00
		44.2	2.00	0.025	22.00	180000.00	21-25	0.90	0.90	2.00	1.00	2.70	0.60	1450.00
		45.2	3.00	0.025	22.00	180000.00	21-23-25	0.90	0.90	3.00	1.00	2.70	0.60	1450.00
		46.2	1.00	0.025	22.00	180000.00	24	0.90	0.90	1.00	1.00	2.70	0.60	1450.00
13.1	Thermal conduction (W/m.K) + density	47.2	2.00	0.025	22.00	180000.00	24-28	0.90	0.90	2.00	1.00	2.70	0.60	1450.00
		48.2	3.00	0.025	22.00	180000.00	24-26-28	0.90	0.90	3.00	1.00	2.70	0.60	1450.00
		49	1.05	0.025	22.00	180000.00	25.00	0.90	0.90	1.00	1.05	2.70	0.60	1450.00
		50	1.10	0.025	22.00	180000.00	25.00	0.90	0.90	1.00	1.10	2.70	0.60	1450.00
13.2	Thermal conduction (W/m.K)	51	1.15	0.025	22.00	180000.00	25.00	0.90	0.90	1.00	1.15	2.70	0.60	1450.00
		52	1.20	0.025	22.00	180000.00	25.00	0.90	0.90	1.00	1.20	2.70	0.60	1450.00
		53	1.25	0.025	22.00	180000.00	25.00	0.90	0.90	1.00	1.25	2.70	0.60	1450.00
		54	1.30	0.025	22.00	180000.00	25.00	0.90	0.90	1.00	1.30	2.70	0.60	1450.00
13.3	Thermal conduction (W/m.K)	55	2.00	0.025	22.00	180000.00	25.00	0.90	0.90	1.00	2.00	0.60	1450.00	
		56	2.50	0.025	22.00	180000.00	25.00	0.90	0.90	1.00	2.50	0.60	1450.00	
		57	3.00	0.025	22.00	180000.00	25.00	0.90	0.90	1.00	3.00	0.60	1450.00	
		58	3.50	0.025	22.00	180000.00	25.00	0.90	0.90	1.00	3.50	0.60	1450.00	
13.4	Thermal conduction (W/m.K)	59	4.00	0.025	22.00	180000.00	25.00	0.90	0.90	1.00	4.00	0.60	1450.00	
		60	4.50	0.025	22.00	180000.00	25.00	0.90	0.90	1.00	4.50	0.60	1450.00	
		61	0.01	0.025	22.00	180000.00	25.00	0.90	0.90	1.00	2.70	0.01	1450.00	
		62	0.04	0.025	22.00	180000.00	25.00	0.90	0.90	1.00	2.70	0.04	1450.00	
13.5	Thermal conduction (W/m.K)	63	0.07	0.025	22.00	180000.00	25.00	0.90	0.90	1.00	2.70	0.07	1450.00	
		64	0.10	0.025	22.00	180000.00	25.00	0.90	0.90	1.00	2.70	0.10	1450.00	
		65	0.13	0.025	22.00	180000.00	25.00	0.90	0.90	1.00	2.70	0.13	1450.00	
		66	0.16	0.025	22.00	180000.00	25.00	0.90	0.90	1.00	2.70	0.16	1450.00	
13.6	Thermal conduction (W/m.K)	67	0.30	0.025	22.00	180000.00	25.00	0.90	0.90	1.00	2.70	0.30	950.00	
		68	0.50	0.025	22.00	180000.00	25.00	0.90	0.90	1.00	2.70	0.50	1250.00	
		69	0.70	0.025	22.00	180000.00	25.00	0.90	0.90	1.00	2.70	0.70	1550.00	
		70	0.90	0.025	22.00	180000.00	25.00	0.90	0.90	1.00	2.70	0.90	1850.00	
13.7	Thermal conduction (W/m.K)	71	1.10	0.025	22.00	180000.00	25.00	0.90	0.90	1.00	2.70	1.10	2150.00	
		72	1.30	0.025	22.00	180000.00	25.00	0.90	0.90	1.00	2.70	1.30	2450.00	
		67	0.30	0.025	22.00	180000.00	25.00	0.90	0.90	1.00	2.70	0.30	1450.00	
		68	0.50	0.025	22.00	180000.00	25.00	0.90	0.90	1.00	2.70	0.50	1450.00	
13.8	Thermal conduction (W/m.K)	69	0.70	0.025	22.00	180000.00	25.00	0.90	0.90	1.00	2.70	0.70	1450.00	
		70	0.90	0.025	22.00	180000.00	25.00	0.90	0.90	1.00	2.70	0.90	1450.00	
		71	1.10	0.025	22.00	180000.00	25.00	0.90	0.90	1.00	2.70	1.10	1450.00	
		72	1.30	0.025	22.00	180000.00	25.00	0.90	0.90	1.00	2.70	1.30	1450.00	

APPENDIX E

Overview with results from the combined optimization showing the correlation between the Heating demand [kWh], the Cooling demand [kWh] and the volume of the PCM panel [m³]

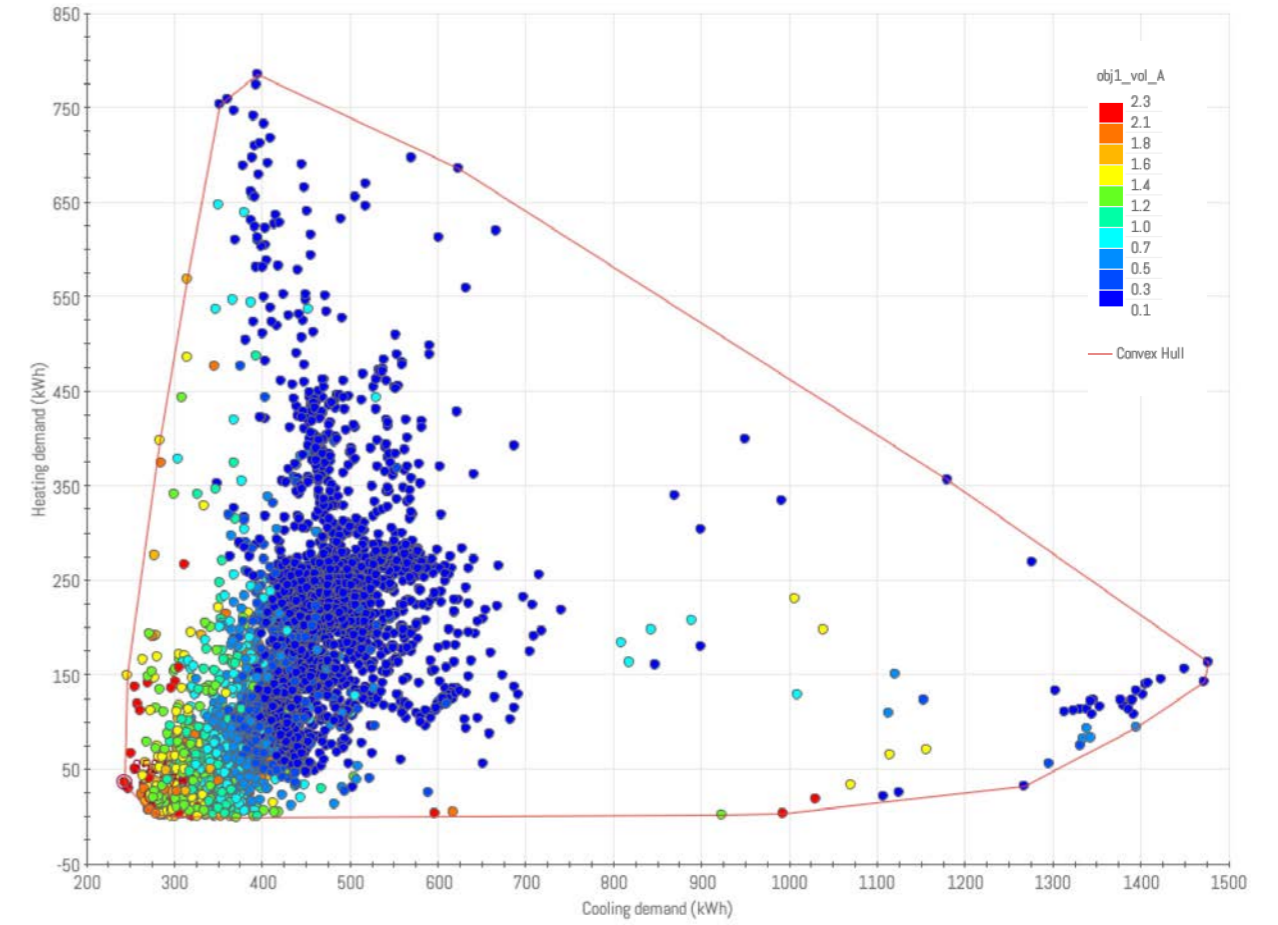


Table 1.30 Optimal design results from the combined heating and cooling optimization

ID #	Panel thickness (m)	Latent heat storage (kJ/kg)	Melting temperature (°C)	Trombe wall ratio 1 (%)	Trombe wall ratio 2 (%)	System layers (no.)	Panel area ratio (%)	Convective heat transfer (W/m²K)	Thermal conduction (W/m.K)	Material density (kg/m³)	Cooling load (kWh)	Heating load (kWh)	Heating and cooling (kWh)	Panel volume (m³)
425	0.0875	215000	25.0	1	0.50	3	1.15	4.1	0.1	1300	276.24	26.41	302.65	2.01
624	0.1000	230000	25.5	1	0.53	3	1.24	3.1	0.1	1400	282.52	11.88	294.41	2.30
639	0.0900	240000	25.0											

APPENDIX F

Overview with results from the cooling optimization showing the correlation between the Heating demand [kWh], the Cooling demand [kWh] and the volume of the PCM panel [m³]

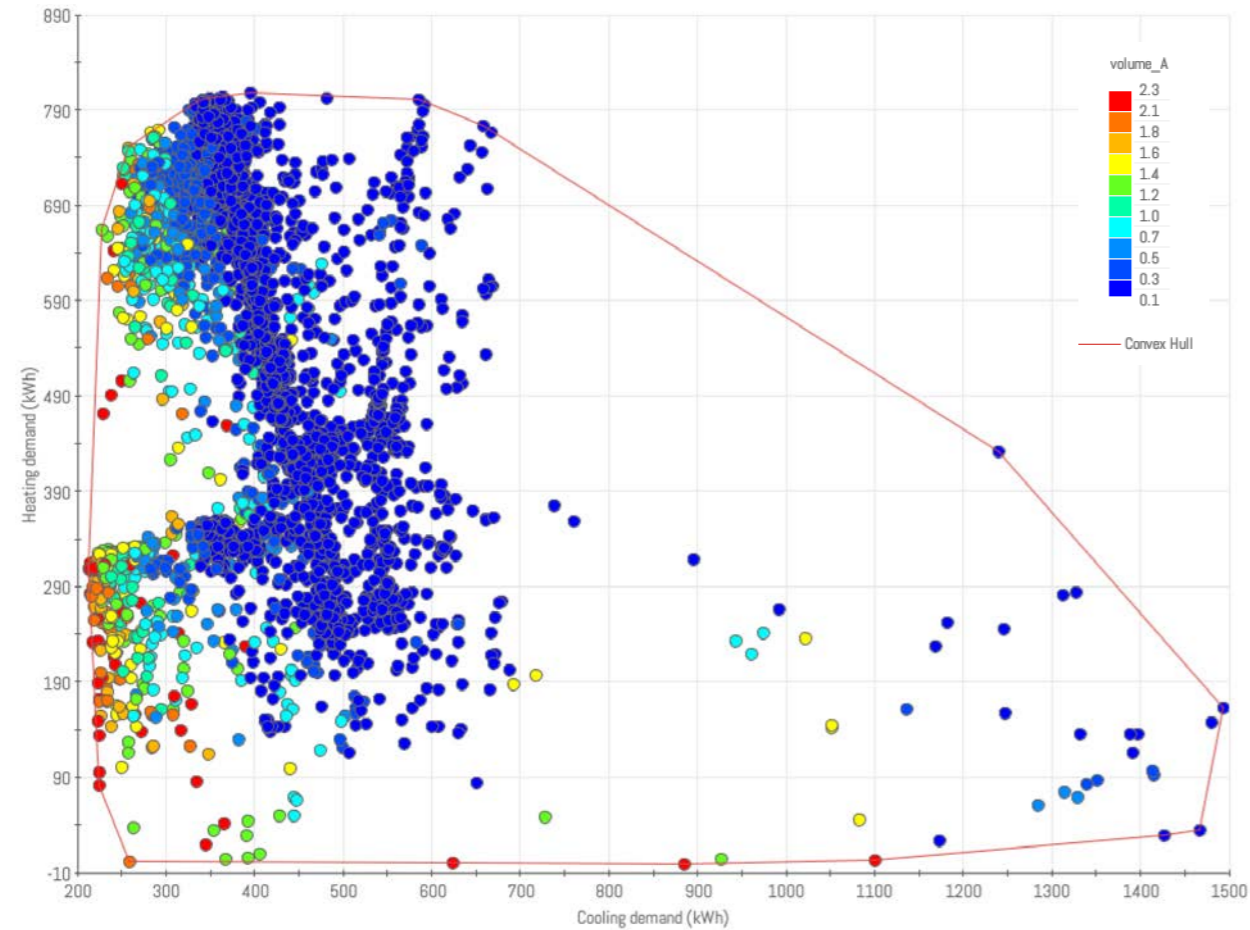
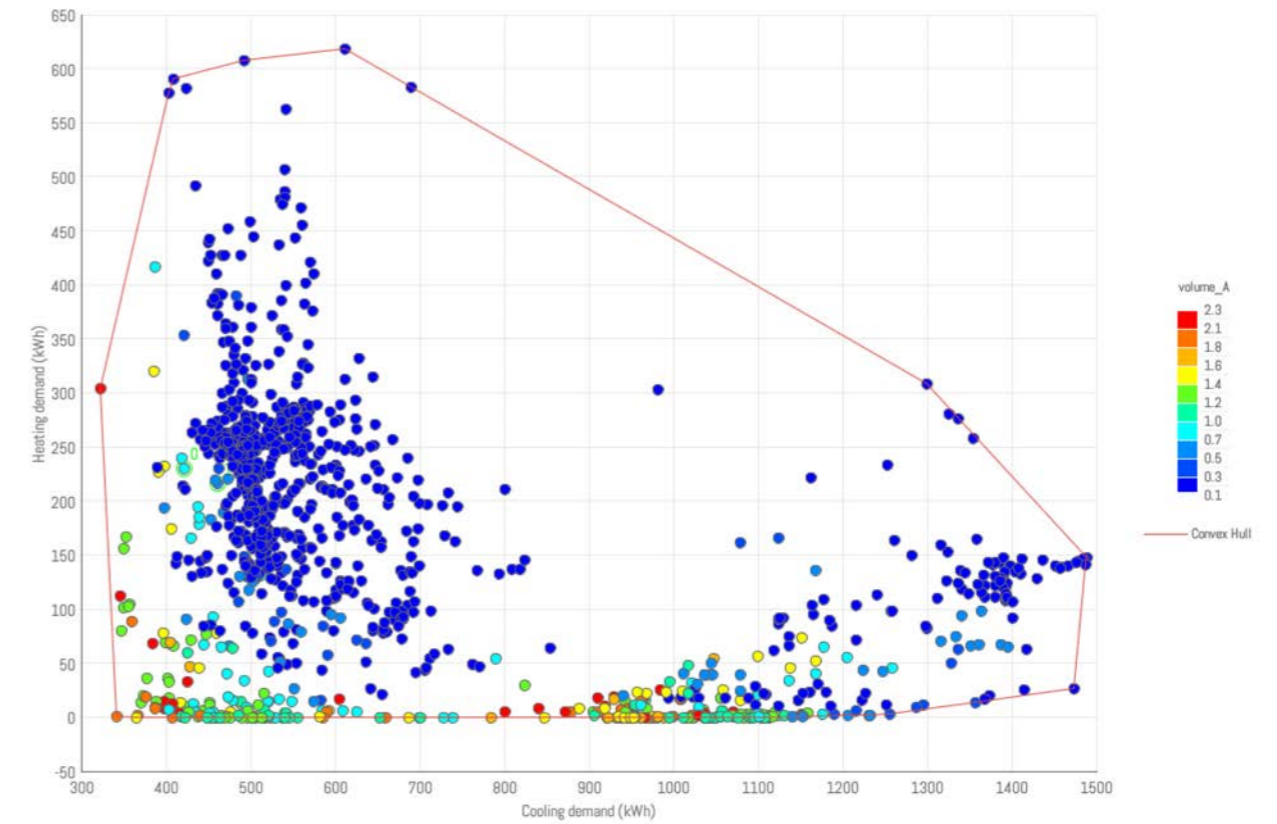


Table 1.31 Optimal design results from the combined heating and cooling optimization

ID #	Panel thickness (m)	Latent heat storage (kJ/kg)	Melting temperature (°C)	Trombe wall ratio 1 (%)	Trombe wall ratio 2 (%)	System layers (no.)	Panel area ratio (%)	Convective heat transfer (W/m²K)	Thermal conduction (W/m.K)	Material density (kg/m³)	Cooling load (kWh)	Heating load (kWh)	Heating and cooling (kWh)	Panel volume (m³)
847	0.095	232500	25.5	1	0.300	1	1.30	6.5	1.3	1400	217.47	316.39	533.86	2.18
850	0.083	232500	25.0	1	0.300	1	1.30	6.5	0.9	1375	218.53	287.19	505.72	1.89
863	0.100	220000	25.5	1	0.300	1	1.30	6.5	1.1	1450	213.72	307.91	521.64	2.30
871	0.100	240000	26.0	1	0.300	1	1.30	6.5	1.3	1450	213.56	315.00	528.55	2.30
875	0.095	232500	25.0	1	0.400	1	1.30	6.5	0.9	1400	216.85	233.17	450.01	2.18
877	0.078	232500	25.0	1	0.300	1	1.30	6.5	1.0	1450	218.26	284.83	503.09	1.78
880	0.095	232500	25.5	1	0.300	1	1.29	6.5	0.8	1425	216.74	308.56	525.31	2.18
887	0.100	220000	25.5	1	0.300	1	1.30	6.5	0.9	1375	216.78	307.58	524.36	2.30
895	0.100	220000	25.5	1	0.300	1	1.29	6.5	1.1	1450	217.56	308.23	525.79	2.30
918	0.093	232500	25.5	1	0.300	1	1.30	6.5	0.9	1425	212.39	309.55	521.94	2.12
1014	0.100	217500	25.5	1	0.300	1	1.30	6.5	1.1	1450	212.85	309.32	522.17	2.30
1064	0.100	240000	26.0	1	0.300	1	1.30	6.5	1.0	1450	216.51	311.15	527.65	2.30
1076	0.075	232500	24.5	1	0.300	1	1.30	6.5	1.1	1450	217.45	269.21	486.66	1.72
1123	0.093	230000	25.5	1	0.300	1	1.30	6.5	1.0	1450	217.11	310.66	527.77	2.12
1198	0.095	232500	25.5	1	0.300	1	1.30	6.5	0.9	1400	215.02	311.45	526.47	2.18
1201	0.075	235000	25.0	1	0.300	1	1.30	6.5	1.1	1450	218.62	281.65	500.27	1.72
1316	0.095	212500	25.0	1	0.300	1	1.30	6.5	1.3	1400	218.58	293.33	511.90	2.18
1471	0.100	217500	25.5	1	0.300	1	1.30	6.5	1.2	1450	215.70	310.60	526.30	2.30
1526	0.090	230000	25.5	1	0.300	1	1.30	6.5	0.9	1450	217.18	313.18	530.36	2.07
1627	0.100	240000	25.5	1	0.300	1	1.30	6.5	1.3	1450	216.45	308.45	524.89	2.30
1702	0.090	232500	25.5	1	0.325	1	1.30	6.5	1.1	1400	218.55	302.03	520.58	2.07
1759	0.090	232500	25.5	1	0.300	1	1.30	6.5	0.9	1450	216.60	310.72	527.31	2.07
1772	0.100	230000	25.0	1	0.300	1	1.30	6.5	1.3	1450	214.04	283.66	497.70	2.30
1775	0.078	240000	25.0	1	0.300	1	1.30	6.5	1.0	1450	216.51	287.67	504.18	1.78
1956	0.090	230000	25.0	1	0.300	1	1.30	6.5	0.9	1450	215.97	290.13	506.10	2.07
2029	0.090	240000	25.5	1	0.300	1	1.30	6.5	0.9	1450	214.85	310.06	524.91	2.07
2093	0.090	240000	25.0	1	0.300	1	1.30	6.5	0.9	1450	214.42	280.93	495.35	2.07
2373	0.100	220000	25.5	1	0.300	1	1.30	6.5	1.3	1450	214.10	309.83	523.93	2.30

APPENDIX G

Overview with results from the heating optimization showing the correlation between the Heating demand [kWh], the Cooling demand [kWh] and the volume of the PCM panel [m³]



ID #	Panel thickness (m)	Latent heat storage (kJ/kg)	Melting temperature (°C)	Trombe wall ratio 1 (%)	Trombe wall ratio 2 (%)	System layers (no.)	Panel area ratio (%)	Convective heat transfer (W/m²K)	Thermal conduction (W/m.K)	Material density (kg/m³)	Cooling load (kWh)	Heating load (kWh)	Heating and cooling (kWh)	Panel volume (m³)
349	0.0750	240000	24.0	1	1.000	3.0	1.000	1.9	0.2	1150	973.52	0.07	973.59	1.72
359	0.0600	227500	22.0	1	0.900	1.0	1.175	1.9	0.5	1100	513.71	0.15	513.86	1.38
448	0.0525	207500	22.5	1	0.875	1.0	1.225	1.9	0.4	1150	496.21	0.14	496.34	1.20
465	0.0750	240000	24.0	1	1.000	3.0	1.000	1.9	0.1	1150	971.31	0.03	971.34	1.72
518	0.0500	220000	22.0	1	1.000	1.0	1.263	1.9	0.6	1100	1040.76	0.18	1040.94	1.15
567	0.0550	220000	22.0	1	1.000	1.0	1.263	1.9	0.4	1150	1022.99	0.14	1023.13	1.26
581	0.0575	220000	22.0	1	1.000	1.0	1.263	1.9	0.4	1150	1021.84	0.15	1022.00	1.32
628	0.0550	220000	22.0	1	1.000	1.0	1.225	1.9	0.1	1450	1082.28	0.02	1082.30	1.26
649	0.0500	220000	22.0	1	1.000	1.0	1.263	1.9	0.4	1175	1041.17	0.11	1041.28	1.15
672	0.0750	240000	24.0	1	1.000	3.0	1.000	5.1	0.1	1150	783.22	0.09	783.31	1.72
686	0.0575	235000	22.0	1	1.000	1.0	1.263	1.9	0.4	1150	1015.71	0.11	1015.82	1.32
695	0.0500	220000	22.0	1	1.000	1.0	1.063	1.9	0.1	1050	1112.27	0.09	1112.36	1.15
702	0.0750	240000	24.0	1	1.000	3.0	1.100	1.9	0.1	1150	960.14	0.03	960.17	1.72
715	0.0500	220000	22.0	1	1.000	1.0	1.263	1.9	0.1	1175	1088.60	0.08	1088.68	1.15
722	0.0500	230000	24.5	1	0.950	3.0	1.000	1.9	0.4	1450	537.61	0.12	537.73	1.15
732	0.0700	240000	24.0	1	1.000	3.0	1.000	1.9	0.1	1450	952.59	0.03	952.62	1.61
737	0.0850	240000	25.0	1	0.975	2.0	1.038	1.9	0.2	1175	584.48	0.08	584.56	1.95
756	0.0750	177500	24.0	1	1.000	3.0	1.113	1.9	1.3	1450	940.70	0.14	940.84	1.72
760	0.0900	210000	22.0	1	0.975	1.0	1.300	1.9	0.1	1450	658.91	0.14	659.05	2.07
779	0.0550	220000	22.0	1	1.000	1.0	1.200	1.9	0.7	1175	1016.07	0.11	1016.18	1.26
789	0.0775	240000	24.0	1	1.000	3.0	1.000	1.9	0.2	1150	979.43	0.09	979.52	1.78
790	0.0500	220000	22.0	1	1.000	1.0	1.225	1.9	0.7	1300	1010.31	0.10	1010.41	1.15
831	0.0500	220000	22.0	1	1.000	1.0	1.225	1.9	0.1	1050	1094.27	0.09	1094.37	1.15
920	0.0500	220000	22.0	1	1.000	1.0	1.063	1.9	0.1	1450	1102.07	0.04	1102.11	1.15
924	0.0500	212500	22.0	1	1.000	1.0	1.063	1.9	0.7	1175	1041.66	0.19	1041.85	1.15
940	0.0700	240000	24.0	1	1.000	3.0	1.000	1.9	0.9	1450	941.60	0.12	941.72	1.61
946	0.0500	220000	22.0	1	1.000	1.0	1.025	1.9	0.1	1175	1107.24	0.06	1107.30	1.15
1026	0.0500	220000	22.0	1	1.000	1.0	1.300	1.9	0.5	1150	1037.34	0.10	1037.44	1.15
1091	0.0700	240000	24.0	1	1.000	3.0	1.038	1.9	0.1	1450	948.62	0.03	948.65	1.61
1109	0.0700	240000	24.0	1	1.000	3.0	1.000	1.9	0.4	1450	952.24	0.09	952.33	1.61

APPENDIX H

Marked detailed results from the economic optimization showing the correlation between the heating power, the cooling power [kW], the heating and cooling energy demand [kWh] and the volume [m³].

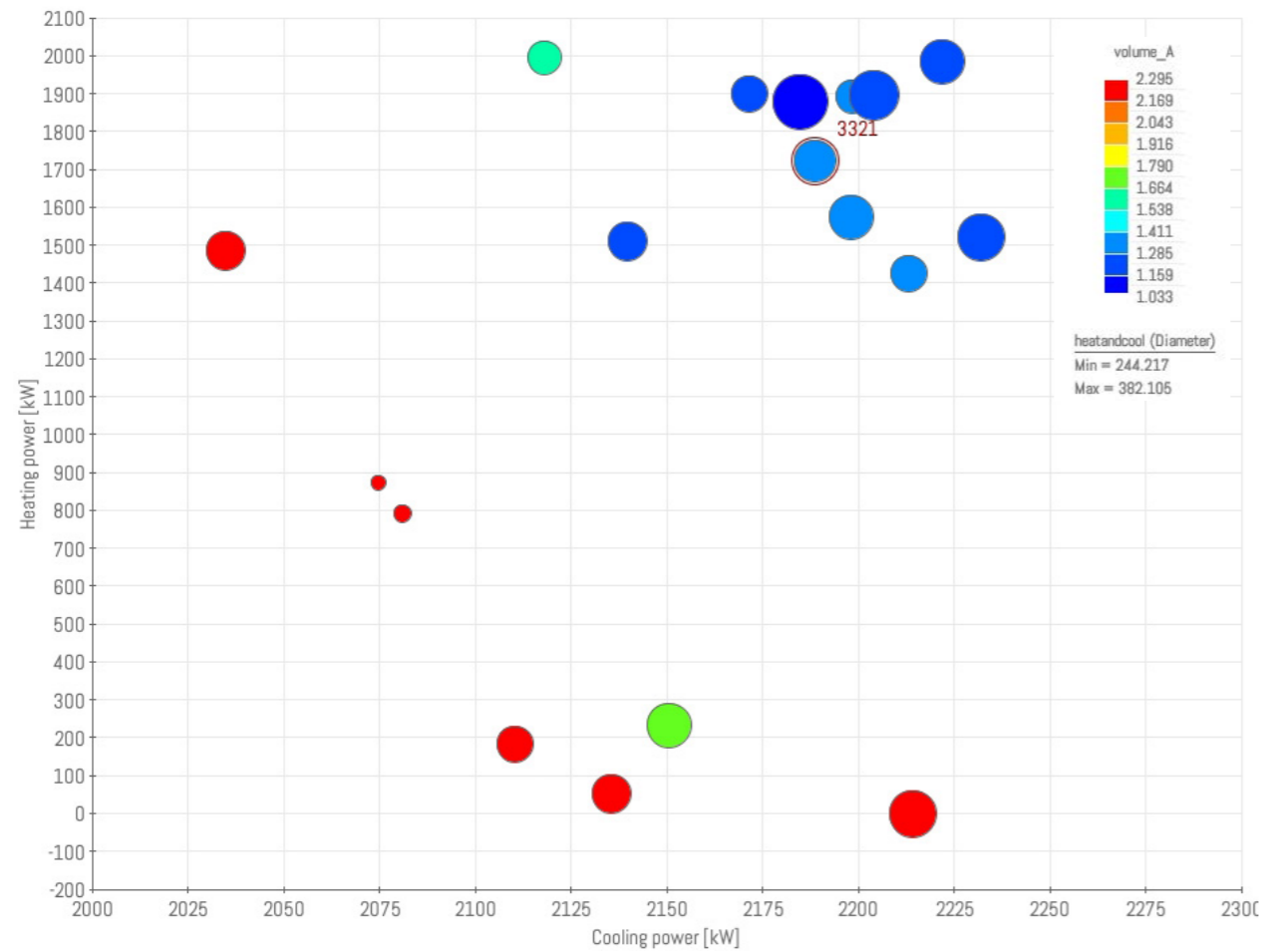
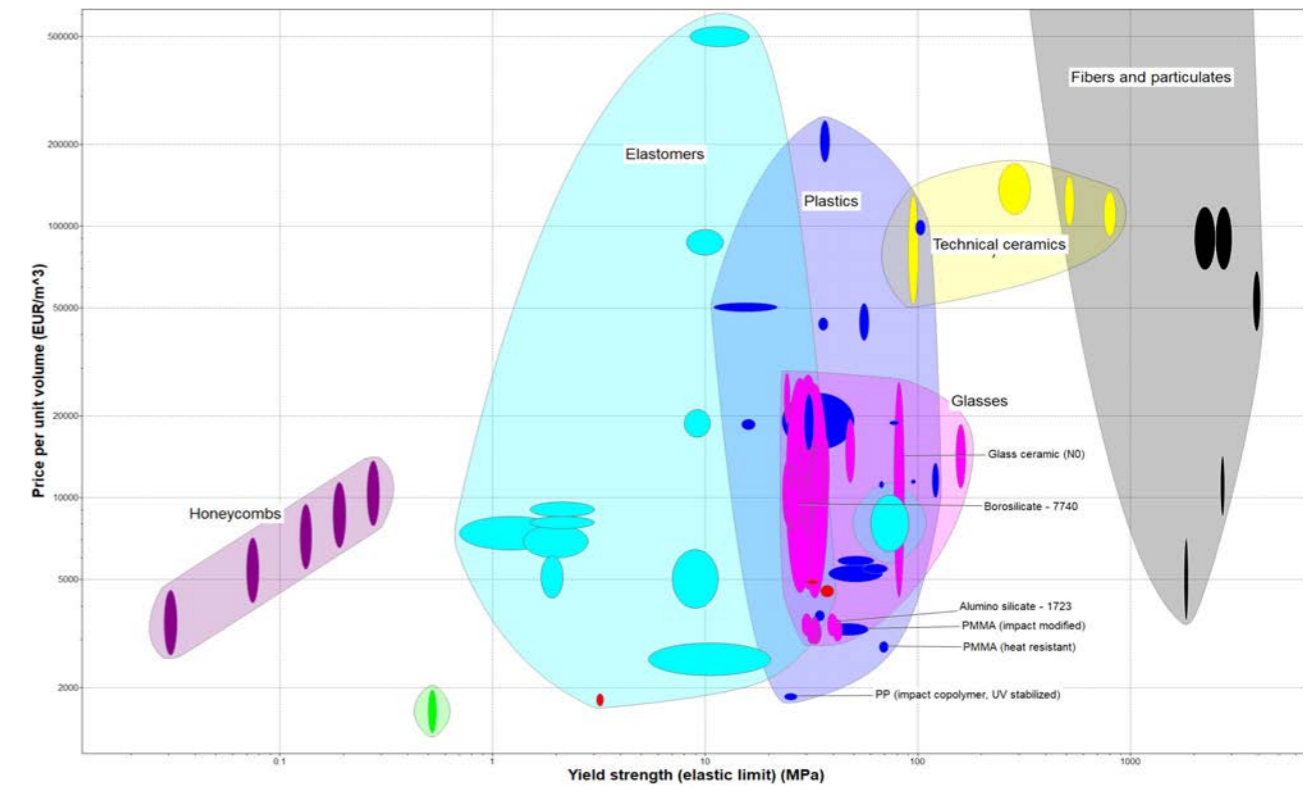


Table 1.32 Optimal design results from the economic optimization

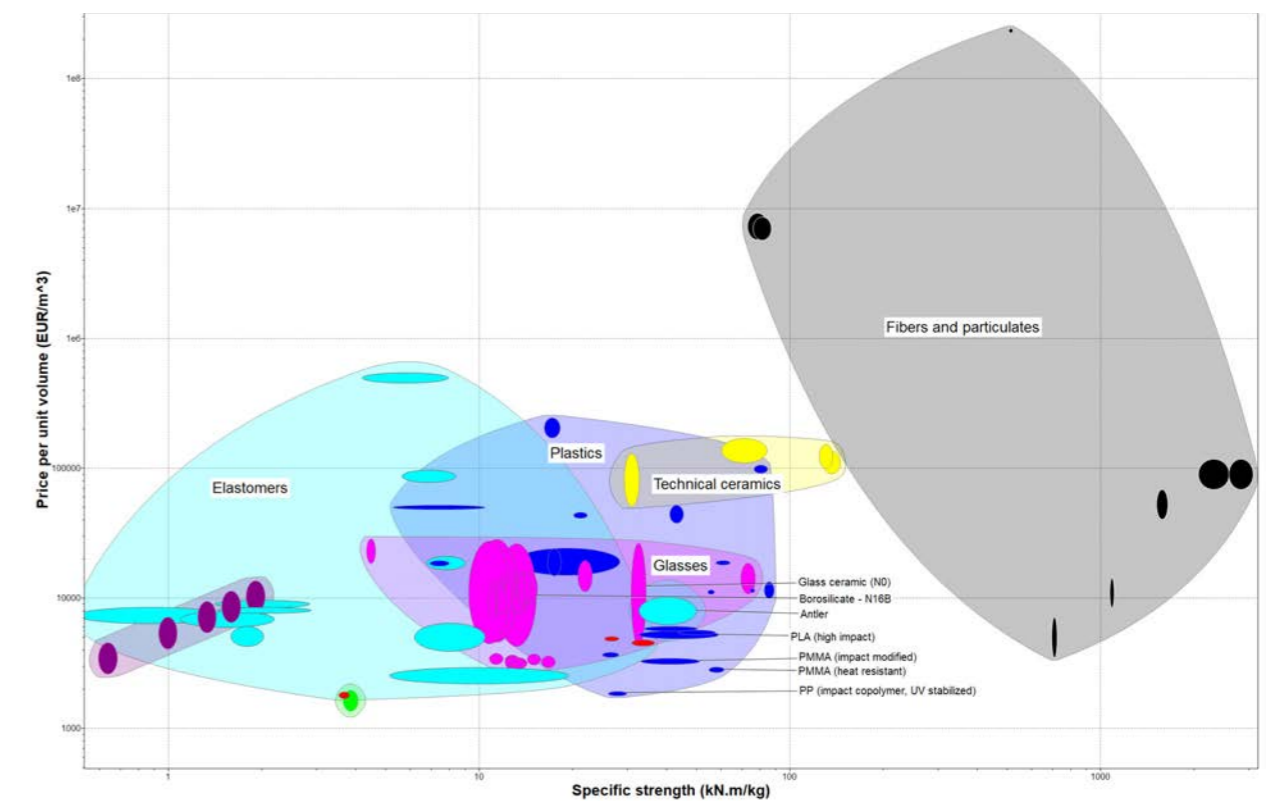
ID (#)	Panel thickness (m)	Latent heat storage (kJ/kg)	Melting temperature (°C)	Trombe wall ratio 1 (%)	Trombe wall ratio 2 (%)	System layers (no.)	Panel area ratio (%)	Convective heat transfer (W/m ² K)	Thermal conduction (W/m.K)	Material density (kg/m ³)	Cooling power (kW)	Heating power (kW)	Heating load (kWh)	Heating an cooling (kWh)	Panel volume (m ³)	
776	0.0775	240000	26	1	0.825	3	1.08	3.1	0.4	1450	2150	236	353.25	0.40	353.65	1.78
885	0.0675	240000	26	1	0.6	3	1.13	4.1	0.1	1450	2118	1996	285.16	32.06	317.22	1.55
1076	0.1	240000	26	1	0.825	3	1.08	3.5	0.4	1450	2135	56	331.98	0.03	332.00	2.30
1097	0.055	230000	26	1	0.75	3	1.15	5.7	0.1	1450	2171	1901	292.59	31.80	324.40	1.26
1726	0.1	232500	26	1	0.7	3	1.30	5.5	0.2	1450	2081	795	249.24	11.14	260.38	2.30
1765	0.0525	240000	26	1	0.7	3	1.00	4.9	0.1	1450	2139	1511	303.97	28.53	332.50	1.20
2146	0.1	240000	25.5	1	0.725	3	1.26	6.5	0.2	1425	2074	875	235.81	8.40	244.22	2.30
2199	0.1	235000	27	1	0.75	3	1.09	6.5	0.1	1450	2035	1488	303.39	24.60	327.99	2.30
2666	0.055	215000	26.5	1	0.775	3	1.18	5.3	0.4	1450	2222	1987	313.55	37.25	350.80	1.26
2775	0.055	237500	26	1	0.85	3	1.21	4.1	0.4	1425	2232	1523	355.17	4.23	359.40	1.26
2845	0.0575	227500	25.5	1	0.775	3	1.24	6.5	0.3	1425	2198	1893	286.17	26.63	312.81	1.32
2997	0.1	240000	25.5	1	0.75	3	1.11	3.1	0.5	1450	2110	187	321.69	0.15	321.84	2.30
3049	0.06	230000	26	1	0.775	3	1.18	6.5	0.1	1425	2213	1428	288.26	30.82	319.08	1.38
3116	0.06	232500	26.5	1	0.8	3	1.11	3.5	0.1	1450	2198	1575	336.92	15.00	351.92	1.38
3135	0.045	240000	26.5	1	0.825	3	1.05	3.5	0.1	1375	2185	1879	362.55	19.56	382.10	1.03
3321	0.06	225000	25.5	1	0.75	1	1.01	5.3	0.1	1450	2188	1725	298.01	43.74	341.74	1.38
3729	0.1	240000	25.5	1	0.9	3	1.20	3.7	1.1	1425	2214	2	358.91	0.00	358.91	2.30
3998	0.055	235000	26.5	1	0.8	3	1.00	4.1	0.3	1450	2204	1900	347.03	17.66	364.69	1.26

APPENDIX I

Design chart showing the price per unit volume (€/m³) on the y-axis and the yield strenght (MPa) on the x-axis.



Material design chart showing the price per unit volume (€/m³) on the y-axis and the specific strength (kN.m/kg) on the x-axis. Specific strength indicate the Yield strength / density ratio, a high value is positive.



PMMA (heat resistant)

Datasheet view: All attributes Show/Hide

Polymers: plastics, elastomers > Plastics > Thermoplastics > **PMMA (Polymethylmethacrylate/acrylic)** > Unfilled >

General information

Designation ⓘ
Polymethylmethacrylate (Heat Resistant, Molding and Extrusion)

Tradenames ⓘ
Acrigel, Acryl, Acrylite, Acrypet, Acryrex, Alathon, Altuglas, Anjacryl, Aristech, Astaglas, Claradex, Colorrx, Cyrolite, Delpet, Diakon, Elvacite, Elvakon, Goldrex, Lucite, Maxiglas, Next, Optix, Parapet, Permastat, Perspex, Plaskolite, Plexiglas, Plexiglas Satinice, Polyman, Polyplex, Shinkolite-P, Solarkote, Sumipex, Terez, Trimma, Tufcoat

Typical uses ⓘ
Light fittings, display signs, domestic baths, packaging, safety spectacles, tool handles, motorcycle windscreens, baby incubators

Composition overview

Compositional summary ⓘ
(CH₂-C(CH₃)COOCH₃)_n

Material family	Plastic (thermoplastic, amorphous)
Base material	PMMA (Polymethyl methacrylate / acrylic)
Polymer code	PMMA

Composition detail (polymers and natural materials)

Polymer	100	%
---------	-----	---

Price

Price	* 2.33	- 2.43	EUR/kg
Price per unit volume	* 2.71e3	- 2.96e3	EUR/m ³

Aluminum, 6016, T1

Datasheet view: All attributes Show/Hide

Metals and alloys > Non-ferrous > **Aluminum** > **Wrought** > **6000 series (Mg and Si-alloyed)** > 6016 >

General information

Designation ⓘ
6016, wrought

Condition ⓘ
T1 (Cooled from elevated temperature shaping process and naturally aged)

UNS number ⓘ
A96016

EN name ⓘ
EN AW-6016

Typical uses ⓘ
Automotive body sheet (in particularly outer panels) and can be laminated with polymer for architectural applications.

Composition overview

Compositional summary ⓘ
Al96-99 / Si1-1.5 / Mg0.25-0.6 (impurities: Fe<0.5, Cu<0.2, Mn<0.2, Zn<0.2, Ti<0.15, Cr<0.1, Other<0.15)

Material family	Metal (non-ferrous)
Base material	Al (Aluminum)

Composition detail (metals, ceramics and glasses)

Al (aluminum)	96.4	- 98.8	%
Cr (chromium)	0	- 0.1	%
Cu (copper)	0	- 0.2	%
Fe (iron)	0	- 0.5	%
Mg (magnesium)	0.25	- 0.6	%
Mn (manganese)	0	- 0.2	%
Si (silicon)	1	- 1.5	%
Ti (titanium)	0	- 0.15	%
Zn (zinc)	0	- 0.2	%
Other	0	- 0.15	%

Price

Price	* 1.68	- 1.81	EUR/kg
Price per unit volume	* 4.49e3	- 4.94e3	EUR/m ³

Physical properties

Density	2.67e3	- 2.73e3	kg/m ³
---------	--------	----------	-------------------

Hot metal extrusion

Datasheet view: All processes Show/Hide

Physical attributes

Mass range	1	- 500	kg
Range of section thickness	1	- 100	mm
Tolerance	0.5	- 2	mm
Roughness	0.8	- 12.5	µm

Process characteristics

Primary shaping processes	✓
Secondary shaping processes	✗
Machining processes	✗
Prototyping	✗
Discrete	✗
Continuous	✓

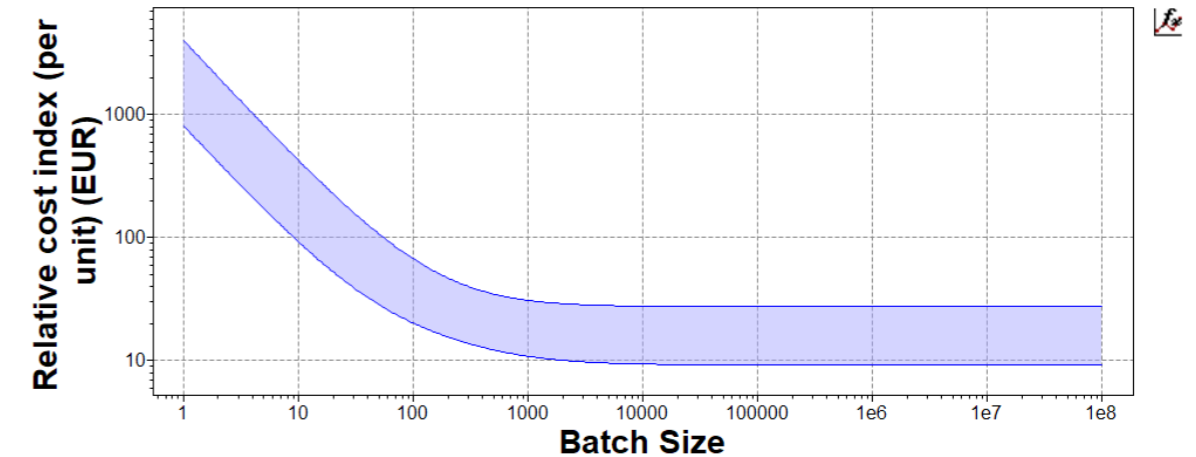
Economic attributes

Economic batch size (units)	50	- 1e4
Labor intensity	low	

Cost modeling

Relative cost index (per unit) ⓘ * 10.9 - 31 EUR

Parameters: Material Cost = 6.77EUR/kg, Component Mass = 1kg, Batch Size = 1e3, Component Length = 1m, Overhead Rate = 127EUR/hr, Discount Rate = 5%, Capital Write-off Time = 5yrs, Load Factor = 0.5



Capital cost	* 1.59e5	- 1.59e6	EUR
Material utilization fraction	0.9	- 0.98	
Production rate (length)	0.01	- 5	m/s
Tool life (length)	100	- 1e5	m
Tooling cost	797	- 3.99e3	EUR

Supporting information

Design guidelines

Limited to shapes of constant cross section. Cross section may be intricate (depending on material extrudability).

Technical notes

Wide variety of metals are extruded. The most common are: aluminum and aluminum alloys, copper and copper alloys, magnesium, low-carbon and medium-carbon steels, low-alloy steels and stainless steels. Symmetrical cross sections and generous radii are advantageous. The ratio of length to thickness of any section of an extrusion should not exceed 14:1 for steels. For magnesium the limit is 20:1.

Injection molding (thermoplastics)

Datasheet view: All processes

Show/Hide

Physical attributes

Mass range	0.01	-	25	kg
Range of section thickness	0.4	-	6.3	mm
Tolerance	0.1	-	1	mm
Roughness	0.2	-	1.6	µm

Process characteristics

Primary shaping processes	✓
Secondary shaping processes	✗
Machining processes	✗
Prototyping	✗
Discrete	✓
Continuous	✗

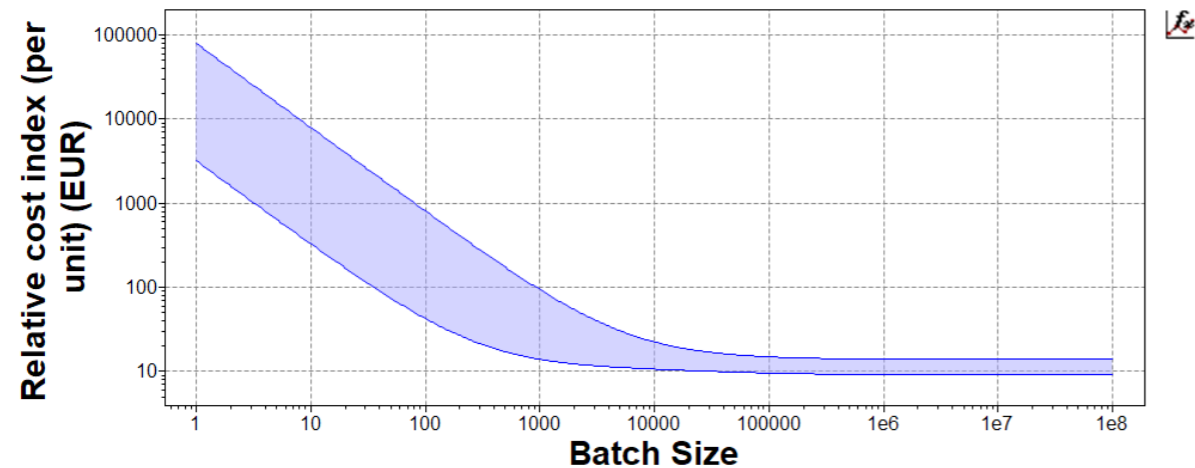
Economic attributes

Economic batch size (units)	1e4	-	1e6
Labor intensity	low		

Cost modeling

Relative cost index (per unit)	13.9	-	94.4	EUR
--------------------------------	------	---	------	-----

Parameters: Material Cost = 6.77EUR/kg, Component Mass = 1kg, Batch Size = 1e3, Overhead Rate = 127EUR/hr, Discount Rate = 5%, Capital Write-off Time = 5yrs, Load Factor = 0.5



Component Mass=1kg, Component Length=1m, Material Cost=6.77EUR/kg, Overhead Rate=127EUR/hr, Capital Write-off Time=5yrs, Discount Rate=5%, Load Factor=0.5

Capital cost	3.19e4	-	7.17e5	EUR
Material utilization fraction	0.6	-	0.9	
Production rate (units)	60	-	3e3	/hr
Tool life (units)	1e4	-	1e6	
Tooling cost	3.19e3	-	7.97e4	EUR

Supporting information

Design guidelines

Complex shapes are possible. Thick sections or large changes in section are not recommended. Small reentrant angles are possible.

Technical notes

Most thermoplastics can be injection molded. Some high melting point polymers (e.g. PTFE) are not suitable. Thermoplastic based composites (short fiber and particulate filled) are also processed. Injection-molded parts are generally thin-walled.

APPENDIX J

Costs overview showing total price according to the different elements integrated within the design solution.

	INPUT VALUES				COST RESULTS		References
	value	unit	value	unit	Total price	Facade price /unit	
1.1 Container	Phase change material (SP25E, $\rho=1450 \text{ kg/m}^3$)	€1.89 /kg	1896.82 kg	€3,584.99	€147.99 /m ²	(S. Klaiher, personal communication, December 20, 2018)	
	Insulation material (Aerogel)	€20.00 /kg	14.83 kg	€296.51	€12.24 /m ²	M. Blau (personal communication, May 22, 2019)	
	Macroencapsulation (3 mm PMMA, $\rho=946 \text{ kg/m}^3$)	€2.33 /kg	30.07 kg	€70.06	€2.89 /m ²	(CES Edupack, 2019)	
	Injection molding (productioncosts) <i>Product and process information: Appendix I</i>	€7.13 /st	64.00 st	€456.32	€18.84 /m ²	(CES Edupack, 2019)	
1.3 Movement mechanism	Steel cable (3 mm)	€0.61 /m	27.36 m	€16.66	€0.69 /m ²	(S3i Group, 2019)	
	Linear guiding rail (LFS-8-2 Linear guide rail)	€26.82 /m ¹	13.68 m	€366.90	€15.15 /m ²	(Banggood, 2019)	
	Guide carriage	€9.40 /st	64.00 st	€601.60	€24.83 /m ²	(RS Components, 2019)	
1.2 Rotation mechanism	Rotation block			<i>included</i>	<i>included</i>		
	Rotation rod (steel, 12 mm)	€2.92 /m	19.00 m	€55.44	€2.29 /m ²	(CES Edupack, 2019)	
	Actuator	€33.99 /st	8.00 st	€271.92	€11.22 /m ²	(Conrad, 2019)	
1.4 Miscellaneous	Protection profile (hot metal extrusion)	€4.13 /st	16.00 st	€66.08	€2.73 /m ²	(CES Edupack, 2019)	
	Protection profile (Aluminium 6016, T1)	€2.33 /kg	25.60 kg	€59.65	€2.46 /m ²	(CES Edupack, 2019)	
	<i>Product and process information: Appendix I</i>						
	Installation procedure	€40.00 /h	8.00 h	€320.00	€13.21 /m ²		
	<i>based on the different design elements</i>			€6,166.12	€254.54 /m ²		
	<i>based on the extra installation needed</i>			€2,977.67	€122.92 /m ²		
	TOTAL CAPITAL COSTS: PCM SYSTEM			€9,143.79	€377.45 /m²		

From: **Markus Blau** Markus.Blau@cabotcorp.com
 Subject: Your inquiry about Cabot's Aerogel
 Date: 22 May 2019 at 15:35
 To: j.c.hendriks@student.tudelft.nl

Dear Mr. Hendriks,

thank you for your inquiry and your interest in Cabot's AEROGEL.

Of course we are helping you with information for the market evaluation of possible new solutions with our Aerogel particles. For the evaluation of the market potential of commercial applications you can use the following target prices for our Aerogel P-grades:
 20 – 28 €/kg.

In general our prices are dependable on the grade and the volume ordered. Hope to help you with these information.

Kind regards

Markus Blau
 Market Development Manager, Aerogel

Cabot GmbH

markus.blau@cabotcorp.com

All sales of Cabot products are subject to Cabot standard terms and conditions of sale, which can be found at <http://www.cabotcorp.com/information/terms-of-sale>.

Office:
 Cabot Aerogel GmbH
 Industriepark Höchst,
 Gebäude D 660
 65926 Frankfurt
 Germany

